DOE/BC/14477-18
Distribution Category UC-122

An Experimental and Theoretical Study to Relate Uncommon Rock/Fluid Properties to Oil Recovery

Final Report

By
R. Watson

July 1995

Work Performed Under Contract No. DE-AC22-89BC14477

Prepared for
U.S. Department of Energy
Assistant Secretary for Fossil Energy

Gene Pauling, Project Manager
Metairie Site Office
900 Commerce Road, East
New Orleans, LA 70123

Prepared by
Pennsylvania State University
102 Mineral Sciences Building
University Park, PA 16802

DISCLAIMER

TABLE OF CONTENTS

Page

Page

LIST OF TABLES

Page

Page

Page

Page

LIST OF FIGURES

Page

Page

Page

Page

Page

Page

Page

Page

Page

NOMENCLATURE

English

A	=	cross-sectional area of core (cm^2)
A	=	pore wall surface area (m^2/g)
AC	=	total amount of cement (percent)
ACC	=	amount of carbonate cement (percent)
ACM	=	amount of clay matrix (percent)
Adj. R-sq.	=	adjusted coefficient of determination (%)
AFG	=	amount of framework grains (percent)
AQO	=	amount of quartz overgrowth (percent)
B.T.	=	breakthrough time
C.I.	=	confidence limits
C_o	=	constant in Kozeny-Carman's equation
C_p	=	C_p criterion
C.S.	=	coefficient of skewness
C.V.	=	coefficient of variation
d	=	capillary tube or pore diameter (micrometer)
D	=	average pore diameter (micrometer)
E	=	expected value
f	=	function of
F	=	formation resistivity factor

F	=	statistical F-test
F.O.	=	floodout time
G	=	dependent variable
h	=	thickness (in)
I_o	=	displacement-by-oil ratio
I_w	=	displacement-by-water ratio
IOIP	=	initial oil-in-place (PV)
k	=	permeability (md)
L	=	length of core (cm)
L	=	apparent total length of the flooded system (cm)
L_a	=	actual total length of the flooded system (cm)
$Lu_w\mu_w$	=	scaling coefficient (cm^2.cp/min)
M	=	median of data set
m_f	=	final mass of core sample (g)
m_i	=	initial mass of core sample (g)
Max.	=	maximum value of a particular data
Min.	=	minimum value of a particular data
mode 1	=	unimodal capillary pressure shape
mode 2	=	bimodal capillary pressure shape
mode 3	=	trimodal capillary pressure shape
mode 4	=	quadramodal capillary pressure shape
MSE_p	=	mean square error

n	=	number of samples
N_{ca}	=	capillary number based on interstitial velocity
N^*_{ca}	=	capillary number based on darcy velocity
OR	=	oil recovery (% IOIP)
P	=	pressure (psia)
p	=	number of parameters
p_1	=	upstream pressure (atm)
p_2	=	downstream pressure (atm)
P_c	=	capillary pressure (psia)
P_i	=	pressure at a particular point (psia)
P_{max}	=	maximum pressure (psia)
P_{min}	=	minimum pressure (psia)
P_{value}	=	significance level
q	=	rate of fluid flow (cc/sec)
Q_1	=	lower quartile or first quartile
Q_3	=	upper quartile or third quartile
r	=	radius of core sample (cm)
R	=	correlation coefficient (fraction)
R^2	=	coefficient of determination (%)
R_N^2	=	coefficient of correlation (%)
R_o	=	resistivity of a rock (ohm-m)
R_p^2	=	R_p^2 criterion

r_i	=	average pore entry radius (cm)
R-sq.	=	coefficient of determination (%)
R_w	=	resistivity of water (ohm-m)
RE	=	mercury recovery efficiency (fraction)
s	=	positive square root of sample variance (fraction)
s	=	standard deviation
S	=	phase saturation (fraction)
S_{Hg}	=	mercury saturation (fraction)
S_j	=	saturation of phase j in core (fraction)
S_{oi}	=	initial oil saturation (fraction)
S_{or}	=	residual oil saturation (fraction)
S_r	=	residual mercury saturation (fraction)
S_s	=	specific surface area (cm^2/cm^3)
S_{wi}	=	irreducible water saturation (fraction)
SA	=	total pore area or surface area (m^2/g)
St. Dev.	=	standard deviation
SSE	=	error sum of squares
SSR	=	regression sum of squares
SSTO	=	total sum of squares
t	=	apparent retention time (sec)
t_a	=	actual retention time (sec)
u	=	darcy or superficial velocity (cm/sec)

u_w	=	flood velocity (cm/min)
UOR	=	ultimate oil recovery (% IOIP)
v	=	interstitial or frontal velocity (cm/sec)
V	=	volume (cc)
V_B	=	bulk volume of sample (cc)
$V_{int.}$	=	total intrusion volume or pore volume (ml/g)
V_j	=	volume of phase j in core (cc)
$(V_o)_{total}$	=	total oil volume displaced (cc)
$(V_o)_{spontaneous}$	=	oil volume displaced spontaneously (cc)
V_p	=	pore volume (cc)
V_S	=	grain volume (cc)
$(V_w)_{total}$	=	total water volume displaced (cc)
$(V_w)_{spontaneous}$	=	water volume displaced by spontaneously (cc)
W	=	work done (erg)
WI	=	wettability index
X	=	independent variable
x	=	mean of data set
x_i	=	individual data set value
Y	=	dependent variable
z	=	statistical z-test
z	=	average
z_c	=	level of significance factor

Greek

α	=	level of significance
β	=	parameter
β	=	linear regression coefficient
$\hat{\beta}$	=	estimated value of linear regression coefficient
ΔS_{Hg}	=	incremental change in mercury saturation
ε	=	random error
θ	=	contact angle for liquid on solid (deg.)
λ	=	lithology factor in Purcell's (1949) equation
μ	=	confidence limits
μ	=	fluid viscosity (cp)
μ_o	=	oil viscosity (cp)
μ_w	=	water viscosity (cp)
ρ	=	fluid density (g/cc)
ρ_B	=	bulk density (g/ml)
ρ_s	=	apparent (skeletal) density (g/ml)
σ	=	surface tension for liquid (dyn/cm)
σ	=	standard deviation
σ^2	=	variance
σ_{ow}	=	interfacial tension between phases (dyn/cm)
Σ	=	summation function
τ	=	tortuosity

ϕ	=	porosity (fraction)
ϕ	=	total porosity (percent)
ϕ_{Hg}	=	mercury porosimetry porosity (fraction)
$\phi_{prim.}$	=	primary porosity (percent)
$\phi_{sec.}$	=	secondary porosity (percent)
χ_i	=	dividing factor in Burdine's (1950) equation

SI METRIC CONVERSION FACTORS

acre x 4.046 873	E+03	=	m^2
acre-ft x 1.233 489	E+03	=	m^3
°API 141.5/(131.5+°API)		=	g/cm^3
bbl x 1.589 873	E-01	=	m^3
cp x 1.0*	E+00	=	mPa.s
ft x 3.048*	E-01	=	m
ft^3 x 2.831 685	E-02	=	m^3
°F (°F-32)/1.8		=	°C
gal x 3.785 412	E-03	=	m^3
in x 2.54*	E+00	=	cm
lbm x 4.535 924	E-01	=	kg
psi x 6.894 757	E-01	=	kPa

*Conversion factor is exact.

ACKNOWLEDGEMENTS

The financial support of the U.S. Department of Energy to The Pennsylvania State University through contract No. DE-AC22-89BC14477 is gratefully acknowledged.

This report is a result of the work performed by the principal investigator, Dr. Robert Watson, Assistant Professor of Petroleum and Natural Gas Engineering, the co-investigator, Dr. Turgay Ertekin, Professor and Section Chairman of Petroleum and Natural Gas Engineering, and the following graduate students: Dr. Fathi H. Boukadi and Dr. Olubunmi O. Owolabi.

Appreciation is expressed to Dr. C. Drew Stahl, Professor Emeritus of Petroleum and Natural Gas Engineering; Dr. Raja V. Ramani, Professor and Head of Mineral Engineering; Dr. Rudy L. Slingerland, Professor of Geology; Dr. William L. Harkness, Professor of Statistics; Dr. Michael A. Adewumi, Associate Professor of Petroleum and Natural Gas Engineering; Dr. Abraham S. Grader, Associate Professor of Petroleum and Natural Gas Engineering; and Dr. Paul J. Hicks, Jr., Assistant Professor of Petroleum and Natural Gas Engineering, for their helpful criticism and suggestions as members of the Graduate Committee of the two Ph.D. theses that resulted from this project. Dr. Robert W. Watson was the advisor for both theses, and both theses Graduate Committee were chaired by Dr. Turgay Ertekin.

The investigators acknowledge the assistance of Mr. Scott Heckman, Senior Research Technician; and other members of the faculty, staff and students of the Petroleum and Natural Gas Engineering Section who have assisted us.

ABSTRACT

The most commonly used secondary oil recovery technique is waterflooding. Macroscopic (or common) rock-pore characteristics such as porosity, permeability and irreducible water saturation and fluid properties such as viscosity have been shown by previous investigators to influence the results of waterflooding and consequently ultimate oil recovery. The objectives of this study are to consider the influence of microscopic (or uncommon) rock-pore characteristics such as wettability, tortuosity, mercury intrusion volume, pore surface area, specific surface area, average pore diameter, median pore-throat diameter, pore length, apparent (skeletal) density and mercury recovery efficiency on residual oil saturation and oil recovery realized in linear-core waterfloods. The results were statistically analyzed to determine the quantitative relations between the various properties, and empirical equations were developed for predicting waterflood performance. The characteristics were analyzed and modeled at both breakthrough and floodout.

To accomplish the above stated objectives, radial-core flood and linear core-flood sets of experimental studies were conducted. The radial core waterflood experiments were conducted on 20 Berea sandstone and 20 Indiana limestone radial-cores. The dimensions of the radial-cores used were 12.7 cm in diameter and 5.08 cm long. Eight core plugs were cut from each waterflooded radial-core. Each of the 8 plugs was cut into 3 sub-plugs giving a total of 24 core plugs for each waterflooded radial core. Altogether, there were a total of 480 sandstone core plugs and 480 limestone core plugs, extracted from the waterflooded radial-cores. The linear-core waterflood experiments were conducted on 21 Berea sandstone and 16 Indiana limestone linear-cores. The sandstone linear-cores ranged from 7.3 to 52.1 cm in length and 3.8 to 3.9 cm in diameter. The limestone linear-cores ranged from 40.0 to 45.7 cm in length and from 3.8 to 3.9 cm in diameter. Six to fifty-four core plugs were

extracted from each of the sandstone linear-cores for a total of 580 sandstone core plugs and thirty-two core plugs were extracted from each of the limestone linear-cores for a total of 512 limestone core plugs.

The core plugs were analyzed by conducting wettability and mercury porosimetry experiments. The wettability indices were determined using the Amott-Harvey method. For a particular core, the sets of data from the core plugs were averaged and single values for the wettability and mercury porosimetry properties were obtained. The sandstone and limestone core samples investigated in this study were all water-wet. The analysis of the results of the mercury porosimetry experiments suggested that steep-convex and steep-concave unimodal capillary pressure curves are characteristic of the investigated sandstone core samples. By contrast, steep-convex unimodal, bimodal, polymodal, and gently-sloping bimodal capillary pressure curves are characteristic of the investigated limestone core samples. Using some of the mercury porosimetry properties, new empirical correlations to aid in the estimations of mercury recovery efficiency and permeability are proposed, for sandstones and limestones.

The results of the radial-core and linear-core flow investigations and the other associated experimental analyses are presented and incorporated into empirical models to improve the predictions of oil recovery resulting from waterflooding, for sandstone and limestone reservoirs. For the radial-core case, the standardized regression model selected, based on a subset of the variables, predicted oil recovery by waterflooding with a standard deviation of 7%. For the linear-core case, separate models are developed using common, uncommon and combination of both types of rock properties. It was observed that residual oil saturation and oil recovery are better predicted with the inclusion of both common and uncommon rock/fluid properties into the predictive models.

Chapter 1

INTRODUCTION

Waterflooding is the most commonly used secondary oil recovery technique. One of the requirements for understanding waterflood performance is a good knowledge of the basic properties of the reservoir rocks.

This study is aimed at correlating rock-pore characteristics to oil recovery from various reservoir rock types and incorporating these properties into empirical models for predicting oil recovery. For that reason, this report deals with the analyses and interpretation of experimental data collected from core floods and correlated against measurements of absolute permeability, porosity, wettability index, mercury porosimetry properties and irreducible water saturation.

An important component of reservoir characterization is the description of the pore systems, which is one of the factors that control the production potential of the reservoir. Pore systems are studied by a family of methods called petrophysical analysis; one of these methods is mercury porosimetry (Kopaska-Merkel and Friedman, 1989a). In this method, mercury is injected into the pore system of a sample under controlled conditions, to produce capillary pressure curves. The properties of interest from the mercury porosimetry include total mercury intrusion volume, pore surface area, specific surface area, average pore diameter, skeletal density, apparent porosity, residual mercury saturation and mercury recovery efficiency.

Empirical models based on data obtained from waterflood, wettability and mercury porosimetry laboratory experiments were developed for the predictions of residual oil saturation and oil recovery at both the breakthrough and floodout conditions. Furthermore,

the various models were developed for sandstones and limestones using unfired linear Berea sandstone and Indiana limestone cores, respectively. The tasks for the investigations were of two main parts. In the first part of the research studies, Boukadi (1991) conducted the investigations using radial core-floods, and in the second part, Owolabi (1993) conducted the investigations using linear core-floods.

1.1 Sandstones

Several quarried sandstone and carbonate rocks are widely used in the petroleum industry as standard porous media for laboratory study of fluid flow phenomena. Berea sandstone which was first identified in the 1950's as a standard porous media for research on oil recovery and Indiana limestone are the most commonly used standard rocks (Churcher et al., 1991; and Ma and Morrow, 1991). Both types of rocks are quarried in Amherst, Ohio by Cleveland Quarries Company. Cores cut from given batches of the quarried rock usually have relatively consistent petrophysical properties, but batches cut from different parts of the quarry provide cores of different permeabilities (Ma and Morrow, 1991).

Sandstones are typically composed of quartz and feldspars, with varying amount of other components such as garnet, magnetite, zircon, apatite, rutile, micas, titanite, tourmaline and corundum (Hurlbut, 1942). The physical characteristics of sandstones are determined by grain composition, the size and shape of grains, cementing materials, and secondary processes which are operative during the life of the rock (Boukadi, 1991). The most important characteristic of sandstone texture is sorting. A well-sorted rock is composed of particles of approximately the same size and a poorly sorted rock is composed of particles with a wide range of sizes.

According to Coogan and Heath (1984), the Berea sandstone in Ohio, which outcrops at the outskirts of Cleveland, is one of the better known rock formations. It is among the

more productive formations in Ohio, where it yields gas, oil, or gas and oil at moderate to very shallow depths, and has been a drilling target for hydrocarbons for more than a century (Ciccarone and Warren, 1985). Stratigraphically, the Berea sandstone is part of the Waverly group and it is underlain by the red and gray Bedford shale and overlain by the black Sunbury shale member of the Cuyahoga formation, all of which are of Late Devonian or Early Mississippian age (Hillebrand and Coogan, 1984).

Berea sandstone is fine-grained, well sorted, and massive to thinly laminated. It consists primarily of detrital, subangular to subrounded, quartz grains with small amounts of feldspar and rock fragments. The sandstone is poorly cemented with cement consisting of overgrowths of secondary quartz and the matrix is clayey in nature (Shakoor and Bonelli, 1991).

1.2 Limestones

Limestones are defined as sedimentary rocks containing over 50% carbonate material, although the proportion often exceeds 95% (Fookes and Hawkins, 1988). According to Fookes and Hawkins, the principal component minerals are calcite (calcium carbonate, $CaCO_3$) and dolomite (calcium magnesium carbonate, $CaMgCO_3$). Other less common carbonate constituents include magnesite ($MgCO_3$), rhodochrosite ($MnCO_3$) and siderite ($FeCO_3$). They also noted that all limestones have a similar basic chemistry, but the processes by which they are formed vary. These processes include:

(a) Skeletal carbonate bodies, such as shells, coral reefs and similar organic material, become cemented to form a rock of mainly biological origin.

(b) Particulate (clastic) material, such as fragments of older limestones, are transported and then cemented to form a rock of mechanical origin.

(c) Material precipitated from water as a result of variation in the pressure, temperature, and concentration of the solution forms a rock or cement of chemical origin.

Indiana limestone, also known as the Salem limestone, was formed in a shallow inland sea during Mississippian time (Patton, 1953; Stevenson, 1979; and Churcher et al., 1991). It has produced oil in Illinois since the late 1930's (Stevenson, 1979). The quarried beds are buff and gray, massive, granular, cross-laminated, high-calcium limestone and are composed largely of small fossils and fossil fragments (Patton, 1953). According to Patton, in order of abundance, the mineral constituents of Indiana limestones are calcite, dolomite, quartz, chert, clay minerals, limonite, hematite, pyrite and leucoxene. Calcite is the principal constituent but locally dolomite and chert are common to abundant. Most of the calcite and some of the quartz were primary, while the remaining mineral contents are secondary and were deposited by ground water and altered from primary grains of magnetite and ilmenite.

It is bioclastic in origin and shows a high degree of size-sorting. Deposition was controlled by marine currents and wave action, and most of the fossil particles are microcrystalline calcite (less than 0.01 mm), but some have recrystallized, so that each fragment consists of a single crystal. Calcites and in some places dolomites, are the cementing material. Calcite crystals in the cement commonly are as broad as the pore space, but dolomite in the cement is microcrystalline (Patton, 1953).

1.3 PUBLICATIONS AND PRESENTATIONS

The following publications, theses, and presentations have resulted from this research project.

1. Watson, R.W., and Boukadi, F.H.: "Effect of Surface Area and Pore-Size Distribution on Oil Recovery at Breakthrough, on Oil Recovery at Infinite Water-Oil Ratio, on Residual Oil Saturation and on Wettability," paper No. SCA 9007, *Proceedings of*

the Society of Core Analysts, Fourth Annual Technical Conference, Dallas, TX., 1990.

2. Watson, R.W., Boukadi, F.H., and Owolabi, O.O.: "The Effects of Clay Matrix, Carbonate Cement and Quartz Overgrowth on Wettability, Porosity, Residual Oil Saturation, Tortuosity and Rock Surface Area of Berea," paper No. 91-76, *Proceedings of the Petroleum Society of CIM and AOSTRA Technical Conference*, Banff, Alberta, 1991, pp. 76-1 - 76-11. Also being reviewed for publication in the *J. Cand. Pet. Tech.*

3. Watson, R.W., and Boukadi, F.H.: "Determination of Fluid Flow Mechanisms in Berea Using Mercury Porosimetry and A Stochastic Model to Relate These Mechanisms to Oil Recovery," paper SCA No. 9123, *Proceedings of the Society of Core Analysts, Fifth Annual Technical Conference*, San Antonio, TX., 1991.

4. Boukadi, B.H.B.: "An Experimental and Theoretical Study to Relate Uncommon Rock/Fluid Properties to Oil Recovery," Ph.D. Dissertation, The Pennsylvania State University, University Park, PA., (Dec. 1991), 238pp.

5. Owolabi, O.O.: "Empirical Modeling of the Microscopic Rock-Pore Characteristics in Sandstone Linear Cores to Residual Oil Saturation and Oil Recovery By Waterflood," paper submitted for the 1992 Mobil Sponsored Student Paper Contest - Ph.D Division.

6. Owolabi, O.O.: "Experimental and Empirical Studies of the Influence of Rock-Pore Properties on Oil Recovery Efficiency in Waterflooded Berea Sandstone Cores," paper presented at the 1992 SPE Rocky Mountain/Mid-Continent Student Paper Contest - Ph.D Division, Butte, Montana, Feb. 28-29, 1992.

7. Owolabi, O.O., and Watson, R.W.: "The Influence of Mercury Porosimetry Properties, Tortuosity, Porosity and Wettability on Sandstone Waterflood Residual Oil

Saturation," *Proceedings of the Eighth Wyoming EOR Symposium*, Casper, WY., 1992.

8. Boukadi, F., Watson, R.W., and Owolabi, O.O.: "The Influence of Reservoir Rocks Skeletal Properties on Ultimate Oil Recovery in Radial-Core Waterfloods," paper No. CIM 92-55, *Proceedings of the Petroleum Society of CIM, 43rd Annual Technical Meeting*, Calgary, Alberta, Canada, 1992. Also accepted for publication in the *J. of Cand. Pet. Tech.*.

9. Owolabi, O.O.: "Relating Uncommon Rock/Fluid Properties to Oil Recovery for Various Types of Oil Bearing Rocks: Experimental and Empirical Studies," Ph.D. Dissertation, The Pennsylvania State University, University Park, PA., (May 1993), 412pp.

10. Owolabi, O.O., and Watson, R.W.: "Empirical Modeling of Fluid Flow Mechanism in Water-Wet Limestones Exhibiting Bimodal Pore-Size Distribution," paper No. CIM 93-53, *Proceedings of the 1993 Annual General Meeting of CIM / 44th Annual Technical Meeting of the Petroleum Society of CIM*, Calgary, Alberta, Canada, 1993.

11. Owolabi, O.O., and Watson, R.W.: "Experiment and Empirical Investigation of Residual Oil Saturation in Limestone Exhibiting Bimodal Pore-Size Distribution Using Mercury Porosimetry," *Proceedings of the Ninth Wyoming EOR Symposium, Casper, WY., 1993.*

12. Owolabi, O.O., and Watson, R.W.: "The Influence of Porosity, Permeability, Tortuosity, Wettability, and Mercury Porosimetry Properties on Limestone Waterflood Residual Oil Saturation," paper No. SCA 9309, *Proceedings of the Society of Core Analysts, Seventh Annual Technical Conference*, Houston, TX., 1993.

13. Owolabi, O.O., and Watson, R.W.: "Effects of Rock-Pore Characteristics on Oil Recovery at Breakthrough and Ultimate Oil Recovery in Water-Wet Sandstones," paper No. SPE 26935, *Proceedings of the 1993 SPE Eastern Regional Conference and Exhibition*, Pittsburgh, PA., 1993.

14. Owolabi, O.O., and Watson, R.W.: "Estimating Recovery Efficiency and Permeability from Mercury Capillary Pressure Measurements for Sandstones," paper No. SPE 26936, *Proceedings of the 1993 SPE Eastern Regional Conference and Exhibition*, Pittsburgh, PA., 1993.

Chapter 2

LITERATURE REVIEW

Over the years, several attempts have been made to develop empirical correlations to better predict ultimate oil recovery. Among these are the work of Craze and Buckley (1945), Guthrie and Greenberger (1955), Carlile (1964), Arnold and Crawford (1964), Donaldson et al. (1969), and Wardlaw and Cassan (1979).

Craze and Buckley's study was conducted in two separate phases. The first phase dealt with gas-drive sandstone fields and the second phase considered water-drive sandstone fields. They showed specific interest in isolating and identifying possible effects on well spacing by measured and estimated values of properties of both the reservoirs and their effluents. They concluded that no systematic variation of oil recovery with well spacing was noticed in both type of drives.

Guthrie and Greenberger determined the effects of the parameters presented by Craze and Buckley on water-drive recovery efficiency. They also made a presentation on the theory of multiple correlation analyses for the interpretation of petroleum engineering data. They reported a significant relationship between porosity and permeability. They further indicated a strong effect of porosity on oil recovery, which was independent of its relationship with permeability. The independent variables included in their final correlation are: permeability, porosity, oil viscosity, net formation thickness and irreducible water saturation.

Carlile developed correlations for recovery, recovery fraction, and residual oil saturation for water-drive sandstone reservoirs. The independent variables used in his correlations are absolute permeability, viscosity ratio, porosity, oil formation volume factor,

net formation thickness, bubble-point pressure, reservoir temperature, depth of horizon, residual oil saturation and oil gravity. The data for his study were collected by the Special Study Committee on Recovery Efficiencies under the auspices of the American Petroleum Institute.

Empirical equations were developed by Arnold and Crawford to show the analytical relation between the fluid and rock properties and oil recovery by waterflooding. Their laboratory studies made use of water-wet consolidated and unconsolidated porous media. Among other properties, their predicting equation utilized an electric rock property, formation resistivity factor.

Donaldson et al. studied the effect of wettability on oil recovery efficiency. They noted that wettability when used as a parameter in designing linear mathematical models for predicting recovery efficiency, is equal in significance to permeability, viscosity and fluid saturations. Their developed correlations for recovery efficiency made use of USBM wettability index, permeability, porosity, oil viscosity and interfacial tension.

Wardlaw and Cassan had as their major objective, the comparison of mercury recovery efficiency, measured by capillary-pressure tests, to oil recovery efficiency obtained from relative-permeability tests. They related the results of both types of tests to other petrophysical data such as porosity and gas permeability, as well as to petrographic observations and direct observations of pore structure made from resin casts. They concluded that for a diverse group of sandstone reservoir rocks, there is a statistically significant correlation between mercury recovery efficiencies and oil recovery efficiencies. Also, the rock-pore properties that were found to be significantly related to high recovery efficiency, are high porosity, small pore-throat size ratio, small mean particle size and low percentage of carbonate.

This present study relates rock/fluid properties from waterflood, wettability and mercury porosimetry to waterflood oil recovery. For this reason, the remaining sections of this chapter review the literature dealing with these properties.

2.1 Waterflood and Petrophysical Properties

The objective of secondary recovery methods is to reduce the fraction of oil left in the reservoir. Currently, waterflooding is the dominant and most effective of these secondary recovery methods. Although waterflooding as a secondary recovery method has been in existence for many decades, there is still a great deal of current research interest in the study of the mechanisms associated with this displacement method.

The residual oil remaining in the swept zone of a waterflood project is usually taken as the target oil for tertiary recovery processes. Rathmell et al. (1973) conducted an investigation of reservoir waterflood residual oil saturation from laboratory tests. They proposed a technique for estimating waterflood residual oil saturations from core saturations where the cores must be taken with water-base muds having a filtrate loss in excess of 5 cc at the bottom-hole conditions. According to Kazemi (1977), the equation proposed by Rathmell et al. must be corrected for waterflood displacement efficiency through multiplication by the reciprocal of the conformance factor. The conformance factor may be obtained from a reservoir simulator that accounts for reservoir heterogeneity, capillary effects, and mobilities of oil and water. Chang et al. (1988) presented a brief review of available residual oil saturation techniques. They summarized the advantages, limitations, problems, and possible improvements of each technique. Furthermore, they presented screening criteria for determining the best residual oil saturation technique under certain wellbore or reservoir conditions.

The factors that determine the amount of residual oil and its microscopic distribution have been studied in the recent years (Wardlaw, 1976; Wardlaw and Cassan, 1978;

Wardlaw and Cassan, 1979; and Chatzis et al., 1983). Chatzis et al. conducted experimental studies that demonstrated the effect of particle size, particle-size distribution, macroscopic and microscopic heterogeneities, microscopic dimensions such as ratio of pore-body to pore-throat size, and pore-to-pore coordination number on residual oil, under water-wet conditions. Major conclusions from their study are:

(1) Residual saturations are independent of absolute pore size, in systems of similar pore geometry.

(2) Well-mixed two-component aggregates of spheres gave virtually the same residual saturations as random packings of equal sized spheres.

(3) Clusters of large pores accessible through small pores, will retain oil.

(4) High aspect ratios (ratio of the pore-body to pore-throat size) tend to cause entrapment of oil as a large number of relatively small blobs, each held in single pores.

(5) The role of pore-to-pore coordination number is generally secondary; hence, correlations that have been proposed between residual oil and coordination number are unreliable.

In 1949 Breston and Hughes presented the results of their laboratory study to propose a relation between pressure and recovery in long core waterfloods. Their experiments were conducted with the aim of duplicating field conditions as closely as possible by using long unextracted consolidated cores, a live crude, and natural brines for both flooding and connate water content. They observed that floods on the long cores showed increased recoveries and lower residual oil saturation with increased flood pressure gradients and flood velocities. It has been documented in the literature that experimental results on flow behavior from flood experiments in small reservoir cores are questionable because of severe end effects resulting from the sudden discontinuity of the capillary forces at the core ends. The significance of this disturbance on the flow pattern is a function of the core length, the

flow velocity, the interfacial tension between the fluids, and the fluid characteristics (Graue et al., 1990). In order to prevent this problem, the laboratory experiments should be well scaled. The required scaling coefficient and the other important waterflood and petrophysical properties investigated are briefly reviewed in the remaining parts of this section.

2.1.1 Scaling Coefficient

In the process of using laboratory experiments to measure the probable performance of a reservoir, the problem of proper scaling arises. Rapoport and Leas (1953) recognized that the flooding behavior is dependent upon the length of the system and the rate of injection. At the same time, it has been determined that systems of different lengths yield the same flooding behavior if the injection rates and/or the fluid viscosities are properly adjusted or scaled (Kyte and Rapoport, 1958). In the discussion of the paper by Edmonson (1985), Odeh and Cook emphasized the fact that it has been shown by Rapoport and Leas (1953) that for linear waterflood to be in the stable region (no capillary end effect), it should conform to the scaling coefficient as shown in Eq. 2.1. This condition was satisfied in each of the corefloods investigated in this phase of the study:

$$L\, u_w\, \mu_w > 5.0 \ \text{cm}^2 \cdot \text{cp/min} \qquad (2.1)$$

where the length of core, L, is in cm, the velocity, u_w, is in cm/min, and the water viscosity, μ_w, is in cp. The suggested scaling causes the capillary pressure gradient in the direction of flow to be small compared to the imposed pressure gradient (Batycky et al., 1980). Batycky et al. in their paper proposed that the scaling factor should be $\geq$ 1.0-5.0.

2.1.2 Capillary Number

Capillary forces often have a detrimental effect on residual oil saturation and oil recovery, since they are responsible for the trapping of oil within the pores. In order to assess the transition between a displacement process dominated by capillary forces and one dominated by viscous forces, it is convenient to consider the dependence of the residual oil saturation and oil recovery efficiency on a suitable dimensionless parameter, such as the capillary number, which is defined as (Melrose and Brandner, 1974; and Willhite, 1986):

$$N_{ca} = \frac{u_w \mu_w}{\phi \sigma_{ow}} \tag{2.2}$$

Equation 2.2 is the capillary number based on interstitial velocity. In the capillary number equations, the velocity, u_w, is in cm/sec, the viscosity, μ_w, is in cp, the porosity, ϕ, is a fraction, and the interfacial tension, σ_{ow}, is in dynes/cm. The capillary number based on darcy velocity, is presented in Eq. 2.3 (Boon, 1984; Willhite, 1986; and Omoregie, 1988):

$$N^*_{ca} = \phi N_{ca} = \frac{u_w \mu_w}{\sigma_{ow}} \tag{2.3}$$

Some authors (Moore and Slobod, 1956; and Latil, 1980) alter the above expression by including the cos θ as follows:

$$N^*_{ca} = \frac{u_w \mu_w}{\sigma_{ow} \cos \theta} \tag{2.4}$$

To make Eqs. 2.2 through 2.4 dimensionless, unit conversion (1 cp = 10^{-2} dyne.s/cm^2) is required in the equations.

The inclusion of the cos θ term will not be used in this study, and the N^*_{ca} will be as defined by Eq. 2.3. Morrow (1970) observed that for a waterflood performed at a low

capillary number, $N^*_{ca} < 10^{-6}$, the residual non-wetting saturation is influenced by capillary forces. For $N^*_{ca} < 10^{-5}$ there is no mobilization of residual oil, but as $N_{ca} > 10^{-5}$ the fraction of the residual oil mobilized increases sharply with increasing capillary number (Boon, 1984; and Willhite, 1986). It has been reported that the lower limit below which the rate of injection has no effect on the nonwetting residual saturation is in the region of 10^{-4} to 10^{-5} (Fulcher, 1982; and Henderson et al., 1991). According to Mohanty et al. (1987), as the capillary number increases, the residual oil saturation decreases and the residual oil blobs tend to be smaller. Also, as the pore size distribution becomes wider, the decrease of residual oil saturation with capillary number becomes more apparent.

2.1.3 Tortuosity and Formation Resistivity Factor

Tortuosity is a concept that describes the complex nature of the interconnecting paths through a rock sample (Winsauer et al., 1952; Wyllie and Spangler, 1952; Amyx et al., 1960; and Given, 1986). As shown in Amyx et al., tortuosity is defined as:

$$\tau = \left[\frac{L_a}{L} \right]^2 \tag{2.5}$$

For the purpose of this study, Eq. 2.5 needs to be modified to a form that could easily be measured in the laboratory. To do this, it should be recalled that:

$$u = \phi v \tag{2.6}$$

where the Darcy or superficial velocity is defined as:

$$u = \frac{L}{t} \tag{2.7}$$

and the interstitial or frontal velocity, which is assumed to relate the actual total length of the flooded system with the actual retention time is defined as:

$$v = \frac{L_a}{t_a} \tag{2.8}$$

Substituting Eqs. 2.7 and 2.8 into Eq. 2.6 results in Eq. 2.9, which describes the length of the actual flow path, L_a, relative to the apparent length, L, across the porous medium.

$$\frac{L_a}{L} = \frac{1}{\phi} \cdot \frac{t_a}{t} \tag{2.9}$$

Hence, substituting Eq. 2.9 into Eq. 2.5 yields:

$$\tau = \left[\frac{1}{\phi} \cdot \frac{t_a}{t} \right]^2 \tag{2.10}$$

As defined by Archie (1942), the formation resistivity factor, F, is the ratio of the electrical resistivity of a rock, R_o, of a porous medium saturated with water to the resistivity, R_w, of the water in the pores.

$$F = \frac{R_o}{R_w} \tag{2.11}$$

In terms of the Archie formation resistivity factor, tortuosity is given by (Amyx et al., 1960):

$$\tau = F\phi \tag{2.12}$$

Givens (1986) and Wyllie and Spangler's (1952) definitions of tortuosity in terms of porosity and formation resistivity factor are different from that given in Eq. 2.12. Givens applied a square-root to the left-hand side of the equation containing the product of formation resistivity factor and porosity, while Wyllie and Spangler squared the product of these properties. These differences arise from the way the authors define tortuosity with respect to the tortuous length as shown in Eq. 2.10. Since tortuosity is a relative measure,

one should be consistent with whatever definition is chosen. Similar to the equation given in Amyx et al. (1960) and Winsauer et al. (1952), the definition of formation resistivity factor adopted in this study is:

$$F = \frac{\tau}{\phi} \tag{2.13}$$

2.1.4 Absolute Permeability

The characteristic of a porous media to allow the flow of a fluid or fluids through it is referred to as permeability. When only one phase is present and flowing through the medium, the measured permeability is referred to as absolute permeability. Absolute permeability is usually the type that is measured in routine core analysis (Guerrero, 1968). The equation for absolute permeability is obtained from Darcy's law (Amyx et al., 1960; Guerrero, 1968; Dake, 1978; and Willhite, 1986).

Equation 2.14 is the steady-state expression for an incompressible fluid flow through a porous medium. If the fluid fully saturates the medium, the permeability determined using this expression is the absolute value. The expression is of the form:

$$k = \frac{\mu q L}{A (p_1 - p_2)} \tag{2.14}$$

Instead of the independent variables of Eq. 2.14, Chilingarian et al. (1990) used multi-variable linear regression analysis to develop empirical correlations for permeability. The correlations are in terms of porosity, specific surface area, and irreducible fluid saturation, for carbonate reservoir rock areas in the former U.S.S.R. They were of the opinion that porosity values do not reflect the number and width of fractures, nor do they reflect the pore sizes or topological structure. Therefore, they advised that permeability should be related simultaneously to porosity, specific surface area, irreducible water/oil

saturation, grain size/pore size/throat size distribution, tortuosity and other petrophysical properties. The coefficient of correlation, R, for their correlations varied from 0.981 to 0.997.

2.1.5 Porosity

Porosity is one of the essential attributes of a reservoir. Porosity is defined as the ratio of the void space in a rock to the bulk volume of that rock (Amyx et al., 1960). It may be categorized according to the mode of origin as original or induced (Amyx et al., 1960). It is mathematically expressed as:

$$\phi = \frac{V_P}{V_B} \tag{2.15}$$

Pores are of three morphological types: catenary, cul-de-sac, and closed (Selley, 1985). Catenary pores are those that communicate with others by more than one throat passage. Cul-de-sac, or dead-end, pores have only one throat passage connecting with another pore. Closed pores have no communication with other pores. Furthermore, catenary and cul-de-sac pores constitute effective porosity, in that hydrocarbon can emerge from them (Selley, 1985). Most of the porosity found in sandstone reservoirs are preserved primary intergranular porosity, but it is generally secondary porosity in the case of carbonate reservoirs.

2.2 Wettability Properties

The term wettability refers to the ability of a fluid to wet a solid surface in the presence of a second fluid (Jadhunandan and Morrow, 1991). Wettability alterations have been known to affect waterflood behavior (Raza et al., 1968; Cuiec, 1987; Treiber et al., 1972 and Wolcott et al., 1991). Generally, the quantification of wettability is dependent on

the method used in the evaluation. The most common methods are the contact angle (Morrow, 1970), the spontaneous and forced displacements (Amott, 1959; Boneau and Clampitt, 1977; and Cuiec, 1984) and the capillary pressure curves (Donaldson et al., 1969). The capillary pressure curves method is also known as the USBM method and it employs imbibition and drainage capillary pressure data as a function of water saturation in determining wettability of a rock sample. Andersen et al. (1989) presented a new device for quantitative determination of wetting preference of crude oil/brine/solid systems. It is known as a dynamic Wilhelmy plate technique. The dynamic Wilhelmy test uses a thin solid plate suspended from a balance that is moved through the crude oil/solid interface inside an anaerobic vessel. The measured change in force as the plate passes through the oil/brine interface relates directly to the adhesion tension at that interface. The apparatus is computer controlled and monitored.

Huang and Holm (1988) presented methods of physically and chemically treating Berea cores to alter the rock wettability. To prepare a strongly water-wet core, a dry Berea core was first saturated with 2% brine. The core was flooded with several pore volumes of brine and then flooded with refined oil (mixture of n-decane, n-tetradecane, and a mineral oil). To prepare a preferentially water-wet core, the procedure was the same as the water-wet core except that a crude-oil was used instead of refined oil. To create a mixed-wettability core, the method used was the same as that for preparing a preferentially water-wet core, except that the core was aged for three month with crude oil in place, before the core was subjected to flooding. Finally, to create an oil-wet core, a dry Berea core was saturated with a crude oil or an oil wetting material. The oil wetting material was an asphaltene solution or 10% surfasil (a short-chain polymeric silicone fluid) dissolved in hexane.

The influence of wettability on waterflood performance has been studied extensively

and the published literature supports the conflicting conclusions as to the optimum wetting condition for recovery (Anderson, 1987, Rao et al., 1992). Jadhunandan and Morrow (1991) reported the findings of their studies on the effect of wettability on waterflood recovery for crude-oil/brine/rock systems and one of their conclusions was that waterflood is optimum at close to neutral wettability. This was in agreement with the earlier findings of Morrow (1990).

In a part of his extensive wettability surveys, Andersen (1987) examined the effects of wettability on waterflooding and on the breakthrough and residual oil saturations. He suggested that when a strong water-wet system is waterflooded, recovery at water breakthrough is high, with little additional oil production after breakthrough. Moreover, water breakthrough occurs much earlier in strongly oil-wet systems, with most of the oil recovered during a long period of simultaneous oil and water production.

2.2.1 Wettability Index

The Amott (1959) wettability test, consists of two parts. The first part is spontaneous imbibition in water followed by forced displacement by water. This is denoted as I_w and expressed below:

$$I_w = \frac{(V_o)_{spontaneous}}{(V_o)_{total}} \tag{2.16}$$

The second part is a test for spontaneous imbibition in oil at a residual oil saturation followed by forced displacement by oil. It is expressed as:

$$I_o = \frac{(V_w)_{spontaneous}}{(V_w)_{total}} \tag{2.17}$$

The Amott-Harvey wettability index (WI) is commonly stated as the subtraction of

displacement-by-oil (I_o) ratio from the displacement-by-water ratio (I_w):

$$WI = I_w - I_o \tag{2.18}$$

This is a relative index and varies from +1.0 for complete water wetness to -1.0 for complete oil wetness (Cuiec, 1984).

2.3 Mercury Porosimetry Properties

Mercury porosimetry analysis for the identification of petrophysical properties is a comparatively rapid procedure (Ghosh and Friedman, 1989). Lowell and Shields (1981a) noted that the experimental method of mercury porosimetry for the determination of porous properties of solids is dependent on several variables such as wetting or contact angle between mercury and the surface of the solid. Capillary pressure data from mercury porosimetry are used to determine petrophysical characteristics such as total intrusion volume, pore surface area, average pore diameter, porosity, residual mercury saturation and mercury recovery efficiency. Such petrophysical information is important to all phases of enhanced recovery, which depends on accurate predictions of the behavior of fluids in rock (Kopaska-Merkel and Amthor, 1988).

According to Moscou and Lub (1981), it is often recommended that double or triple distilled mercury has to be used for mercury porosimetry tests, because of the implication that mercury impurities affects its contact angle and surface tension. They further stated that in practice though, no influence of mercury impurities could be found, This was concluded from the experiments they performed with chemically pure mercury and with mercury which had been used many times already for penetration analysis of some oxides. Before re-use, the mercury was purified from solid particles by filtration. Chemical analysis of the original mercury and the used mercury showed that only minor pollution of the mercury occurred.

2.3.1 Capillary Pressure

The size of the pore invaded by the mercury is related to the pressure necessary to overcome capillary forces. This relationship is shown by Washburn (1921) as:

$$P_c = -\frac{4\,\sigma\cos\theta}{d} \tag{2.19}$$

Here, the capillary pressure, P_c, is in dynes/cm^2; the interfacial tension, σ, is in dynes/cm; and the capillary tube diameter, d, is in cm. The equation assumes a cylindrical pore, but pores are rarely cylindrical, hence Eq. 2.19 constitutes a special model. Such a model may not best represent pores in actual materials, but its use is generally accepted as the practical means for treating what otherwise would be a most complex problem.

The capillary pressure, P_c, is the minimum pressure required to displace a wetting liquid ($\theta < 90°$) from, or inject a non-wetting liquid ($\theta > 90°$) into a capillary of diameter, d, when the interfacial tension is σ and the angle of contact which this interface forms with the solid of the capillary is θ (Leverett, 1941; Purcell, 1949; and Fatt, 1956). It is inversely proportional to the diameter and hence may be used as a measure of capillary size (Purcell, 1949; Burdine et al., 1950; Orr, Jr., 1969/70; Moscou and Lub, 1981; Bell et al., 1981; Mukaida, 1981; Etris et al., 1988; and Kopaska-Merkel and Amthor, 1988).

The surface tension of mercury varies with purity; its usually accepted value and the value used in this study is 485 dynes/cm. The contact angle between mercury and the solid containing the pores varies somewhat with solid composition. A value of 130° is used here, in the absence of specific information to the contrary.

If d is measured in micrometers and P_c in psia, then this equation reduces for the purpose of routine analysis to:

$$P_c = \frac{180.863}{d} \tag{2.20}$$

2.3.2 Pore Surface Area and Specific Surface Area

Pore surface area is calculated from the pressure-volume work expended in forcing mercury into the pores. The work, dW, required to immerse an area, dA, of pore wall is expressed by (Lowell and Shields, 1981c):

$$dW = \sigma \cos\theta \, dA = -P \, dV \tag{2.21}$$

The total pore area is then (Lowell and Shields, 1981c; and Van Brakel et al., 1981):

$$SA = -\frac{1}{\sigma \cos\theta} \int_{V_{min}}^{V_{max}} P \, dV \tag{2.22}$$

where V_{max} corresponds to the volume of mercury to first penetrate and fill the maximum sized pores. V_{min} is the volume of mercury which subsequently filled the minimum sized pores. This surface area value reflects the pore space whose walls are wetted by mercury at a specified pressure, and does not represent the total surface area of the pore space which would be measured by the adsorption of gas molecules.

For pressure in psia, volume in cc, pore surface area in m^2/g, $\theta = 130°$, and $\sigma = 485$ dynes/cm, Eq. 2.22 becomes:

$$SA = 0.0221 \int_{V_{min}}^{V_{max}} P \, dV \tag{2.23}$$

Howard (1991) suggested that it is important to distinguish between the available surface area of a pore and its total surface area. He referred to available pore surface area as the portion of the pore space that contributes to the fluid flow paths. It is expected that any measurement of available pore surface area would be less than the total surface area.

Some authors (Chilingarian and Yen, 1987; Chilingarian et al., 1990; Borner and

Schon, 1991; and Raffensperger and Ferrell, Jr., 1991) introduced the term specific surface area in their studies. It is defined as:

$$S_s = \frac{SA}{V_{int.}} \tag{2.24}$$

In Eq. 2.24, the units of specific surface area, S_s, are in terms of m^2/cm^3. In order to convert it to the units of cm^2/cm^3, as used in this study, it is redefined as:

$$S_s = \frac{10^4\ SA}{V_{int.}} \tag{2.25}$$

2.3.3 Average Pore Diameter

The pore entry diameter represents the equivalent circle diameters calculated from capillary pressure measurements (Dullien and Dhawan, 1975). The average pore diameter is therefore the equivalent diameter of all the effective pores and throats. The average pore diameter in micrometers is estimated from the following equation (Lowell and Shields, 1981c):

$$\overline{D} = \frac{4\ V_{int.}}{SA} \tag{2.26}$$

A pore-throat is defined as the constriction of minimum cross-sectional area of a conduit which connects one pore to another (Dullien, 1979). Etris et al. (1988) noted that one of the factors controlling capillary pressure is pore-throat radius. Small pore-throats require high pressure in the non-wetting phase for it to displace the wetting phase, while larger pore-throats require lower pressures. He further stated that pore-throats are the features that limit the amount of mercury saturations. At any given pressure, mercury will invade all pores that are mutually connected by throats larger than a given value. Increased

pressure permits the filling of pores connected by smaller throats and so on.

According to Orr, Jr. (1969/70), if pores were all either straight-walled or V-shaped cracks, all the mercury forced into them under pressure would recede as the pressure was diminished. Given the fact that this behavior is not often observed indicates that most materials contain at least some so called "ink-well" pores. Ink-well pores are pores with narrow throats opening into large cavities. The extent of this type of pore structure is indicated by the hysteresis revealed by increasing pressure and decreasing pressure determinations.

2.3.4 Permeability from Capillary Pressure Data

As reported in Amyx et al. (1960), Purcell (1949) and Burdine (1950) have both provided equations for computing permeability from capillary pressure data which were obtained by the mercury-penetration method. Purcell utilized the concept of pore-size distribution without evaluating the distributions. Burdine provided pore-size distribution as well as the results of the computation of permeability.

The equation presented by Purcell for the calculation of permeability in millidarcies, from the pore properties of a rock is given as:

$$k = 10.24 (\sigma \cos \theta)^2 \phi \lambda \int_{S_{Hg}=0}^{S_{Hg}=1} \frac{d S_{Hg}}{(P_c)^2} \qquad (2.27)$$

In Eq. 2.27, the lithology factor, λ, is assumed to be constant for the porous medium.

The permeability (in millidarcies) equation developed by Burdine (1950) is based on an analogy to a bundle of capillary tubes and it is given as:

$$k = 1.266 \times 10^7 \phi \sum_{i=1}^{i=n} \frac{\Delta S_{HG} \bar{r}_i^2}{\chi_i^2} \qquad (2.28)$$

In Eq. 2.28, the subscript, i, represents a particular capillary tube in the bundle. χ_i^2 is the factor to account for more complex geometry of the system and it is termed dividing factor. Empirically determined values of the dividing factor as a function of permeability are presented by Burdine.

Bear (1972) provided an excellent review of the different models that have been used to represent flow through porous media. The models cited by Bear are essentially classified into four different categories: capillary tube models; fissure models; hydraulic radius models; and resistance to flow models. The well known Kozeny-Carman model (Amyx et al., 1960; Bear, 1972; and Raffensperger and Ferrell, Jr., 1991), which is based on a theoretical analysis of fluid flow through a bundle of capillary tubes, is one example of the hydraulic radius models. The Kozeny-Carman equation may be given as:

$$k = \frac{C_o \phi^3}{\tau^2 S_s^2 (1 - \phi)^2} \tag{2.29}$$

In Eq. 2.29, C_o is a shape factor, porosity, ϕ, is a fraction, specific surface area, S_s, is expressed in terms of cm^2/cm^3, and permeability, k, is expressed in terms of cm^2. The common unit for permeability is in terms of darcy; 1 darcy = 9.869×10^{-9} cm^2, and 1 millidarcy = 9.869×10^{-12} cm^2.

2.3.5 Mercury Porosity

Porosity is calculated from the grain volume and bulk volume of the sample as (Amyx et al., 1960; and Dake, 1978):

$$\phi = \frac{V_B - V_S}{V_B} \tag{2.30}$$

Mercury porosimetry measured porosity can also be estimated from the relationship given

below:

$$\phi_{Hg} = V_{int.}\,\rho_B \tag{2.31}$$

The definition given in Eq. 2.30 is for the absolute porosity and the one presented in Eq. 2.31 is for the effective porosity. It is expected that the porosity measured by the mercury porosimetry would be less than the porosity measured by the routine methods because of the limited intrusion pressure employed.

2.3.6 Mercury Recovery Efficiency

Recovery efficiency in mercury porosimetry is the fraction of the mercury intruded at maximum pressure which is extruded during pressure reduction to final minimum pressure (usually 14-15 psia, or atmospheric pressure) (Wardlaw, 1976; Wardlaw and McKellar, 1981; Melas and Friedman, 1992). From the capillary pressure curve data, it is calculated using the equation given below:

$$RE = \frac{\text{Cum. Volume at } P_{max} - \text{Cum. Volume at } P_{min}}{\text{Cum. Volume at } P_{max}} \tag{2.32}$$

and residual mercury saturation is:

$$S_r = 1 - RE \tag{2.33}$$

also, the mercury saturation at any pressure point can be estimated from the relationship below:

$$S_{Hg} = \frac{\text{Cum. Volume at } P_i}{\text{Cum. Volume at } P_{max}} \tag{2.34}$$

According to Li and Wardlaw (1986), the effects of pore-throat size, shape,

connectivity, and arrangement (topology), in combination with the prevailing contact angle for fluid interfaces, determine the mechanism of disconnection and the amount of location of trapped fluid. They further noted that interface movements during imbibition are influenced by the sizes, shapes and arrangement of both pores and throats with respect to the direction of advancing displacement phase. Chatzis et al. (1983) observed a strong relationship between trapping and aspect ratio, which is the ratio of the pore-body to pore-throat size. As aspect ratio increases, the trapping mechanism goes through a transition from bypassing to snap-off. At high aspect ratio, which is typical of Berea sandstones, the recovery of oil is low and comes mostly from volume contributed by the pore throats.

2.3.7 Density

In many areas of petrophysical analyses the need to measure the rock volume or density often arises. For example, rock-bed porosities in permeametry, volume specific surface area, sample cell void volumes, as well as numerous other calculated values, all require accurately measured rock densities or specific volumes. The volume occupied by the solid plus the volume of voids when divided into the rock mass yields the bulk density. The equation needed for the calculation of bulk density of a sample is:

$$\rho_B = \frac{\text{Wt. of Sample}}{V_B} \tag{2.35}$$

When densities are determined by liquid displacement an apparent (skeletal) density is obtained which can differ according to the liquid used, because of their different capabilities of penetrating small pores (Lowell and Shields, 1981a).

2.3.8 Capillary Pressure Curve Mode

Mode refers to the various forms of the capillary-pressure curves for each of the samples. Unimodal form is "1", bimodal form is "2", trimodal form is "3", quadramodal form is "4", and so on. Bimodal, trimodal, quadramodal and higher modes are sometime referred to as "polymodal". The unimodal forms can exhibit "steep-convex", "steep-concave", or "gentle sloping" shapes (Amthor et al., 1988). The form of capillary-pressure curves is controlled by a variety of factors, including the volume distribution of throats, microscopic spatial heterogeneity of the pore system, connectivity, randomness of the spatial distribution of throat sizes and intrusion rate (Wardlaw and Taylor, 1976).

Water-air capillary-pressures are about 1/5th of equivalent mercury-air capillary-pressure (Purcell, 1949), whereas average conversion factors from gas-water and oil-water systems to the mercury-air systems are 1/5th and 1/10th, respectively (Smith, 1966). These numbers are highly sensitive to fluid densities, contact angles, and interfacial angles, and are therefore rough approximations (Kopaska-Merkel and Amthor, 1988).

2.4 Thin-Section Analysis

Besides surface area and wettability, porosity origin permit a better assessment of oil recovery. Porosity origin could be determined by the use of thin-section analysis. Thin-section analysis is used to investigate the influence of small scale geological heterogeneities on porosity and ultimately on fluid flow and non-wetting phase trapping. Hove et al. (1985) investigated the presence of small scale heterogeneities that may influence fluid movements, trapping, movement of flood fronts, dispersion, viscous fingering, and other flow conditions in cores.

Wellington and Vinegar (1987) measured porosity and fluid saturation during multiphase flow and studied oil displacement mechanisms in homogeneous cores. Tomutsa

et al. (1990) investigated the application of integrated pore-to-core image analysis for the study of fluid distribution in reservoir rocks. They concluded that thin-section analysis along with CT scanning provides supplemental information about the effect of heterogeneities on microscopic fluid distribution and movement.

The consistency with which pore structure controls residual non-wetting phase saturation was demonstrated by Kimbler and Caudle (1957). In a series of experiments utilizing a photographic technique, they observed non-wetting phase distribution after water drive. Results indicated that residual fluid distribution was not a random chance phenomenon but rather was strictly controlled by the geometry of the pore continuum. These authors indicated that changing the conditions of the experiment by altering the flow rate or interfacial tension, or by substituting oil for gas as the non-wetting phase, resulted in only very slight change in the configuration of the residual oil distribution.

One of the objectives of this study was to determine the geometrical and topological characteristics of individual fluid phases at the microscale. As indicated by Dullien et al. (1974), oil during the secondary oil recovery process is left behind as isolated blobs called ganglia. This occurs at floodout and was attributed to the heterogeneity of the porous matrix and the attendant non-wetting phase snap-off at the entry pores. Based on the theory of capillary trapping and experimental observations, Jasti et al. (1990) suggested that these ganglia may occupy a part of a single pore or may extend to several pores.

Ruzyla (1986) used thin sectional image analysis to quantify the microstructure of porous media. To examine two-dimensional polished thin sections and to generate digitized maps of the porous matrix, the optical microscope or scanning microscope was used. Simon et al. (1977) indicated that thin-section analysis is a powerful tool in identifying rock types.

They noted that the degree of fluid sensitivity is related to rock type, permeability and especially porosity. Furthermore, Pathak et al. (1982) showed that residual oil saturation was strongly dependent on the specific genus of the porous media.

2.5 Summary

The literature has been reviewed to understand the rock/fluid properties investigated in this study. To assist with the optimal design of the laboratory experiments, the scaling factor as initially proposed by Rapoport and Leas (1953) and the concept of capillary number were introduced into the review.

The part of this study that deals with the linear-core experimental investigations attempted to eliminate the problems associated with outlet end-effects, by having well designed laboratory experiments. Furthermore, rock/fluid properties will be related to both residual oil saturation and oil recovery. The relationships are to be developed at both breakthrough and floodout.

To assist those who are interested in future work in this or similar areas, a detailed multi-disciplinary list of related literature is provided in the bibliography.

Chapter 3

PROBLEM STATEMENT

The overall objectives of this study are:

- To develop a better understanding of some important but not really well investigated rock/pore properties such as: wettability, tortuosity, pore size distribution, pore surface area, specific surface area, pore diameter, pore length, apparent (skeletal) density, mercury porosity, mercury recovery efficiency, and develop a better insight on capillary pressure variation with respect to wettability and pore geometry of Berea sandstones and Indiana limestones.
- To improve the understanding of fluid flow in porous media under conditions of secondary and tertiary recovery through the laboratory study of the performance of secondary recovery methods such as waterflooding, using radial and linear-cores.
- To develop empirical relationships between residual oil saturation and oil recovery at breakthrough and the uncommon rock/pore properties for various types of porous media. Develop correlations between residual oil saturation and ultimate oil recovery at floodout and the uncommon rock/pore properties for various types of porous media. Furthermore, variations of irreducible water saturation, porosity and absolute permeability with respect to the rock/pore properties, residual oil saturation and oil recovery will be investigated.

Chapter 4

EXPERIMENTAL PROCEDURE

Figures 4.1 and 4.2 show schematics of the radial-core and linear-core experimental procedures. As illustrated on Fig. 4.1 for the radial-cores, 8 core plugs were cut from each waterflooded core. The core plugs made an angle of 45° with each other. They were spaced in such a way as to ensure coverage of all lithologies and better rock characterization. Each of the 8 plugs was cut into 3 sub-plugs giving a total of 24 core plugs for each waterflooded radial-core. The dimensions of the plugs are approximately 1.27 cm in diameter and 1.69 cm long, and weighed approximately 2.50 g. As indicated in the Fig. 4.2 for the linear-cores, flow of the injected oil or brine was parallel to the bedding planes. Core plugs were extracted from each of the waterflooded linear-cores. The core plugs were cleaned and retained for utilization in the wettability and mercury porosimetry tests.

4.1 Waterflood Experiments

Waterflooding experiments were conducted using unfired Berea sandstone and Indiana limestone cores. The experimental apparatus used for this investigation was a fully automatic core-flooding station developed by Core Test Systems, Mountain View, California. A schematic of the flow system is shown in Fig. 4.3. For this figure, the description of the identification numbers is provided in Table 4.1. This system permitted the simulation of both reservoir temperature and overburden pressure. Three fluid separators are provided to hold the oil. Figure 4.4 shows a cut-away of one of the flow system separators. The experimental oil was filled into the bladder with end-plugs fixed on both ends. The annulus of the fluid separator was filled with hydraulic fluid to apply pressure on the bladder and in turn to regulate the flow rate with the aid of the oil pump. Figure 4.5 shows

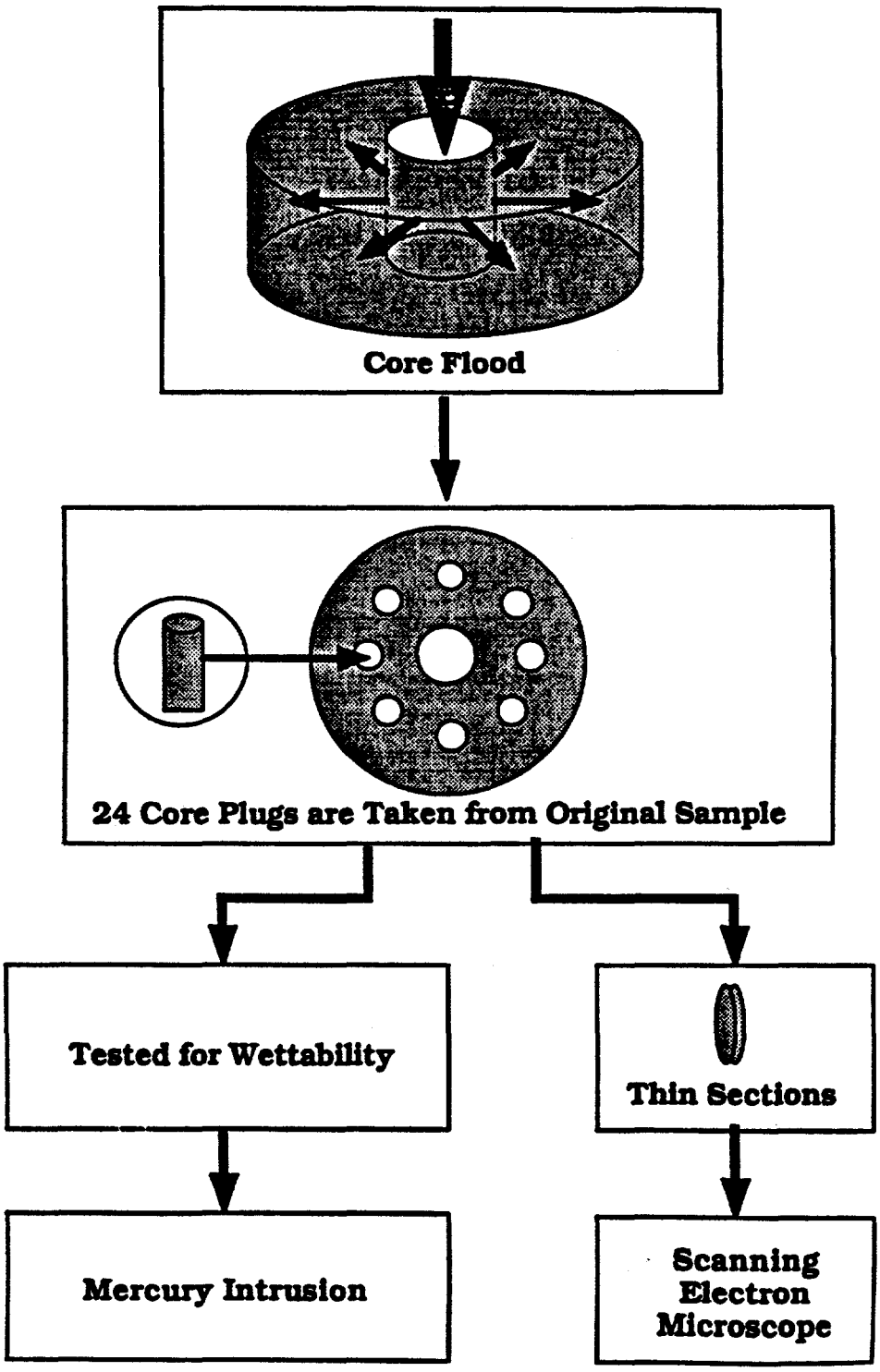

Fig. 4.1: Schematic of the Radial-Core Experimental Procedure.

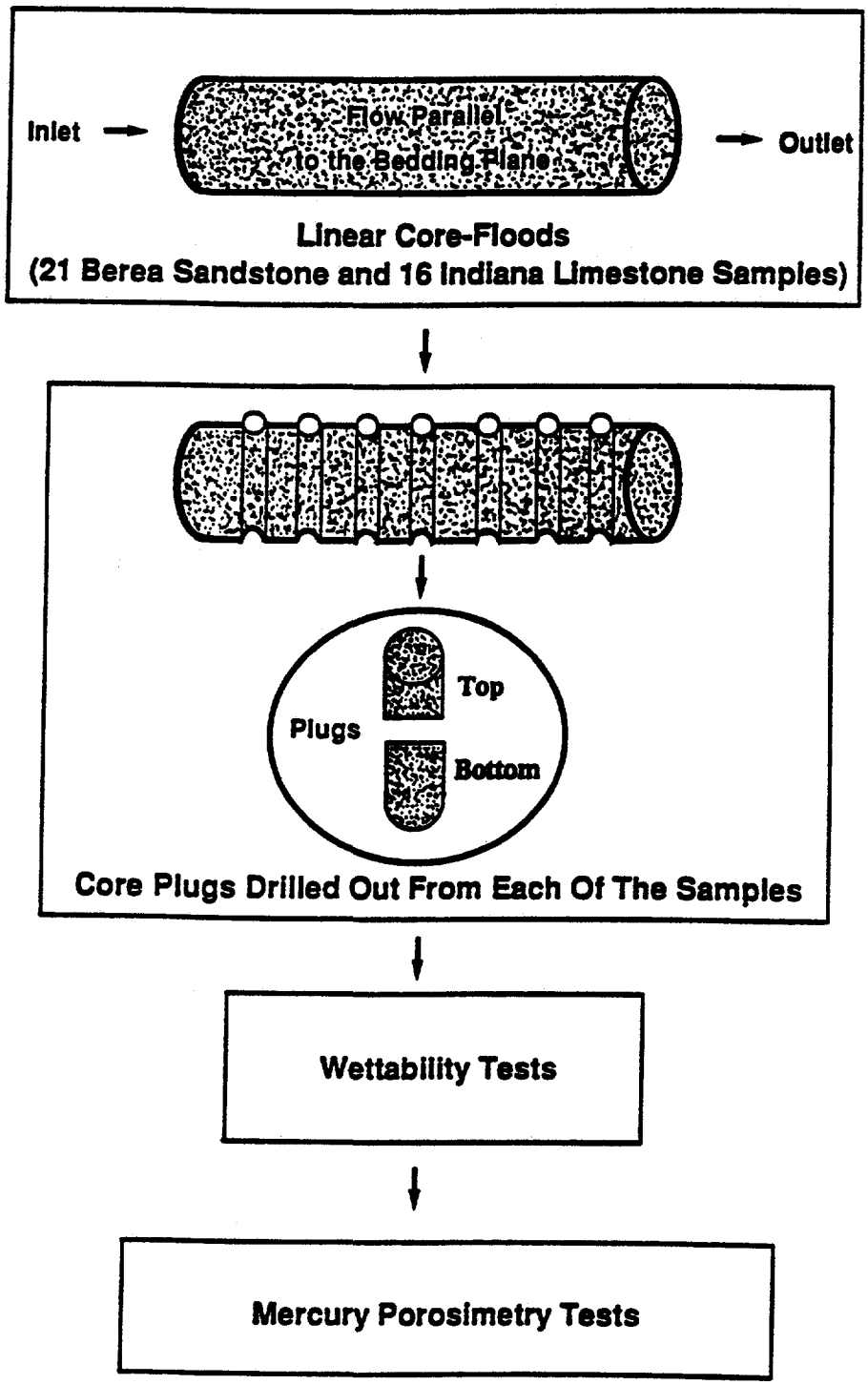

Fig. 4.2: Schematic of the Linear-Core Experimental Procedure.

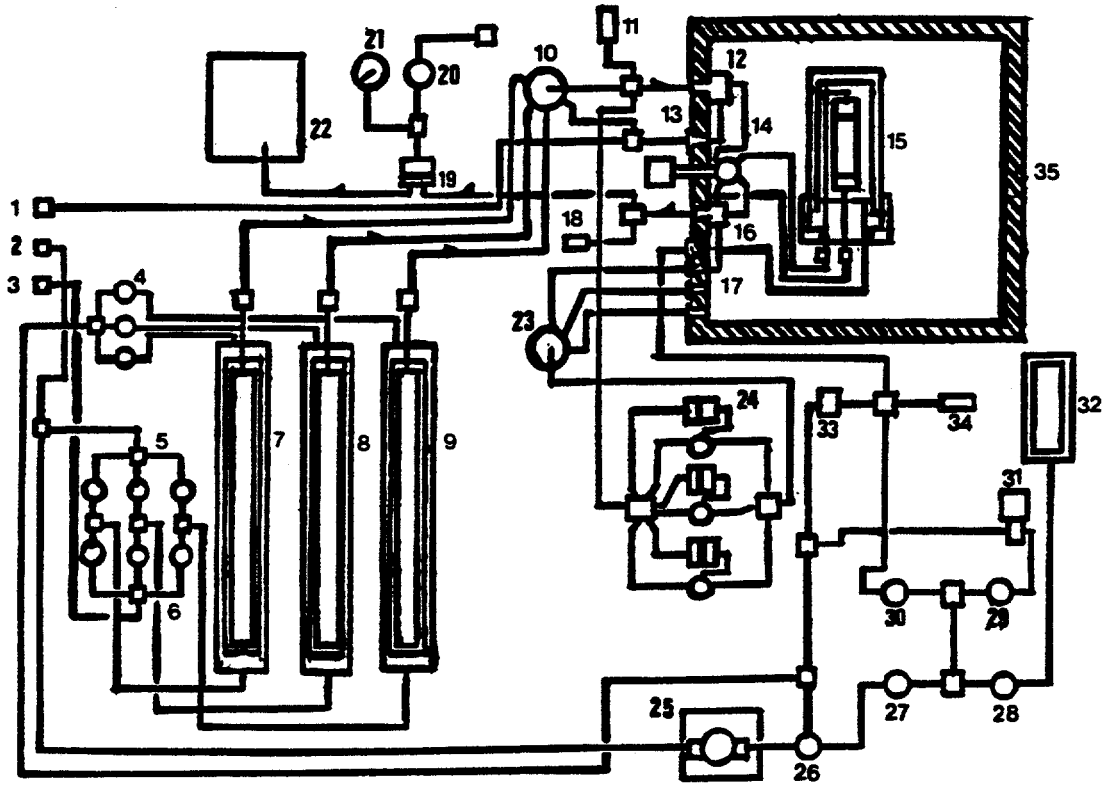

Fig. 4.3: Schematic of Flow System (After Coretest Systems, Inc., 1988).

Table 4.1: Index for Fig. 4.3

ITEM	DESCRIPTION
1	Brine Pump Outlet
2	Oil Pump Inlet
3	Oil Pump Outlet
4	Separator Air Bleed Valves
5	Separator Pressure Valves
6	Separator Bleed Valves
7	Fluid Separator #1
8	Fluid Separator #2
9	Fluid Separator #3
10	Fluid Select Valve
11	Inlet Pressure Transducer
12	Inlet Bulk-Head Connector
13	Brine Pump Inlet
14	Fluid Direction Valve
15	Core Holder Pressure Vessel
16	Outlet Bulk-Head Connector
17	Differential Pressure Ports
18	Outlet Pressure Transducer
19	Back Pressure Regulator
20	Gas Pressure Control Valve
21	Pressure Gauge
22	Fractional Collector
23	ΔP Port Select Valve
24	ΔP Transducers and Isolate Valves
25	Overburden Fluid Pump
26	Prime/Purge Valve
27	Pump Isolate Valve
28	Accumulator Isolate Valve
29	Bleed Rate Valve
30	Vessel/Core Holder Isolate
31	Air Operated Bleed Valve
32	Accumulator
33	Pressure Relief Valve
34	Overburden Pressure Transducer
35	Core Holder Oven

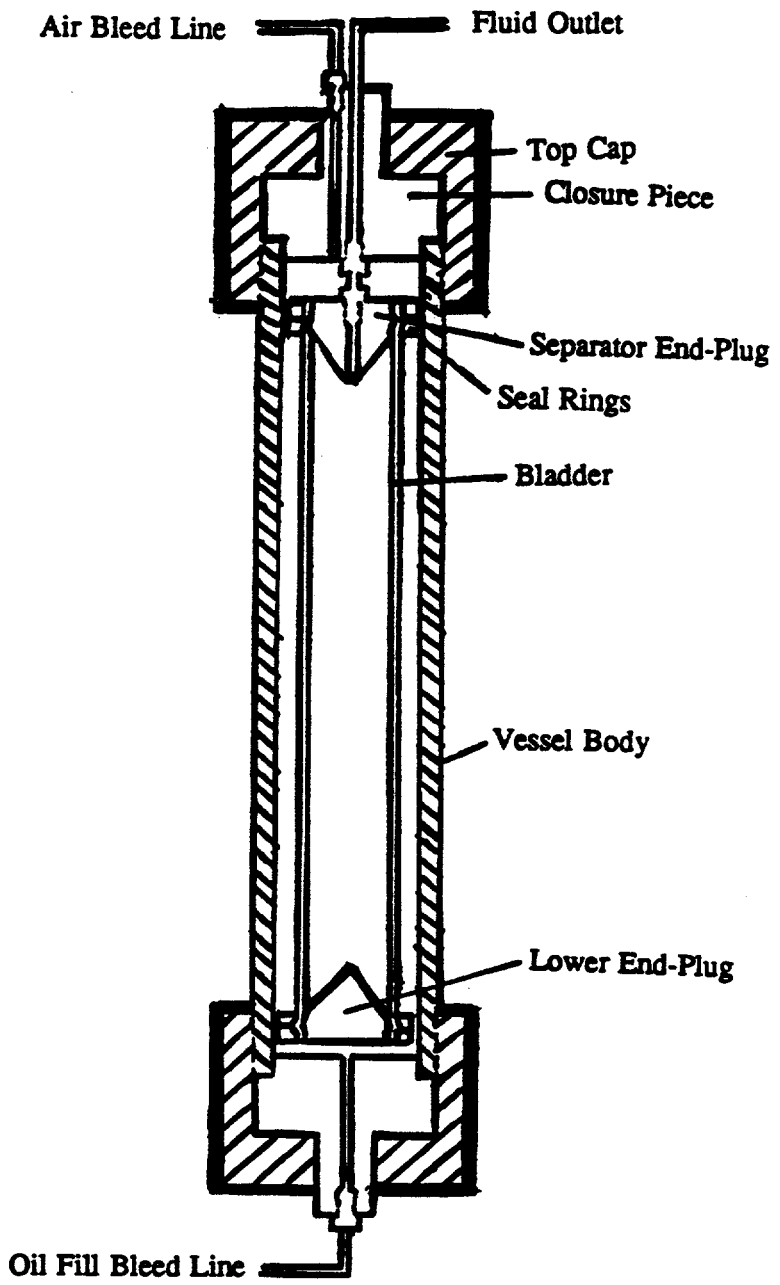

Fig. 4.4: Flow System Separator Cutaway (After Coretest Systems, Inc., 1988).

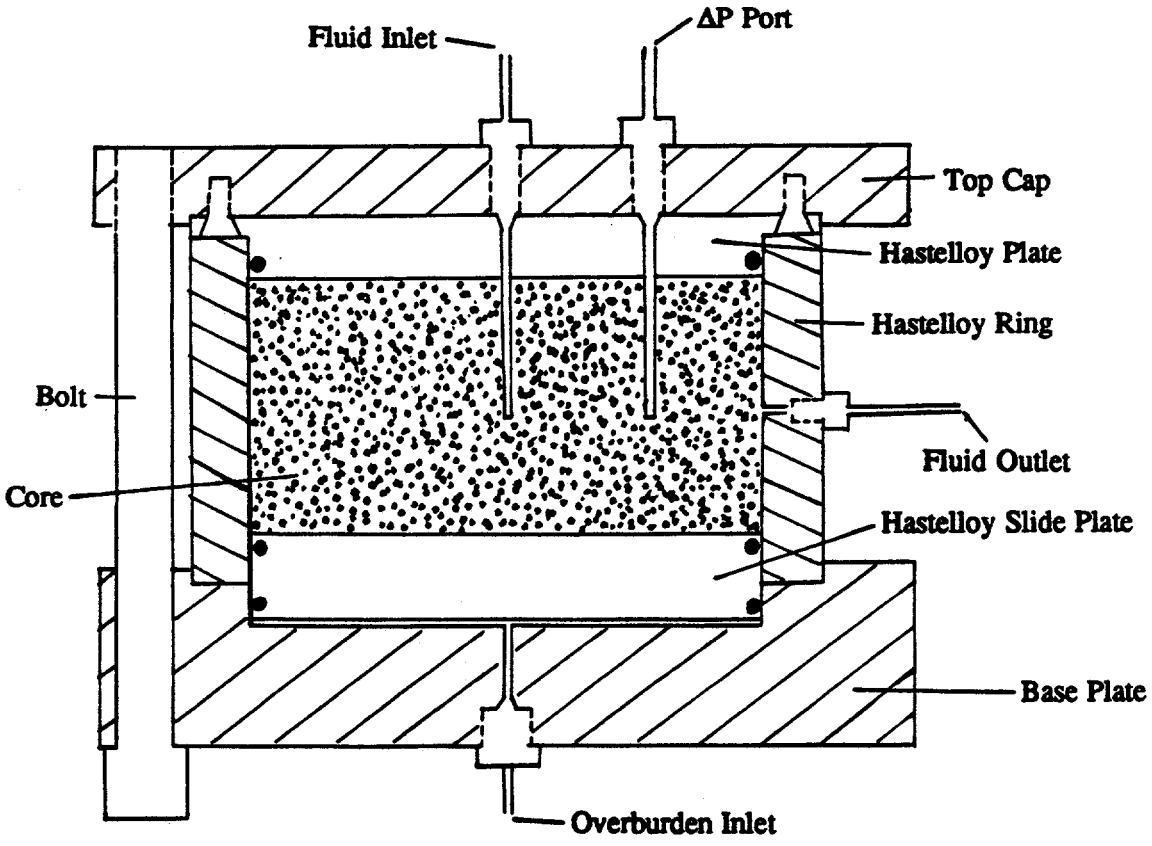

Fig. 4.5: Radial-Core holder (After Coretest Systems, Inc., 1988).

a schematic of the radial flow core holder. The radial-core holder is manufactured from 304 stainless steel and Hastelloy C-276 (Micromeritics, 1987). The disk holder is rated for operation at pressures to 2500 psi and at a temperature of 300°F. The base plate has a bore into which the Hastelloy pressure plate rests. When pressure is introduced on the plate, the rock is subjected to an overburden pressure. The base plate is a two part construction with a Hastelloy seal plate and a 304 stainless steel base plate. Eight large socket head bolts are used to hold the whole assembly together. Seven pressure taps are located on the top of the vessel and two on the sides. Pressure lines for connecting to the inlet and outlet pore fluid ports, differential pressure ports, overburden pressure ports, and thermocouple are provided in the set-up of the radial-core holder. Several plugs are also provided for closing off un-used holes. To apply overburden pressure on the linear-core, the annulus of the linear-core holder, an example of which is shown in Fig. 4.6 was filled with light hydraulic fluid. The linear-core was also loaded into a bladder. Both ends of the linear-core were fixed with end-plugs. The long linear-core holder which was utilized in the linear flow studies can be used to perform experiments on core samples 1 in. and 1.5 in. in diameter and up to 36 in. long. The pressure vessel is designed to operate at pressure to 5000 psi and at temperatures of up to 300°F. Several long thermocouples are also provided in the set-up of the long linear-core holder.

For the radial core-floods, the cores used were 12.7 cm in diameter and 5.08 cm long. Prior to mounting in a cylindrical core holder, an injection well located at the center was drilled through the core. A 0.159 cm clearance between the core and the core holder around the circumference was maintained. This clearance was necessary to permit the development of radial flow behavior. To model a field situation where water advance is moderate, displacement studies were conducted at injection rates equivalent to a field drainage rate of 1 foot/day for the waterflooding experiments. This was equivalent to an injection rate of

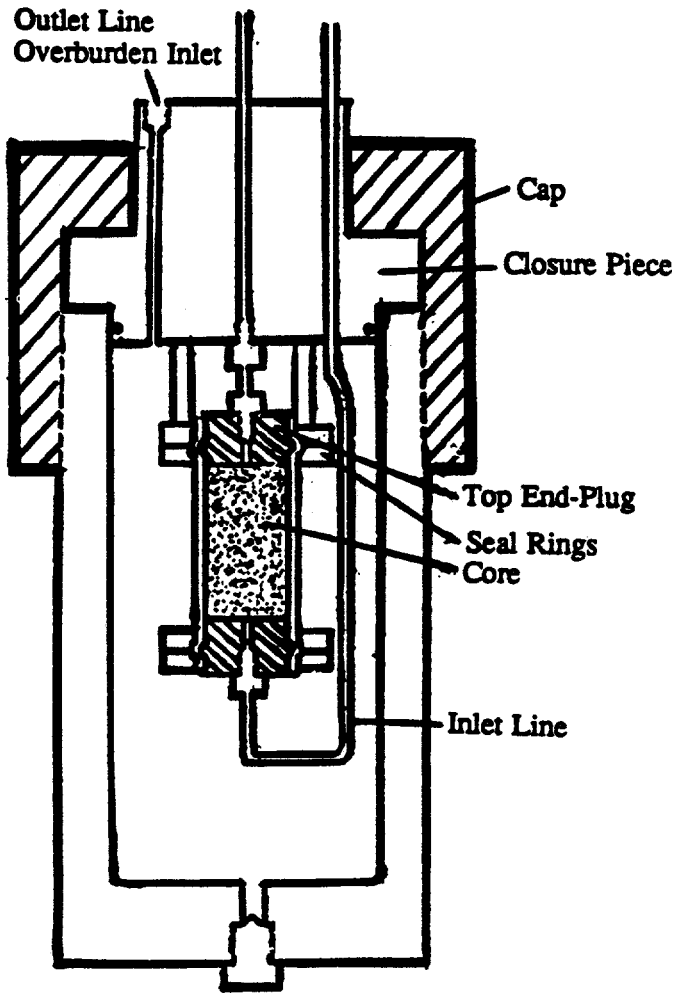

Fig. 4.6: Standard Linear-Core holder (After Coretest Systems, Inc., 1988).

0.61 cc/min or 36.6 cc/hr.

For the case of the linear-core floods, 21 Berea sandstone and 16 Indiana limestone core-floods were performed. The Berea sandstone and Indiana limestone cores were ordered with the specification that they should be of varying permeability values, from Cleveland Quarries Company, Amherst, Ohio. The Berea sandstone cores used in these experiments ranged from 7.34 cm to 52.07 cm in length and from 3.79 cm to 3.88 cm in diameter. The Indiana Limestone cores used ranged from 40.00 cm to 45.72 cm in length and from 3.76 cm to 3.89 cm in diameter.

The experimental procedure required that the core be evacuated to a pressure of 50-100 microns of mercury. After this requirement was satisfied, the core was then saturated with brine. The pore volume was determined by measuring the amount of brine used to completely saturate the core. After the core was saturated with brine, the absolute permeability was determined. The core was then subjected to the drainage and imbibition processes of flooding to determine properties such as irreducible water saturation, residual oil saturation at breakthrough, cumulative oil recovery at breakthrough, residual oil saturation at floodout, cumulative oil recovery at floodout (ultimate oil recovery), and the rock tortuosity expressed as the wetting-phase retention time.

According to Chang et al. (1988), residual oil saturation is the oil saturation remaining in the reservoir after extraction by conventional recovery methods, such as waterflooding. Rathmell et al. (1973) made mention of residual oil saturation at breakthrough and at floodout in their study. In the context used in this study, residual oil saturation at breakthrough is the oil saturation remaining in the flooded core at breakthrough and the residual oil saturation at floodout is the oil remaining in the flooded core after extraction by waterflooding. Residual oil saturation is used not only to judge the waterflood performance, but also to evaluate the potential for a tertiary recovery project. It is also used to calculate

the sweep efficiency, which in turn leads to an estimation of the remaining reserves.

The brine used consisted of 1.5% by weight sodium chloride, 0.3% by weight formalin (37% by volume formaldehyde), and 98.2% by weight distilled water. The formalin was used to preserve the brine and prevent bacterial growth. The non-wetting phase was a binary system containing 70% by volume Blandol and 30% by volume of Soltrol 160. This combination was selected to yield a viscosity of 10.0 cp at 35°C. A viscosity of 10.0 cp was selected to simulate the viscosity of common reservoir oil. Before mixing and prior to each experimental run, the wetting and the non-wetting phases were filtered through a 0.45 μm Metricel filter. The physical properties of the fluids are shown in Table 4.2. For the linear core-floods, the physical and petrophysical properties of the cores are as shown in Tables 4.3 and 4.4 for Berea sandstone and Indiana limestone cores, respectively.

The densities of the brine and oil are determined using Mettler KEM DA-300 Density Meter[a] which gives a direct digital readout of density. The viscosities of the fluids are measured using Cannon-Fenske Routine Viscometers[b]. The time required to flow a fixed volume of liquid under gravity through a calibrated glass capillary tube is measured. The kinematic viscosity is given by multiplication of the time by a calibration constant. Multiplication of the kinematic viscosity by the fluid density gives the dynamic viscosity, μ. The interfacial tension between the brine and oil is measured using the du Nouy type Surface Tensiometer[c] which uses the principle of pulling a platinum-iridium ring through the interface of two immiscible liquids and recording the force at which the distended interface breaks. The scaling coefficient, $Lu_w\mu_w$, was maintained at approximately 5.0 cm^2 . cp/min, in order to prevent end-effects.

[a]Kyoto Electronic Manufacturing Company, Japan
[b]Cannon Instrument Company, State College, Pennsylvania
[c]Fisher Scientific Company, Pittsburgh, Pennsylvania

Table 4.2: Physical Properties of the Oil and Brine

Oil Density @ 35°C (gm/cc)	0.83
Brine Density @ 35°C (gm/cc)	1.01
Oil Viscosity @ 35°C (cp)	10.00
Brine Viscosity @ 35°C (cp)	1.00
Interfacial Tension (dynes/cm)	26.33

Table 4.3: Physical and Petrophysical Properties of the Berea Sandstone Linear-Cores

Core No.	Length (cm)	Dia. (cm)	Inj. Rate (cc/min)	Scaling Coeff., $Lu_w\mu_w$ (cm^2.cp/min)	Core Pore Vol. (cc)	Brine Porosity (frac)	Absolute Perm. (md)	Pore Vol. Inj. (cc)	H.C. Pore Vol. (cc)	Cap. Number, N^*_{ca} (E-07)
1A	50.07	3.82	1.20	5.24	135.46	0.227	269.78	3.02	43.12	6.63
1B	7.34	3.81	7.80	5.03	17.17	0.206	251.37	5.56	4.95	43.41
2A	50.80	3.79	1.20	5.41	124.81	0.218	276.02	2.53	51.19	6.74
2B	39.37	3.81	1.50	5.18	100.49	0.224	211.34	2.87	41.15	8.33
3A	45.09	3.82	1.30	5.11	64.33	0.124	75.75	4.40	29.75	7.17
3B	44.45	3.85	1.40	5.35	70.70	0.137	78.03	3.01	33.10	7.62
4A	43.34	3.82	1.40	5.29	82.86	0.167	81.85	4.50	35.55	7.72
4B	44.57	3.82	1.30	5.04	90.70	0.177	85.03	2.53	41.00	7.16
5A	45.24	3.86	1.30	5.01	75.14	0.142	80.91	5.14	31.10	7.01
5B	45.40	3.88	1.30	4.99	80.91	0.151	82.68	4.69	35.85	6.96
6A	45.56	3.81	1.30	5.20	103.14	0.199	195.89	6.06	46.10	7.23
6B	44.77	3.81	1.30	5.10	120.31	0.235	291.27	3.03	44.00	7.20
7A	30.32	3.84	2.00	5.24	64.93	0.185	119.18	3.14	44.71	10.93
7B	29.53	3.84	2.00	5.11	77.51	0.227	241.31	2.13	48.41	10.96
7C	28.58	3.84	2.10	5.17	61.66	0.186	120.63	4.52	49.09	11.45
8A	18.73	3.82	3.10	5.07	41.50	0.194	272.11	5.04	36.30	17.15
8B	13.41	3.82	4.30	5.03	31.28	0.203	203.71	7.45	26.85	23.75
8C	9.22	3.84	6.30	5.03	23.87	0.224	276.43	6.97	21.33	34.50
8D	9.28	3.83	6.30	5.08	22.17	0.207	179.61	5.44	20.00	34.63
8E	7.34	3.83	7.90	5.04	17.85	0.211	249.74	3.86	4.89	43.50
8F	8.04	3.83	7.20	5.03	20.83	0.225	321.22	3.02	5.40	39.63

Table 4.4: Physical and Petrophysical Properties of the Indiana Limestone Linear-Cores

Core No.	Length (cm)	Dia. (cm)	Inj. Rate (cc/min)	Scaling Coeff., $Lu_w\mu_w$ (cm^2.cp/min)	Core Pore Vol. (cc)	Brine Porosity (frac)	Absolute Perm. (md)	Pore Vol. Inj. (cc)	H.C. Pore Vol. (cc)	Cap. Number, N^*_{ca} (E-07)
9A	45.64	3.78	1.23	5.00	82.75	0.162	19.83	2.18	49.5	6.94
9B	45.16	3.76	1.23	5.00	80.37	0.160	18.10	1.36	43.9	7.01
10A	45.32	3.77	1.24	5.04	78.28	0.155	14.99	1.62	48.5	7.02
10B	45.08	3.77	1.25	5.03	78.54	0.156	14.51	2.25	37.7	7.07
11A	45.24	3.87	1.31	5.03	84.46	0.158	9.70	1.57	48.9	7.04
11B	45.24	3.89	1.32	5.03	83.08	0.155	8.47	1.71	46.5	7.04
12A	45.48	3.83	1.27	5.00	77.81	0.148	10.51	2.41	40.3	6.96
12B	45.24	3.83	1.28	5.03	75.82	0.145	14.23	2.42	41.6	7.03
13A	45.24	3.81	1.27	5.03	77.51	0.150	16.31	1.84	35.3	7.03
13B	45.32	3.81	1.27	5.03	77.78	0.150	11.09	2.44	47.4	7.03
14A	45.40	3.84	1.28	5.01	74.39	0.141	10.09	2.48	44.6	6.99
14B	45.08	3.83	1.28	5.01	74.10	0.143	11.20	2.49	42.1	7.04
15A	45.72	3.79	1.24	5.02	75.74	0.147	12.30	2.40	41.7	6.95
15B	44.93	3.80	1.25	4.96	77.60	0.152	10.92	2.49	48.8	6.99
16A	45.56	3.86	1.29	5.02	80.57	0.151	10.48	2.13	41.9	6.97
16B	40.00	3.88	1.48	5.00	69.96	0.148	9.12	3.42	39.4	7.91

After the completion of the waterflood experiments and in readiness for the wettability and mercury porosimetry experiments, core plugs were extracted from the waterflooded cores. For the linear cores, depending on the length of the waterflooded cores, 6 to 54 core plugs were taken from each of the 21 Berea sandstone linear cores, for a total of 580 Berea sandstone core plugs. In the case of the 16 Indiana limestone linear cores, 32 core plugs were extracted from each of them, for a total of 512 Indiana limestone core plugs. The core plugs were drilled perpendicular to the bedding planes on each of the sandstone and limestone linear cores, using a diamond core bit with water as the coolant and lubricant. Each core plug was identified by a sample number, using blue color wax-base pencil. On the average, the extracted core plugs were 1.3 cm in diameter and 1.7 cm long. The core plugs were cleaned prior to performing the wettability and mercury porosimetry tests by using the method presented in the next section.

4.2 Samples Cleaning

The core plugs were cleaned by soaking for 48 hours in solution containing 50% by volume acetone and 50% by volume isopropyl alcohol (IPA). This was followed by an additional soaking for 24 hours in acetone solution only. Finally, the core plugs were dried in a vacuum oven for 24 hours at a temperature of 60°C. This technique was developed by Texaco Research Laboratory (Kopaska-Merkel and Amthor, 1988). Results derived from samples cleaned in this way are as reliable as other more rigorous methods of cleaning core plugs which are presented in the paper by Ghosh and Friedman (1989).

4.3 Wettability Experiments

Wettability is a major factor controlling the location, flow and distribution of fluids in a reservoir. The term is generally used to describe the ability of a fluid to wet a solid

surface in the presence of the second fluid. Wettability changes have been shown to affect waterflood behavior, irreducible water saturation and residual oil saturation (Raza et al., 1968).

According to Morrow (1990), reservoir wettability is determined by complex interface boundary conditions acting within the pore space of sedimentary rocks. These conditions have a dominant effect on interface movement and associated oil displacement.

The Amott-Harvey (Trantham and Clampitt, 1977; and Boneau and Clampitt, 1977) method was used to measure the average wettability of the core plugs which were extracted from the waterflooded cores. This method, which is similar to the Amott (1959) wettability measurement technique, is based on the fact that the wetting fluid will generally imbibe spontaneously into the core, thereby displacing the non-wetting phase. The method compares the tendency of a permeable plug at irreducible oil to imbibe oil with the tendency of the same plug at irreducible water to imbibe water (Trantham and Clampitt, 1977). In determining the wettability index, the ratio of spontaneous imbibition to forced imbibition is utilized to reduce the influence of other factors, such as relative permeability, viscosity, and the initial saturation of the rock because only the surface forces are changed (Anderson, 1986). A description of the experimental procedure (Boneau and Clampitt, 1977; Cuiec et al., 1979; Cuiec, 1984; Anderson, 1986), is summarized as follows:

1. Centrifuge core plug under brine.
2. Centrifuge under reservoir crude.

   Carefully weigh the core plug at the end of step 2.
3. Submerge in brine for 20 hours and find "A".

   The value of "A" is equal to the weight of the core plug at the end of step 3 less the weight of the core plug at the end step 2.

4. Centrifuge under brine and find "B".

   The value of "B" is equal to the weight of the core plug at the end of step 4 less the weight of the core plug at the end step 3.

5. Submerge in reservoir crude oil for 20 hours and find "C".

   The value of "C" is equal to the weight of the core plug at the end of step 5 less the weight of the core plug at the end step 4.

6. Centrifuge under crude oil and find "D".

   The value of "D" is equal to the weight of the core plug at the end of step 6 less the weight of the core plug at the end step 5.

7. Determine relative displacement (wettability) index as:

$$WI = \left[\frac{A}{A+B}\right] - \left[\frac{C}{C+D}\right] \qquad (4.1)$$

   The samples are centrifuged for 1 hour with the speed control knob of the centrifuge set at between one-half to full speed or at about 1500 RPM.

The centrifuge used for the forced imbibitions was supplied by International Equipment Company (A division of Damon), Needham Heights, Massachusetts.

Wettability is well established in the literature as a dominant variable in controlling the performance of displacement of oil by water in the porous media and it is often described with the terms "water-wet", "intermediate", or "oil-wet" (Rathmell et al., 1973). For the Amott-Harvey method, water-wet range is from +0.3 to +1.0, the intermediate range is from -0.3 to +0.3 and the oil-wet range is from -0.3 to -1.0 (Cuiec, 1987). The intermediates are further broken down to a range of +0.1 to +0.3 for slightly water-wet, -0.1 to +0.1 for neutral and -0.1 to -0.3 for slightly oil-wet.

4.4 Mercury Porosimetry Experiments

The experiments were carried out on a mercury porosimeter (Pore Sizer Model Autopore II 9220) supplied by Micromeritics, Norcross, Georgia. Figure 4.7 shows front view of a mercury porosimetry Autopore II 9220. To embark on the tests, the samples were weighed and installed in penetrometers individually. Figure 4.8 shows diagram of an assembled and unassembled penetrometer. Four samples in penetrometers were installed in the low-pressure ports at a time and evacuated simultaneously in the low pressure ports until a stabilized pressure of about 50 μm was obtained. Mercury was then allowed to fill the penetrometers and low-pressure tests were performed in discrete increments from 1.5 psia to 14 psia (about atmospheric pressure).

At the conclusion of the low pressure runs, the penetrometers containing mercury and samples were weighed and two of them were installed in the high-pressure chambers at a time. The high-pressure runs could be performed at specific values from 14 to 60,000 psia (air-mercury) by raising the pressure incrementally and allowing equilibration at each increment. With each increment of pressure, smaller pore throats were invaded by mercury. For this study, the maximum pressure was limited to 11,000 psia, because the amount of mercury intrusion above this pressure is negligible for the types of samples being investigated. Kopaska-Merkel and Amthor (1988) pointed out that any capillary-pressure study done to evaluate reservoir rock should at least cover the pressure range corresponding to pressures which might be encountered in the subsurface (probably at least 10,000 psia) or one runs the risk of under-estimating available porosity by up to 30% or more.

Pore size information are obtained from mercury intrusion (drainage) curves based on the assumption of a cylindrical pore configuration. It is assumed that mercury is the non-wetting phase which displaces completely the wetting phase (mercury vapor or air) in the rock samples. The extrusion (imbibition) curves are obtained by releasing pressure and

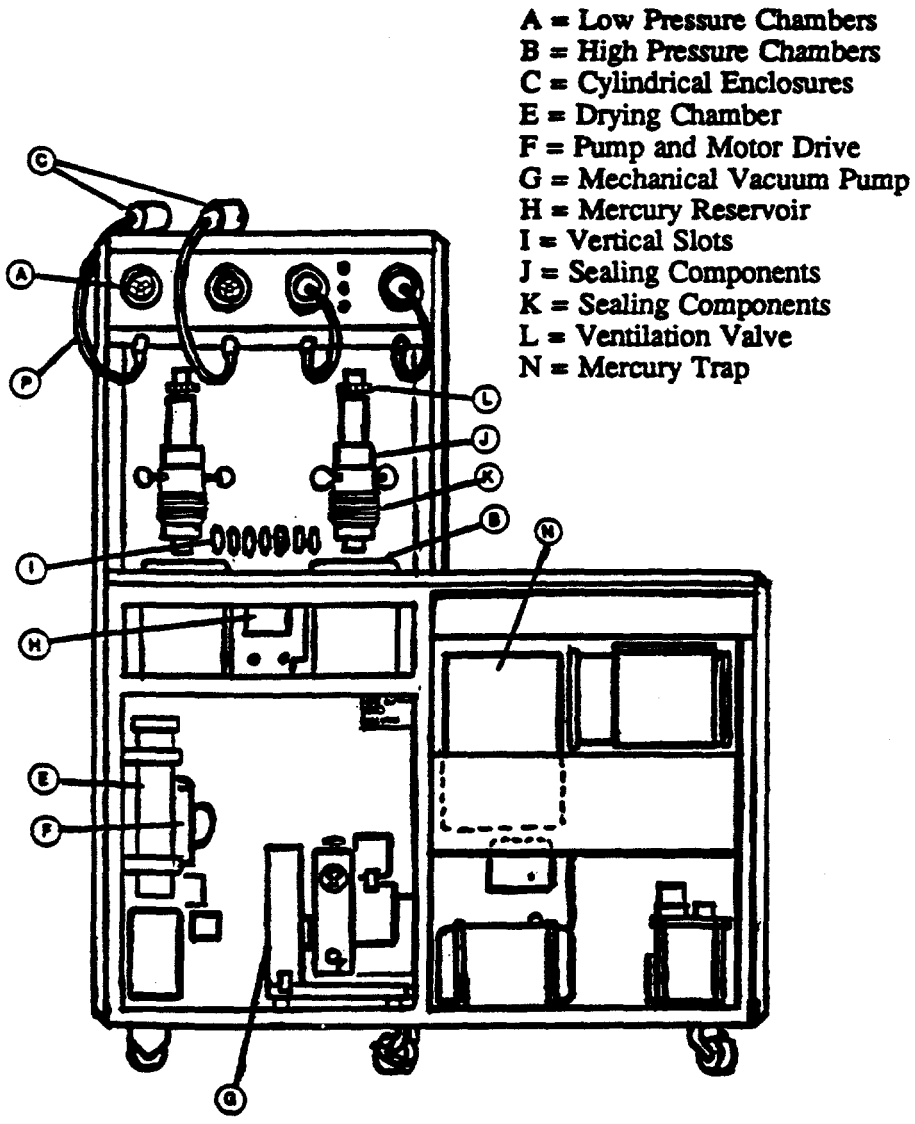

Fig. 4.7: Front View of Mercury Porosimetry Autopore II 9220 (After Micromeritics, 1987).

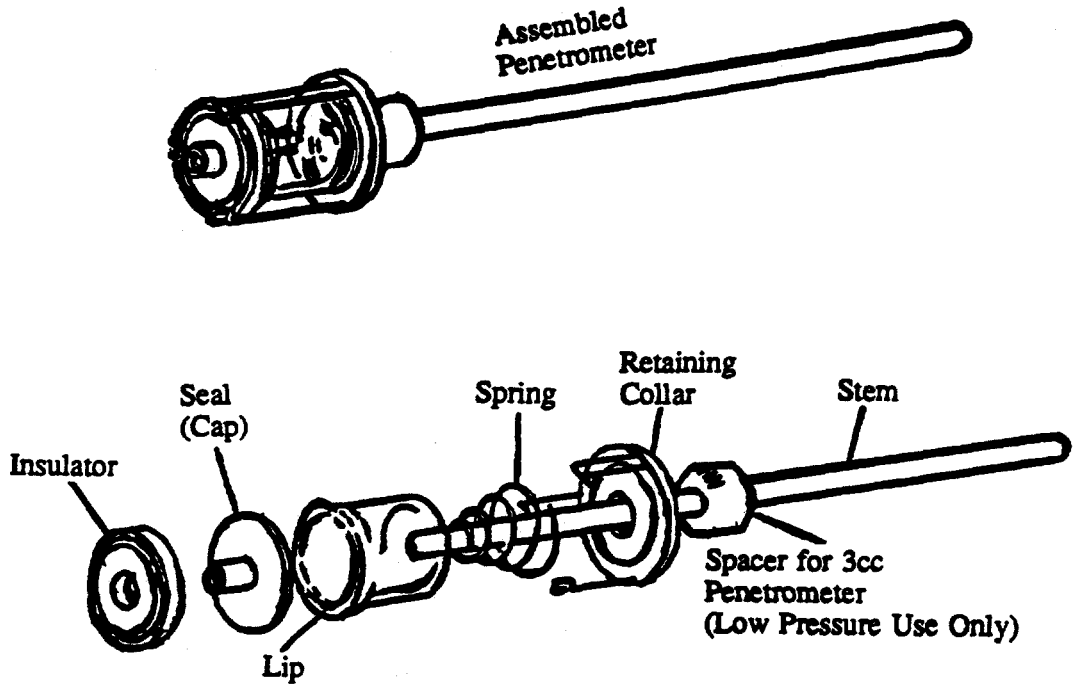

Fig. 4.8: Mercury Porosimetry Penetrometer Assembly (After Micromeritics, 1987).

recording equilibrated values and taking readings at successively lower pressures (Ghosh and Friedman, 1989).

4.5 Thin-Section Analysis

To better interpret waterflooding, wettability and porosimetry data, 10 sandstone cores were thin-sectioned and impregnated with blue epoxy. Approximately 400 points were counted per section using an optical microscope at 10x power.

Chapter 5

RESULTS AND DISCUSSION

5.1 Sandstone Radial-Core Case

Twenty sets of waterflooding displacement tests were conducted in Berea sandstone radial-cores of 12.7 cm diameter, 5.08 cm long, with 0.159 cm clearance between the core's circumference and the core holder. The containment pressure on the cores was maintained at 500 psig for the sandstone radial-cores. The pressure of 500 psig permitted water injection without the inducement of fracture.

5.1.1 Waterflood Properties

As part of data collection and analysis, waterflood experimental results are used to identify the mechanisms of fluid flow pertinent to this study. In addition, waterflood experimental results are used to determine the functional relationships between oil recovery and residual water and oil saturations and tortuosity. Tortuosity which is expressed in terms of the true rock retention time (in seconds) for the purpose of this study, was measured by recoding the amount of time required for the injected brine to travel from the core inlet to the outlet face.

Statistical descriptions of the different waterflood experimental variables are listed in Table 5.1. The variables include initial oil saturation, residual oil saturation, porosity, permeability, tortuosity (expressed in terms of retention time), oil recovery at breakthrough, and ultimate oil recovery. Figure 5.1 shows a plot of residual oil saturation versus initial oil saturation. The plot indicates that there is a tendency for residual oil to increase as the initial oil saturation increases. This observation is in agreement with Pickell et al. (1966), who indicated that residual oil saturation is dependent on initial oil content.

Table 5.1: Statistical Description of Waterflood Experimental Variables for Berea Sandstone Radial-Cores

	UOR (% IOIP)	OR @ B.T. (% IOIP)	S_{oi} (%)	S_{or} (%)	ϕ_{brine} (%)	ϕ_{air} (%)	k_{air} (md)	τ
Mean	43.99	32.25	54.41	30.41	19.55	18.51	302.7	652.0
Median	43.62	32.69	54.84	31.07	20.09	18.96	361.9	666.9
Min.	39.86	20.05	46.58	24.46	16.88	16.20	63.00	347.1
Max.	51.30	37.66	61.93	34.88	21.83	20.34	583.8	897.0
Q1	42.10	31.80	50.94	28.07	17.79	16.64	73.40	572.4
Q3	44.97	34.60	57.79	33.14	21.48	20.02	483.8	743.7
St. Dev.	2.928	2.400	3.950	3.234	1.893	1.500	188.2	139.1

B.T. = Breakthrough

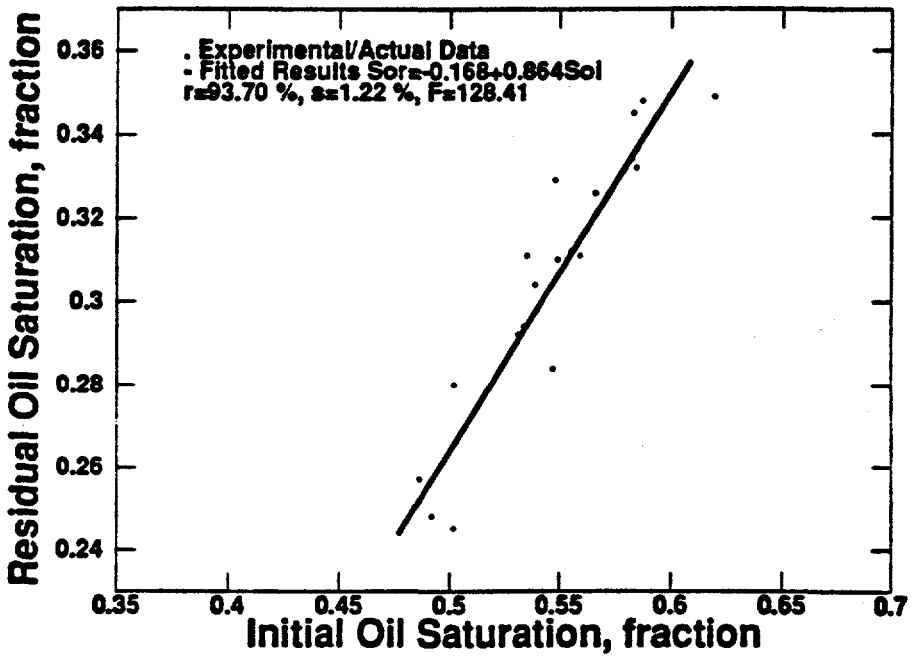

Fig. 5.1: Residual Oil Saturation vs. Initial Oil Saturation for Berea Sandstone Radial-Cores.

In this study, the ratio of capillary to viscous forces was calculation to be $1.859 \times 10^{+6}$, corresponding to a capillary number, N_{ca} , of $1.344 \times 10^{-7} < 10^{-6}$. Capillary forces here are defined using interfacial tension only. A N_{ca} value of 1.344×10^{-7} indicates a capillary force dominance. Therefore, the residual oil saturation resulting from the waterflooding was influenced by capillary forces only.

5.1.2 Wettability Properties

Wettability indices were obtained from the results of wettability experiments. These results were used to determine the average wettability index of the Berea sandstone radial-cores. Furthermore, the results are used to determine functional relationships between oil recovery and average wettability index.

Using the Amott-Harvey method, Berea sandstone radial-cores surface wettability indices were determined and shown to vary from a minimum value of +0.45 to a maximum value of +1.0. Wettability variations in the less permeable rocks were more pronounced. This was attributed to the relative abundance of shaly streaks in the tighter cores and led to the conclusion that with respect to the core plugs tested, the wettability is heterogeneous or "dalmatian" with some parts of the surface area being water-wet and others being oil-wet.

The frequency distribution of the wettability indices was skewed to the left since the median of the distribution is larger than the mean (Fig. 5.2). Figure 5.3 shows that the average wettability index was found to be directly related to the initial water saturation. However, Fig. 5.4 indicates that the residual oil saturation in Berea sandstone cores is inversely related to the average wettability index. Figure 5.5 indicates that ultimate oil recovery directly relates to the average wettability index in Berea sandstone radial-cores.

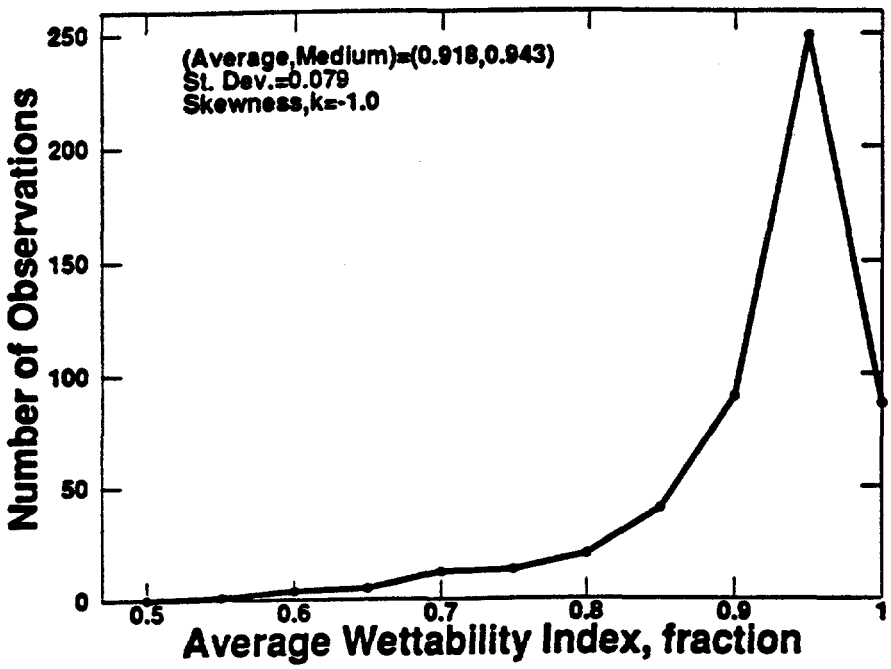

Fig. 5.2: Frequency Distribution for Wettability Indices for Berea Sandstone Radial-Cores.

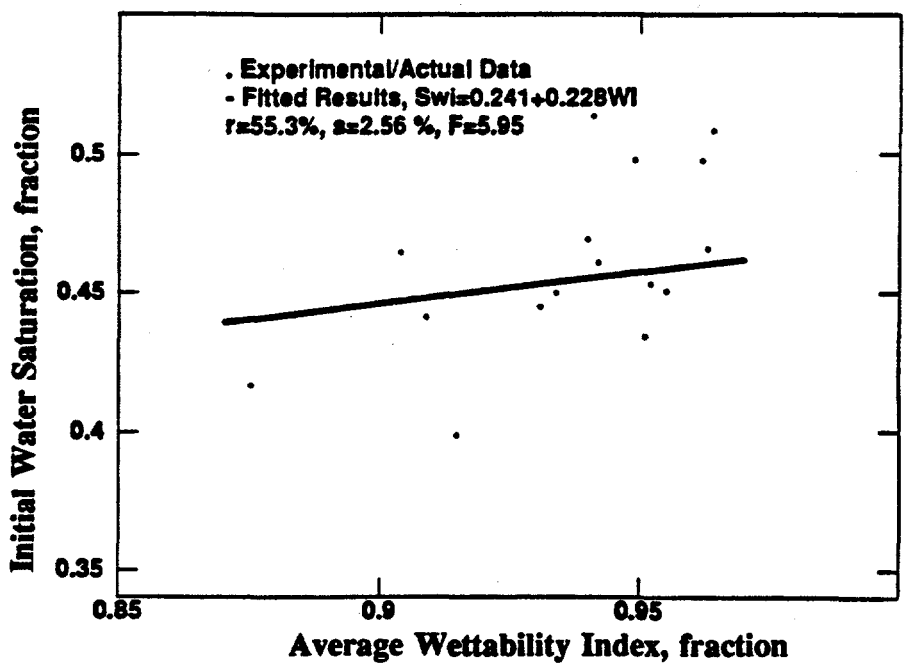

Fig. 5.3: Initial Water Saturation vs. Average Wettability Index for Berea Sandstone Radial-Cores.

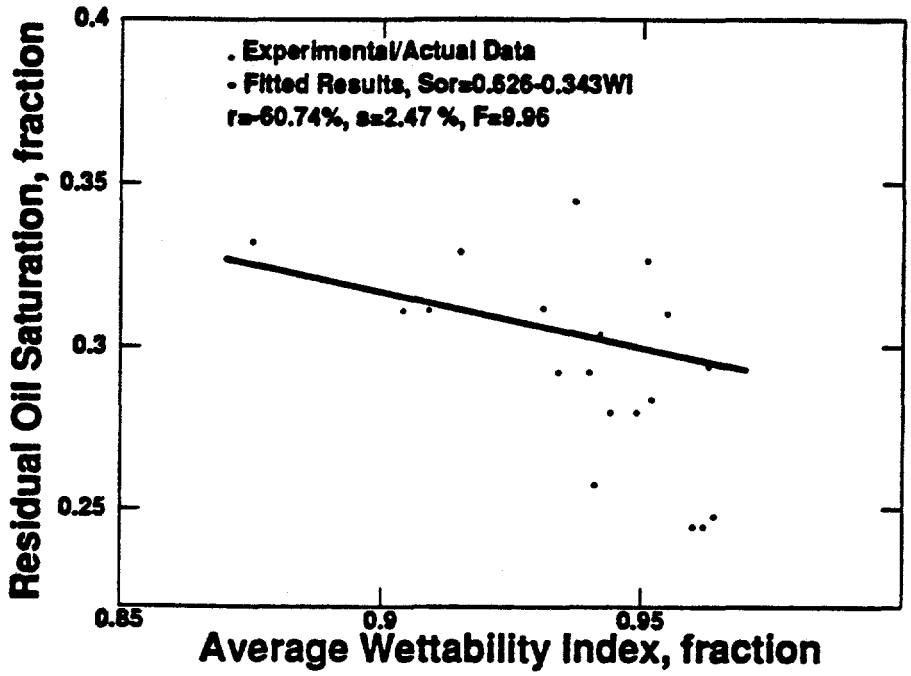

Fig. 5.4: Residual Oil Saturation vs. Average Wettability Index for Berea Sandstone Radial-Cores.

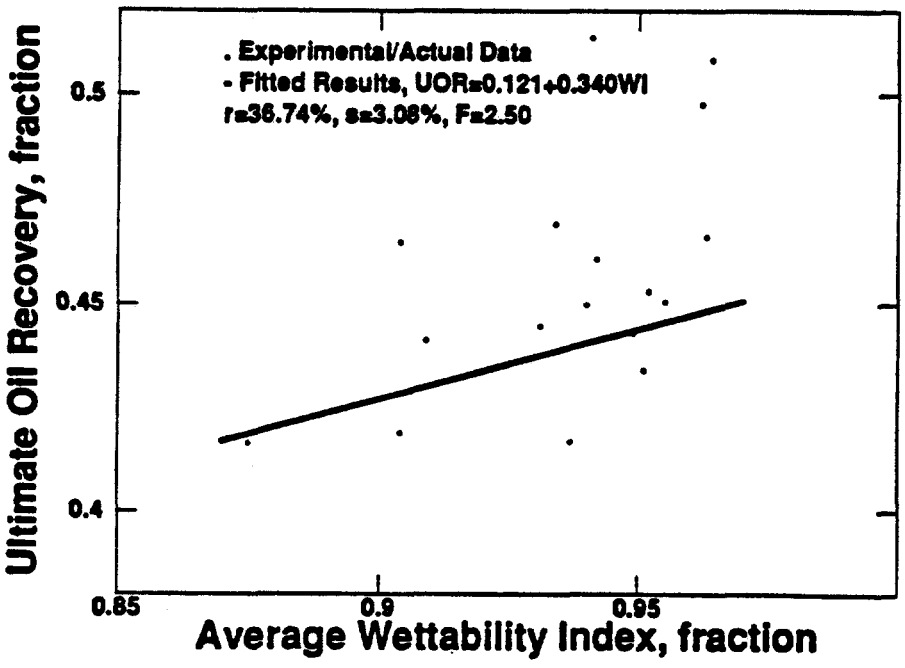

Fig. 5.5: Ultimate Oil Recovery vs. Average Wettability Index for Berea Sandstone Radial-Cores.

5.1.3 Mercury Porosimetry Properties

In mercury porosimetry experiments, incremental and cumulative intrusion curves are used to determine the non-wetting phase mechanisms of trapping in Berea sandstone radial-cores investigated. Additionally, using mercury porosimetry, measurements of pore-throat diameter, rock surface area and pore length are obtained. The data resulting from these measurements are used to determine the functional relationships between oil recovery and median pore-throat diameter, rock surface area and pore length.

Figure 5.6 which relates ultimate oil recovery to average rock surface area indicates a trend that is directly related. Hence, for water-wet rocks, ultimate oil recovery is higher, for larger average rock surface area. Figure 5.7 contain a plot of the pore-throat size distribution for permeable Berea sandstone core. The plot indicates that the distribution is centered around a median pore-throat size of approximately 15 μm. Figure 5.8 shows plots of the extrusion and intrusion cycles. The location of the extrusion cycle above the intrusion cycle indicates that the hysteresis loop does not close and suggests that some mercury is entrapped in the pores. Similar intrusion-extrusion curves behavior was observed by Lowell and Shields (1981). Orr (1969/70) suggested that intrusion-extrusion hysteresis is due mainly to "ink-well" shaped pores. In pores of this type, intrusion cannot occur until sufficient pressure is attained to force mercury into the narrow neck, whereupon the entire pore will fill. However, upon extrusion, the wide-pore body can not empty until a lower pressure is reached, leaving entrapped mercury in the wide inner portion.

Figure 5.9 is the plot relating the permeability of Berea sandstone cores to porosity. According to Fig. 5.10, rock permeability and average rock surface area are inversely proportional. Also, as indicated in Fig. 5.11, average surface area is correlatable to the median pore-throat diameter. Since the Berea sandstone average rock surface area is inversely related to its median pore-throat size, the rock surface area was found to be

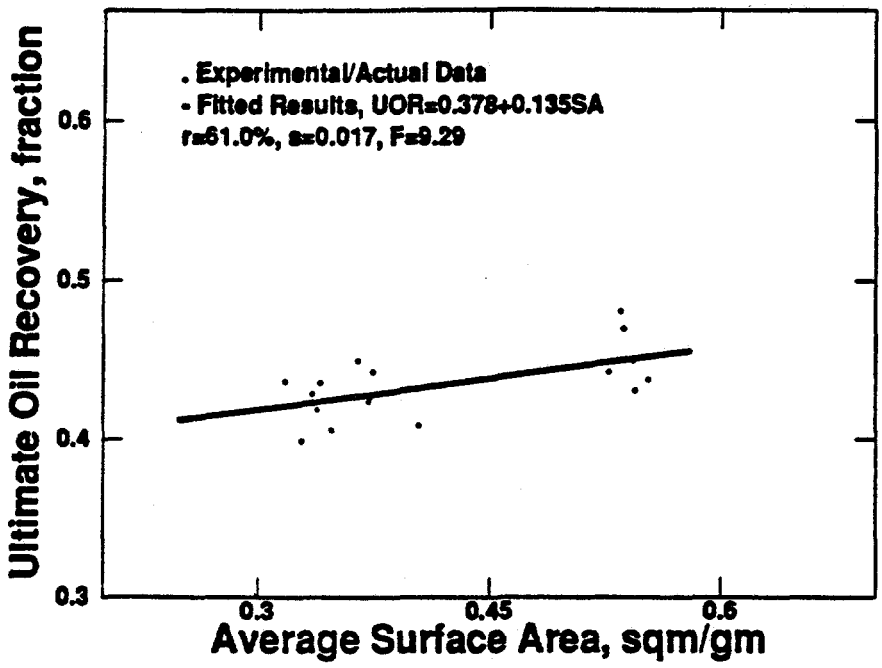

Fig. 5.6: Ultimate Oil Recovery vs. Average Surface Area for Berea Sandstone Radial-Cores.

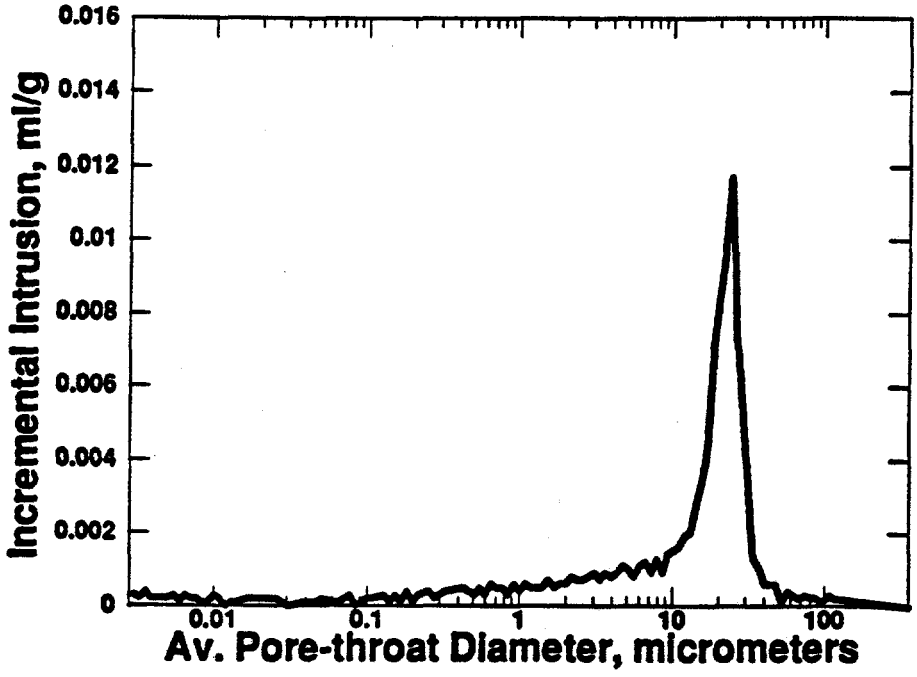

Fig. 5.7: Pore-Throat Size Distribution for Permeable Berea Sandstone Radial-Cores.

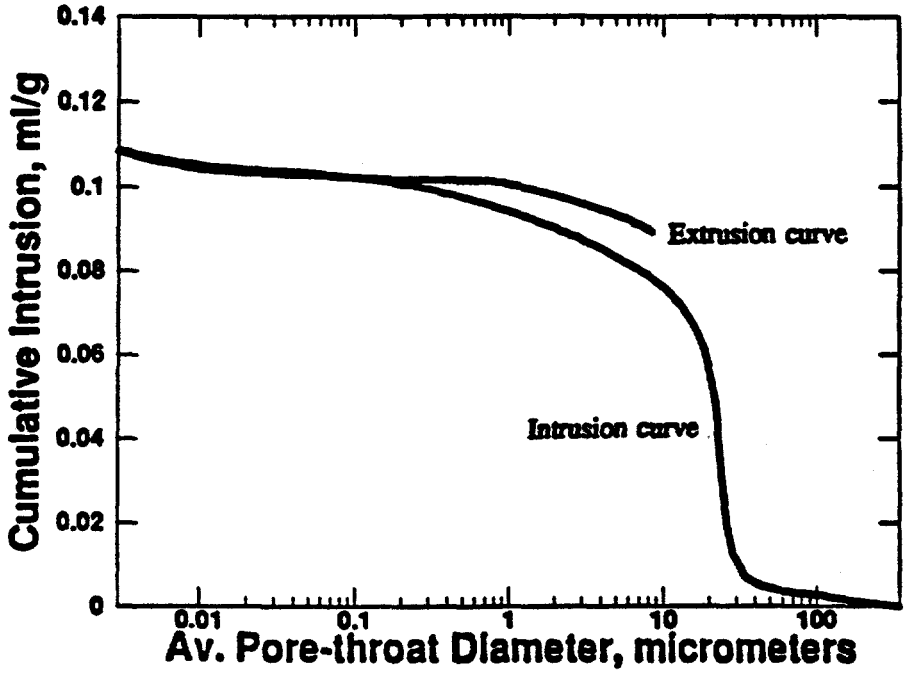

Fig. 5.8: Steep-Convex Unimodal Capillary-Pressure Curve for Permeable Berea Sandstone Radial-Cores.

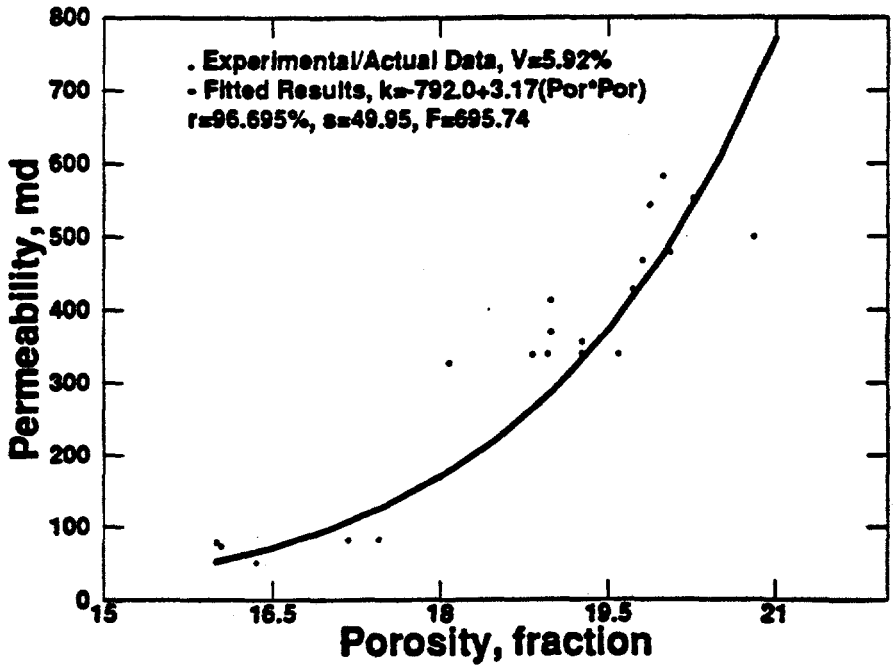

Fig. 5.9: Permeability vs. Porosity for Berea Sandstone Radial-Cores.

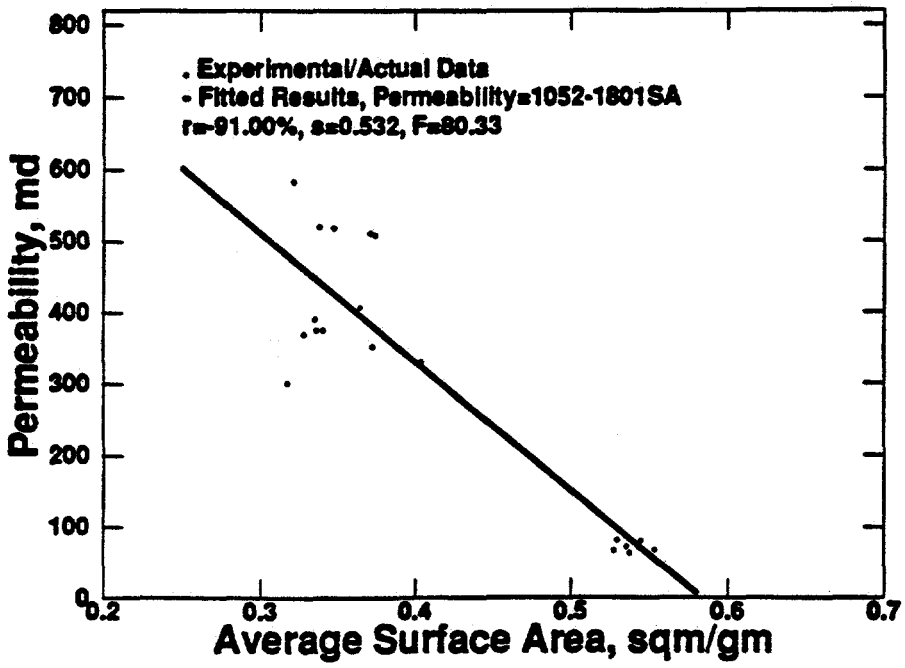

Fig. 5.10: Permeability vs. Average Surface Area for Berea Sandstone Radial-Cores.

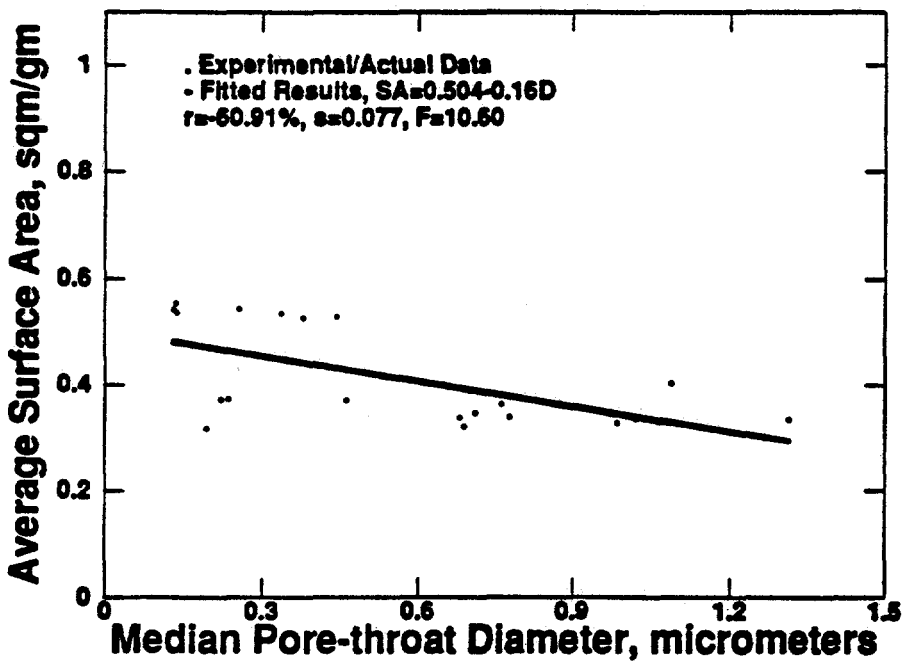

Fig. 5.11: Average Surface Area vs. Median Pore-Throat Diameter for Berea Sandstone Radial-Cores.

inversely related to rock permeability. As pointed out by Amthor et al. (1988), porosity was found to be positively related to rock median-throat size. In this study, as indicated in Fig. 5.12, rock porosity was found to be inversely proportional to average rock surface area. Our findings appear to be in accordance with the conclusions of Amthor et al. since rock surface area is an inverse function of the rock median pore-throat size.

Further analysis indicated that one form of capillary pressure curves was distinguishable. Similar to the plot shown in Fig. 5.8, all the curves from the 524 core plugs tested show a steep-convex unimodal trend. Unimodal curves are strong indications of unimodal throat-size distributions. Amthor et al. suggested that rocks are classified by their capillary pressure curve forms which are strongly correlatable to recovery efficiencies.

Figure 5.13 indicates that median pore length and oil recovery are found to be directly proportional. As shown in Fig. 5.14, ultimate oil recovery is inversely proportional to median pore-throat diameter. Furthermore, Fig. 5.15 shows that tortuosity is related to the median pore length. A longer flow pathway affects the rock retention time in such a way that it retards the time of appearance of the first liquid droplet coming out of the porous medium.

5.1.4 Thin-Section Analysis Properties

With the aid of thin-section analyses, the effects of clay matrix, carbonate cement and quartz overgrowth on wettability, porosity, residual oil saturation, and rock surface area of Berea sandstones were investigated. Mercury porosimetry and spectro-electromicroscopic analyses indicated that carbonate and quartz overgrowth were the predominant types of cement present in Berea sandstone rocks.

It was previously concluded that Berea sandstone wettability could be described as "dalmatian" with some parts of the rock surface area being water-wet and others being oil-

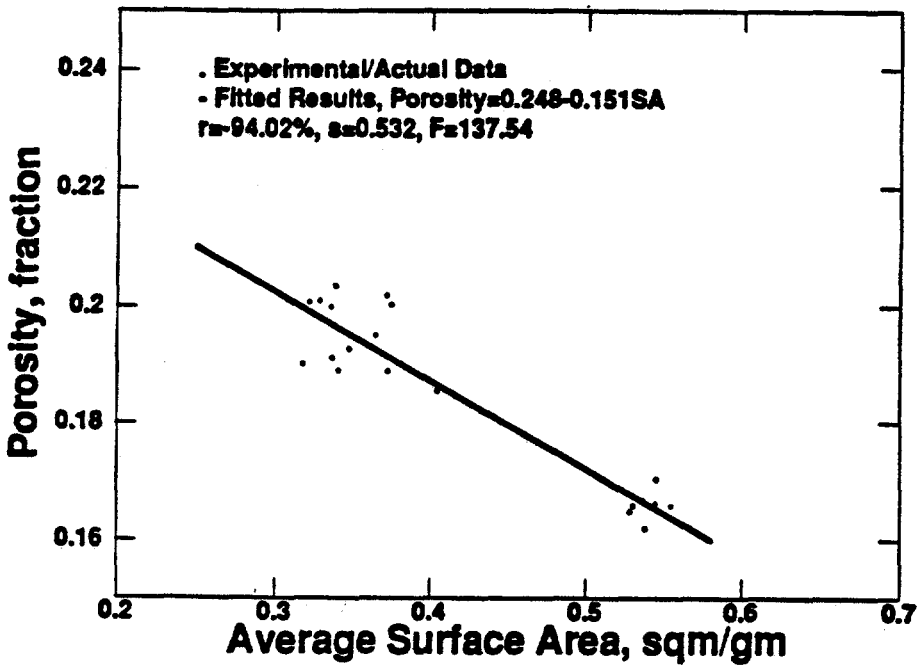

Fig. 5.12: Porosity vs. Average Surface Area for Berea Sandstone Radial-Cores.

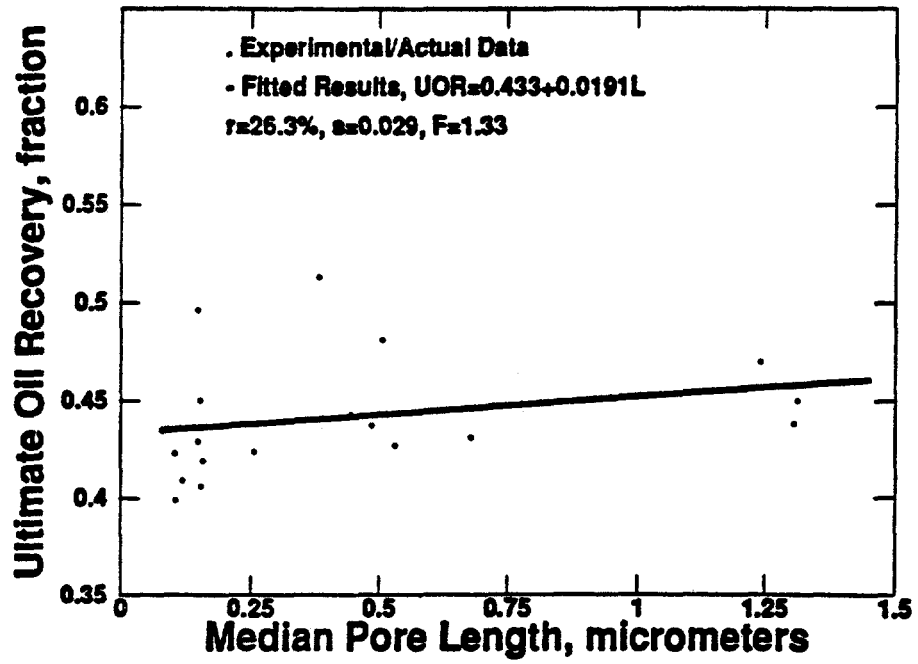

Fig. 5.13: Ultimate Oil Recovery vs. Median Pore Length for Berea Sandstone Radial-Cores.

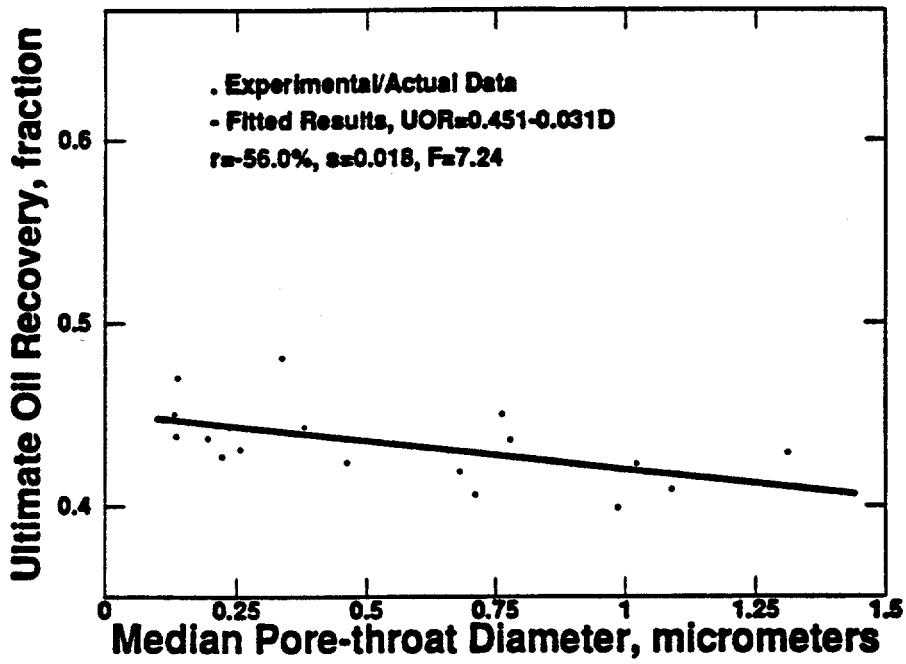

Fig. 5.14: Ultimate Oil Recovery vs. Median Pore-Throat Diameter for Berea Sandstone Radial-Cores.

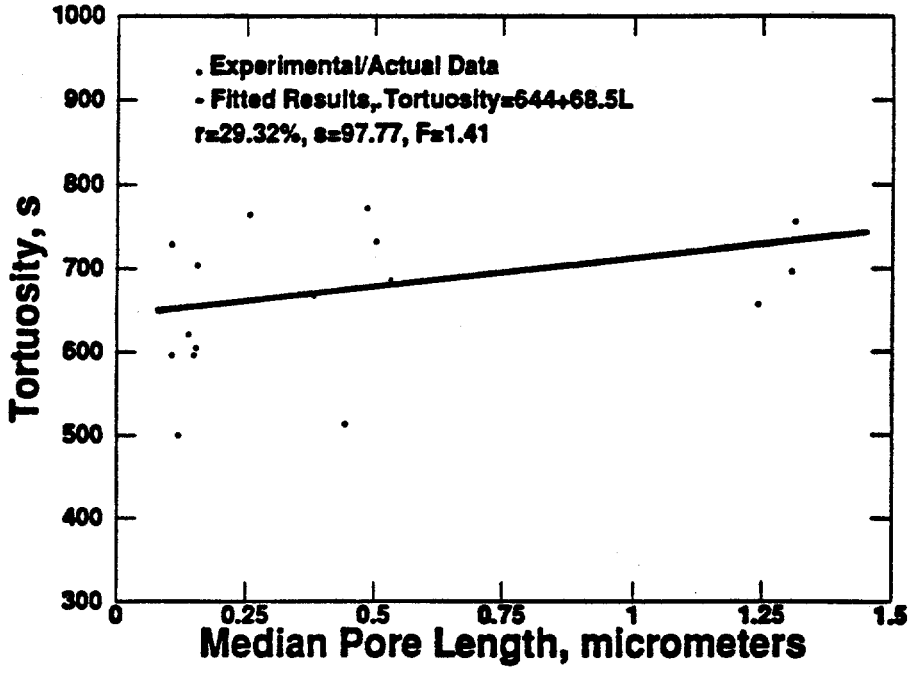

Fig. 5.15: Tortuosity vs. Median Pore Length for Berea Sandstone Radial-Cores.

wet. Furthermore, wettability is "dalmatian" mainly because of the occurrence of shaly streaks were more abundant in tighter cores. The mean wettability was found to be functionally related to the amount of hydrophobic or hydrophilic surface area present in each core sample. The impact of rock surface type, clay and cement contents on wettability were examined. Higher amount of clays, as indicated in Fig. 5.16, reduce the wettability of the rock surface area. Therefore, an inversely proportional relationship relates the cores average wettability index to the clay content. Consequently, it was concluded that larger amount of clays prevents the spreading of the wetting phase on the rock surface area.

Thin-section analysis supported the conclusion that wettability is "dalmatian". As shown in Fig. 5.16, average wettability index is slightly related to the amount of clay present. Higher rock clay content reduces the affinity of the rock surface area to the wetting phase. The relationship is weak with a R^2 of 6% and it is statistically not significant at α = 0.1 level. Since the coefficient of variance of the relationship is less than 1.0, it indicates that no erratic data points are present.

In mercury porosimetry studies, high surface areas resulted from ink-well shaped pores which are characterized by a narrow entrance and a comparatively wide inner body. Intrusion into the wide inner body does not occur until a sufficiently high pressure is applied to force mercury through the narrow throats into the pore body. As a result errors in volume are associated with narrow pores which result in a high calculated surface area. It was observed that low surface areas were associated with more porous and permeable formations. In these types of rocks, median pore-throat sizes were found to be larger than the median pore-throat sizes associated with the less porous and less permeable formations. These observations are in agreement with those of Amthor, Kopaska-Merkel and Friedman (1988). These investigators indicated that low permeability was due to small median pore-throat sizes. Moreover, higher surface areas were associated with core samples having

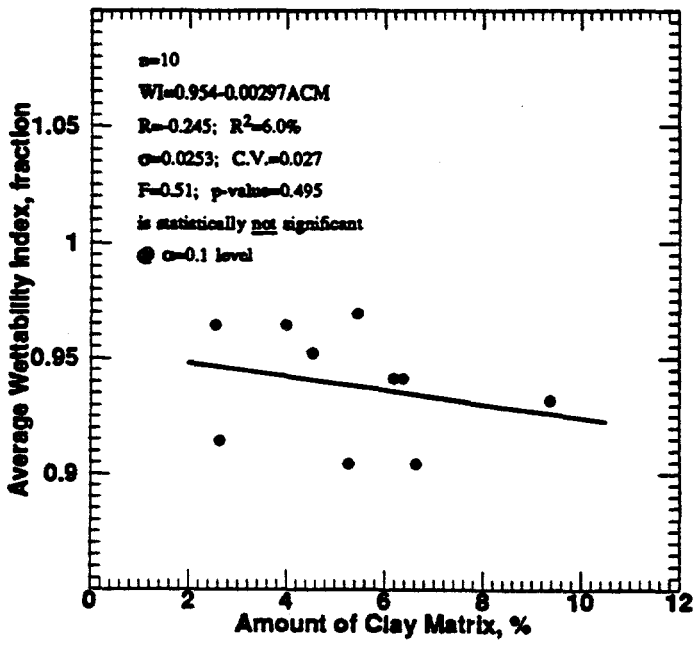

Fig. 5.16: Average Wettability Index vs. Amounts of Clay Matrix for Berea Sandstone Radial-Cores.

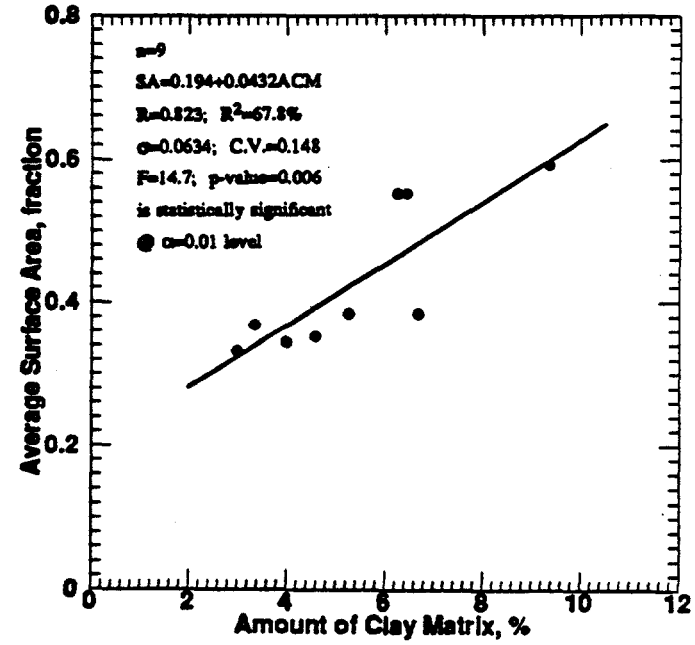

Fig. 5.17: Average Surface Area vs. Amounts of Clay Matrix for Berea Sandstone Radial-Cores.

smaller median pore-throat diameters. These types of samples were found in tighter cores where shale streaks were abundant. Higher surface areas reflected the expansion of clay minerals in the tighter formations. Therefore, as described in Fig. 5.17, rock surface area is affected by the amount of clay minerals present in a core. Higher amount of clays results in higher surface areas. As shown in Fig. 5.18, there is no defined trend for the relationship between average surface area and the amount of cements in the core.

Further, using thin-section analysis technique, it was noted that the matrix of Berea sandstone was made up of monocrystalline quartz, polycrystalline quartz, chert, plagioclase, alkali feldspar, rock fragments, mica flakes and heavy minerals Tables 5.2, 5.3, and 5.4 show the point count results from thin sections of bedded and unbedded cores. As Table 5.2 shows, the dominant cement appears to be quartz overgrowths. Nearly all quartz grains had at least a thin layer of overgrowth. Tables 5.3 and 5.4 show the point count results on coarse and finer laminations in the bedded cores, respectively. On the other hand, the unbedded cores could be described as well-sorted quartzose sandstone (Fig. 5.19). Indications of bedding or laminations were not seen under the microscope or from the thin-section analysis; therefore, these cores were referred to as unbedded. By contrast, the bedded Berea sandstone cores could be described as moderately well-sorted quartzose sandstone (Fig. 5.20). The bedding laminations in these cores were very distinct. These laminations were differentiated mainly on the basis of grain size. The coarser laminations were well-sorted within their own boundaries, while the finer laminations were moderately well-sorted. Figs. 5.19 and 5.20 show that porosity connectivity was not homogeneous as was true in the case of the thin sections from well-sorted, unbedded cores. However, the thin sections obtained from the bedded cores indicate that the pores were better connected along the bedding planes. As indicated in Tables 5.3 and 5.4, there was no significant differences apparent in the proportions of framework grains (i.e. monoquartz, polyquartz,

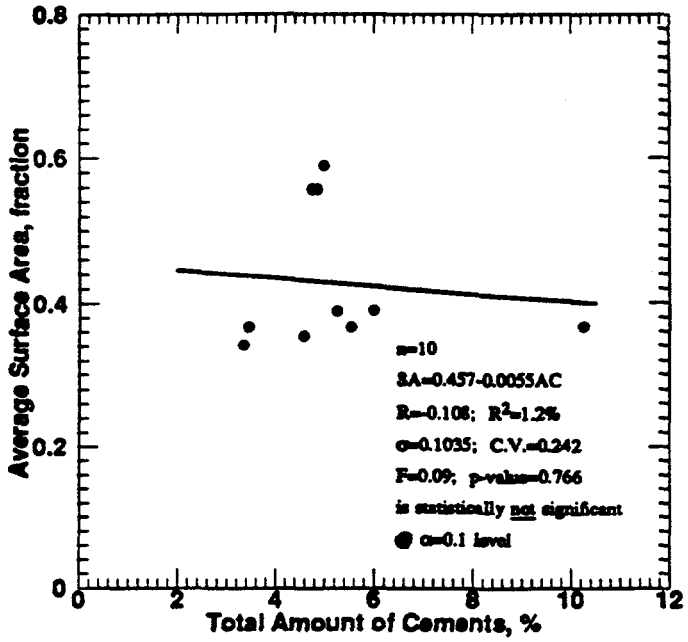

Fig. 5.18: Average Surface Area vs. Total Amounts of Cements for Berea Sandstone Radial-Cores.

Table 5.2: Point Count Results for Slide 8-2

		No.	%
Framework Minerals	Monocrystalline Quartz	257	44.5
	Polycrystalline Quartz	46	8.0
	Chert	6	1.0
	Plagioclase	35	6.0
	Alkali Feldspar (k)	14	2.4
	Rock Fragments	5	0.9
Porosity	Primary Porosity	67	11.6
	Oil (Interstitial)	69	11.9
	Secondary Porosity	7	1.2
Matrix and Cement	Clay Matrix	27	4.7
	Quartz Overgrowths	33	5.7
	Carbonate Cement	8	1.4
	Clay Alteration Rim	5	0.9
	Total:	578	
	%Framework Grains	62.8	
	%Porosity (Total)	24.7	
	%Matrix	4.7	
	%Cement	7.1	
		99.3	

Count covered 14 traverses perpendicular to bedding

Table 5.3: Point Count Results for Slide 17-2 (Finer Laminations)

		No.	%
Framework Minerals	Monocrystalline Quartz	154	48.3
	Polycrystalline Quartz	27	8.5
	Chert	1	0.3
	Alkali Feldspar (k)	6	1.9
	Rock Fragments	19	6.0
	Mica Flakes	1	0.3
Porosity	Primary Porosity	53	16.6
	Oil (Interstitial)	27	8.5
	Secondary Porosity	6	1.9
Matrix and Cement	Clay Matrix	14	4.4
	Quartz Overgrowths	4	1.3
	Carbonate Cement	7	2.2
	Total:	319	
	%Framework Grains	65.3	
	%Porosity (Total)	27.0	
	%Matrix	4.4	
	%Cement	3.5	
		99.2	

Table 5.4: Point Count Results for Slide 17-2 (Coarse Laminations)

		No.	%
Framework Minerals	Monocrystalline Quartz	159	50.2
	Polycrystalline Quartz	29	9.1
	Chert	2	0.6
	Alkali Feldspar (k)	5	1.6
	Rock Fragments	16	5.0
	Mica Flakes	1	0.3
	Heavy Minerals	2	0.6
Porosity	Primary Porosity	47	14.8
	Oil (Interstitial)	16	5.0
	Secondary Porosity	4	1.3
Matrix and Cement	Clay Matrix	17	5.3
	Quartz Overgrowths	5	1.6
	Carbonate Cement	14	4.4
	Total:	317	
	%Framework Grains	67.4	
	%Porosity (Total)	21.1	
	%Matrix	5.3	
	%Cement	6.0	
		99.8	

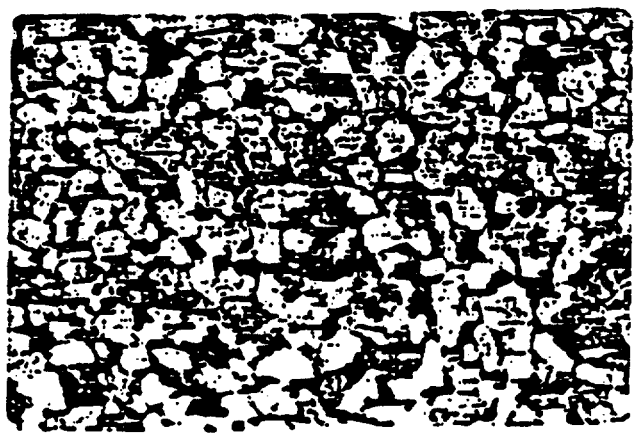

Fig. 5.19: SEM Photograph of Epoxy-Filled Unbedded Thin-Section for Berea Sandstone Radial-Cores.

Fig. 5.20: SEM Photograph of Epoxy-Filled Bedded Thin-Section for Berea Sandstone Radial-Cores.

feldspars and shale rock fragments) between laminations. Additionally, as Tables 5.3 and 5.4 show, there was a significant decrease in total porosity in the finer laminations (27-28% coarse versus 20-22% fine) of the thin sections obtained from bedded cores. This decrease resulted from both larger amount of clay matrix and carbonate in the finer laminations.

Quartz overgrowths were detected with greater frequency in the unbedded cores. Figure 5.21 shows that as the total porosity decreases, amount of quartz overgrowth increases. The relationship between total porosity and the amount of quartz overgrowth for the bedded cores, is statistically not significant at $\alpha = 0.1$ level. The total porosity decrease seemed to be more pronounced in the unbedded cores. Moreover, the amount of quartz overgrowth appears to have little influence on total porosity variation in the tight and less permeable cores.

Additionally, patchy carbonate was present as a cement. Where present, it tended to fill the entire pore and appeared to have been deposited at a time subsequent to the quartz overgrowth. Figure 5.22 indicates that presence of carbonate cements in Berea sandstone cores lowers the total porosity. The amount of carbonate cements were higher in the thin sections obtained from bedded cores than in those obtained from unbedded cores. In the latter case, the presence of incipient secondary porosity was determined. Incipient secondary porosity occurs where feldspar grains (plagioclase and alkali feldspars) and shale rock fragments were partially dissolved (filled with epoxy). If the pore size was large enough and is connected to the primary porosity, oil will be trapped in cul-de-sacs or dead ends. Figure 5.23 indicates that total and secondary porosity are related. A high total porosity is associated with a high induced secondary porosity.

The matrix in Berea sandstone cores was predominantly clay. The clay matrix, on rare instances, was replaced by a very patchy amount of silica. It was observed that large amount of clay matrix reduces the total porosity (Fig. 5.24). Porosity, on the other hand, did

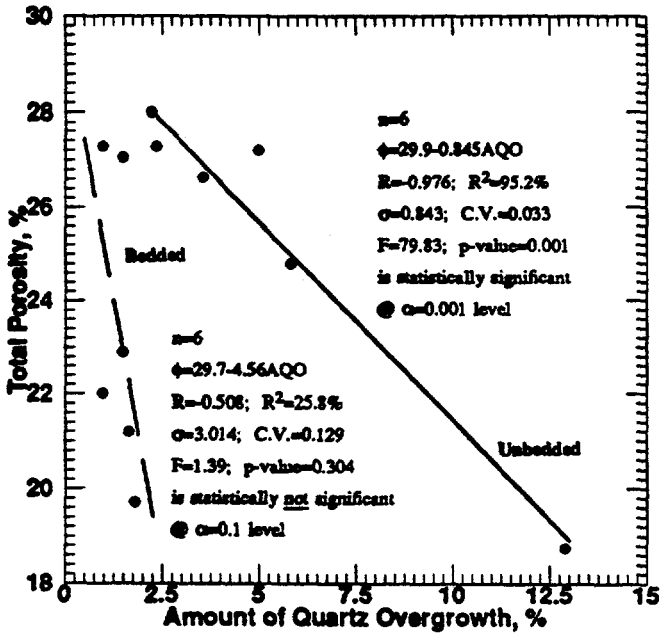

Fig. 5.21: Total Porosity vs. Amounts of Quartz Overgrowth for Berea Sandstone Radial-Cores.

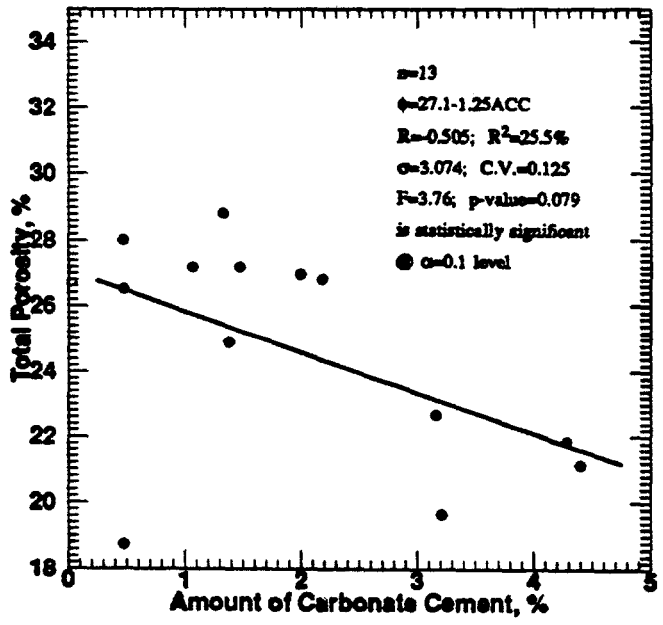

Fig. 5.22: Total Porosity vs. Amounts of Carbonate Cement for Berea Sandstone Radial-Cores.

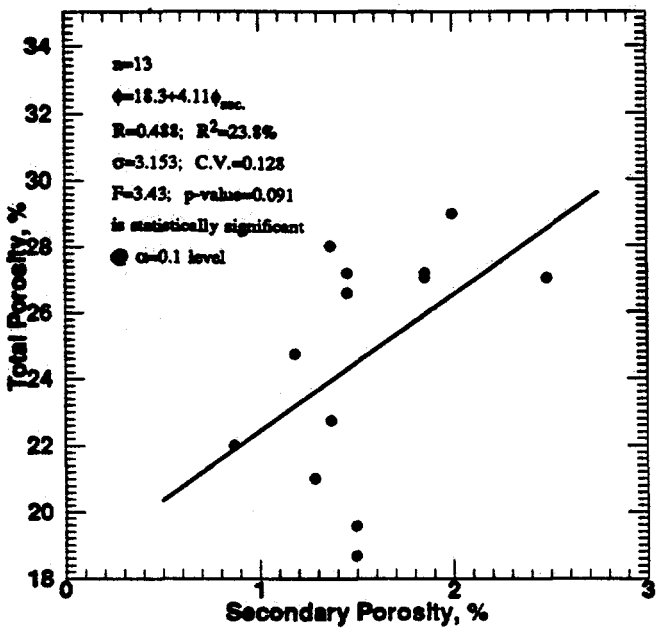

Fig. 5.23: Total Porosity vs. Secondary Porosity for Berea Sandstone Radial-Cores.

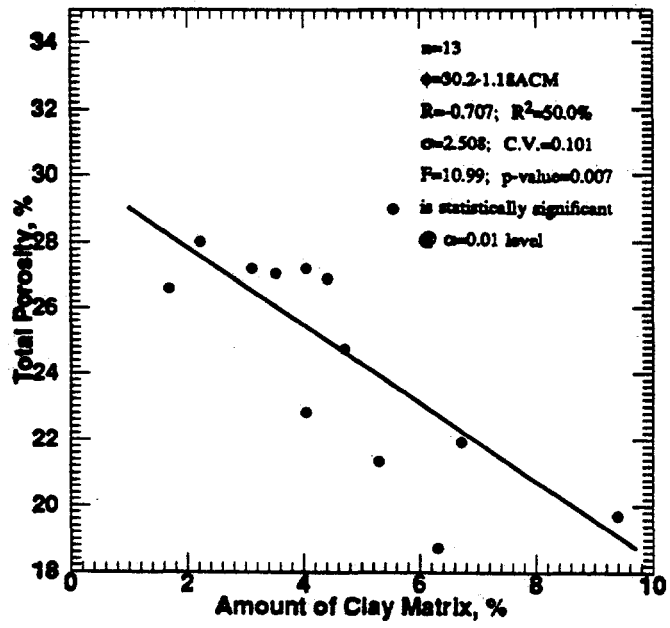

Fig. 5.24: Total Porosity vs. Amounts of Clay Matrix for Berea Sandstone Radial-Cores.

not seem to be related to the amount of framework grains in the bedded and unbedded cores (Fig. 5.25). Furthermore, there do not appear to be any significant differences in the proportions of framework grains in the thin sections obtained from bedded and unbedded cores.

The extent of degree of primary porosity was higher in the thin sections obtained from bedded cores. The total porosity was found to be directly proportional to the primary porosity, as illustrated by Fig. 5.26. The relationship for the unbedded cores is statistically not significant at $\alpha = 0.1$ level. The two distinct curves support the fact that the contrast in porosity was mainly due to two different primary porosity ranges.

When capillary forces dominate the fluid flow mechanisms, as is true in the case of a strongly water-wet system, less porous formations are best suited for piston-like displacement. Consequently, a low residual oil saturation is associated with tighter formations because of a better sweep efficiency and a more uniform frontal displacement. As indicated in Fig. 5.27, the residual non-wetting phase saturation increased with an increase in total porosity. This result seems to support Watson and Boukadi's (1990) conclusion that the ratio of pore body to pore throat diameters (the aspect ratio) affects the residual non-wetting phase saturation in Berea sandstone cores. Figure 5.27 also seems to suggest that a highly porous system permits by-passing and non-wetting phase snap-off when capillary forces dominate the displacement process.

5.2 Limestone Radial-Core Case

Twenty sets of waterflooding displacement tests were conducted in Indiana limestone radial-cores of 12.7 cm diameter, 5.08 cm long, with 0.159 cm clearance between the core's circumference and the core holder. The containment pressure on the cores was maintained at 200 psig for the limestone radial-cores. The containment pressure for limestone radial-core

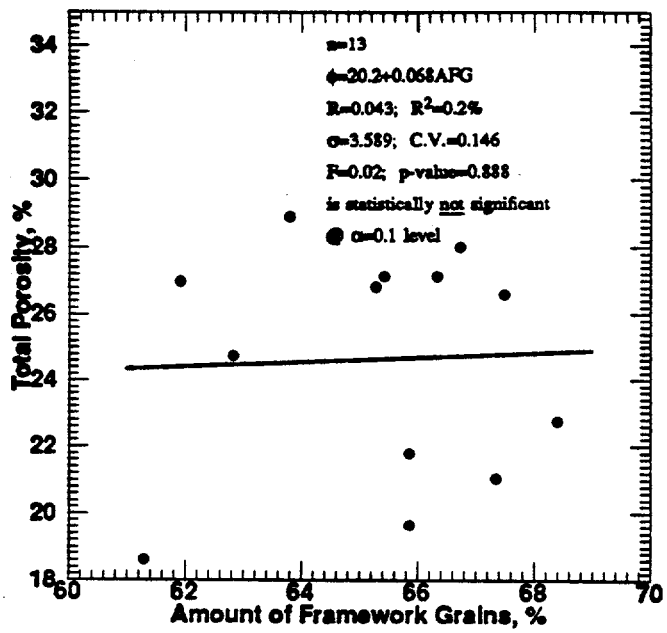

Fig. 5.25: Total Porosity vs. Amounts of Framework Grains for Berea Sandstone Radial-Cores.

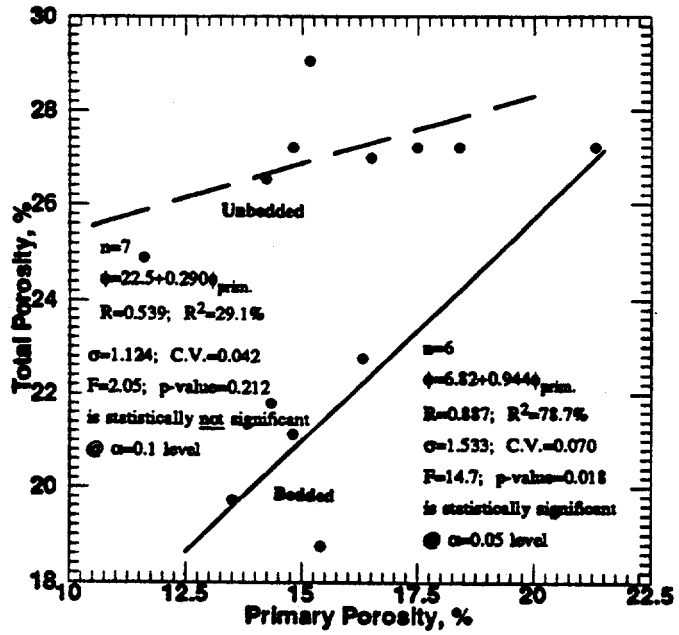

Fig. 5.26: Total Porosity vs. Primary Porosity for Berea Sandstone Radial-Cores.

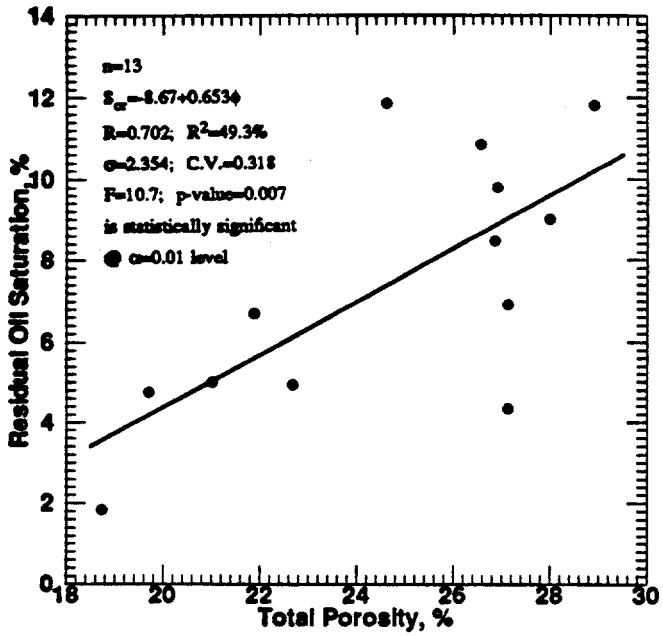

Fig. 5.27: Residual Oil Saturation vs. Total Porosity for Berea Sandstone Radial-Cores.

Table 5.5: Statistical Description of Waterflood Experimental Variables for Less Porous Indiana Limestone Radial-Cores
($10.099\% \leq \phi \leq 11.851\%$)

	UOR (% IOIP)	OR @ B.T. (% IOIP)	S_{oi} (%)	S_{wi} (%)	S_{or} (%)	ϕ_{brine} (%)
Mean	44.87	22.17	51.53	48.47	28.42	11.34
Median	43.74	20.79	51.73	48.27	29.32	11.47
Min.	39.33	18.05	46.77	44.92	23.49	10.09
Max.	52.70	27.41	55.08	53.28	31.55	11.85
Q1	41.55	20.04	49.92	46.71	25.62	11.15
Q3	47.91	24.79	53.29	50.08	30.88	11.66
St. Dev.	4.650	3.130	2.508	2.508	2.900	0.498

B.T. = Breakthrough

was 300 psig lower than that used for the sandstone radial-core. Experience indicated that the limestone radial-cores failed at containment pressures equal to or greater than 300 psig.

5.2.1 Waterflood Properties

Statistical descriptions of initial oil saturation, residual oil saturations, porosity, oil recovery at breakthrough and ultimate oil recovery with respect to less porous and more porous Indiana limestone cores are presented in Tables 5.5 and 5.6, respectively. For the two porosity ranges combined, the description of the data is shown in Table 5.7. Correlation matrices (Tables 5.8 and 5.9) were used to correlate the ultimate oil recovery to porosity, initial water saturation and residual oil saturation for the two porosity ranges used. The correlation indicated that the ultimate oil recovery was directly proportional to initial oil saturation and inversely proportional to porosity and residual oil saturation.

Figures 5.28 and 5.29 are plots of residual oil saturation and initial water saturation versus porosity, respectively. Figure 5.28 indicates that residual oil saturation is proportional to porosity for the low porosity range cores and inversely proportional to porosity in the high porosity range cores. Figure 5.29 indicates that initial water saturation is inversely proportional to porosity for the low porosity range cores. In the high porosity range cores, as the porosity increases, higher levels of initial water saturations are realized.

5.2.2 Wettability Properties

In determining the wettability indices of the Indiana limestone waterflooded cores, 480 core plugs were used to ensure a better lithology characterization and a better frequency distribution of the wettability indices and hence a more accurate average rock wettability index. A frequency polygon of the wettability indices is shown in Fig. 5.30. It was observed that the wettability of Indiana limestone cores is slightly heterogeneous with hydrophilic dominance. This heterogeneity is attributed to the fact that different amounts of

Table 5.6: Statistical Description of Waterflood Experimental Variables for More Porous Indiana Limestone Radial-Cores ($14.437\% \leq \phi \leq 17.047\%$)

	UOR (% IOIP)	OR @ B.T. (% IOIP)	S_{oi} (%)	S_{wi} (%)	S_{or} (%)	ϕ_{brine} (%)
Mean	38.72	25.32	41.54	58.46	25.49	16.12
Median	38.48	25.79	41.35	58.65	24.63	16.37
Min.	30.15	18.25	36.55	49.37	21.35	14.44
Max.	46.64	30.18	50.62	63.45	31.59	17.05
Q1	37.19	21.97	37.86	56.25	22.65	15.60
Q3	40.83	28.84	43.75	62.14	27.94	16.66
St. Dev.	4.210	4.020	4.150	4.150	3.450	0.818

B.T. = Breakthrough

Table 5.7: Statistical Description of Waterflood Experimental Variables for Indiana Limestone Radial-Cores

	UOR (% IOIP)	S_{oi} (%)	S_{or} (%)	ϕ_{brine} (%)	ϕ_{air} (%)	k_{air} (md)
Mean	41.79	46.51	26.96	13.73	16.44	48.8
Median	41.09	48.09	26.89	13.14	16.36	30.7
Min.	30.15	36.55	21.35	10.10	11.12	1.60
Max.	52.70	55.08	31.59	17.05	20.80	154.4
Q1	38.42	40.74	23.64	11.46	13.15	4.00
Q3	45.65	52.24	30.48	16.39	19.63	89.7
St. Dev.	5.340	6.100	3.449	2.535	3.424	50.8

Table 5.8: Correlation Matrix for More Porous Indiana Limestone Radial-Cores

	UOR	S_{or}	S_{wi}	S_{oi}
S_{or}	-0.701			
S_{wi}	0.248	-0.865		
S_{oi}	-0.248	0.865	-1.000	
ϕ	-0.430	-0.264	0.666	-0.666

Table 5.9: Correlation Matrix for Less Porous Indiana Limestone Radial-Cores

	UOR	S_{or}	S_{wi}	S_{oi}
S_{or}	-0.878			
S_{wi}	0.119	-0.579		
S_{oi}	-0.119	0.579	-1.000	
ϕ	-0.411	0.602	-0.568	0.568

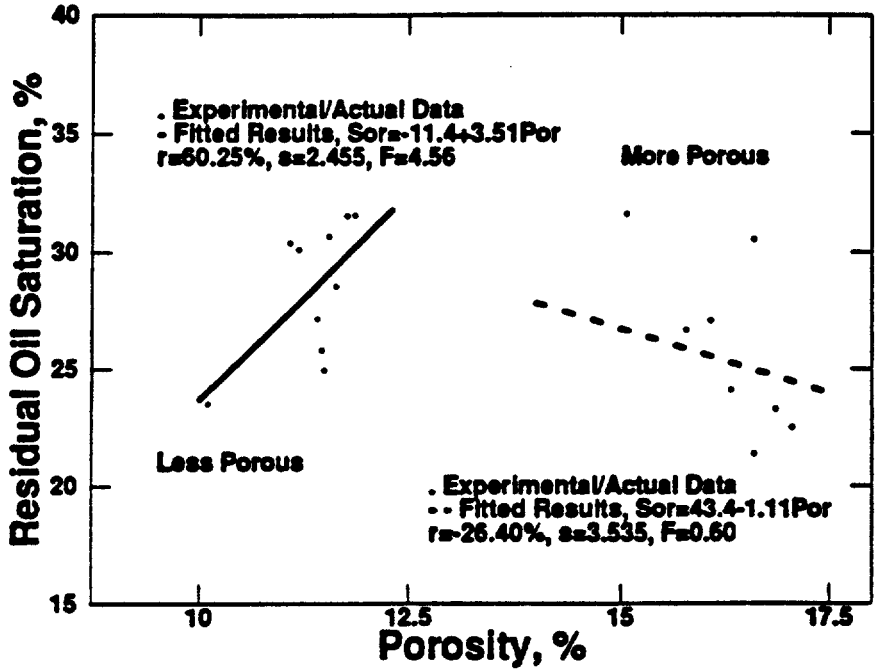

Fig. 5.28: Residual Oil Saturation vs. Porosity
for Indiana Limestone Radial-Cores.

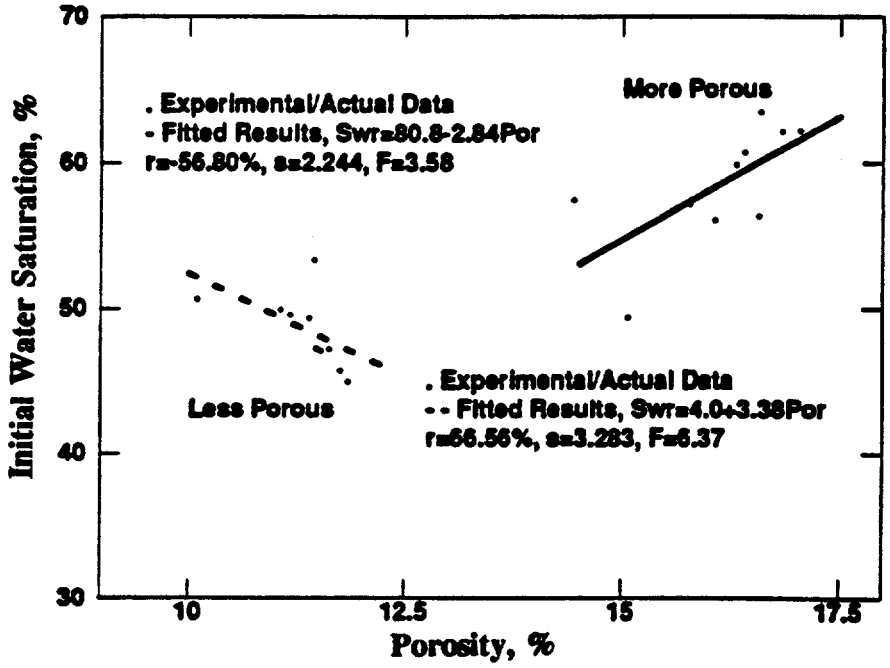

Fig. 5.29: Initial Water Saturation vs. Porosity
for Indiana Limestone Radial-Cores.

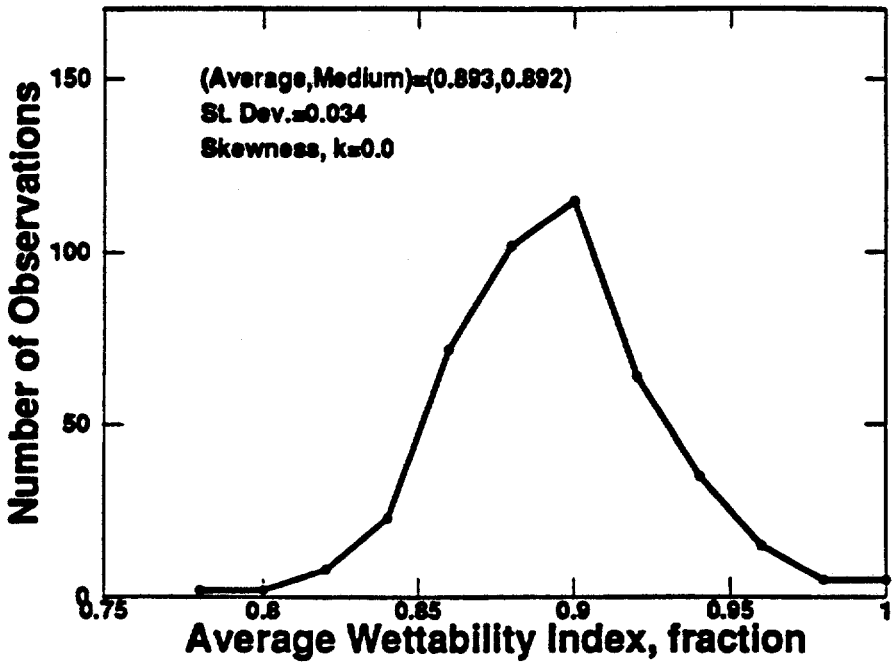

Fig. 5.30: Frequency Distribution for Wettability Indices for Indiana Limestone Radial-Cores.

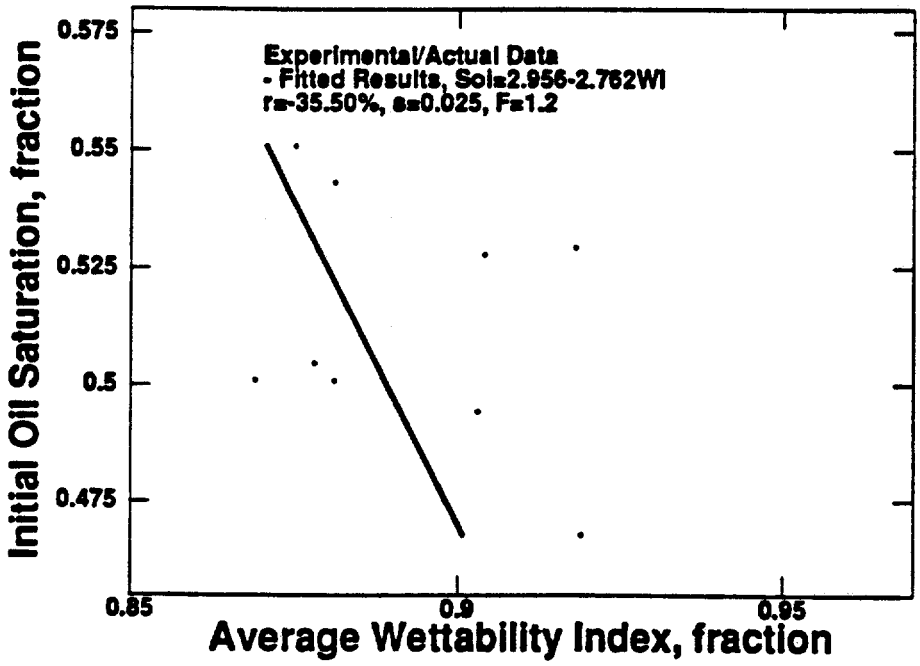

Fig. 5.31: Initial Oil Saturation vs. Average Wettability Index for Less Porous Indiana Limestone Radial-Cores.

shale are present in the matrix of the cores.

Figure 5.31 shows that initial oil saturations in Indiana limestone cores were inversely proportional to average wettability indices, for the less permeable cores. For the more permeable cores, average wettability index was found to be directly proportional to the initial oil saturation as shown in Fig. 5.32. This observation indicates that more porous Indiana limestone cores tend to be less water-wet than the less porous cores.

5.2.3 Mercury Porosimetry Properties

Conclusions regarding recovery efficiency relationships with respect to surface area and median pore-throat size are identical to the conclusions reached for Berea sandstone. Based on capillary pressure curves of pore-entry diameters and differential intrusion curves, pore-size distribution of Indiana limestone can be unimodal, bimodal or polymodal, as shown in Figs. 5.33 through 5.40. Unimodal and bimodal pore-size distributions are characteristic of the more permeable and more porous Indiana limestone core plugs. By contrast, the less porous and less permeable cores are associated with bimodal and polymodal pore-size distributions. This indicates that the pore-size distributions in the less porous and less permeable cores are not homogeneous. As indicated in Figs. 5.39 and 5.40, mercury recovery resulting from a core plug where a polymodal distribution predominates, is poor. However, as shown in Figs. 5.33 and 5.34, a unimodal pore-size distribution is associated with the highest mercury recovery. Figures 5.41 and 5.42 indicate that unimodal pore-size distributions which are associated with areas of discontinuity lead to lower recovery. Domains of secondary porosity are penetrated at high pressures. Extrusion from these domains is not complete which leads to the conclusion that areas of discontinuity are associated with secondary porosity and not with primary porosity as is the case of Berea sandstone rocks.

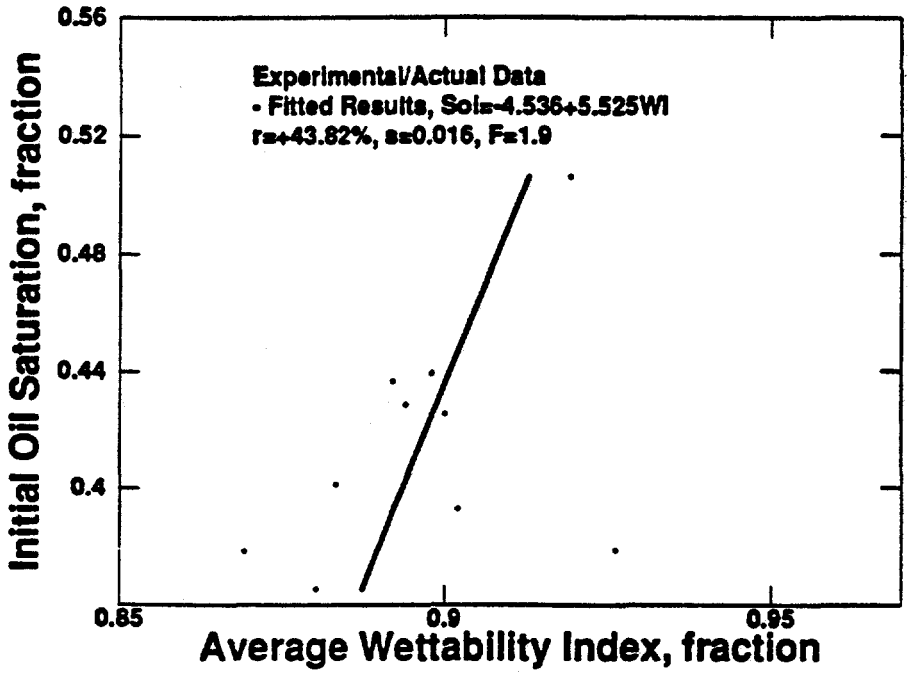

Fig. 5.32: Initial Oil Saturation vs. Average Wettability Index for More Porous Indiana Limestone Radial-Cores.

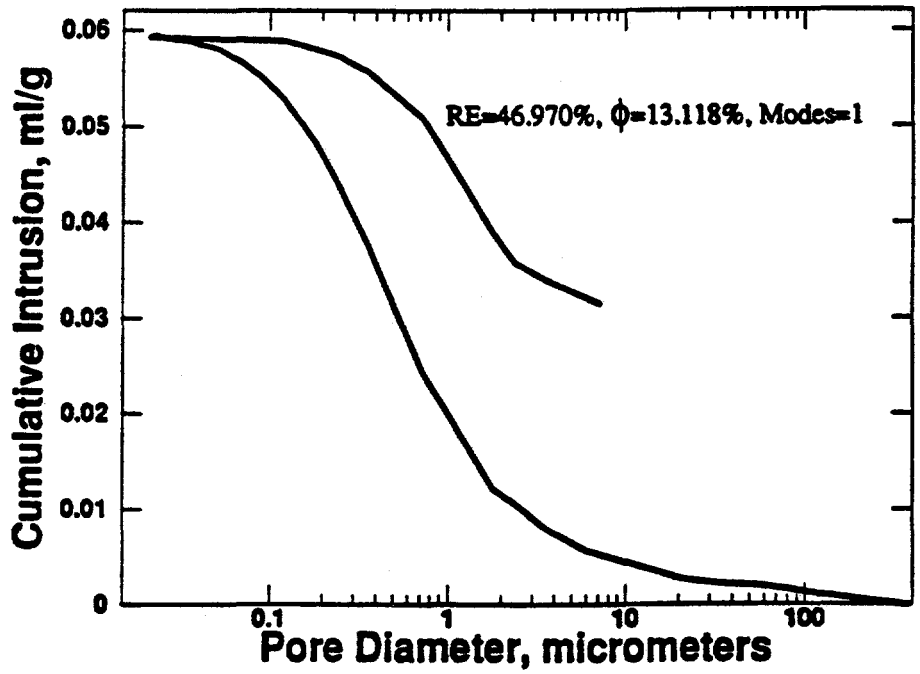

Fig. 5.33: Steep-Convex Unimodal Capillary-Pressure Curve for Tight Indiana Limestone Radial-Cores.

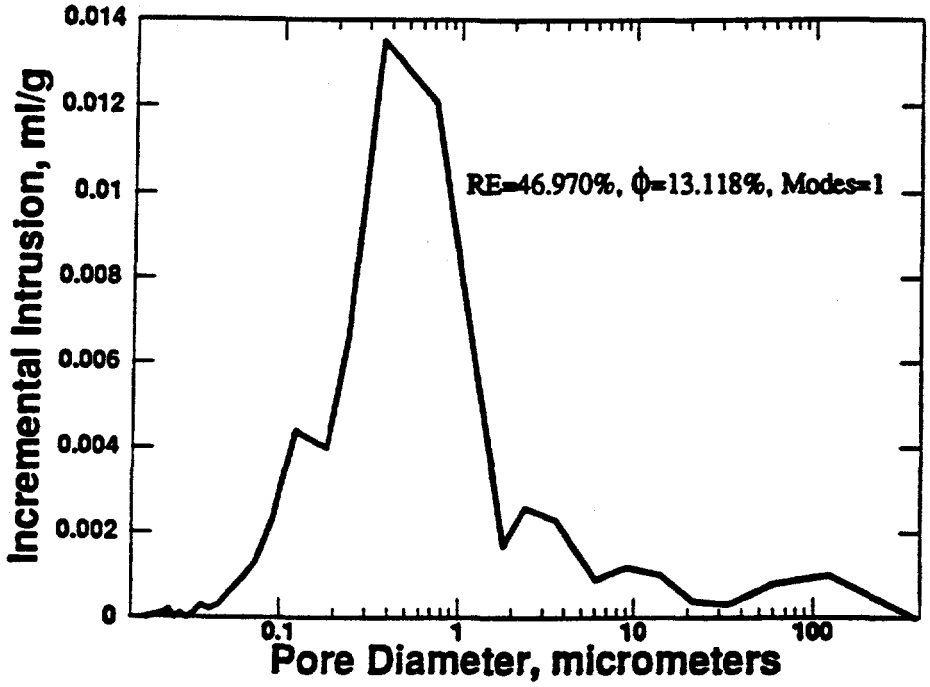

Fig. 5.34: Pore-Throat Size Distribution for Unimodal Tight Indiana Limestone Radial-Cores.

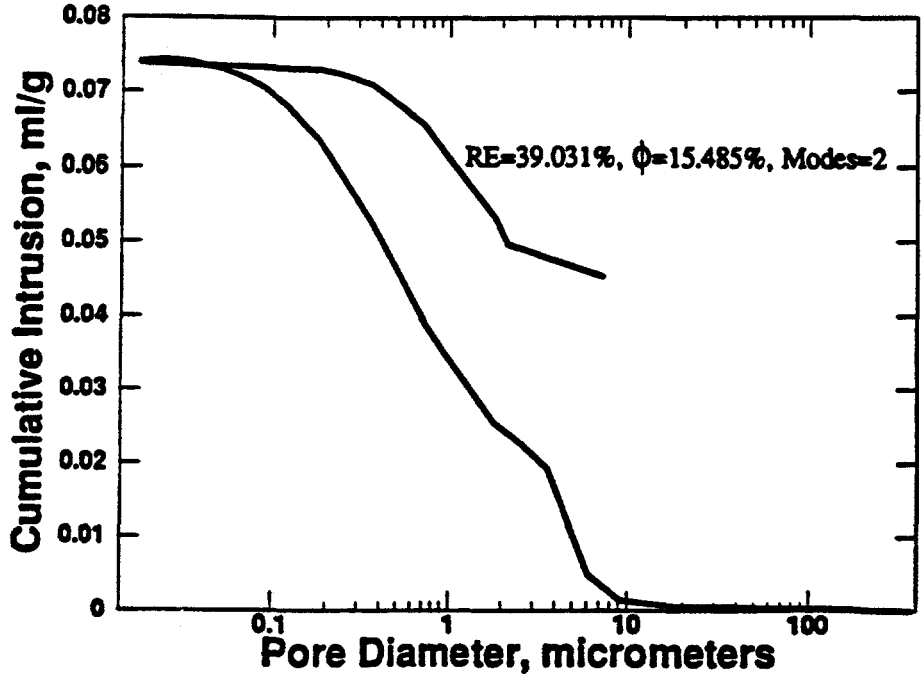

Fig. 5.35: Steep-Convex Bimodal Capillary-Pressure Curve for Permeable Indiana Limestone Radial-Cores.

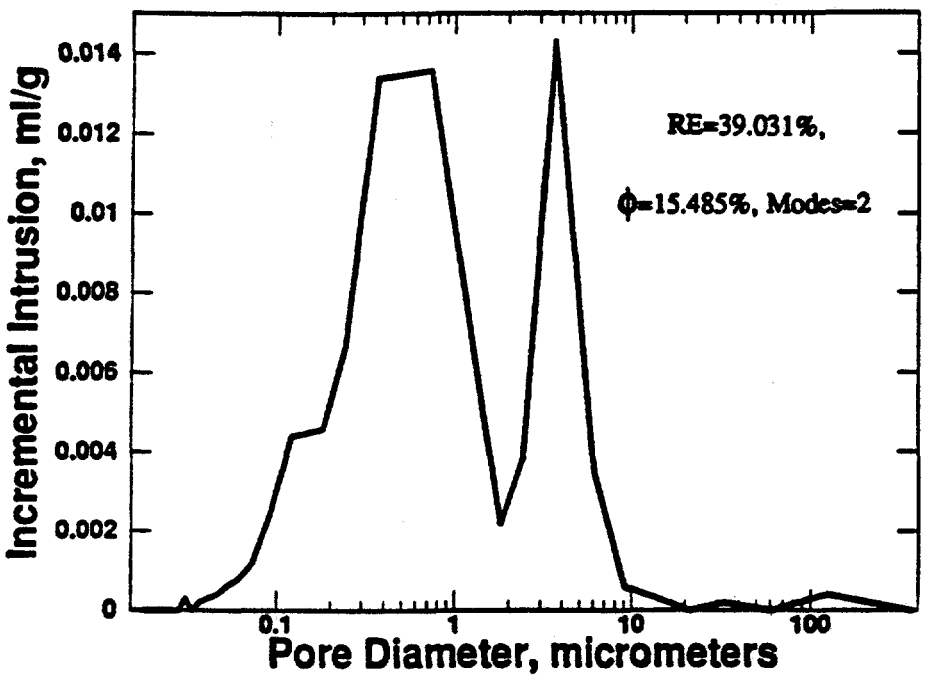

Fig. 5.36: Pore-Throat Size Distribution for Bimodal Permeable Indiana Limestone Radial-Cores.

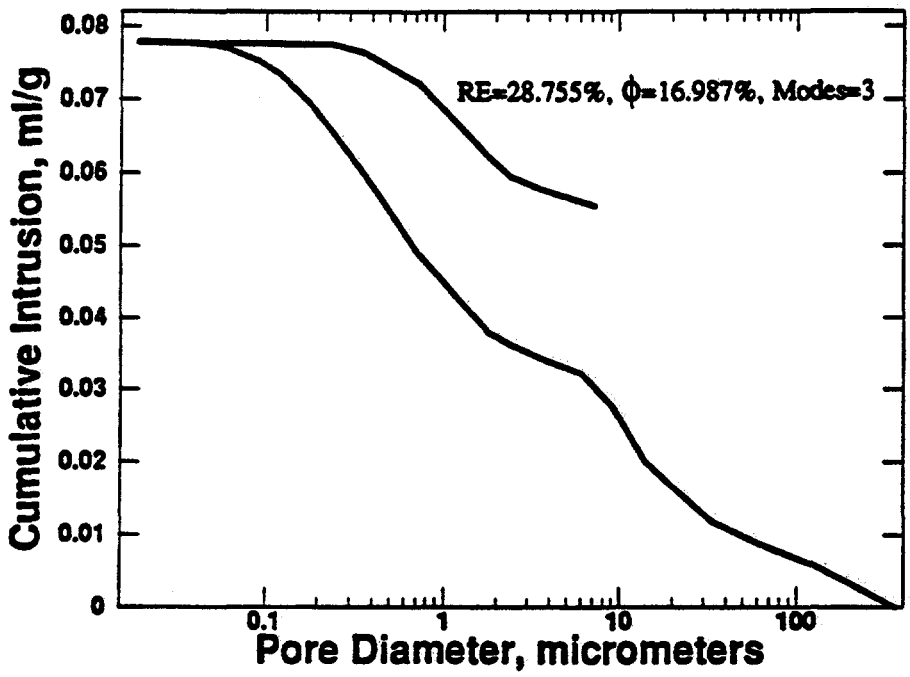

Fig. 5.37: Steep-Convex Trimodal Capillary-Pressure Curve for Permeable Indiana Limestone Radial-Cores.

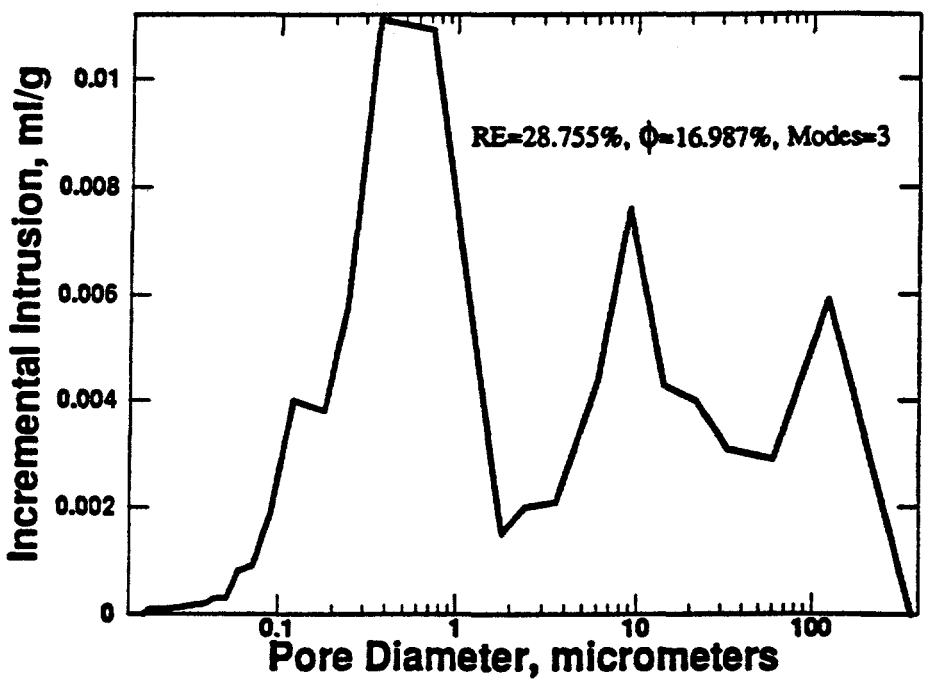

Fig. 5.38: Pore-Throat Size Distribution for Trimodal Permeable Indiana Limestone Radial-Cores.

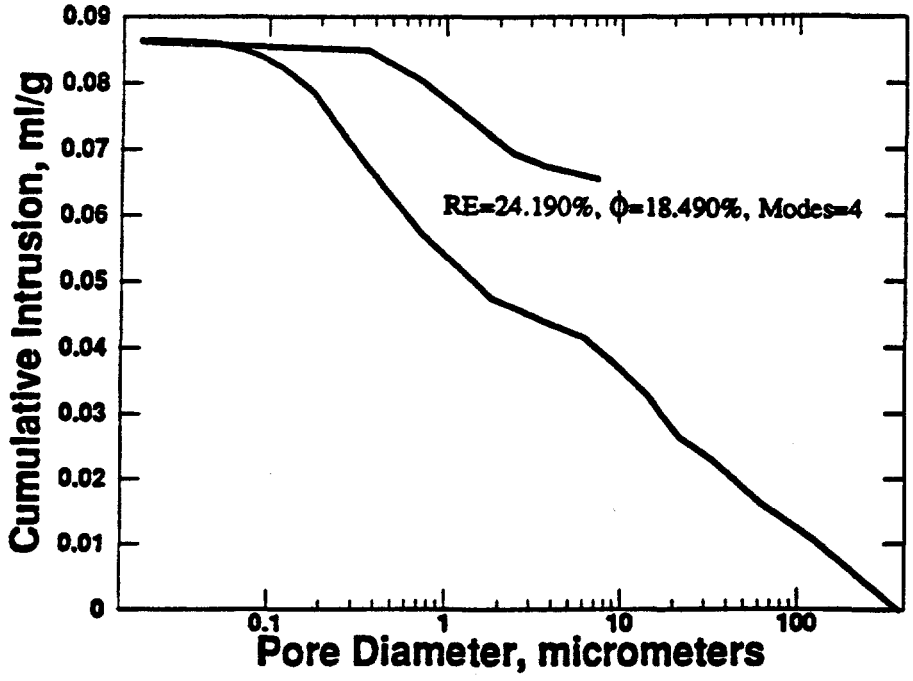

Fig. 5.39: Steep-Convex 4-modal Capillary-Pressure Curve for Permeable Indiana Limestone Radial-Cores.

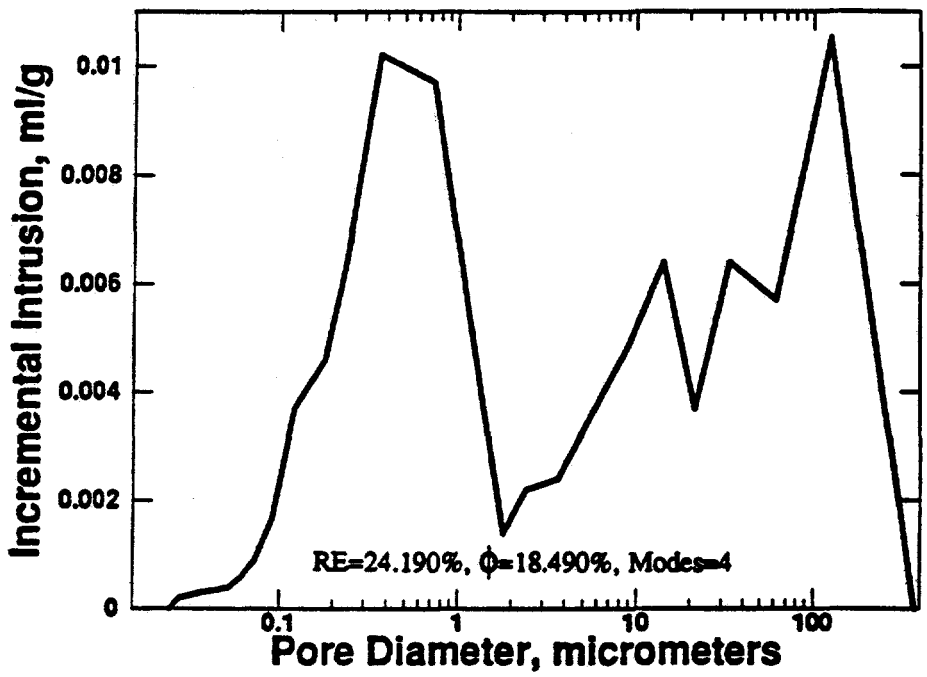

Fig. 5.40: Pore-Throat Size Distribution for 4-modal Permeable Indiana Limestone Radial-Cores.

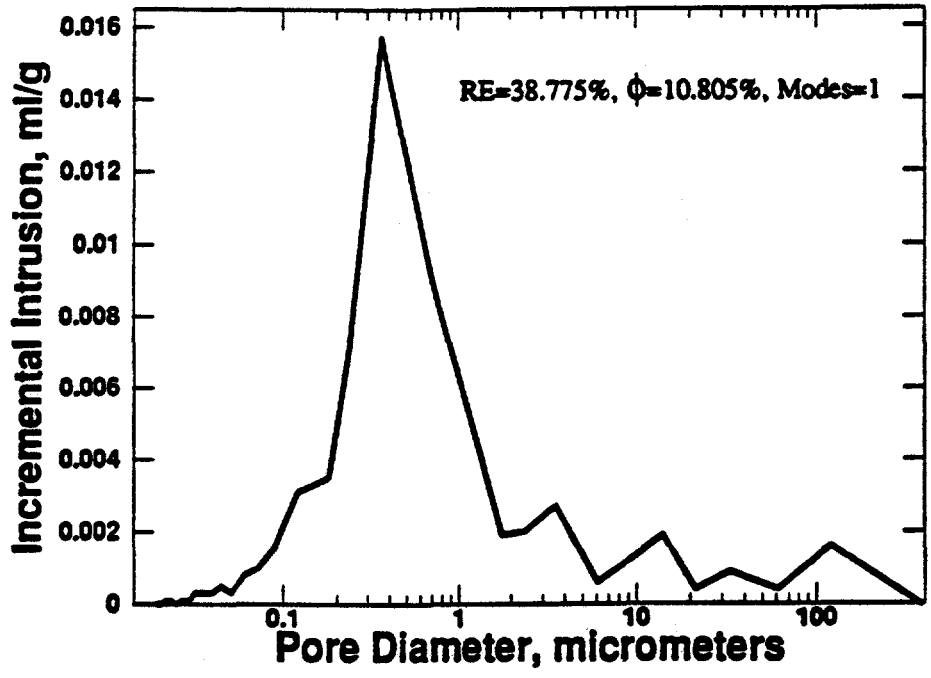

Fig. 5.41: Steep-Convex Unimodal Capillary-Pressure Curve for Tight Indiana Limestone Radial-Cores Associated With Areas of Discontinuity.

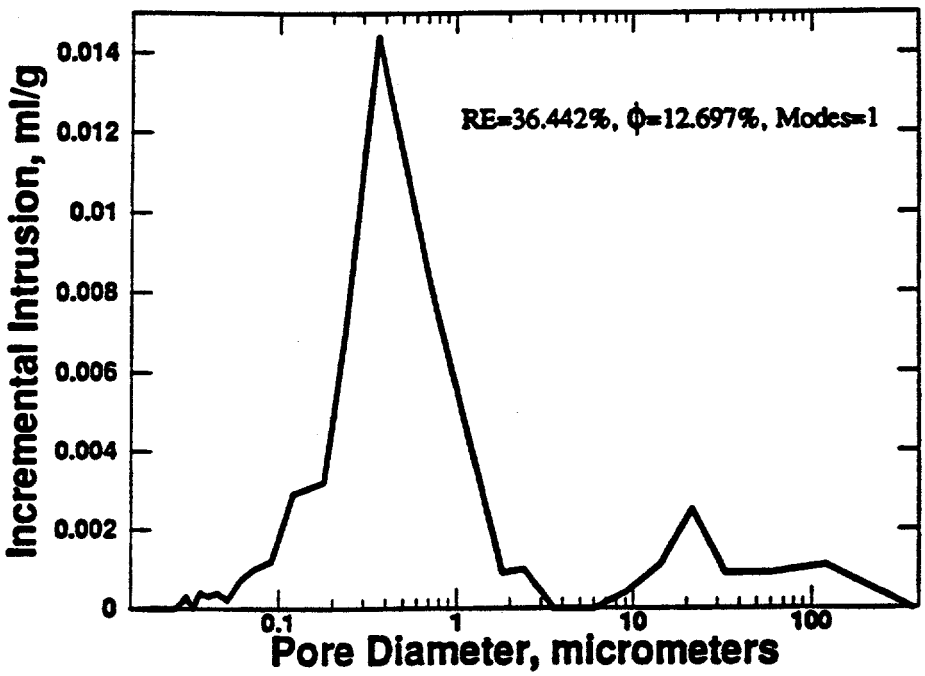

Fig. 5.42: Pore-Throat Size Distribution for Unimodal Tight Indiana Limestone Radial-Cores Associated With Areas of Discontinuity.

5.3 Sandstone Linear-Core Case

Twenty-one sets of waterflooding displacement tests were conducted in Berea sandstone linear-cores of varying lengths. Oil was displaced from the cores by brine at an overburden pressure of 500 psig and at a fixed temperature of 35°C. Brine was injected at rates varying from 1.2 to 7.9 cc/min, depending on the diameter and length of the core being tested. The injection rate for each core was determined using Eq. 2.1. In this study, the same numbered cores were taken from the same 3 ft. long core.

5.3.1 Introduction

Table 5.10 shows the waterflood properties of the Berea sandstone linear-cores. It also contains data for the cores average wettability indices. From the development, the error in porosity measurement is between 0.10 to 0.20%. The error in absolute permeability measurement is about 12.0% and the error in saturation measurement is between 0.07 to 0.23%.

Most of the figures in this chapter are fitted with trend lines using regression methods and the goodness of the correlations analyzed on the figures. The regressions were performed using MINITAB statistical computer package (Ryan et al., 1985). Statistical significance of the regressed equations were analyzed at significance levels, α, of 0.001, 0.005, 0.01, 0.05 and 0.1. These correspond to F-test statistic values of 17.27, 11.13, 8.90, 4.61 and 3.11, respectively (Neter et al., 1990). The plots of relationships that were found not to be statistically significant were either not presented in this report or not fitted with the trend lines. A brief discussion on various types of statistics used in these evaluations is provided in Appendix A.

A detailed statistical description of the experimental variables are shown in Table 5.11. Table 5.12 presents the correlation matrix for the waterflood and wettability properties

Table 5.10: Waterflood and Wettability Properties of the Berea Sandstone Linear-Cores

Core No.	S_{wi} (frac)	WI	S_{or} @ B.T. (frac)	S_{or} @ F.O. (frac)	OR @ B.T. (% IOIP)	UOR @ F.O. (% IOIP)
1A	0.682	0.569	0.113	0.102	64.40	67.89
1B	0.712	0.749	0.228	0.108	20.81	62.63
2A	0.598	0.569	0.298	0.197	27.43	51.96
2B	0.591	0.749	0.299	0.186	26.86	51.48
3A	0.538	0.616	0.347	0.239	24.87	48.44
3B	0.532	0.712	0.263	0.171	43.79	63.44
4A	0.571	0.423	0.319	0.194	25.64	54.77
4B	0.548	0.464	0.159	0.133	64.71	70.63
5A	0.586	0.856	0.324	0.173	21.74	56.23
5B	0.557	0.592	0.363	0.243	18.05	45.19
6A	0.553	0.514	0.322	0.184	27.97	58.89
6B	0.634	0.390	0.181	0.142	50.58	61.25
7A	0.311	0.633	0.241	0.228	64.99	66.88
7B	0.375	0.638	0.249	0.242	60.04	61.29
7C	0.204	0.602	0.321	0.301	59.66	62.15
8A	0.125	0.642	0.290	0.249	66.88	71.52
8B	0.142	0.519	0.313	0.223	63.49	74.00
8C	0.107	0.636	0.279	0.204	68.82	77.22
8D	0.098	0.562	0.357	0.263	60.41	70.85
8E	0.726	0.379	0.124	0.042	54.75	84.66
8F	0.741	0.391	0.114	0.060	55.93	77.04

Table 5.11: Statistical Description of the Waterflood and Wettability Experimental Variables for Berea Sandstone Linear-Cores

	OR @ B.T. (% IOIP)	UOR @ F.O. (%IOIP)	S_{or} @ B.T. (frac)	S_{or} @ F.O. (frac)	ϕ (frac)	k (md)	WI	$Ln_{w}\mu_{w}$	S_{wi} (frac)	N^{o}_{ca} (E-07)
Mean	46.28	63.73	0.262	0.185	0.194	188.8	0.581	5.132	0.473	16.65
Median	54.75	62.63	0.290	0.194	0.204	203.7	0.592	5.096	0.553	8.33
Min.	18.05	45.19	0.113	0.042	0.124	75.7	0.379	4.992	0.098	6.63
Max.	68.82	84.66	0.363	0.301	0.235	321.2	0.856	5.410	0.741	43.50
Q1	26.25	55.50	0.204	0.138	0.172	83.9	0.489	5.034	0.258	7.16
Q3	63.95	71.18	0.321	0.241	0.224	270.9	0.640	5.221	0.616	29.12
St. Dev.	18.71	10.32	0.080	0.015	0.033	85.9	0.127	0.118	0.219	13.64

Table 5.12: Correlation Matrix for the Waterflood and Wettability Properties for Berea Sandstone Linear-Cores

	ϕ	k	WI	S_{wi}	S_{or}	S_{or}	OR
k	0.884						
WI	-0.329	-0.267					
S_{wi}	-0.030	0.059	-0.176				
S_{or} @ B.T.	-0.473	-0.493	0.443	-0.496			
S_{or} @ F.O.	-0.296	-0.399	0.350	-0.755	0.826		
OR @ B.T.	0.436	0.338	-0.304	-0.547	-0.437	-0.026	
UOR @ F.O.	0.447	0.461	-0.377	-0.257	-0.588	-0.409	0.787

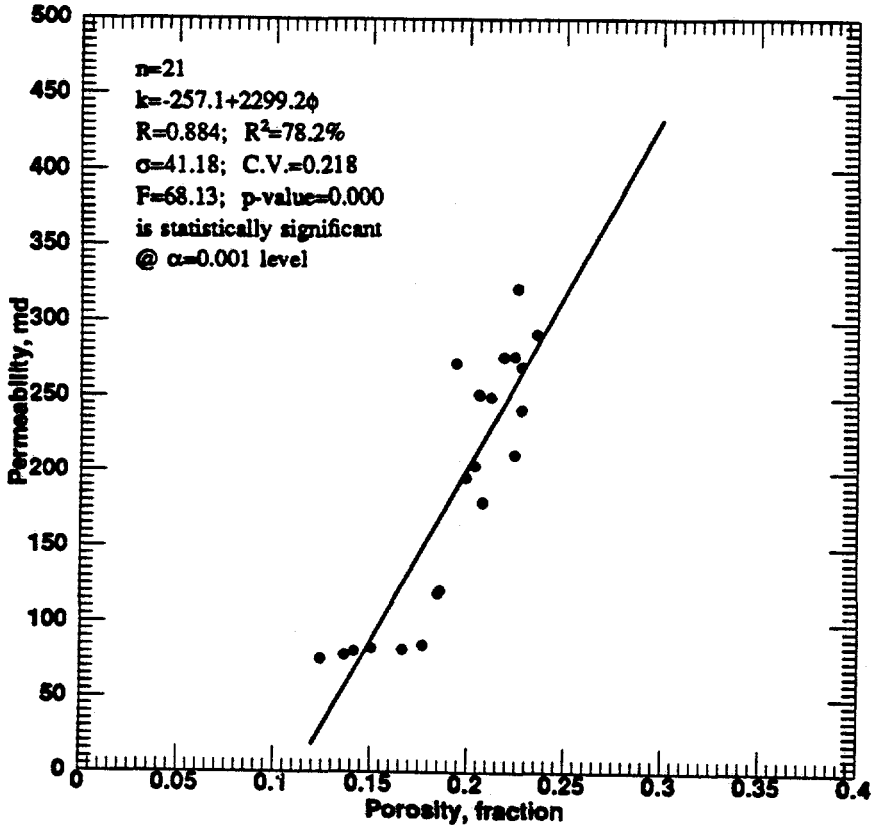

Fig. 5.43: Permeability vs. Porosity for Berea Sandstone Linear-Cores.

for the Berea sandstone linear-cores. In this table, a positive value of correlation coefficient in the matrix implies a direct relationship between two specified variables. A negative value of correlation coefficient implies an inverse relationship between two specified variables, in the correlation matrix.

5.3.2 Petrophysical Properties

In this report, the term petrophysical properties include porosity, and permeability data determined from standard core analyses technique. For all the 21 Berea sandstone cores combined, the porosities varied from 12.4 to 23.5%, and the absolute permeabilities varied from 75.7 to 321.2 md. The core samples of the same numbered cores exhibited porosity values that vary only slightly, but the variations in the absolute permeability values are more pronounced.

The absolute permeability versus porosity for the 21 core samples are plotted in Fig. 5.43. As expected for Berea sandstones, permeability is directly related to porosity for sandstones. The relationship of absolute permeability with porosity is strong with a R^2 of about 78% and the relationship is statistically significant at $\alpha = 0.001$ level. Since the coefficient of variance of the relationship is less than 1.0, it indicates that no erratic data points are present. This form of trend between permeability and porosity is similar to published trends in the literature (Archie, 1942; Wyllie and Gregory, 1953; Amyx et al., 1960; and Lynch, 1962).

5.3.3 Waterflood Properties

Waterflood properties include irreducible water saturation, residual oil saturation and oil recovery data. The residual oil saturation and the oil recovery are measured at breakthrough and at floodout. Breakthrough occurs when water is first produced at the

outlet and floodout occurs at infinite water to oil ratio (or at a water to oil ratio of about 400:1, for the purpose of this study). Plots of the cumulative oil recovery in percent of initial oil-in-place as a function of cumulative brine injected in pore volume for the 21 core samples tested are presented in Figs. 5.44 through 5.47. The results of all the same numbered linear-core samples were similar, whereas those of the six core samples numbered 1, 3 and 4 varied widely, but are of the same trend. This might be due to the fact that these six samples were slightly shaly. Visual inspection of the cores indicated the shaly nature of the samples considered. Moreover, compared to the other Berea sandstone cores that were greyish in color, these cores were reddish-orange in color with streaks of shaly minerals. Berea sandstone cores similar to these were also studied by Churcher et al. (1991). They referred to them as Orange Berea sandstones. These Orange Berea sandstones rest unconformably in the lower unit of the underlying red Bedford and Chagrin shales in Ohio. This type of Berea sandstone is characterized by its high angle cross-bedding and it is coarser-grained and more poorly-sorted than the other types of Berea sandstones.

The production performance (producing water/oil ratio as a function of cumulative oil recovery in percent initial oil-in-place) for each of the 21 core samples are shown in Figs. 5.48 through 5.51. In all the tests, the water breakthrough point occurred at less than 0.4 pore volume of injected brine. After breakthrough, increasing amounts of water and decreasing amounts of oil are produced.

Furthermore, another observation from Table 5.10 and Figs. 5.44 through 5.51 is that in strongly water-wet floods, breakthrough occurs relatively late and very little oil is produced after water breakthrough, as shown for example in the plots of Core Sample Nos. 1A, 4B, 7A, 7B, and 7C. Also, the water/oil ratio in strongly water-wet floods rises rapidly. However, in weakly water-wet floods, breakthrough occurs at an earlier time and the water/oil ratio rises gradually, as shown for example in the plots of Core Sample Nos. 1B,

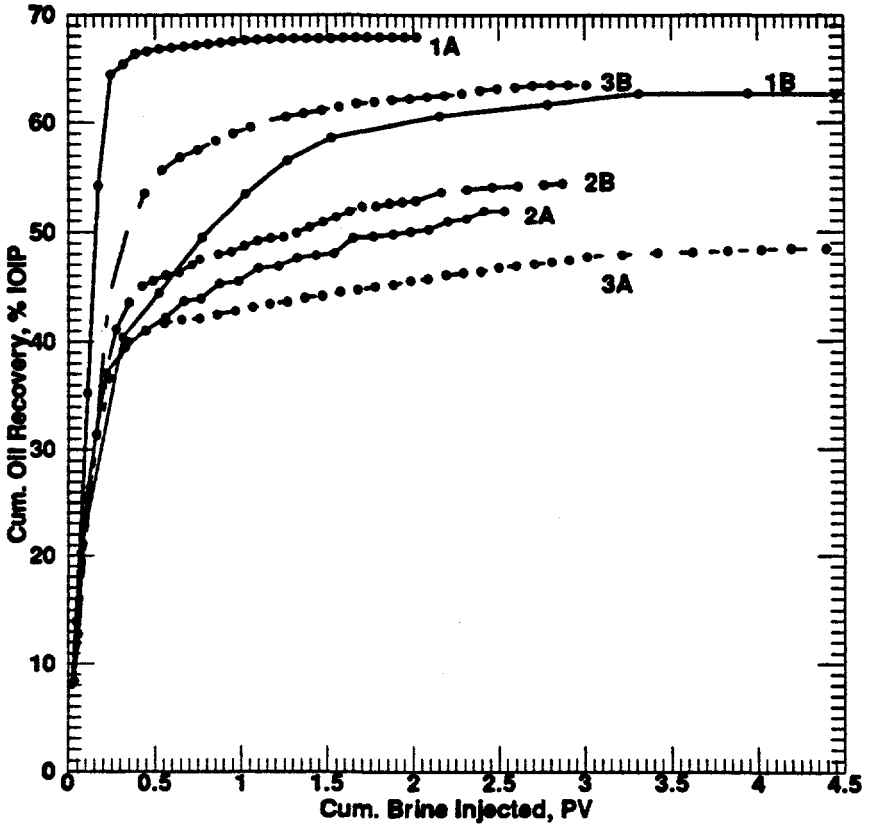

Fig. 5.44 Cumulative Oil Recovery vs. Cumulative Brine Injected for Berea Sandstone Linear-Core Samples 1A, 1B, 2A, 2B, 3A and 3B.

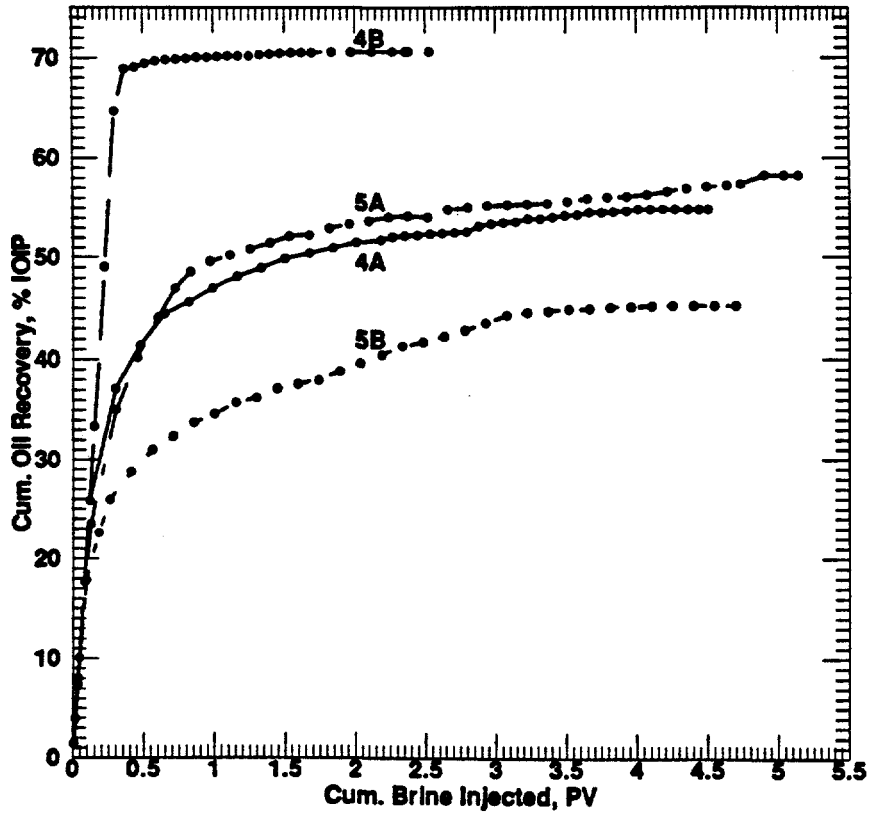

Fig. 5.45: Cumulative Oil Recovery vs. Cumulative Brine Injected for Berea Sandstone Linear-Core Samples 4A, 4B, 5A and 5B.

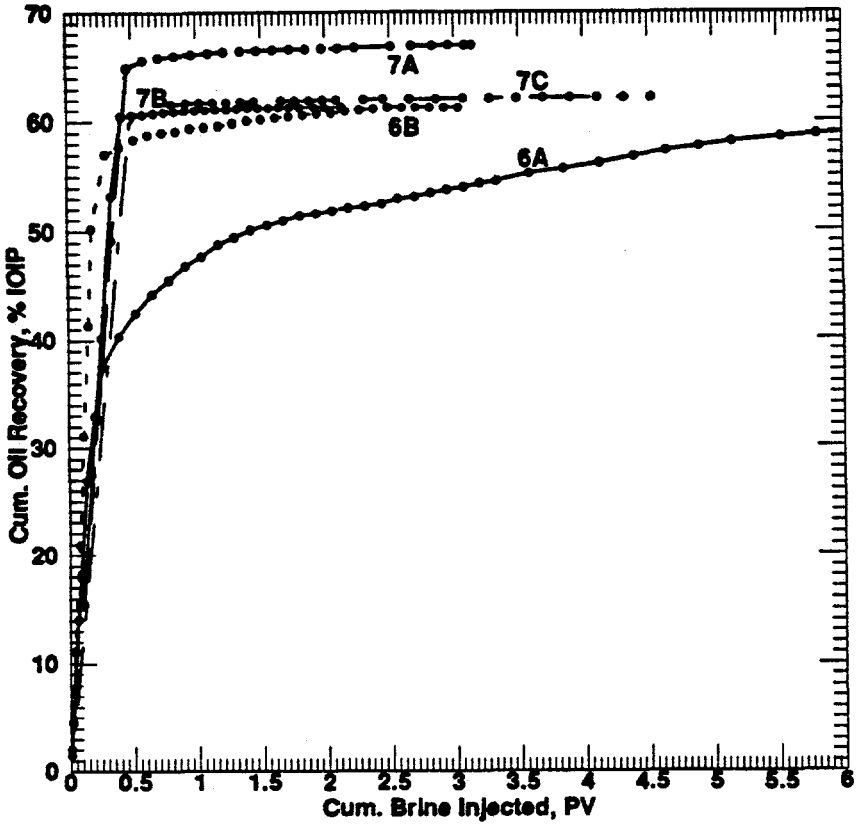

Fig. 5.46: Cumulative Oil Recovery vs. Cumulative Brine Injected for Berea Sandstone Linear-Core Samples 6A, 6B, 7A, 7B and 7C.

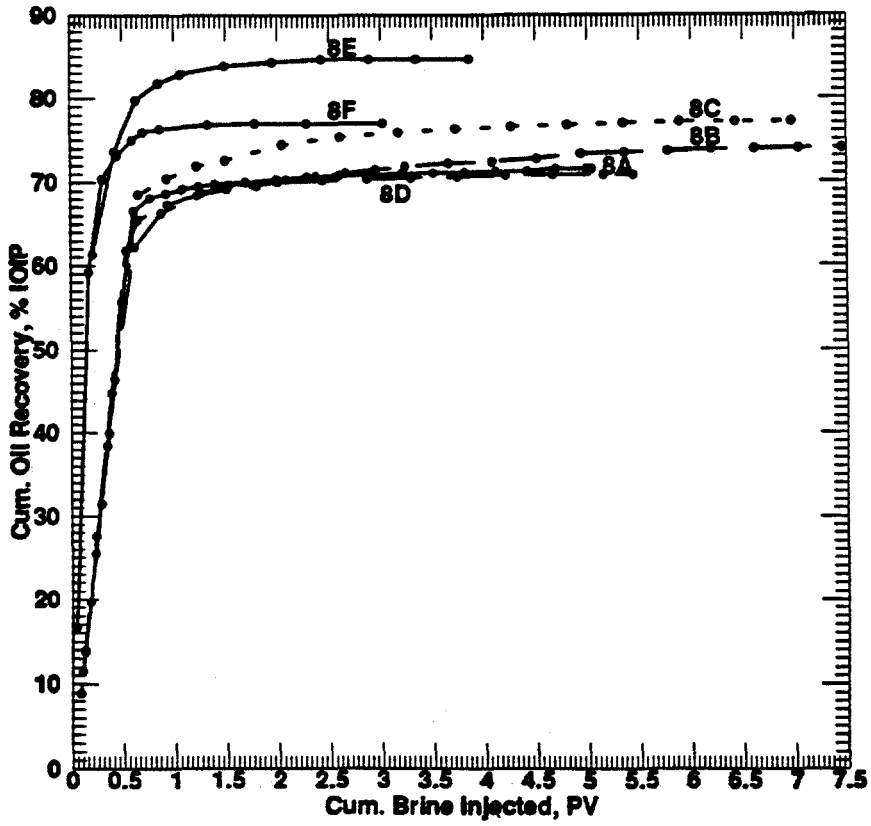

Fig. 5.47: Cumulative Oil Recovery vs. Cumulative Brine Injected for Berea Sandstone Linear-Core Samples 8A, 8B, 8C, 8D, 8E and 8F.

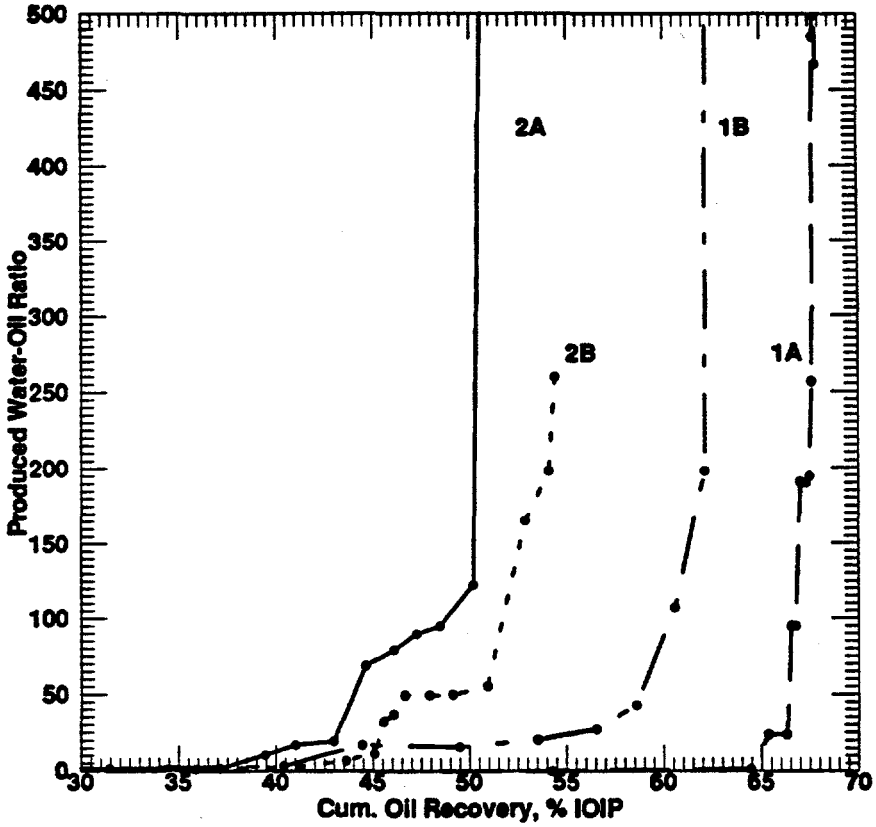

Fig. 5.48: Produced Water-Oil Ratio vs. Cumulative Oil Recovery for Berea Sandstone Linear-Core Samples 1A, 1B, 2A, and 2B.

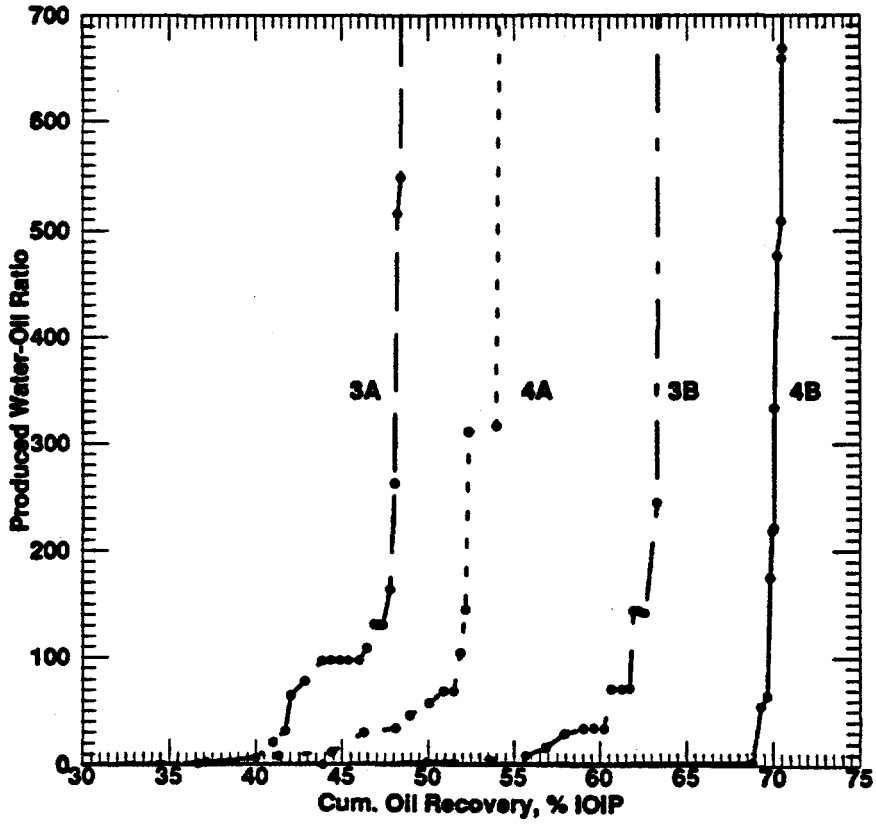

Fig. 5.49: Produced Water-Oil Ratio vs. Cumulative Oil Recovery for Berea Sandstone Linear-Core Samples 3A, 3B, 4A and 4B.

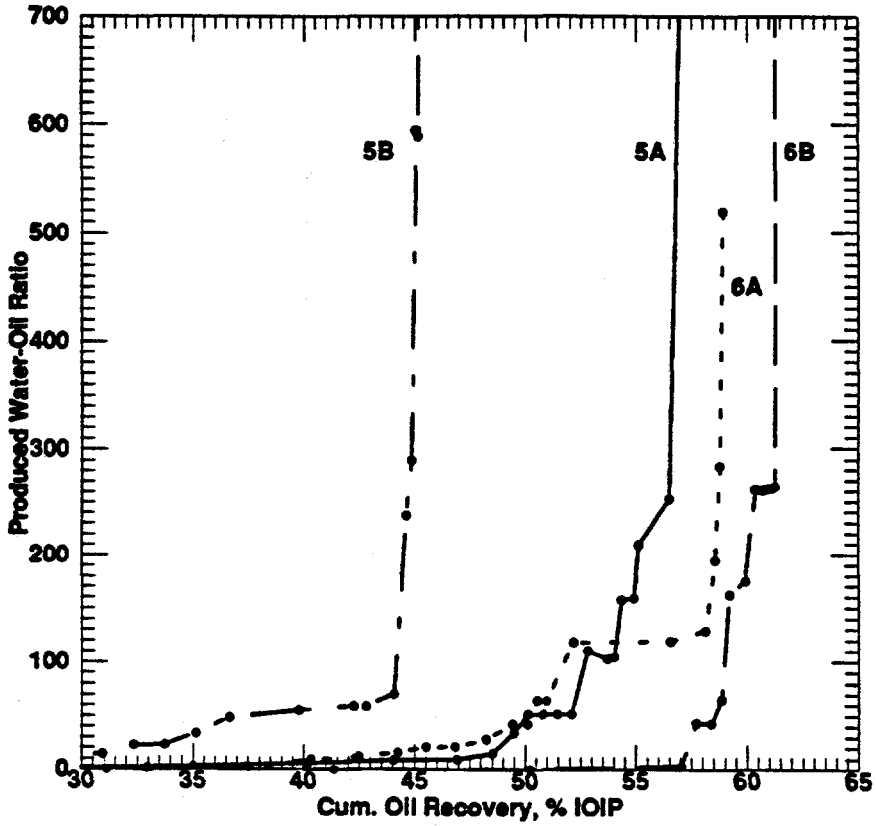

Fig. 5.50: Produced Water-Oil Ratio vs. Cumulative Oil Recovery for Berea Sandstone Linear-Core Samples 5A, 5B, 6A and 6B.

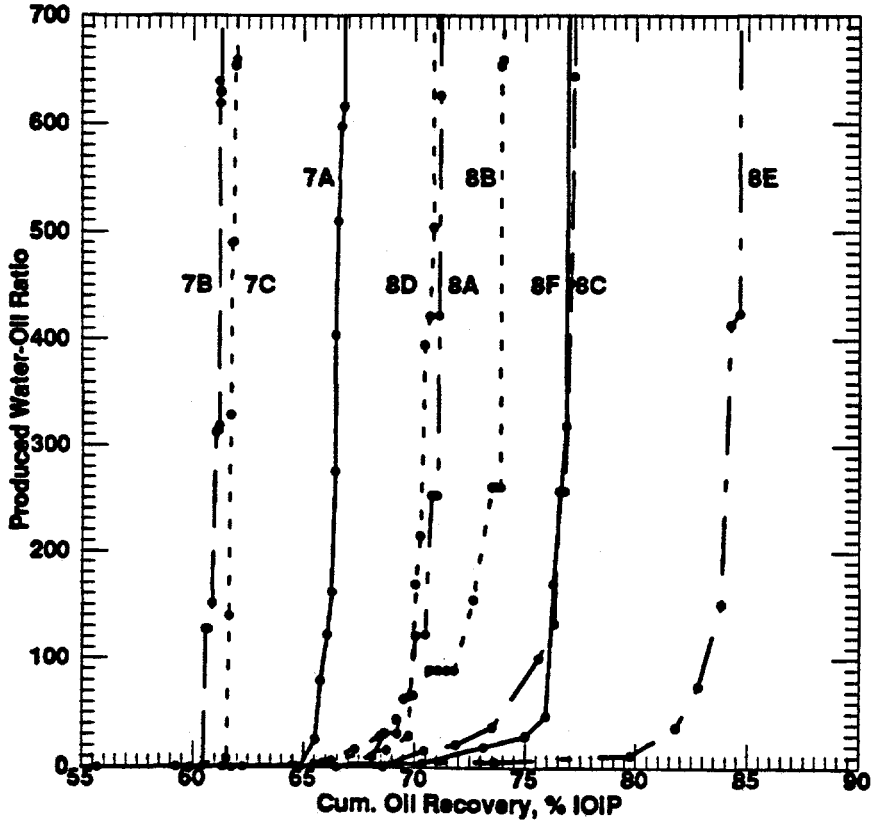

Fig. 5.51: Produced Water-Oil Ratio vs. Cumulative Oil Recovery for Berea Sandstone Linear-Core Samples 7A, 7B 7C, 8A, 8B, 8C, 8D, 8E and 8F.

2A, 2B, 3A, 3B, 4A, 5A, 5B, 6A, and 8E. More amount of water must be injected to recover the same amount of oil in the weakly water-wet system. It is generally agreed that the residual oil saturation at floodout is lower in water-wet systems. That is, more oil is produced in a uniformly water-wet system than would be produced in uniformly oil-wet system with the same pore geometry (Anderson, 1987c).

According to Anderson (1987c), there are different oil saturations of interest in waterflooding: breakthrough saturation, practical (or economical) saturation, and true residual saturation. He noted that all the three saturations are essentially equal in a strongly water-wet systems with a moderate oil/water viscosity ratio. The saturations can differ greatly however, in intermediate and oil-wet systems or in water-wet systems with a large oil/water viscosity ratio. The lower the oil saturation in the reservoir rock at breakthrough (and the higher the oil recovery), the more economically attractive a waterflood will be.

For the purpose of this study, residual oil saturation at breakthrough and at floodout, correspond to Anderson's (1987c) breakthrough saturation and practical (or economical) saturation, respectively. The corresponding oil recovery values are oil recovery at breakthrough and at floodout (or ultimate oil recovery). Figure 5.52 is the residual oil saturation profiles at breakthrough and at floodout for sandstone cores. The oil recovery profiles at breakthrough and at floodout is shown in Fig. 5.53. As presented in Table 5.11, the residual oil saturation ranged from 0.113 to 0.363 at breakthrough and from 0.042 to 0.301 at floodout. At breakthrough the oil recovery values ranged from 18.1 to 68.8 %IOIP and at floodout the ultimate oil recovery ranged from 45.2 to 84.7 %IOIP. The irreducible water saturation ranged from 0.098 to 0.741, with a value of 0.473. Chatzis et al. (1983) observed that Berea sandstone usually retains a high residual oil saturation, approximately 0.350, following waterflooding.

The irreducible water saturation versus residual oil saturation at breakthrough and at

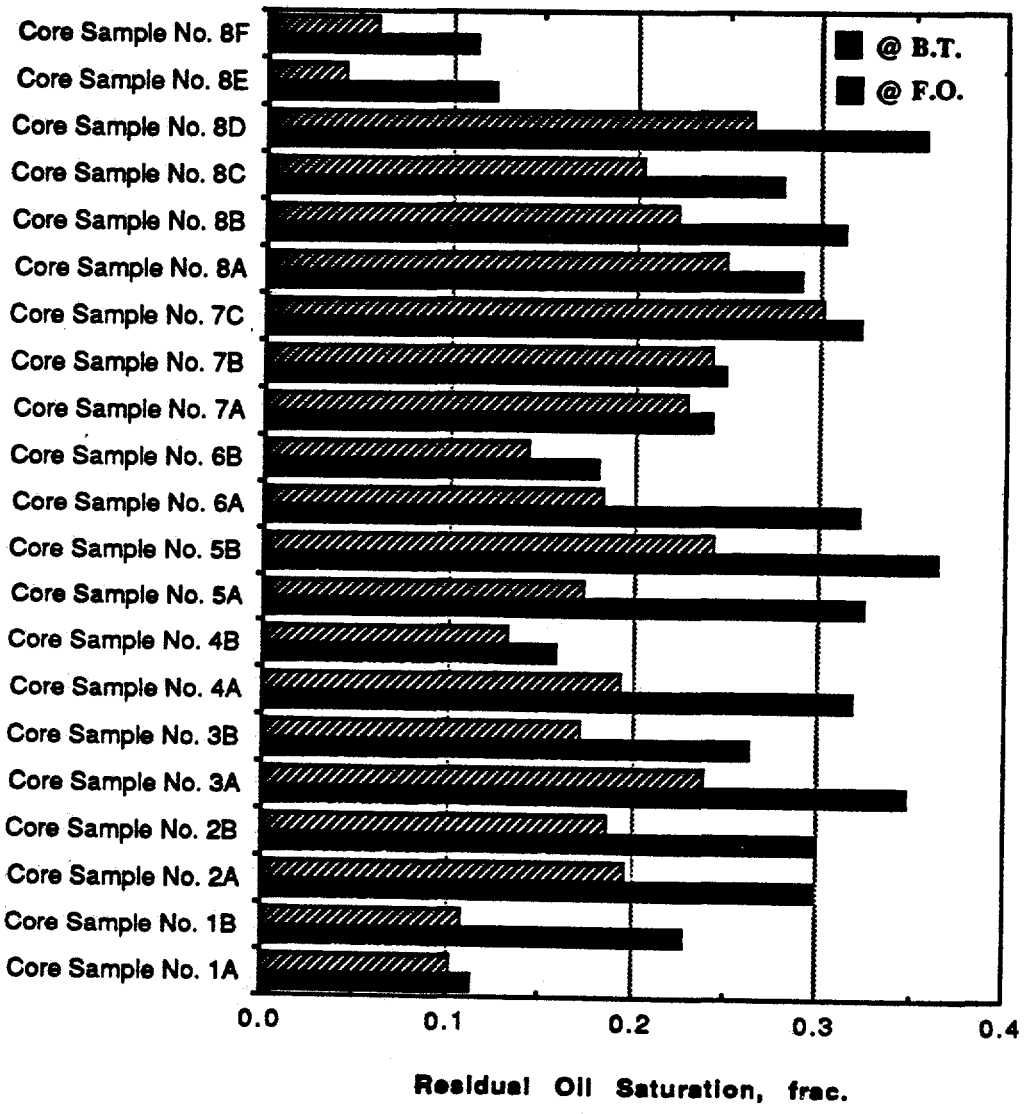

Fig. 5.52: Residual Oil Saturation Profiles at Breakthrough and Floodout for Berea Sandstone Linear-Cores.

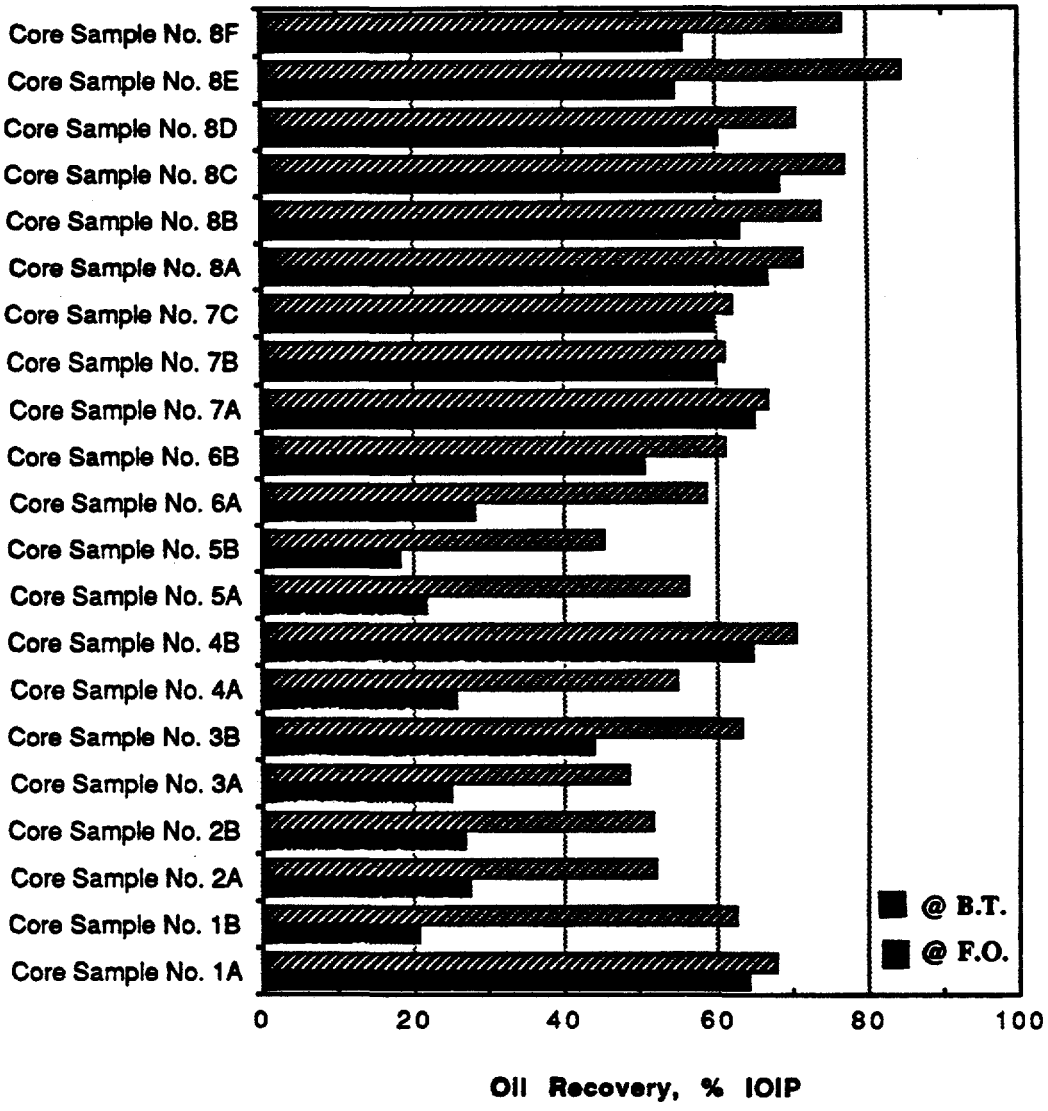

Fig. 5.53: Oil Recovery Profiles at Breakthrough and Floodout for Berea Sandstone Linear-Cores.

floodout are plotted in Figs. 5.54 and 5.55. The irreducible water saturation is inversely related to residual oil saturation at breakthrough and at floodout. The irreducible water saturation versus oil recovery at breakthrough and at floodout are plotted in Figs. 5.56 and 5.57. The irreducible water saturation is inversely related to oil recovery at breakthrough. This observation is in agreement with Pickell et al. (1966) who observed that residual oil saturation is dependent on initial oil content. The relationship of irreducible water saturation with ultimate oil recovery at floodout is not statistically significant. Figures 5.58 and 5.59 show the relationships between oil recovery and residual oil saturation at breakthrough and floodout, respectively. The plots show that oil recovery is inversely related to residual oil saturation, at $\alpha = 0.05$ level for case at breakthrough, and at $\alpha = 0.1$ for the case at floodout.

5.3.3.1 Relation Between Waterflood and Petrophysical Properties

The relationships of petrophysical properties such as porosity, and permeability on residual oil saturation and oil recovery from waterflooding were also investigated. As shown in Table 5.12, the relationships are weak in the case of porosity and permeability. From inspection of Table 5.12, a tendency for oil recovery to increase as porosity and permeability increased was observed. There is a tendency for residual non-wetting-phase saturation to increase as porosity and permeability decreased.

5.3.3.2 Scaling Coefficient and Capillary Number

The experimental design was properly scaled by keeping the scaling coefficient close to a value of 5.0 cm^2.cp/min. The values of the capillary number varied from $6.63*10^{-7}$ to $4.35*10^{-6}$, with a mean value of $1.67*10^{-6}$, as presented in Table 4.3. Core floods having capillary number values that are larger than 10^{-6}, such as core samples 1B, and 7A through 8F, were expected not to have their residual oil saturation values influenced by capillary

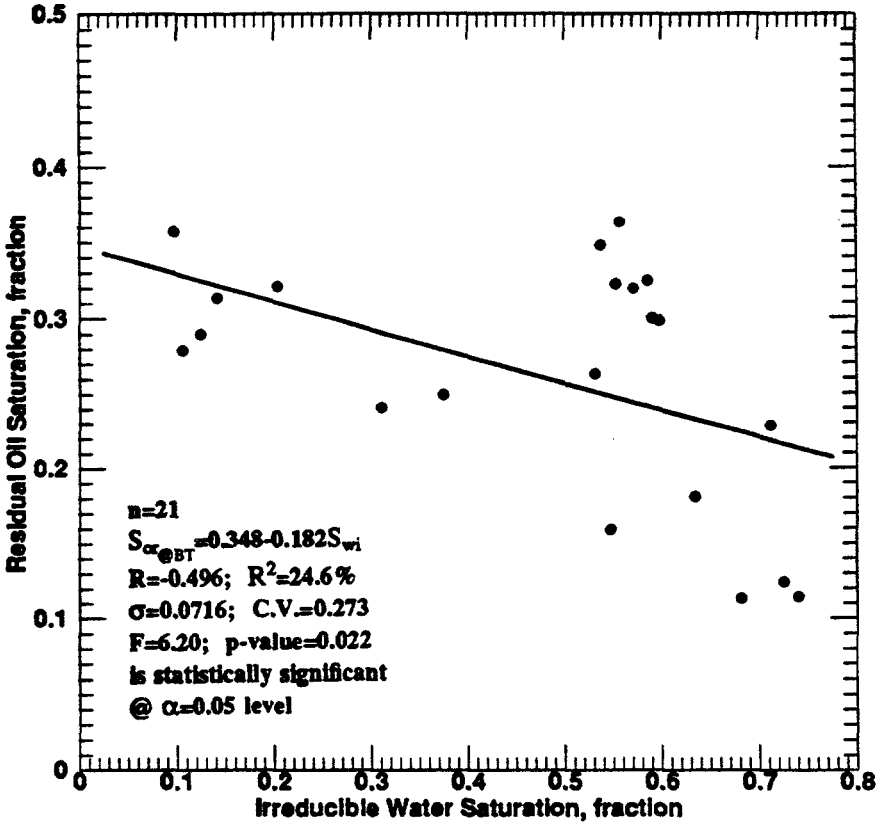

Fig. 5.54: Residual Oil Saturation vs. Irreducible Water Saturation for Berea Sandstone Linear-Cores at Breakthrough.

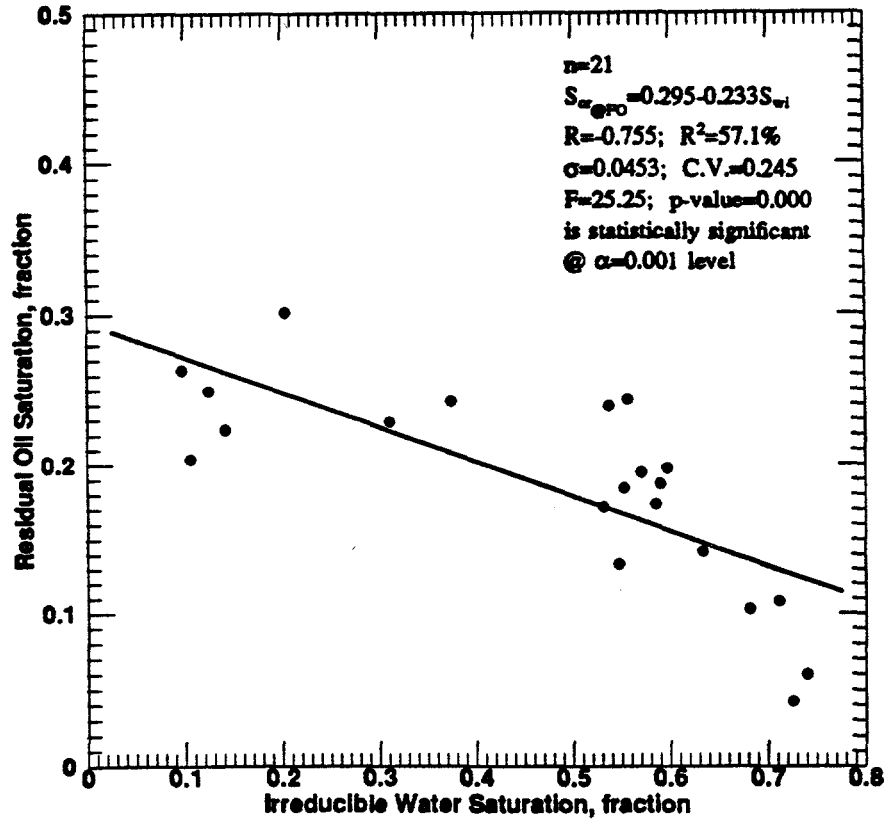

Fig. 5.55: Residual Oil Saturation vs. Irreducible Water Saturation for Berea Sandstone Linear-Cores at Floodout.

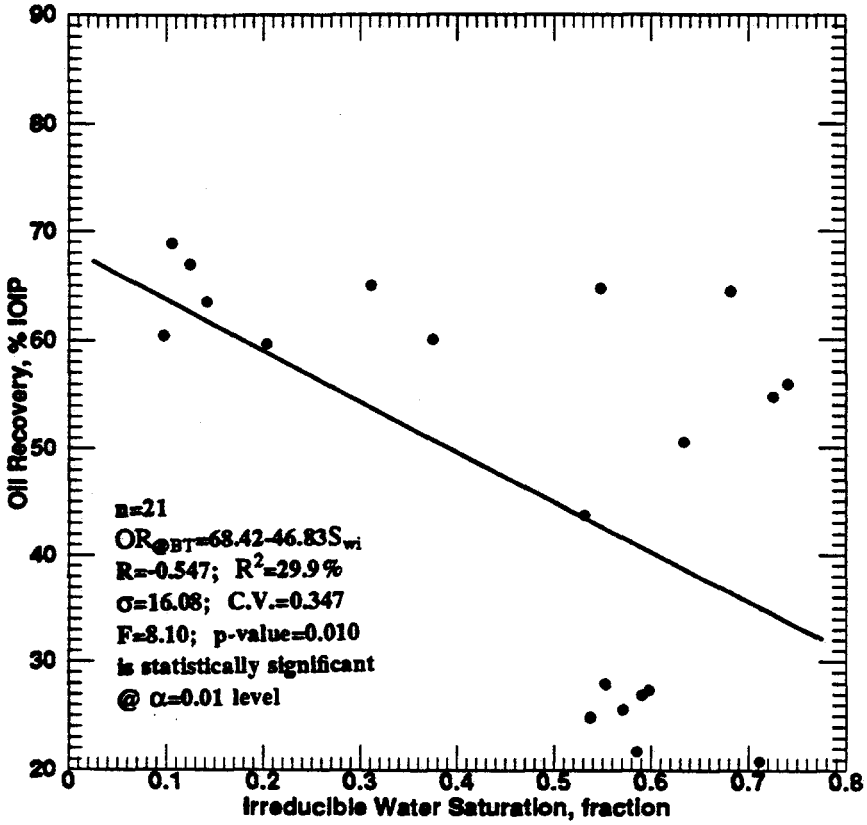

Fig. 5.56: Oil Recovery vs. Irreducible Water Saturation for Berea Sandstone Linear-Cores at Breakthrough.

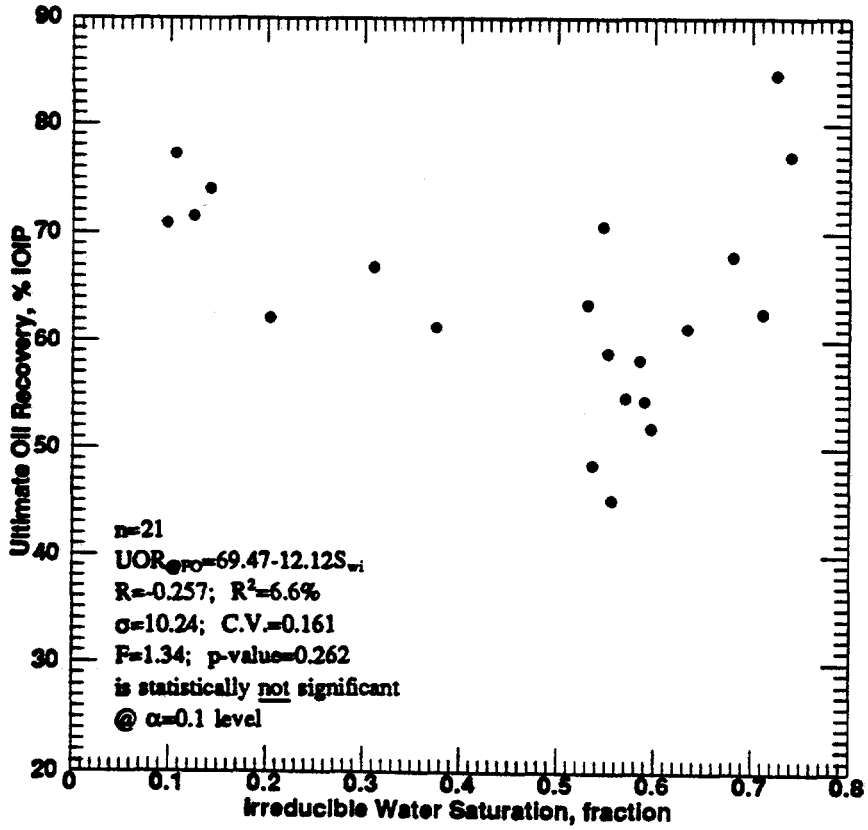

Fig. 5.57: Ultimate Oil Recovery vs. Irreducible Water Saturation for Berea Sandstone Linear-Cores at Floodout.

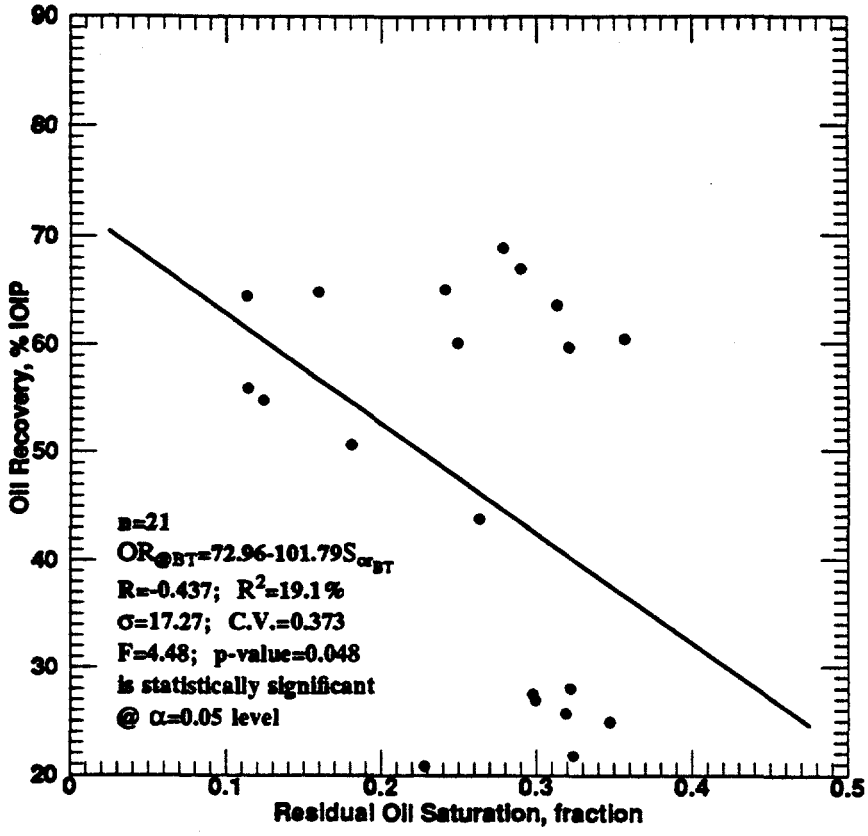

Fig. 5.58: Oil Recovery vs. Residual Oil Saturation for Berea Sandstone Linear-Cores at Breakthrough.

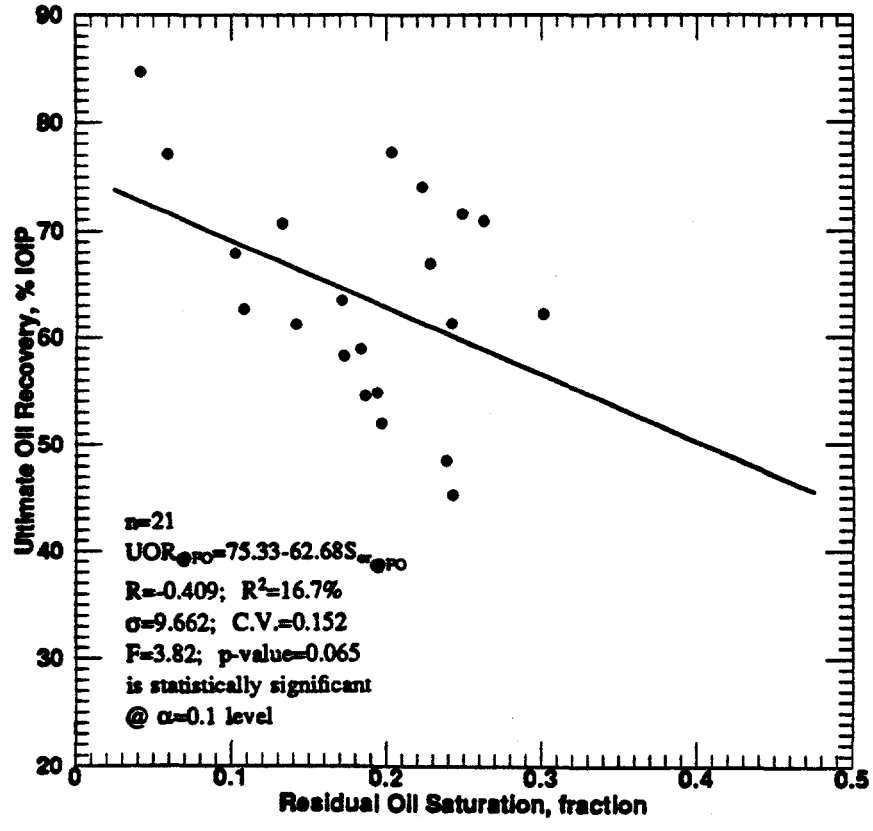

Fig. 5.59: Ultimate Oil Recovery vs. Residual Oil Saturation for Berea Sandstone Linear-Cores at Floodout.

forces.

It is expected that as the scaling coefficient increases, the oil recovery at breakthrough increases. However, above the critical value of scaling factor, the oil recovery at breakthrough should be constant and independent of rate, length, and water viscosity. By controlling the values of the scaling coefficient, a better balance in the capillary forces and the viscous forces will result, and less oil will be bypassed in the large pores. Theoretically, a maximum in recovery would result if the viscous forces were increased sufficiently, for water-wet systems.

5.3.4 Wettability Properties

From each of the waterflooded cores, six to fifty-four core plugs were extracted from along the flow path at about 2.0 cm intervals. The core plugs were perpendicular to the flood plane. During the process of the extraction, the distance of each core plug relative to the inlet face of the core was noted. For a given distance, two core plugs were obtained, one from the top and the other from the bottom of the core, as earlier shown in Fig. 4.2. An average value of the wettability index is obtained for the two core plugs from a given distance. Distances are normalized by dividing the value of the measured distance relative to the core inlet by the total length of the core.

Figure 5.60 shows the distribution of the wettability index per number of sandstone core plug samples. The core plugs wettability index values varied from 0.00 to 1.00, with a mean of 0.59. Included in this and the other frequency distribution plots are simple summaries of statistical data, which include number of samples, mean, median, minimum, maximum, lower quartile, upper quartile, and standard deviation values.

The plots of the core plugs wettability indices versus the normalized distances for each of the 21 cores are presented in Figs. 5.61 through 5.69. Except for core Nos. 1B and 8E,

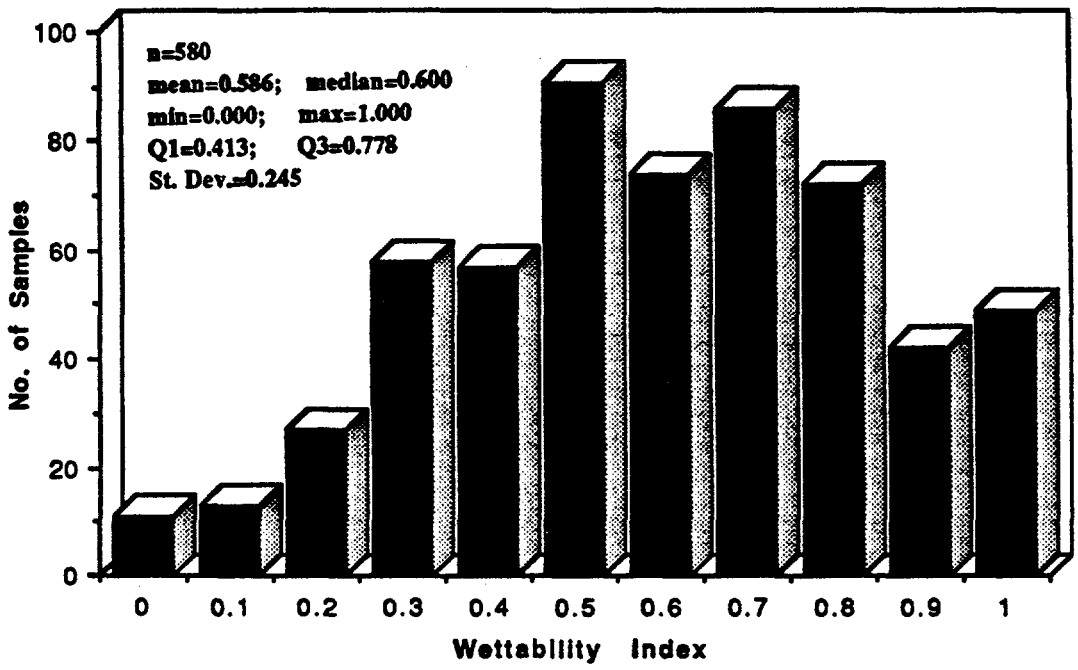

Fig. 5.60: Distribution of Wettability Index per Number of Berea Sandstone Linear-Core Plug Samples.

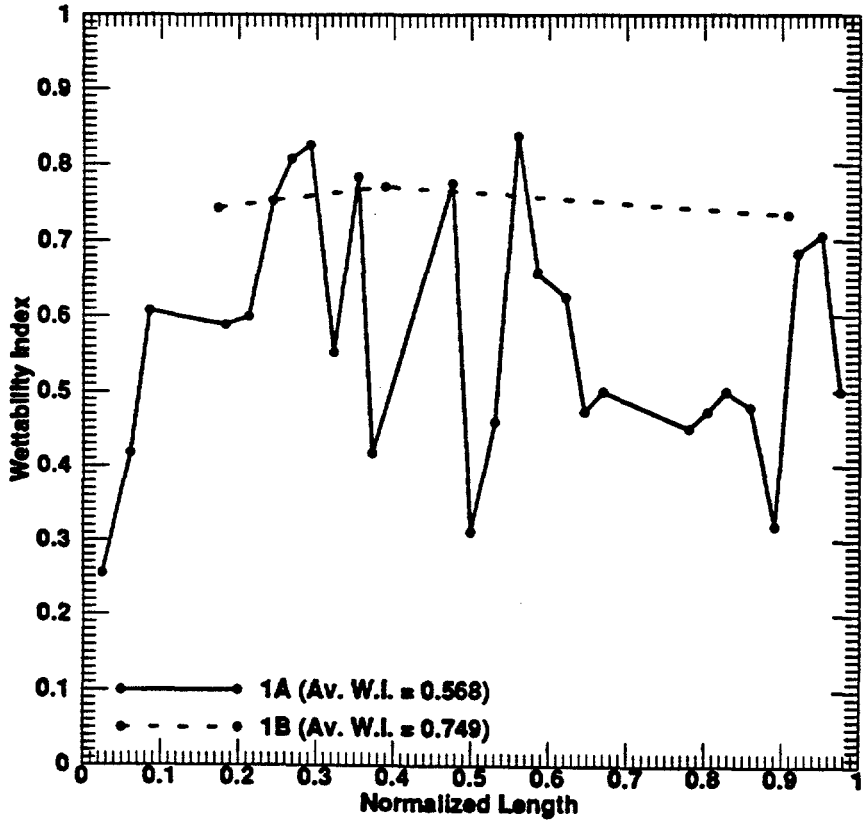

Fig. 5.61: Wettability Index vs. Normalized Length for Berea Sandstone Linear-Core Samples 1A and 1B.

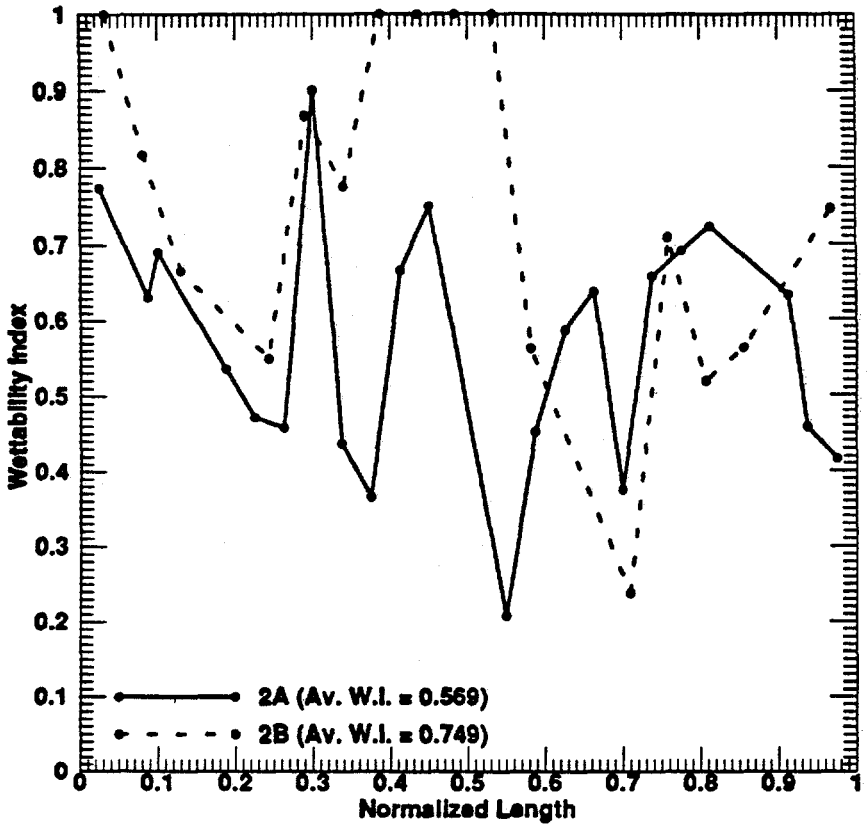

Fig. 5.62: Wettability Index vs. Normalized Length for Berea Sandstone Linear-Core Samples 2A and 2B.

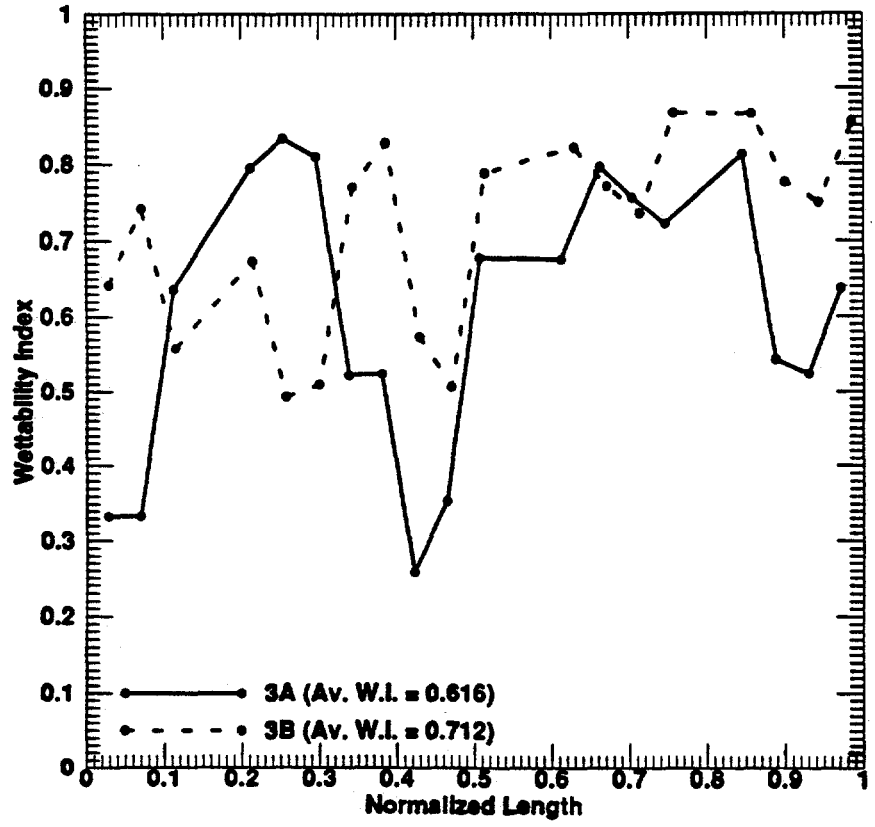

Fig. 5.63: Wettability Index vs. Normalized Length for Berea Sandstone Linear-Core Samples 3A and 3B.

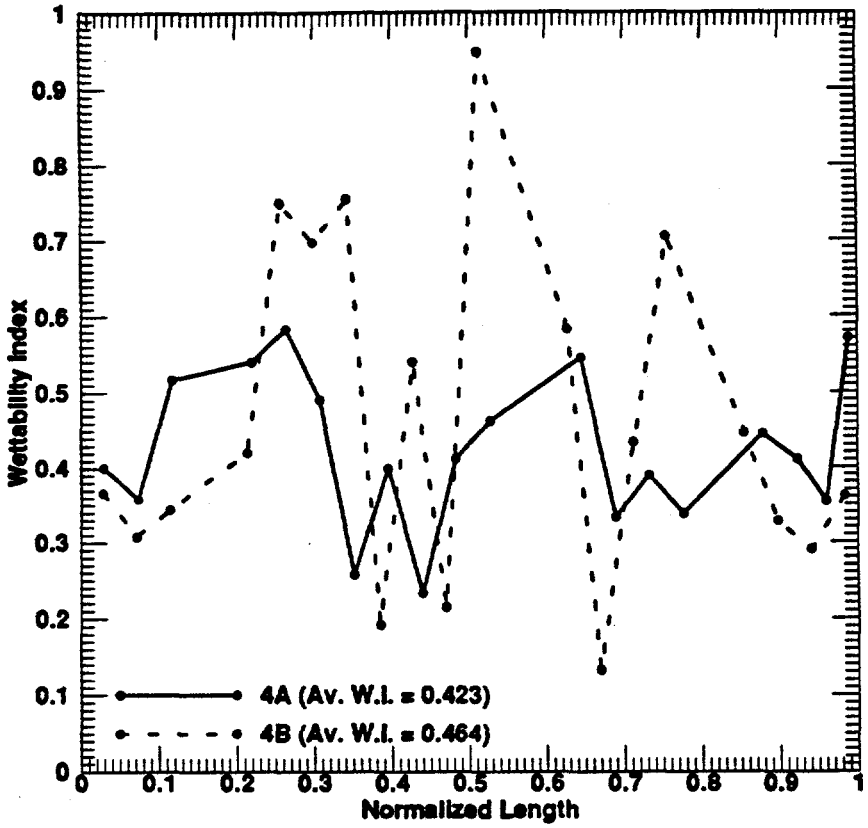

Fig. 5.64: Wettability Index vs. Normalized Length for Berea Sandstone Linear-Core Samples 4A and 4B.

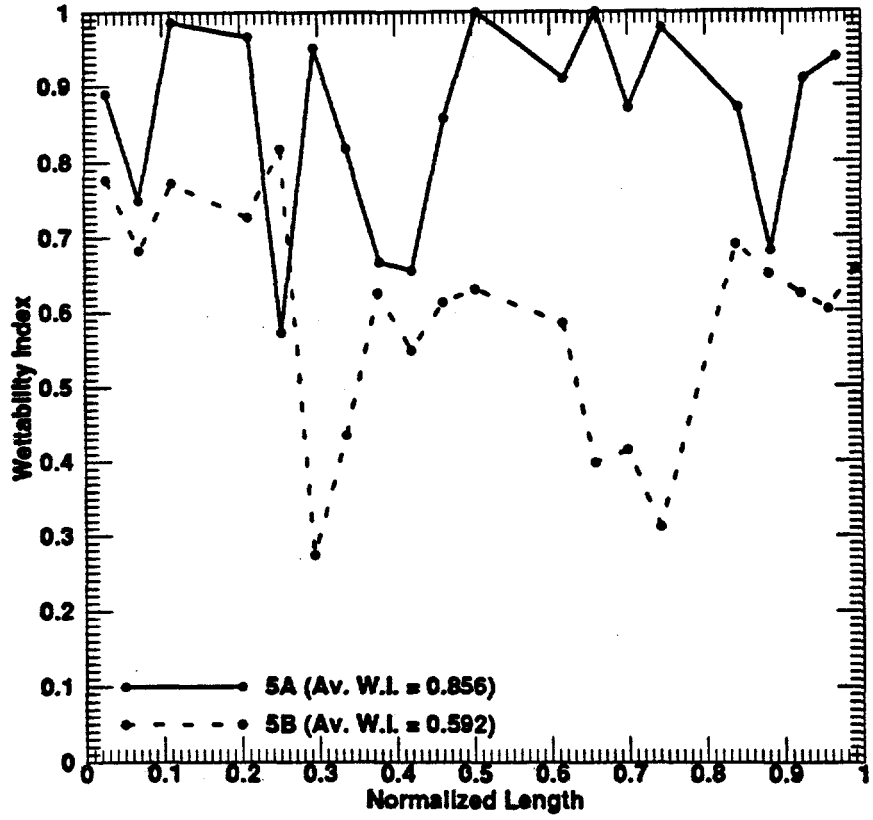

Fig. 5.65: Wettability Index vs. Normalized Length for Berea Sandstone Linear-Core Samples 5A and 5B.

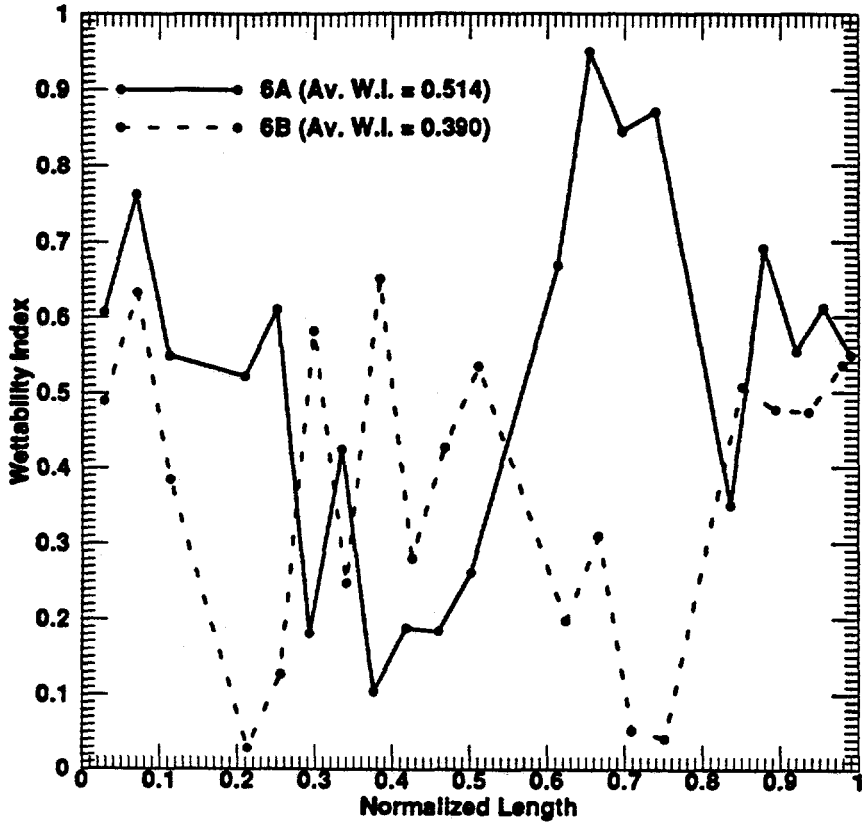

Fig. 5.66: Wettability Index vs. Normalized Length for Berea Sandstone Linear-Core Samples 6A and 6B.

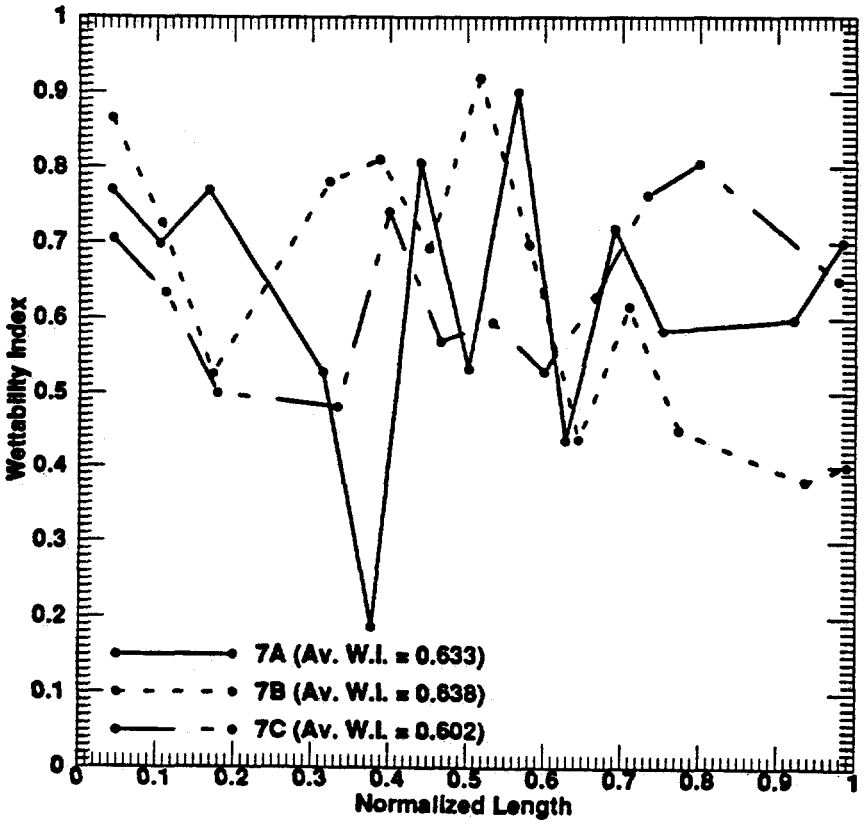

Fig. 5.67: Wettability Index vs. Normalized Length for Berea Sandstone Linear-Core Samples 7A, 7B and 7C.

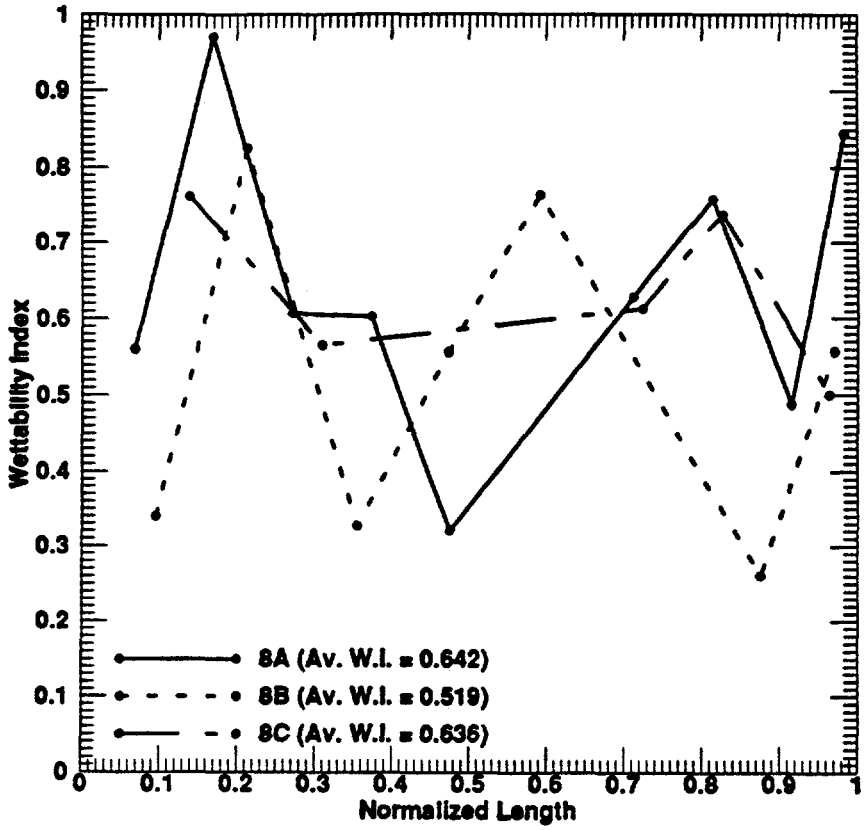

Fig. 5.68: Wettability Index vs. Normalized Length for Berea Sandstone Linear-Core Samples 8A, 8B and 8C.

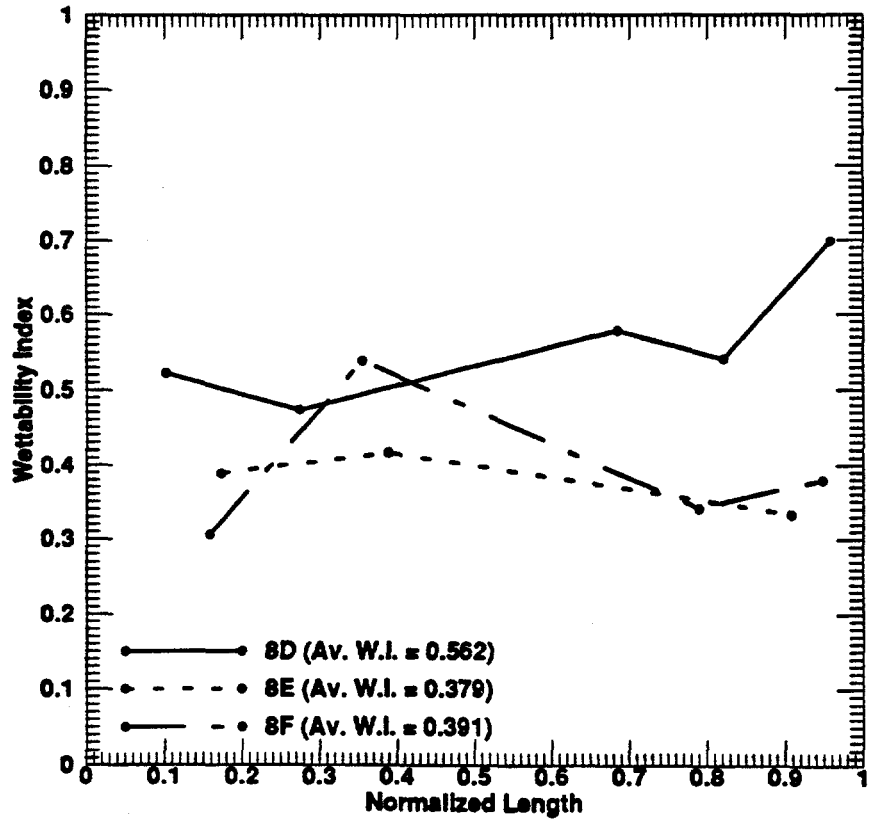

Fig. 5.69: Wettability Index vs. Normalized Length for Berea Sandstone Linear-Core Samples 8D, 8E and 8F.

the trends are generally not constant. From the core plugs, an average value of wettability index was obtained for each of the cores. The average wettability index for the 21 cores ranged from 0.38 to 0.86, with a mean of 0.58. Based on these determinations, the sandstone cores investigated in this study are classified as water-wet rocks.

5.3.4.1 Relation Between Wettability and Petrophysical Properties

The relationships of porosity, and permeability, with the average wettability index were also investigated. At $\alpha = 0.1$ level, this relationships failed the statistical tests, so they were found not to be significant.

5.3.4.2 Relation Between Wettability and Waterflood Properties

Figures 5.70 through 5.73 show the plots of residual oil saturation and oil recovery versus average wettability index at both the breakthrough and floodout. Wettability of sandstone cores governs the residual oil saturation and oil recovery values. It affects waterflooding by controlling the flow and spatial distribution of fluids in a porous medium. Wardlaw (1983) noted that wettability may strongly affect residual oil saturation, the fractional flow fluids for a given saturation and areal and volumetric sweep efficiency. Wardlaw emphasized that changes in wettability can greatly change the arrangement of water and oil within a pore system. He also indicated that for a given rock, the critical end-point saturation may differ greatly for different conditions of wettability.

Figures 5.70 and 5.71 show the relationships of average wettability index on residual oil saturation at breakthrough and at floodout, respectively. Average wettability index was found to be directly related to the residual oil saturation at breakthrough, but the relationship at floodout slightly failed the significance test. An explanation for this occurrence is that residual oil saturation at floodout is less sensitive to wettability than is residual oil saturation at breakthrough. Residual oil saturation appears to be slightly lower

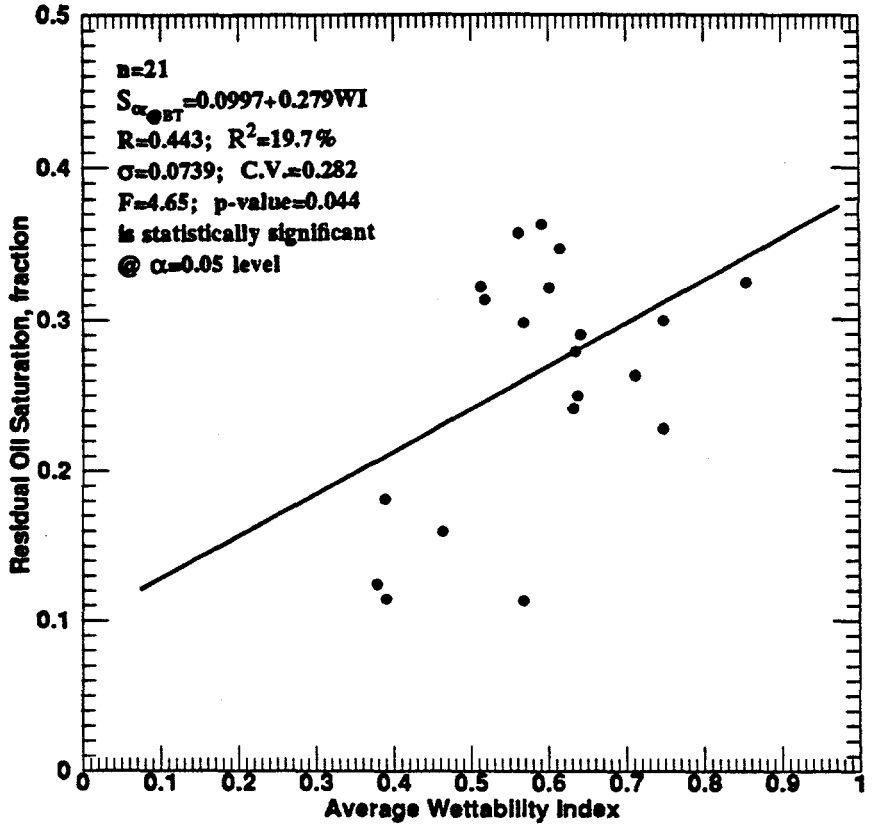

Fig. 5.70: Residual Oil Saturation vs. Average Wettability Index for Berea Sandstone Linear-Cores at Breakthrough.

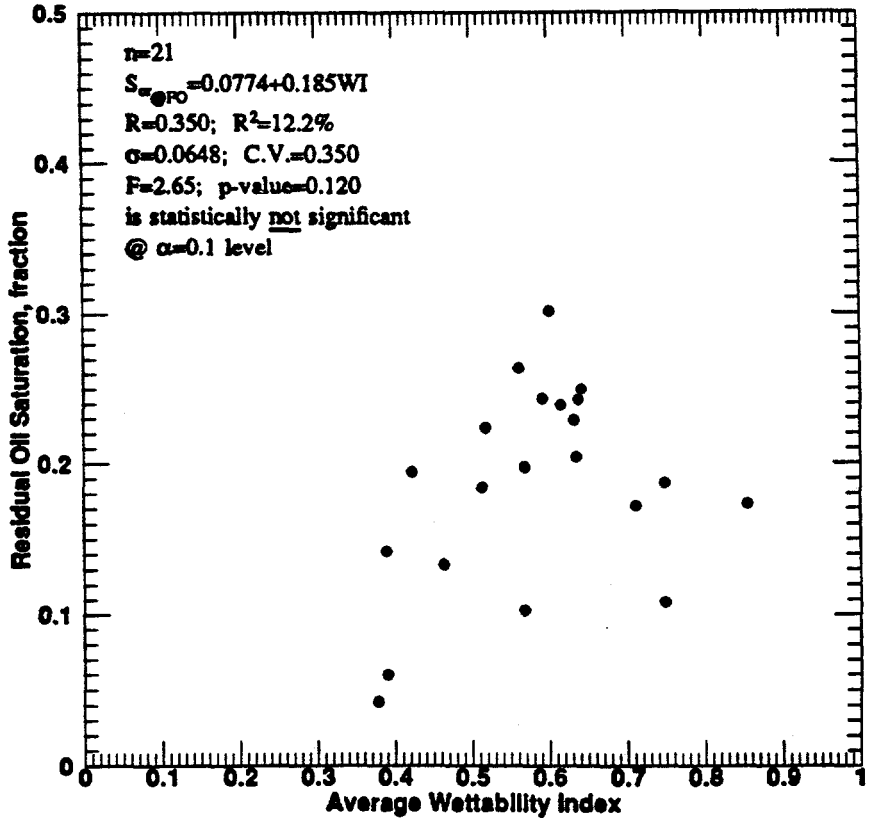

Fig. 5.71: Residual Oil Saturation vs. Average Wettability Index for Berea Sandstone Linear-Cores at Floodout.

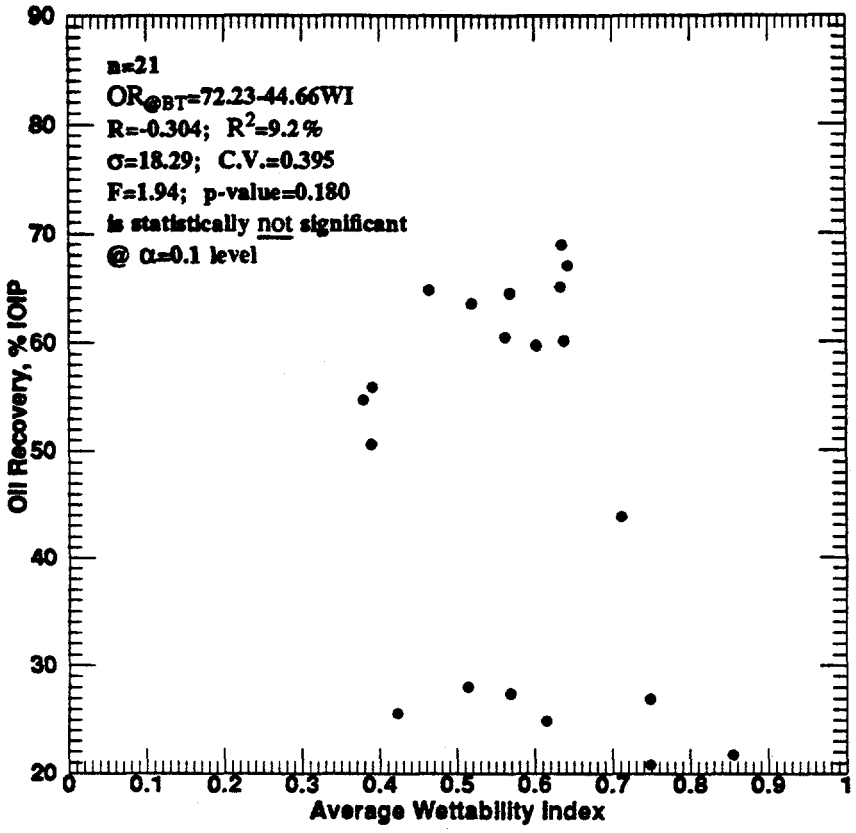

Fig. 5.72: Oil Recovery vs. Average Wettability Index for Berea Sandstone Linear-Cores at Breakthrough.

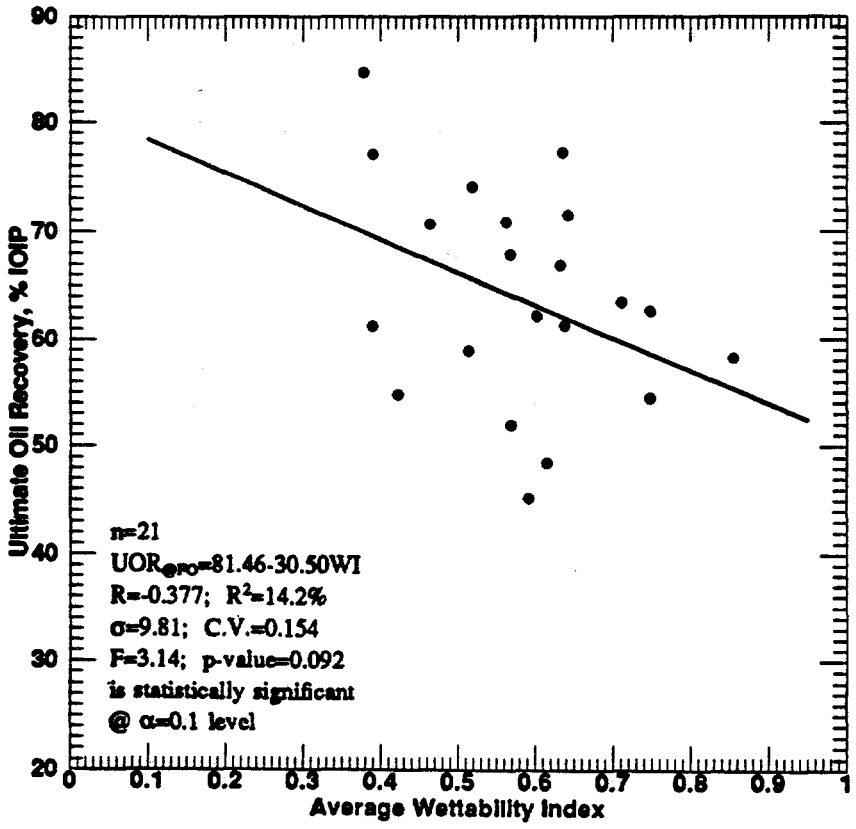

Fig. 5.73: Ultimate Oil Recovery vs. Average Wettability Index for Berea Sandstone Linear-Cores at Floodout.

near neutral wettability, which corresponds to higher oil recovery. However, Fig. 5.73 indicates that the average wettability index in sandstone cores is inversely related to ultimate oil recovery at floodout. The relationship with oil recovery at breakthrough slightly failed the significance test at $\alpha = 0.1$ level, as shown in Fig. 5.72. As a result of these findings, one can deduce that for water-wet sandstone rocks, as the wettability index increases, the residual oil saturation also increases and the oil recovery by waterflood decreases. These observation are in agreement with the findings of Morrow (1990) and Jadhunandan and Morrow (1991), that systems with weakly imbibe water give higher oil recovery by waterflooding than very strongly water-wet systems.

5.3.5 Mercury Porosimetry Properties

A porous system may be modeled as a network of relatively large voids (pores) connected by smaller constrictions (throats). According to Kopaska-Merkel and Friedman (1989), mercury porosimetry is currently the only effective quantitative means of studying pore throats, which control the movement of fluids into and out of reservoir rocks.

Intrusion of mercury into the system of voids involves penetration of the throats. Once the mercury attains the pressure required to enter a throat, it proceeds to fill the pore connected to it. Only those throats connected to an empty pore at the time of their penetration are actually measured by mercury porosimetry. Extrusion is controlled by the size of the pores. During extrusion, some regions of filled pores become isolated from the exterior and are on longer accessible. This isolation results in mercury retention within the samples. Ideally, the fraction of retained mercury is characteristic of the type of porous network geometry being measured. Further, the number of pores measured at a given radius of the sample is less than the number of pores actually present in the network. This phenomenon primarily affects the largest pores because they tend to be the last to extrude

and are most likely to be stranded. If no volume of mercury is extruded from them, they are not measured (Lane et al., 1985).

A total of 580 core plugs were extracted from along the flow path of the 21 waterflooded Berea sandstone linear-cores. These extracted plugs are the same that were previously tested for wettability and later cleaned in readiness for the mercury porosimetry tests. After the completion of low-pressure and high-pressure runs, the plugs were discarded because they were contaminated with mercury and rendered unsuitable for future analyses.

Similar to the analysis of the wettability data, average values of mercury porosimetry properties were obtained for each of the core samples from the core plugs. These values are presented in Table 5.13 for the types of mode, pore intrusion volumes, pore surface areas, pore specific surface areas, average pore diameters, apparent densities, mercury porosities, residual mercury saturations and mercury recovery efficiencies. Melas and Friedman (1992) noted that mercury porosimetry characteristics determine the shape of the capillary-pressure curve to which they correspond, and as such, an understanding of them is important for various phases of reservoir production, especially secondary and tertiary recovery.

Table 5.14 shows the statistical description of the mercury porosimetry measured data obtained. For all the core samples combined, intrusion volumes varied from 0.06 to 0.11 ml/g, with an average of 0.08 ml/g; the surface areas varied from 0.16 to 0.68 m^2/g, with an average of 0.29 m^2/g; the specific surface area varied from $1.84*10^4$ to $8.58*10^4$ cm^2/cm^3, with an average of $3.62*10^4$ cm^2/cm^3; the average pore diameters varied from 1.32 to 13.79 μm, with an average of 5.24 μm; the apparent (skeletal) densities varied from 2.46 to 2.61 g/ml, with an average of 2.53 g/ml; the porosities varied from 12.8 to 22.1%, with an average of 17.0%; and the mercury recovery efficiencies varied from 6.6 to 18.5%, with an average value of 11.2%.

Table 5.13: Mercury Porosimetry Properties of the Berea Sandstone Linear-Cores

Core Sample No.	No. of Plugs	Type of Mode	$V_{int.}$ (ml/g)	SA (m^2/g)	S_s (cm^2/cm^3) (E+04)	$\bar{D}$ (μm)	ρ_s (g/ml)	ϕ_{Hg} (frac)	RE (frac)
1A	54	1	0.0787	0.675	8.577	13.793	2.567	0.159	0.071
1B	6	1	0.0753	0.608	8.074	8.860	2.553	0.161	0.142
2A	44	1	0.0783	0.238	3.040	3.819	2.514	0.162	0.110
2B	32	1	0.0801	0.165	2.060	5.472	2.498	0.163	0.102
3A	38	1	0.0601	0.213	3.544	9.442	2.460	0.128	0.066
3B	38	1	0.0598	0.159	2.659	6.781	2.492	0.128	0.096
4A	38	1	0.0782	0.224	2.864	5.505	2.524	0.164	0.092
4B	38	1	0.0756	0.198	2.619	5.850	2.477	0.151	0.112
5A	38	1	0.0599	0.396	6.611	2.880	2.556	0.132	0.159
5B	40	1	0.0639	0.346	5.415	1.316	2.564	0.140	0.185
6A	40	1	0.0851	0.280	3.290	2.707	2.583	0.177	0.131
6B	38	1	0.0848	0.246	2.901	2.418	2.542	0.170	0.131
7A	26	1	0.0948	0.236	2.489	5.447	2.582	0.196	0.100
7B	26	1	0.0865	0.257	2.971	6.251	2.472	0.175	0.118
7C	24	1	0.0792	0.245	3.093	4.262	2.485	0.164	0.149
8A	18	1	0.0927	0.394	4.250	1.373	2.510	0.188	0.143
8B	14	1	0.0998	0.236	2.365	4.306	2.592	0.203	0.101
8C	10	1	0.0985	0.243	2.467	3.597	2.554	0.200	0.104
8D	10	1	0.0863	0.159	1.842	9.336	2.494	0.177	0.069
8E	6	1	0.1025	0.226	2.205	5.076	2.548	0.207	0.075
8F	8	1	0.1088	0.295	2.711	1.507	2.607	0.221	0.101

Table 5.14: Statistical Description of the Mercury Porosimetry Experimental Variables for Berea Sandstone Linear-Cores

	$V_{int.}$ (ml/g)	SA (m^2/g)	S_s (cm^2/cc) (E+04)	$\bar{D}$ (μm)	ρ_s (g/ml)	ϕ_{Hg} (frac)	RE (frac)
Mean	0.0823	0.288	3.621	5.238	2.531	0.170	0.112
Median	0.0801	0.243	2.901	5.076	2.542	0.164	0.104
Min.	0.0598	0.159	1.842	1.316	2.460	0.128	0.066
Max.	0.1088	0.675	8.577	13.793	2.607	0.221	0.185
Q1	0.0755	0.218	2.478	2.793	2.493	0.155	0.094
Q3	0.0938	0.320	3.897	6.516	2.565	0.192	0.137
St. Dev.	0.0141	0.135	1.920	3.126	0.042	0.026	0.031

In water-wet reservoir rocks, the non-wetting-phase is oil and in such a situation, experimentally trapping of mercury is similar to trapping of oil in the subsurface. Hence, these rocks with less than 25% mercury recovery efficiencies and good porosities, would not perform well during primary oil recovery period, but they would be good candidates for enhanced oil recovery methods (Kopaska-Merkel and Friedman, 1989).

Figures 5.74 through 5.80 show the distribution plots of the sandstone core plug samples for total intrusion volume, surface area, specific surface area, average pore diameter, apparent (skeletal) density, mercury porosity, and mercury recovery efficiency, respectively. Due to the removal of all the bad mercury porosimetry experimentally measured data, only 552 out of the original 580 core plugs were utilized for these analyses. The bad mercury porosimetry experimentally measured data, were those with stem volume below 25% or higher than 90% (Micromeritics, 1987). The plots of the plug's mercury porosities versus the normalized distances for each of the 21 linear-cores are presented in Figs. 5.81 through 5.89. There is a strong similarity between the variability in these figures and those presented in Figs. 5.61 to 5.69 for wettability indices. Similar to the case of the wettability indices, except for core Nos. 1B and 8E, the exhibited trends are generally not constant.

The correlation matrix shown in Table 5.15 confirms the trends of Figs. 5.90 through 5.93. Figure 5.90 shows a strong relationship between the total intrusion volume and the mercury porosity, with a R^2 value of about 99% and high F-test statistic value. The relationship has a strong statistical significance at $\alpha = 0.001$ level. Figure 5.91 shows that mercury recovery efficiency is inversely related to average pore diameter. The mercury recovery efficiency versus average pore diameter relationship has a strong statistical significance at $\alpha = 0.005$ level. This is in agreement with the findings of Amthor et al. (1988), that the larger the pore throat size, the poorer the mercury recovery efficiency for

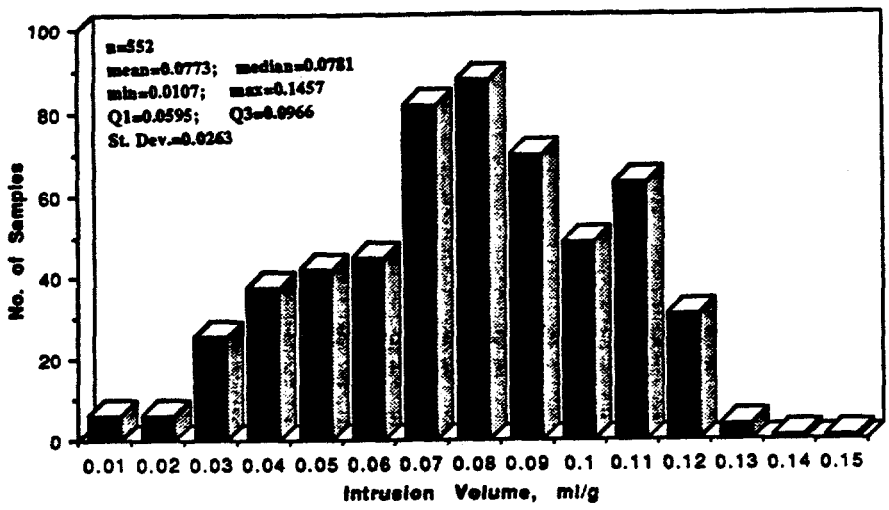

Fig. 5.74: Distribution of Total Intrusion Volume per Number of Berea Sandstone Linear-Core Plug Samples.

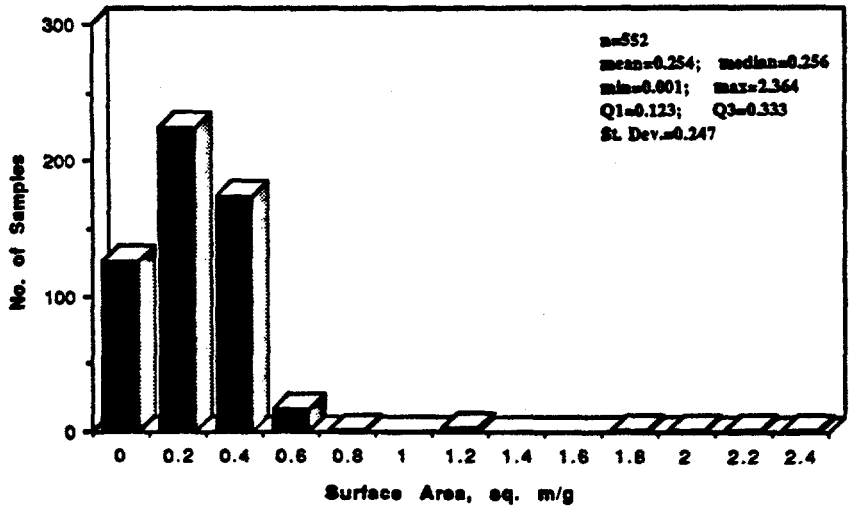

Fig. 5.75: Distribution of Surface Area per Number of Berea Sandstone Linear-Core Plug Samples.

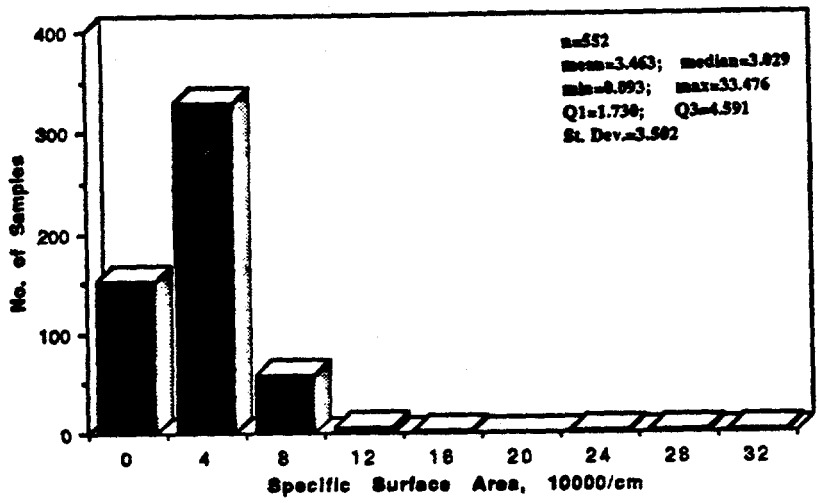

Fig. 5.76: Distribution of Specific Surface Area per Number of Berea Sandstone Linear-Core Plug Samples.

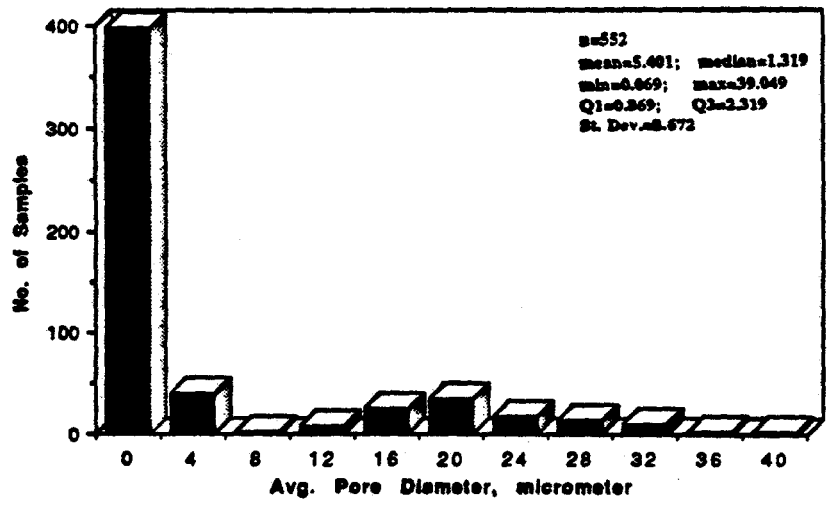

Fig. 5.77: Distribution of Average Pore Diameter per Number of Berea Sandstone Linear-Core Plug Samples.

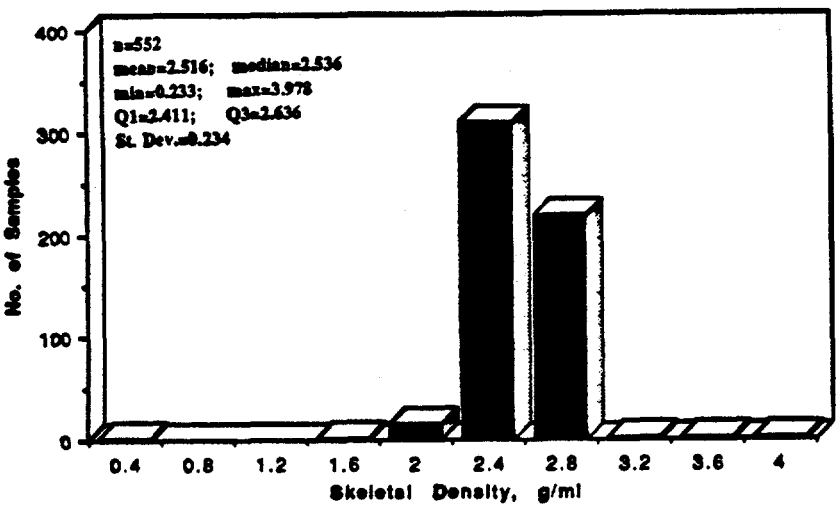

Fig. 5.78: Distribution of Apparent (Skeletal) Density per Number of Berea Sandstone Linear-Core Plug Samples.

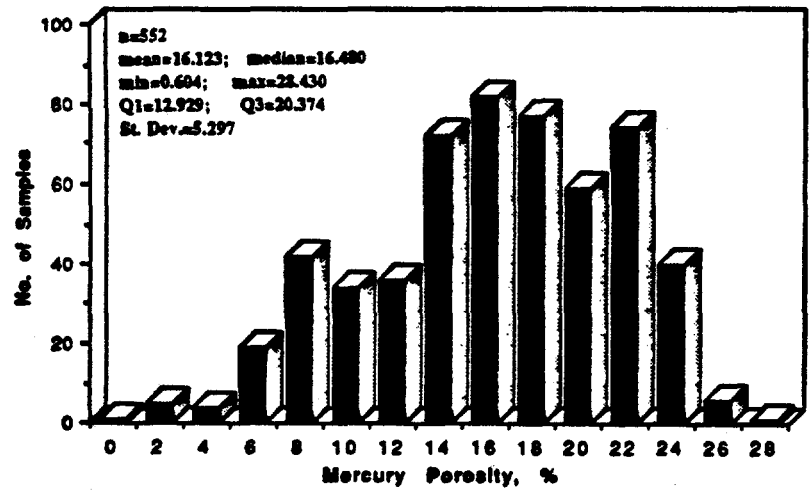

Fig. 5.79: Distribution of Mercury Porosity per Number of Berea Sandstone Linear-Core Plug Samples.

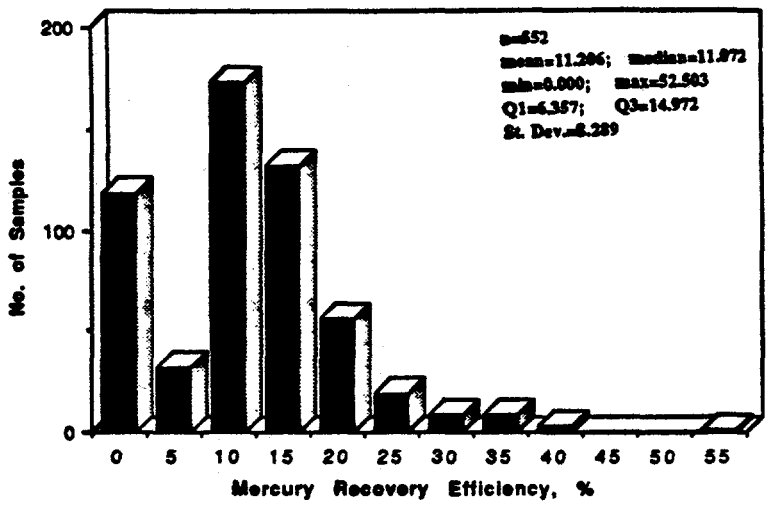

Fig. 5.80: Distribution of Mercury Recovery Efficiency per Number of Berea Sandstone Linear-Core Plug Samples.

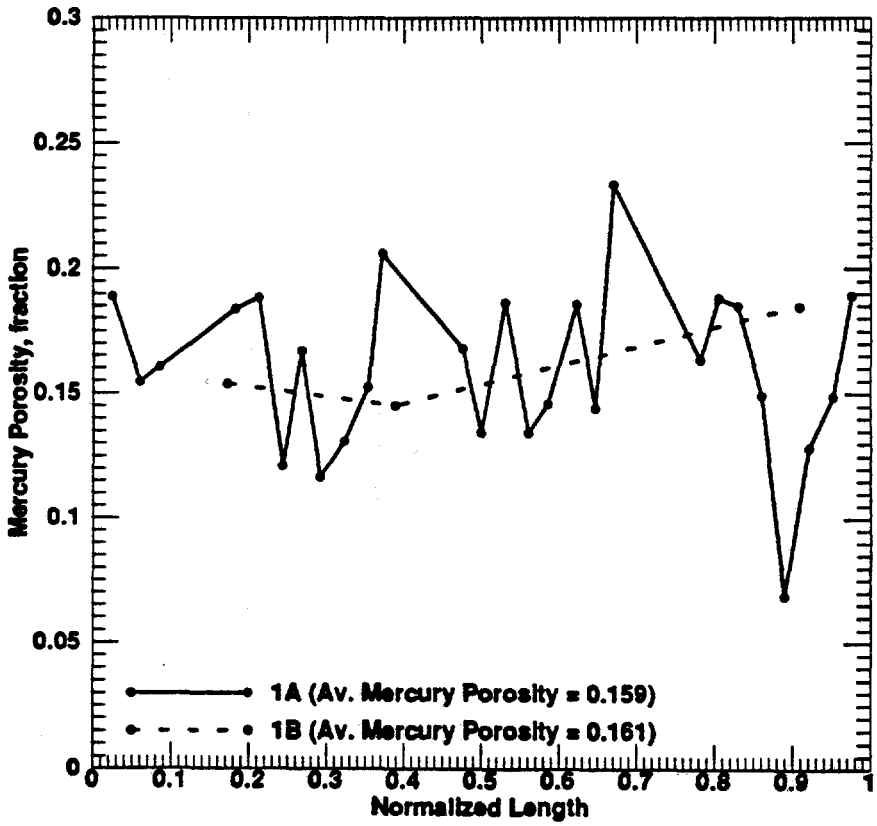

Fig. 5.81: Mercury Porosity vs. Normalized Length for Berea Sandstone Linear-Core Samples 1A and 1B.

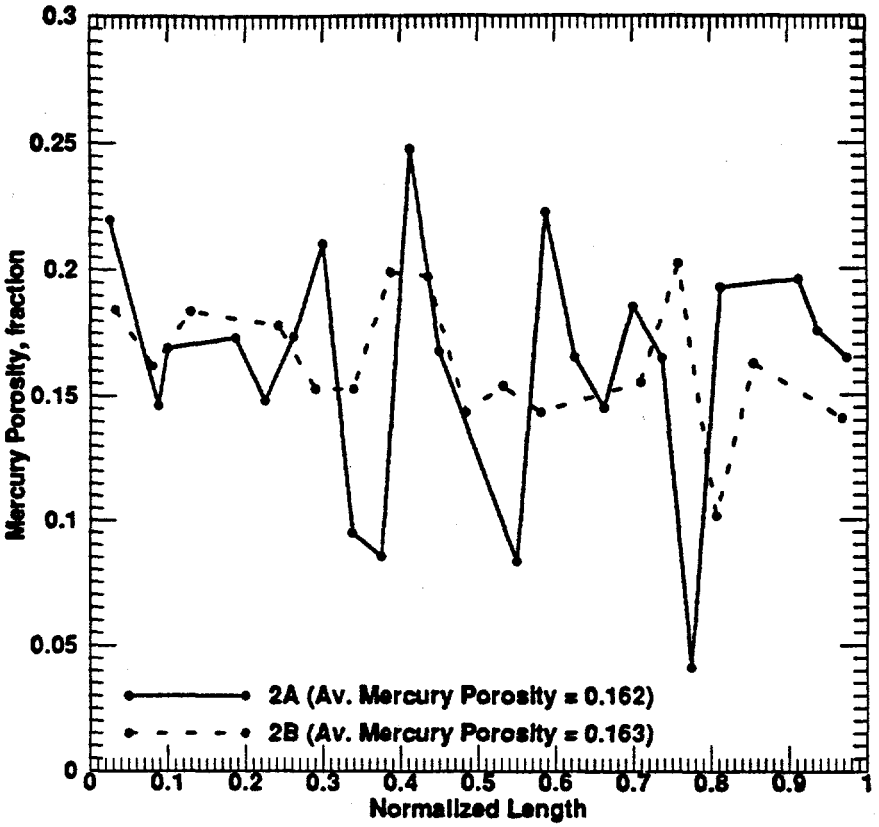

Fig. 5.82: Mercury Porosity vs. Normalized Length for Berea Sandstone Linear-Core Samples 2A and 2B.

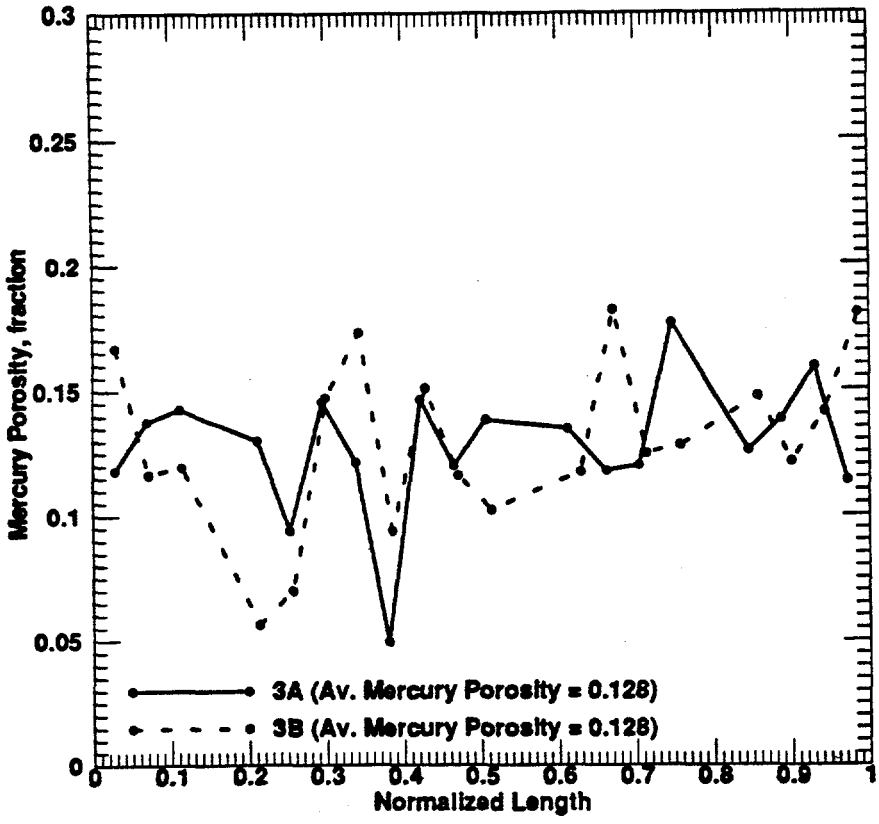

Fig. 5.83: Mercury Porosity vs. Normalized Length for Berea Sandstone Linear-Core Samples 3A and 3B.

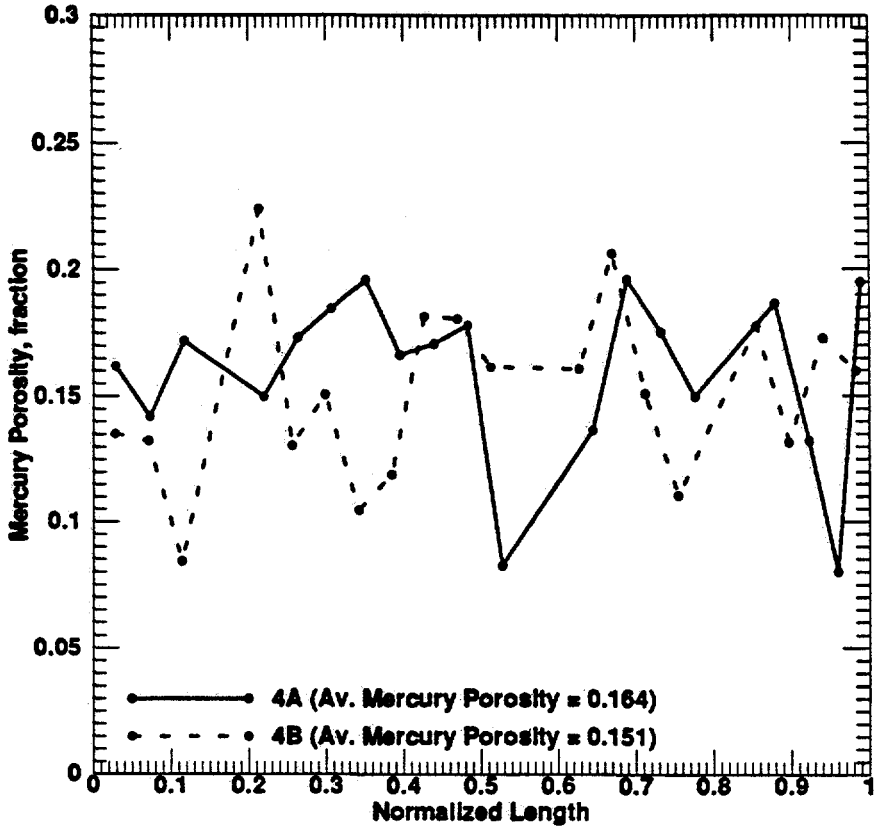

Fig. 5.84: Mercury Porosity vs. Normalized Length for Berea Sandstone Linear-Core Samples 4A and 4B.

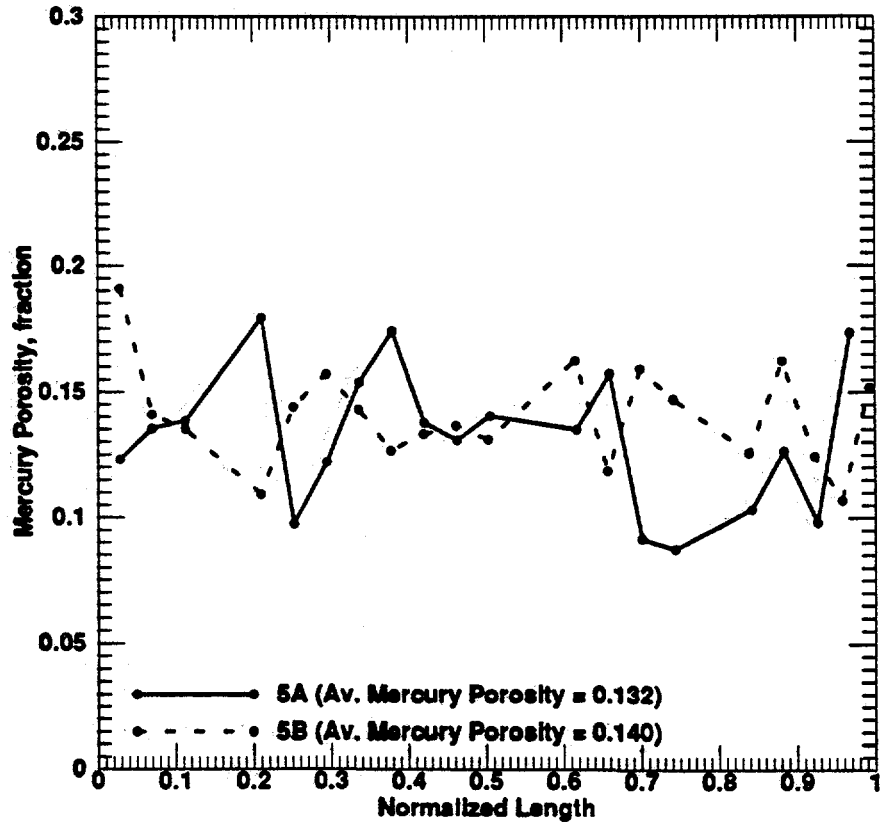

Fig. 5.85: Mercury Porosity vs. Normalized Length for Berea Sandstone Linear-Core Samples 5A and 5B.

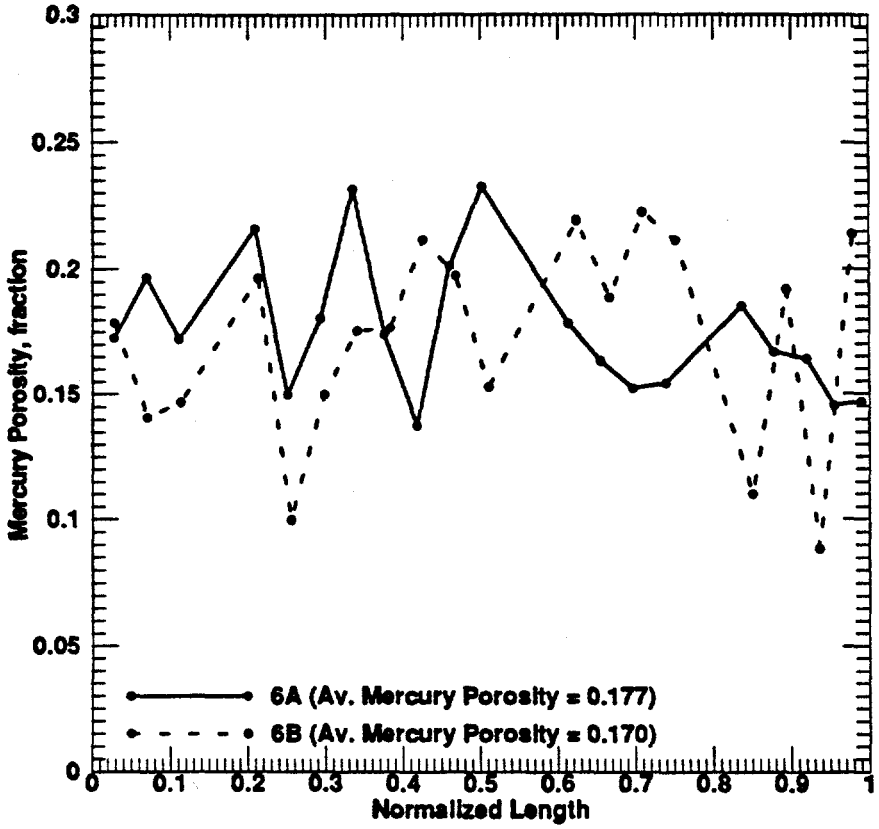

Fig. 5.86: Mercury Porosity vs. Normalized Length for Berea Sandstone Linear-Core Samples 6A and 6B.

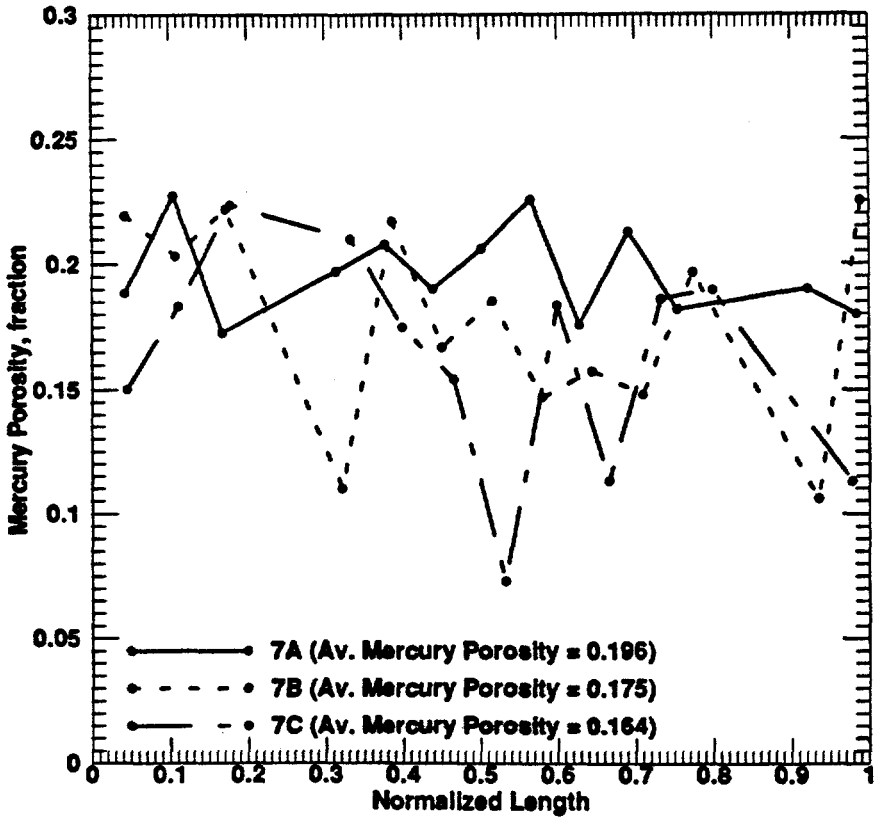

Fig. 5.87: Mercury Porosity vs. Normalized Length for Berea Sandstone Linear-Core Samples 7A, 7B and 7C.

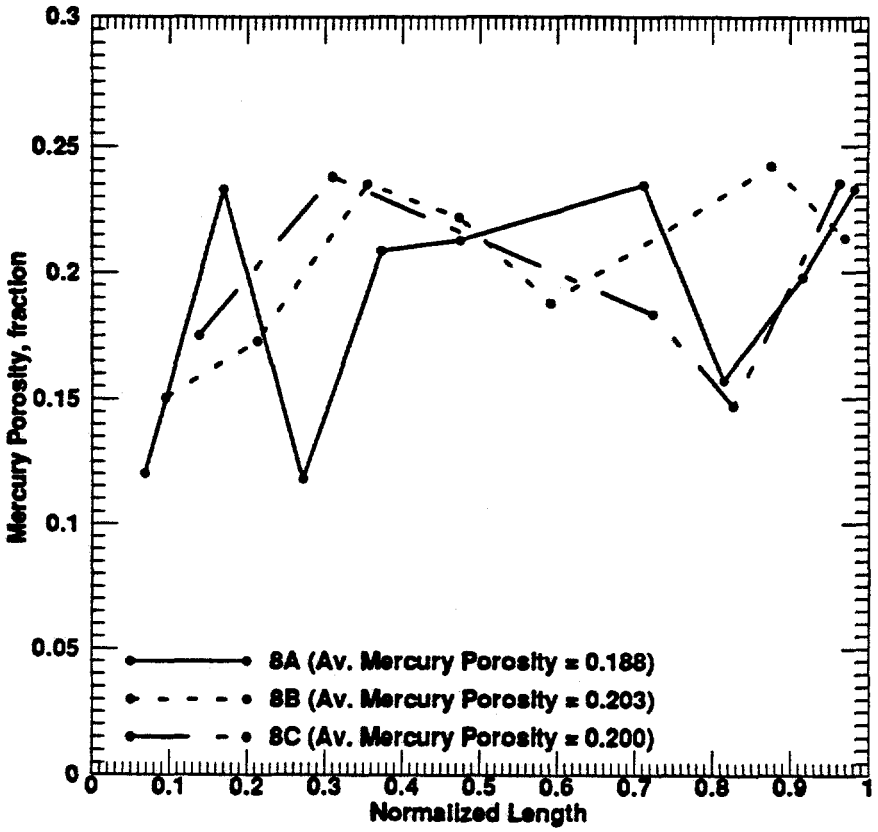

Fig. 5.88: Mercury Porosity vs. Normalized Length for Berea Sandstone Linear-Core Samples 8A, 8B and 8C.

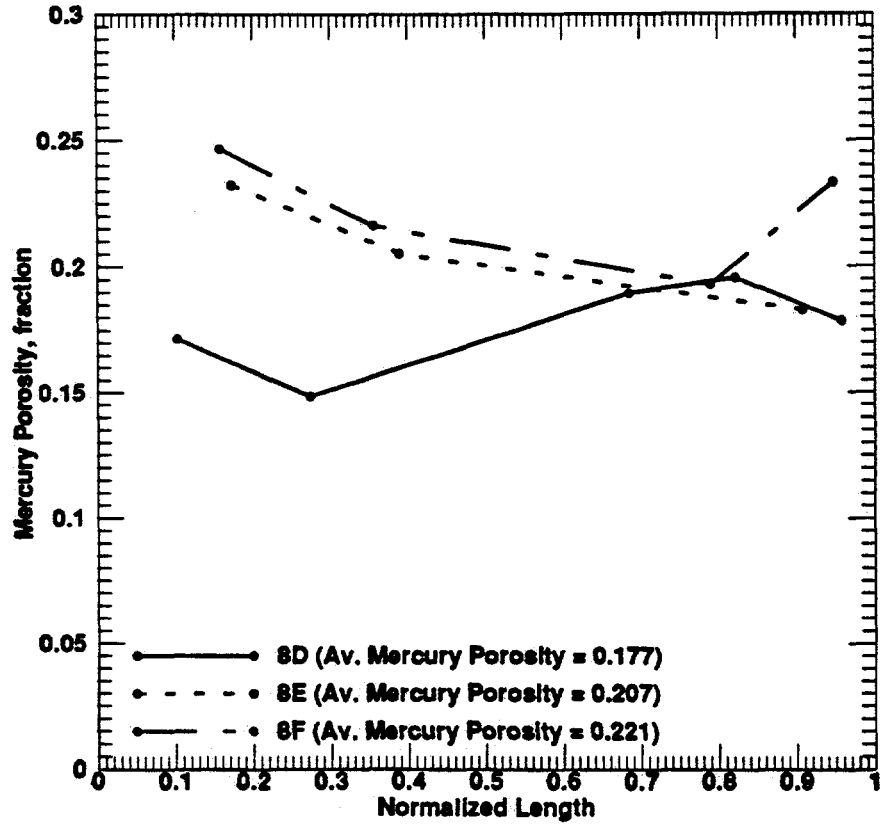

Fig. 5.89: Mercury Porosity vs. Normalized Length for Berea Sandstone Linear-Core Samples 8D, 8E and 8F.

Table 5.15: Correlation Matrix for the Mercury Porosimetry Properties for Berea Sandstone Linear-Cores

	$V_{Int.}$	SA	S_o	$\bar{D}$	ρ_s	ϕ_{Hg}
SA	-0.108					
S_o	-0.410	0.945				
$\bar{D}$	-0.263	0.326	0.348			
ρ_s	0.447	0.399	0.269	-0.295		
ϕ_{Hg}	0.994	-0.091	-0.386	-0.295	0.504	
RE	-0.261	0.251	0.337	-0.620	0.171	-0.221

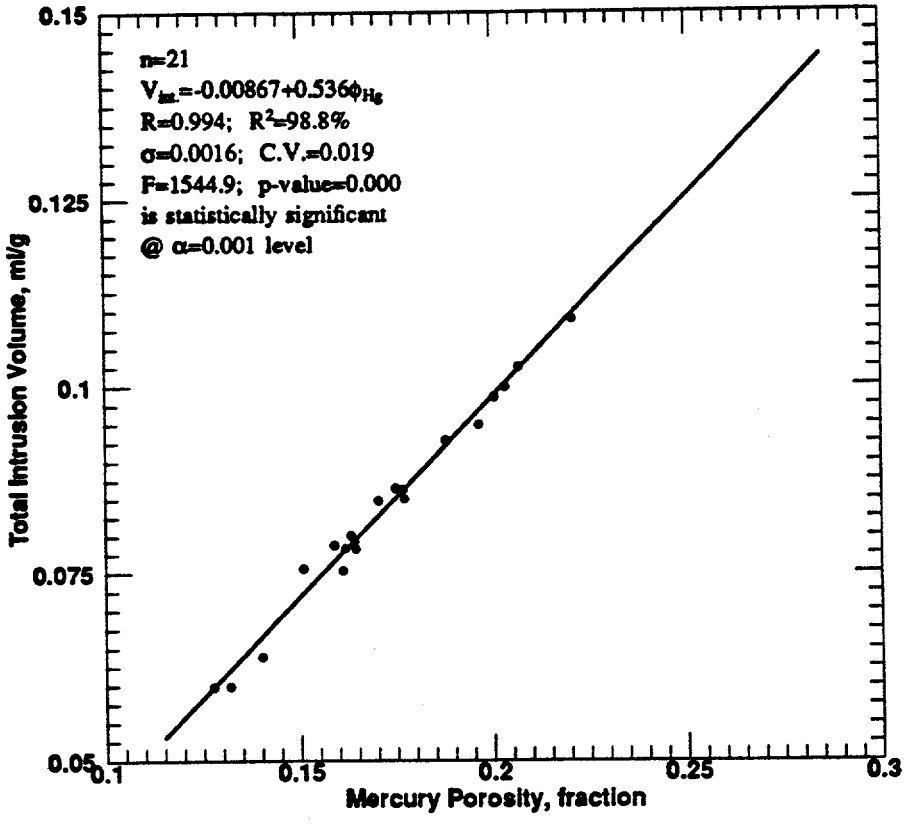

Fig. 5.90: Total Intrusion volume vs. Mercury Porosity for Berea Sandstone Linear-Cores.

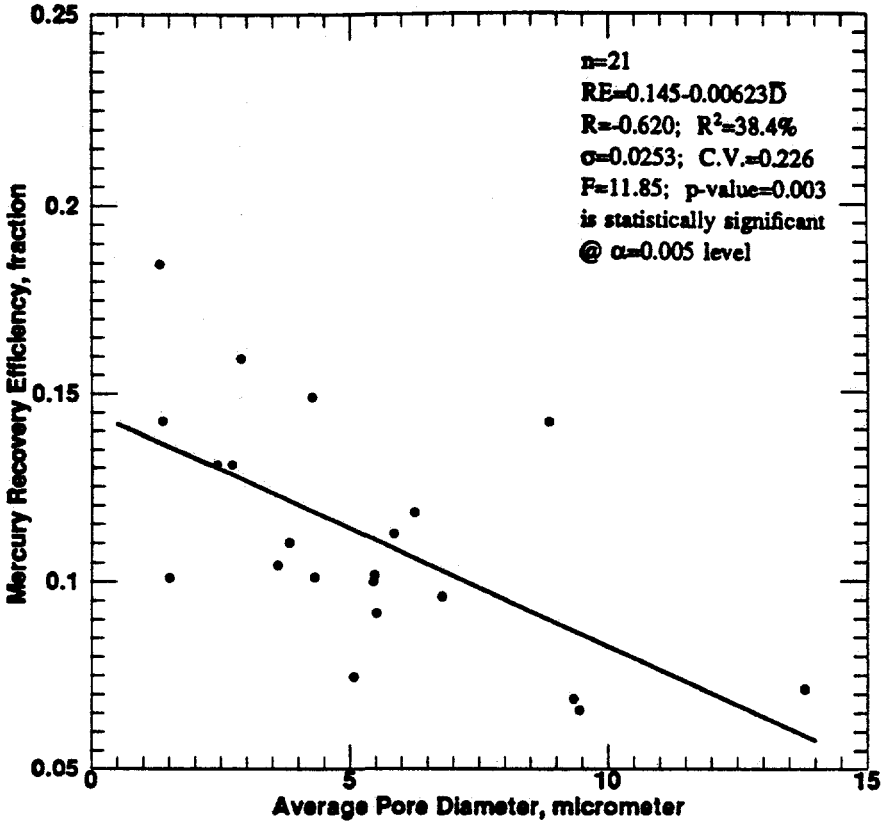

Fig. 5.91: Recovery Efficiency vs. Mercury Porosity for Berea Sandstone Linear-Cores.

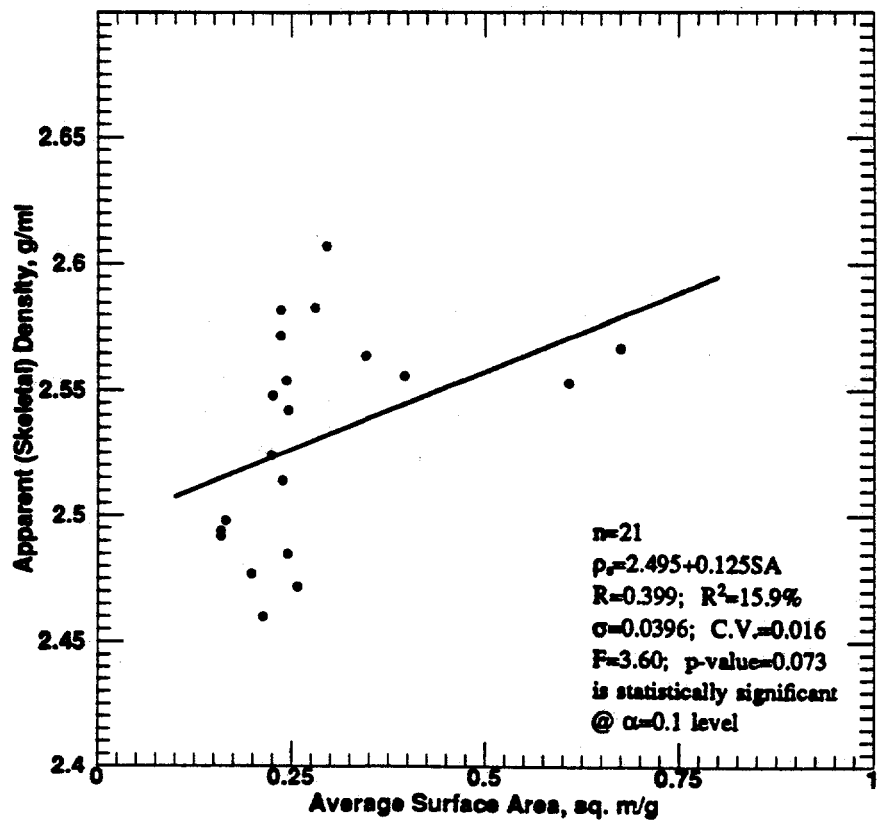

Fig. 5.92: Skeletal Density vs. Surface Area for Berea Sandstone Linear-Cores.

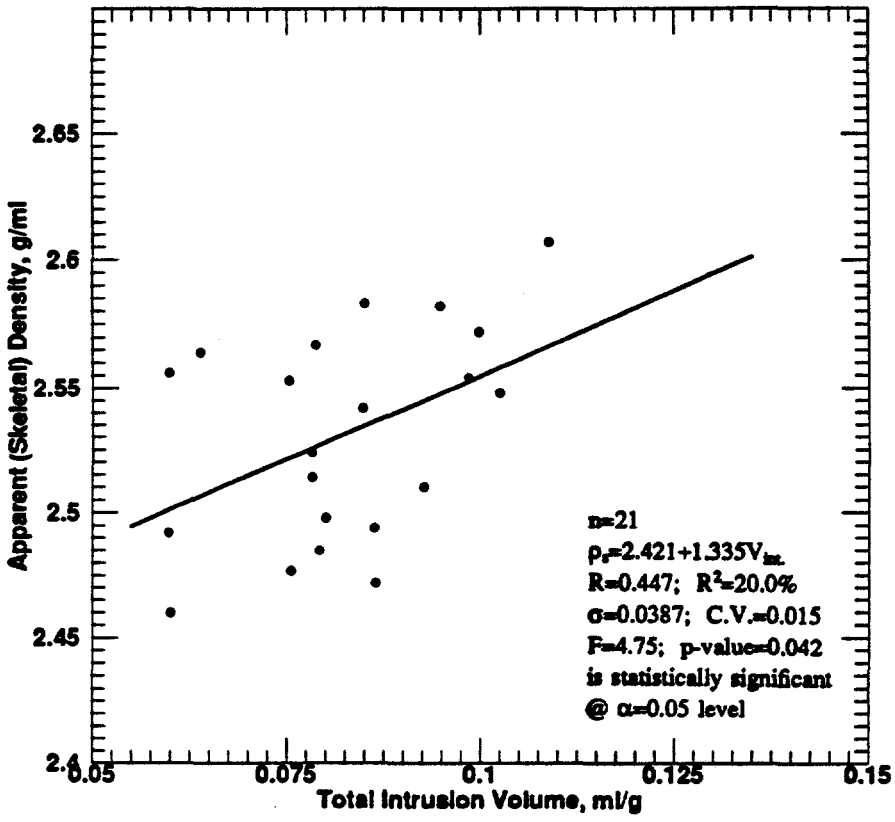

Fig. 5.93: Skeletal Density vs. Total Intrusion Volume for Berea Sandstone Linear-Cores.

steep-concave unimodal systems. They suggested that this is a consequence of three controlling factors: accessibility ratio, hysteresis, and experimental procedure. Accessibility ratio is a measure of the propensity for isolation of throats by snap-off and related phenomena during extrusion (withdrawal), and it is inversely related to the throat size (Wardlaw and Taylor, 1976). As evidenced in Fig. 5.92, the relationship between skeletal density and surface area is direct and statistically significant at $\alpha = 0.1$ level. Figure 5.93 shows a direct trend between the skeletal density and the total intrusion volume. The relationship is statistically significant at $\alpha = 0.05$ level. The relationship between mercury recovery efficiency and porosity was found not to be statistically significant, with low value of correlation coefficient ($R = -0.22$), as shown in the correlation matrix of Table 5.15.

Another explanation for the inverse relationship between mercury recovery efficiency and average pore diameter, can be deduced from the fact that the pore system in a porous medium consists of the main open spaces (pores) and the smaller channels (pore throats) connecting the pores. The smaller voids or throats, control access to the larger ones (pores) because higher pressures are needed to force mercury into the smaller spaces. Further, the pore throats are the bottle-necks in the pore systems and their critical capillary pressures must be exceeded for mercury or other non-wetting fluids to enter the pores they surround (Kopaska-Merkel and Friedman, 1989).

5.3.5.1 Mercury Recovery Efficiency Correlation

Adequate prediction of the field behavior during primary or enhanced recovery period requires representative laboratory measurements. Using non-linear multiple regression analysis, the correlation for estimating mercury recovery efficiency values for sandstones is developed from 450 experimentally obtained mercury porosimetry data. It was initially assumed that:

$$RE = f(V_{int.}, SA, S_s, \overline{D}, \rho_s, \phi_{Hg}) \quad (5.1)$$

After a series of analyses using the best subset algorithms, as outlined in the next chapter, it was observed that specific surface area could be removed from the list of independent variables in Eq. 5.1. The equation can then be re-written as:

$$RE = f(V_{int.}, SA, \overline{D}, \rho_s, \phi_{Hg}) \quad (5.2)$$

Again, with further modification, Eq. 5.2 is assumed to be of the general form:

$$RE = \frac{SA^E \phi_{Hg}^F}{A V_{int.}^B \overline{D}^C \rho_s^D} \quad (5.3)$$

In Eq. 5.3, A, B, C, D, E, and F are coefficients of the correlation. By regressing the available mercury porosimetry data obtained from 450 Berea sandstone core plug samples, the values of the coefficients were obtained. After the substitution of the values of the coefficients into Eq. 5.3, it results into the new correlation for estimating mercury recovery efficiency for sandstones, as presented in Eq. 5.4:

$$RE = \frac{SA^{0.689} \phi_{Hg}}{26.9 V_{int.}^{1.65} \overline{D}^{0.242} \rho_s^{0.369}} \quad (5.4)$$

The units of mercury recovery efficiency, RE, mercury porosity, ϕ_{Hg}, and the other variables in Eq. 5.4 are as defined in the nomenclature.

To test the quality of the correlation, a crossplot to compare the predicted mercury recovery efficiency values using Eq. 5.4 with the measured values is shown in Fig. 5.94. The solid 45° line in the figure represents a perfect correlation between the measured and estimated mercury recovery efficiencies. Most of the plotted data points of this new correlation fall close to the 45° line, indicating its good degree of correlation. It has a standard deviation value of 0.0569, F-test statistic value of 232.0, and statistically

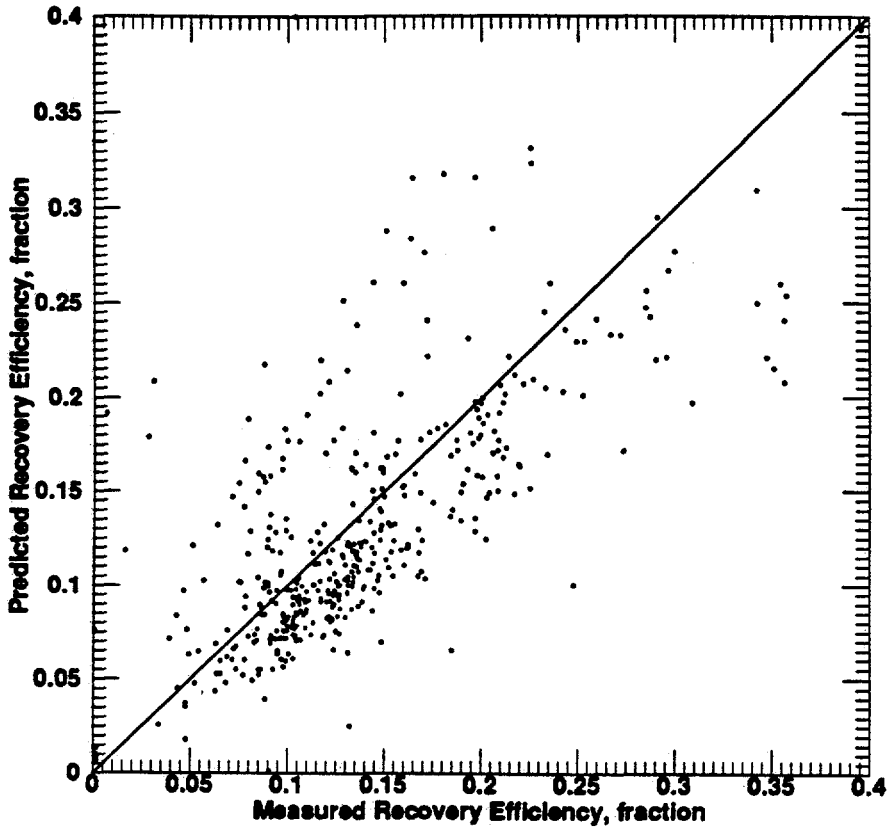

Fig. 5.94: Comparison of Measured Mercury Recovery Efficiency Values for Sandstones with those Predicted by the New Correlation.

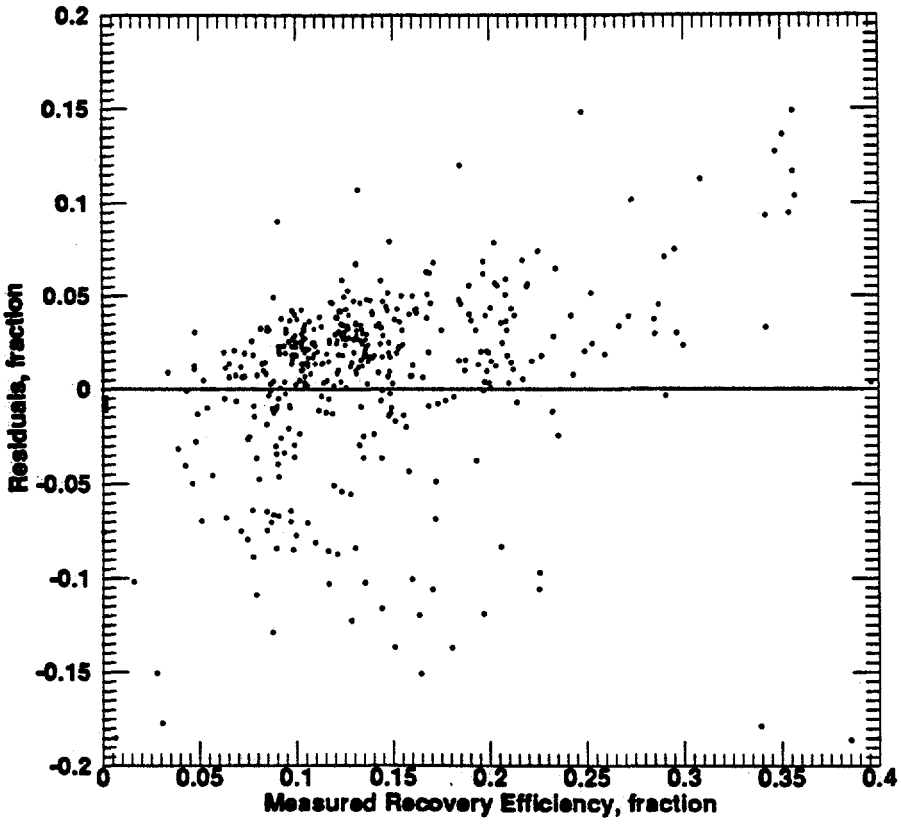

Fig. 5.95: Plotted Residuals Using the New Correlation vs. Measure Mercury Recovery Efficiency for Sandstones.

significant with p-value of 0.000.

Furthermore, another method of evaluating the adequacy of the regressed correlation is to examine a plot of the residuals, which are simply the differences between the individual measured values of the dependent variable and the predicted values. This plot of residuals versus measured mercury recovery efficiency for sandstones is shown in Fig. 5.95. The behavior of the plot suggests that the independent variables in the correlation were enough to define the dependent variable.

5.3.5.2 Relation Between Porosimetry and Petrophysical Properties

Correlation matrices for the full models (making use of data from waterflood, wettability, and mercury porosimetry experiments) at breakthrough and at floodout for Berea sandstones were investigated and presented in Tables 5.16 and 5.17, respectively. The agreement between porosity values obtained using mercury porosimetry and those obtained from the corefloods were not as good as expected, as shown in Fig. 5.96. It was observed that if a 45° degree line is drawn on the plot, most of the data points lie above the line. This indicates that the brine porosities were larger than the mercury porosities for these data points. According to Howard (1991), it is expected that the porosity measured by mercury porosimetry would be less than the porosity measured by routine methods because of the limited intrusion pressures employed. He reiterated that experience with a wide range of sandstones and carbonates indicates that all of the void spaces are not filled at the maximum intrusion pressure of 60,000 psi. This results in porosities that are several percent less than standard brine porosity measurements.

The relationship of brine permeability versus total intrusion volume is presented in Fig. 5.97. Porosity and permeability were found to be directly related to total intrusion volume. The relationships of porosity, and permeability with specific surface area, were both found not to be statistically significant.

Table 5.16: Correlation Matrix for the Full Model for Berea Sandstone Linear-Cores at Breakthrough

	ϕ brine	k	WI	S_{wi}	$V_{int.}$	SA	S_s	$\bar{D}$	ρ_s	ϕ Hg	RE	S_{or} @ B.T.
k	0.884											
WI	-0.329	-0.267										
S_{wi}	-0.030	0.059	-0.176									
$V_{int.}$	0.720	0.679	-0.520	-0.268								
SA	0.145	0.295	0.246	0.297	-0.108							
S_s	-0.112	0.039	0.405	0.364	-0.410	0.945						
$\bar{D}$	-0.009	-0.091	0.158	0.109	-0.263	0.326	0.348					
ρ_s	0.271	0.343	-0.205	0.219	0.447	0.399	0.269	-0.295				
ϕ_{Hg}	0.682	0.653	-0.489	-0.269	0.994	-0.091	-0.386	-0.295	0.504			
RE	-0.159	-0.118	0.316	-0.013	-0.261	0.251	0.337	-0.620	0.171	-0.221		
S_{or} @ B.T.	-0.473	-0.493	0.443	-0.496	-0.421	-0.307	-0.135	-0.177	-0.296	-0.373	0.288	
OR @ B.T.	0.436	0.338	-0.304	-0.547	0.637	-0.090	-0.306	0.079	0.003	0.585	-0.314	-0.437

B.T. = Breakthrough

Table 5.17: Correlation Matrix for the Full Model for Berea Sandstone Linear-Cores at Floodout

	ϕ brine	k	WI	S_{wi}	$V_{int.}$	SA	S_g	$\bar{D}$	ρ_g	ϕ Hg	RE	S_{or} @ F.O.
k	0.884											
WI	-0.329	-0.267										
S_{wi}	-0.030	0.059	-0.176									
$V_{int.}$	0.720	0.679	-0.520	-0.268								
SA	0.145	0.295	0.246	0.297	-0.108							
S_g	-0.112	0.039	0.405	0.364	-0.410	0.945						
$\bar{D}$	-0.009	-0.091	0.158	0.109	-0.263	0.326	0.348					
ρ_g	0.271	0.343	-0.205	0.219	0.447	0.399	0.269	-0.295				
ϕ_{Hg}	0.682	0.653	-0.489	-0.269	0.994	-0.091	-0.386	-0.295	0.504			
RE	-0.159	-0.118	0.316	-0.013	-0.261	0.251	0.337	-0.620	0.171	-0.221		
S_{or} @ F.O.	-0.296	-0.399	0.350	-0.755	-0.238	-0.324	-0.235	-0.108	-0.441	-0.223	0.242	
OR @ F.O.	0.447	0.461	-0.377	-0.257	0.758	0.010	-0.223	0.010	0.286	0.736	-0.357	-0.409

F.O. = Floodout

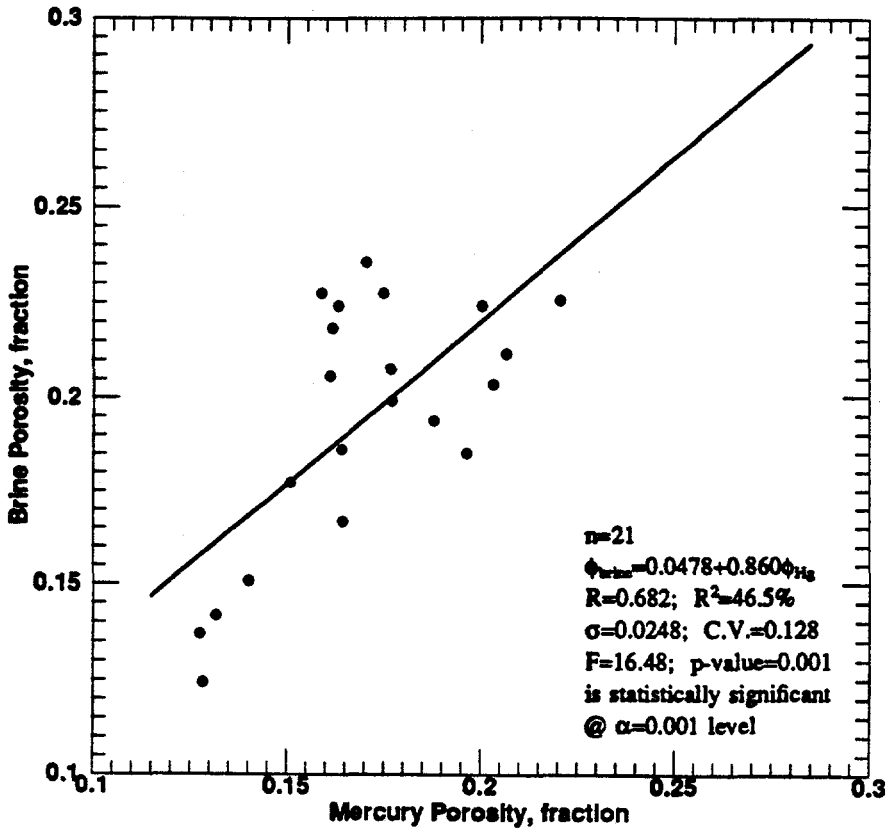

Fig. 5.96: Brine Porosity vs. Mercury Porosity for Berea Sandstone Linear-Cores.

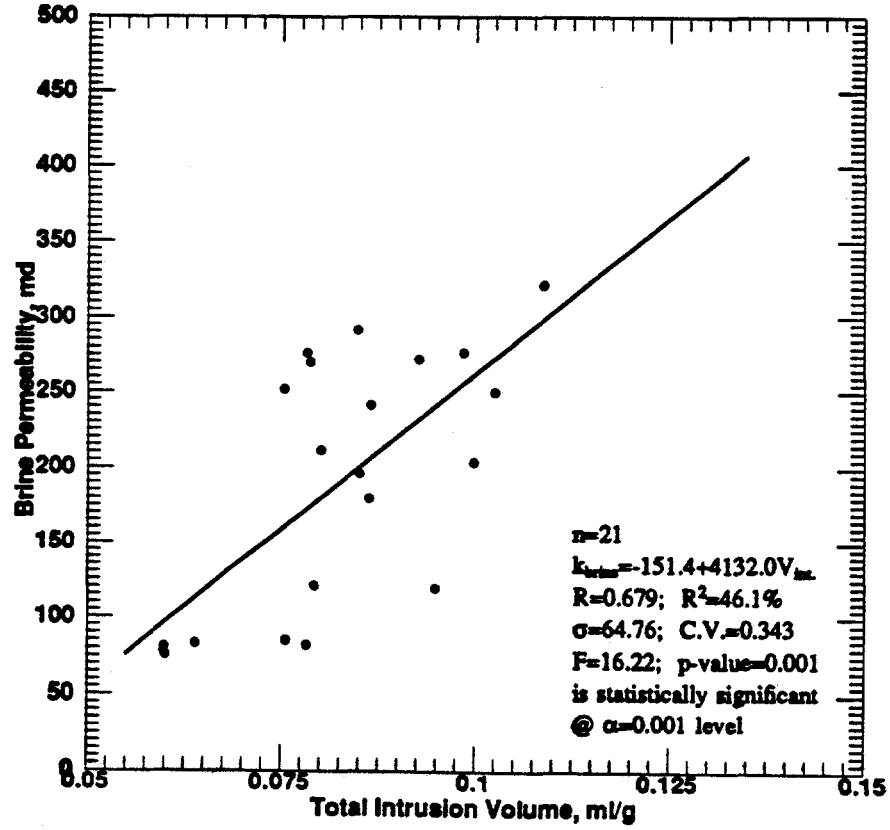

Fig. 5.97: Brine Permeability vs. Total Intrusion Volume for Berea Sandstone Linear-Cores.

5.3.5.3 Relation Between Porosimetry and Waterflood Properties

The mercury porosimetry properties were individually related to the residual oil saturation and oil recovery at breakthrough and at floodout, as shown in Tables 5.16 and 5.17. Except for the relationship between oil recovery (at breakthrough and at floodout) with total intrusion volume and with mercury porosity, the relationships were observed to be not statistically significant at $\alpha = 0.1$ level. The relatively low correlation coefficients resulting from these relationships indicate that except for total intrusion volume and mercury porosity, none of these mercury porosimetry properties dominantly controls waterflood results. Instead, all of them together influence residual oil saturation and oil recovery in reservoir rocks, as will be shown in next chapter (which deals with the development of the empirical models).

5.3.5.4 Permeability Correlation

The permeability dictates the speed at which fluid flow through various layers of reservoir rock (Pugh et al., 1991). There is an increasing need for good, simple to use correlation to estimate permeability. The estimation of reservoir rock permeability from mercury porosimetry data is important when routine permeability measurements cannot be performed, as in the case of very small core plugs or drill-cuttings. This estimate is also important when there is a need to minimize core analysis cost or when measurements of permeability are of questionable accuracy, as in the case of reservoir rocks with microfractures.

Using non-linear multiple regression analysis, as in the case of mercury recovery efficiency, a new correlation for estimating permeability values for sandstones using coreflood or mercury porosimetry measured data has been developed. The development was initiated using the 21 sandstone linear-cores waterflood and mercury porosimetry experimentally obtained data. Here, it was initially assumed that:

$$k = f(\phi, V_{int.}, SA, S_g, \overline{D}, \rho_g) \tag{5.5}$$

The primary reason for using only the initial independent variables contained in Eq. 5.5, was to develop a correlation to estimate permeability based on the rock properties determined using mercury porosimetry.

In Eq. 5.5, the independent variable, ϕ, can either be brine porosity or mercury porosity, depending on whether the permeability is to be estimated from waterflood experimental core data (brine permeability) or from mercury porosimetry experimental core plug data (mercury permeability). After a series of analyses, it was observed that permeability could be correlated with only porosity, surface area, and specific surface area as the independent variables in Eq. 5.5. The equation can then be re-written as:

$$k = f(\phi, SA, S_g) \tag{5.6}$$

To further improve the correlation, Eq. 5.6 was modified by dividing the dependent variable by $(1-\phi)^2$, which implies that:

$$\frac{k}{(1-\phi)^2} = f(\phi, SA, S_g) \tag{5.7}$$

After applying multiple regression analysis methods on Eq. 5.7, the resulting developed correlation for estimating permeability is given as:

$$k = \frac{7.834 * 10^5 \, \phi^{3.46} (1-\phi)^2 \, SA^{0.230}}{S_g^{0.192}} \tag{5.8}$$

In Eq. 5.8, permeability, k, is expressed in millidarcy and porosity, ϕ, is expressed in fraction. The other variables in the equation are as defined in the nomenclature.

To show how good the correlation is, a crossplot to compare the predicted brine permeability values using the new correlation, as presented in Eq. 5.8, with the measured

values is shown in Fig. 5.98. Most of the plotted data points of this new correlation fall close to the 45° line, indicating its a good correlation. It has a standard deviation of 0.0546, F-test statistic value of 191.3, and statistically significant at $\alpha = 0.001$ level. The plotted residuals versus measured brine permeability values for sandstones is shown in Fig. 5.99. The behavior of the plot suggests that porosity, surface area, and specific surface area were enough to develop a good correlation for permeability.

Equation 5.8 was also used to estimate mercury permeability of the core plug samples. The resulting estimates of mercury permeability values for the 450 sandstone core plug samples were plotted against the respective values of their measured mercury porosity values, as shown in Fig. 5.100. The plotted data points fall very close to an exponential trend as expected for the relationship of porosity with permeability. Finally, the estimated average mercury permeability values were compared with the measured brine permeability values as shown in Fig. 5.101. Similar to the observation in Fig. 5.96, which is the plot of brine porosity versus mercury porosity, the comparison was not perfect.

Swanson (1981) developed permeability correlations for sandstones and carbonates using parameters from capillary-pressure curves. His data base consists of 116 carbonates and 203 sandstones from 74 formations. Thompson et al. (1987) used percolation theory to develop theoretical models to predict permeability from mercury porosimetry data. They proposed that the theory was valid for essentially all porous rocks. Other recent permeability correlations include those of Pittman (1992) and Kamath (1992). The predictive strength of the new correlation for sandstones is not compared with that of these correlations. This was because the conductivity formation factor values for the rock samples needed to use Thompson et al.'s model, were not measured in this study. Also, it is time consuming to estimate the values of the maximum of the parameter, S_{Hg}/P_c, needed to be able to use the various models developed by Swanson, Pittman, and Kamath.

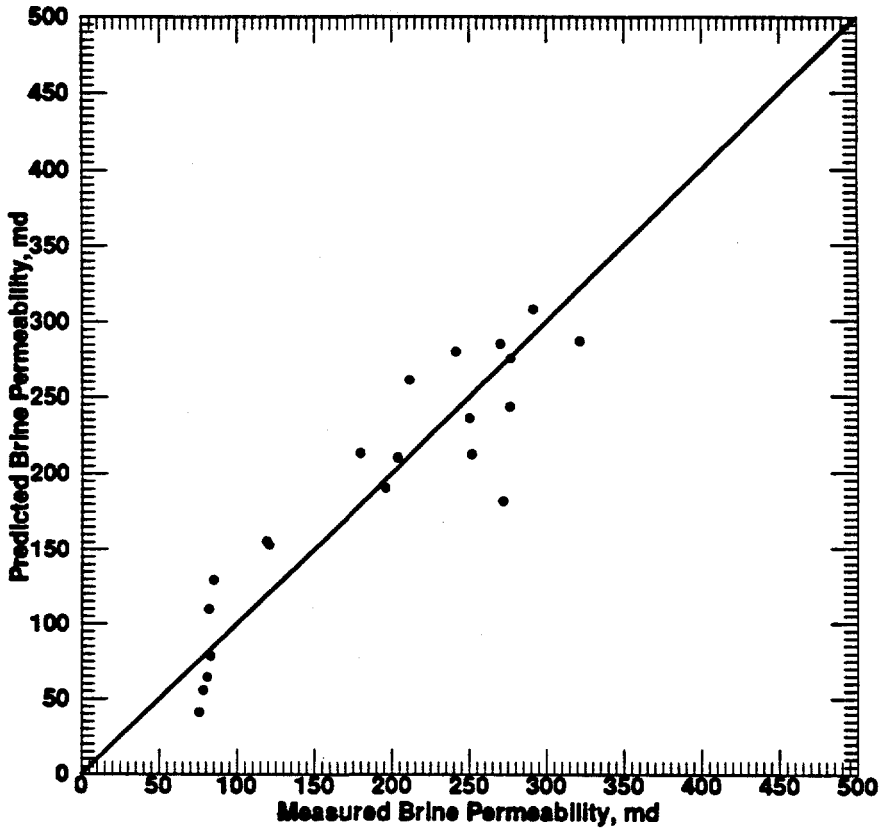

Fig. 5.98: Comparison of Measured Permeability Values for Sandstones with those Predicted by the New Correlation.

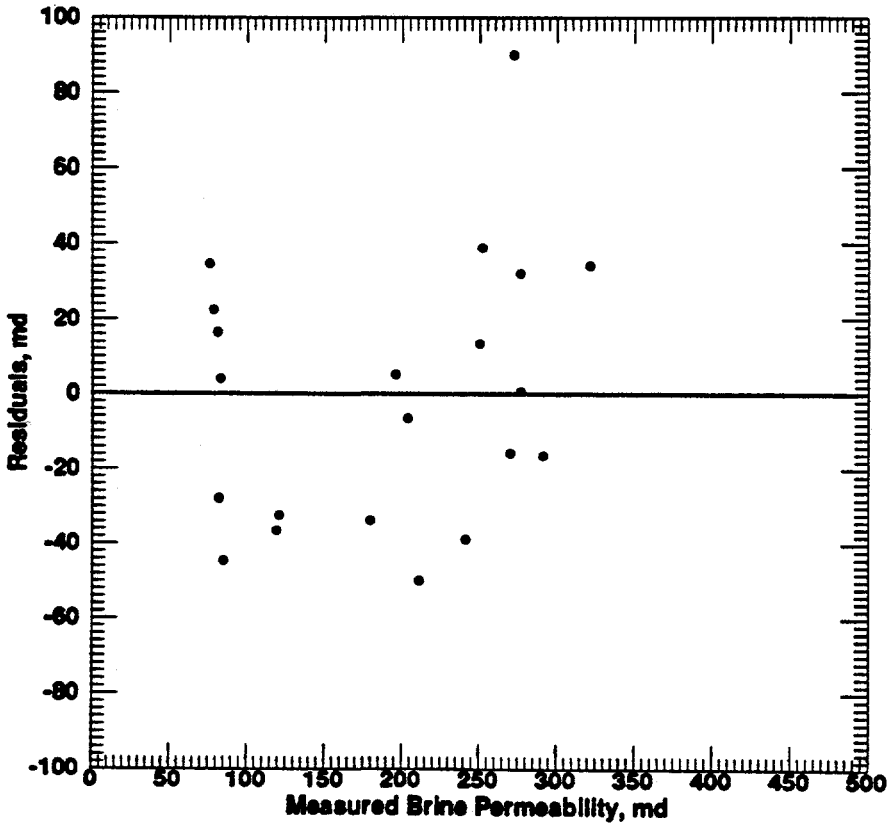

Fig. 5.99: Plotted Residuals Using the New Correlation vs. Measure Permeability for Sandstones.

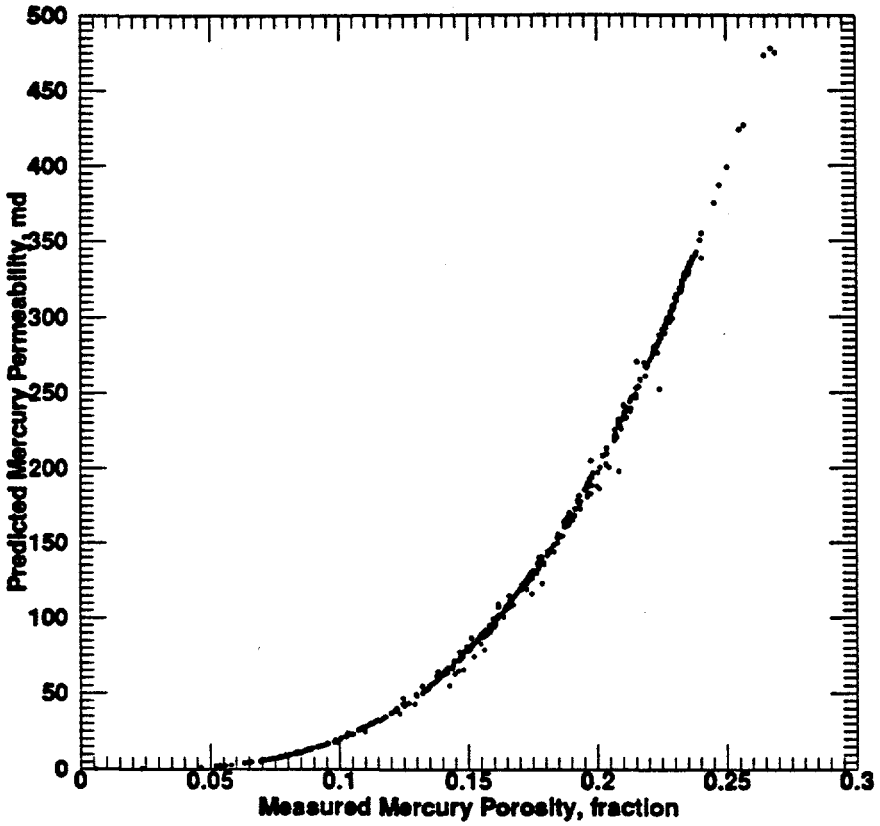

Fig. 5.100: Mercury Permeability for Sandstones Predicted by Using the New Correlation vs. Measured Mercury Porosity.

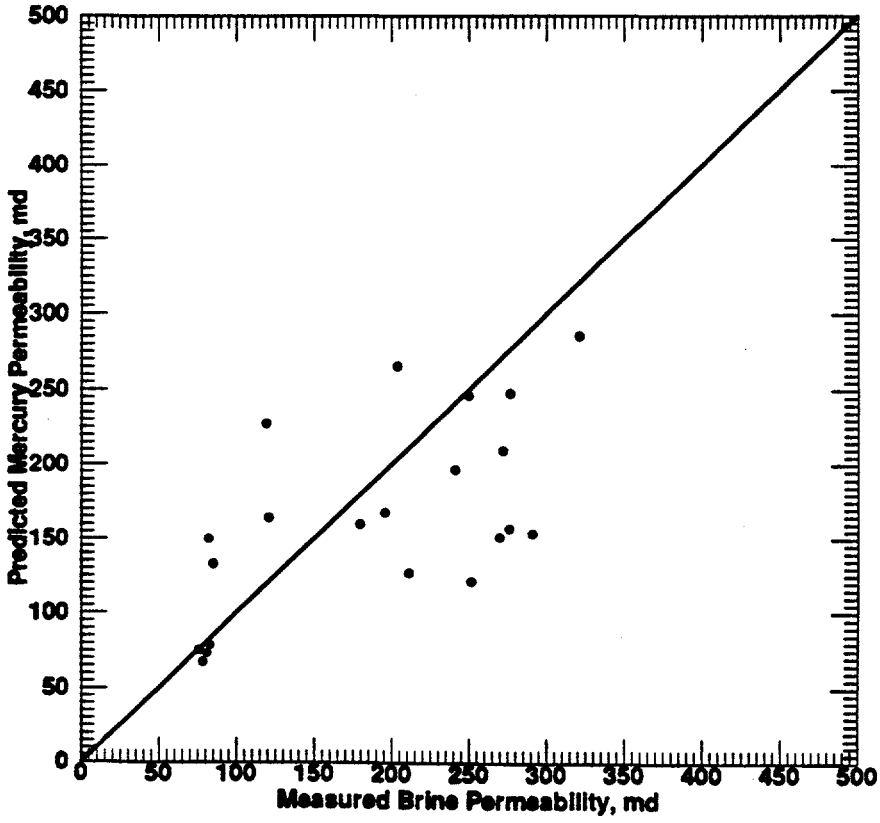

Fig. 5.101: Comparison of Measured Brine Permeability Values for Sandstones with Mercury Permeability Predicted by the New Correlation.

5.3.5.5 Relation Between Porosimetry and Wettability Properties

The relationship of the average wettability index with the total intrusion volume is presented in Fig. 5.102. The trend is inverse and statistically significant at $\alpha = 0.05$ level. Average wettability index relationships with the other mercury porosimetry properties are shown in Tables 5.16 and 5.17. A direct relationship was observed with specific surface area and an inverse relationship was observed with mercury porosity was inverse. The relationships of average wettability index with all the other mercury porosimetry properties were found not to be statistically significant.

The observation of the effects of wettability on mercury porosimetry properties could be explained by the postulation of Roof (1970). He said that because of the small size of the pores in the reservoir rock or sand, capillary forces at the oil-water interface are of considerable importance in determining the nature of the flow through the pores. He showed that "snap-off" of oil in water-wet pores does not occur until the protrusion has grown to a radius much larger than that of the throat of the constriction.

5.3.5.6 Shape of Capillary Pressure Curve

The term capillary-pressure, as used in the reservoir analysis literature and in this paper, refers to the injection pressure necessary to inject non-wetting fluids (such as mercury) into the pore spaces of a rock. Capillary pressure curves and their hysteresis depend on the geometry of the pore structure, the wetting properties of the individual pores of a porous sample, and also on the accessibility of the pores from the surface of the sample (Larson and Morrow, 1981; Amthor and Friedman, 1988; Kopaska-Merkel and Friedman, 1989).

Reservoir rocks are classified in terms of their capillary-pressure curve form. This is because capillary-pressure curve form is controlled by various properties which can be

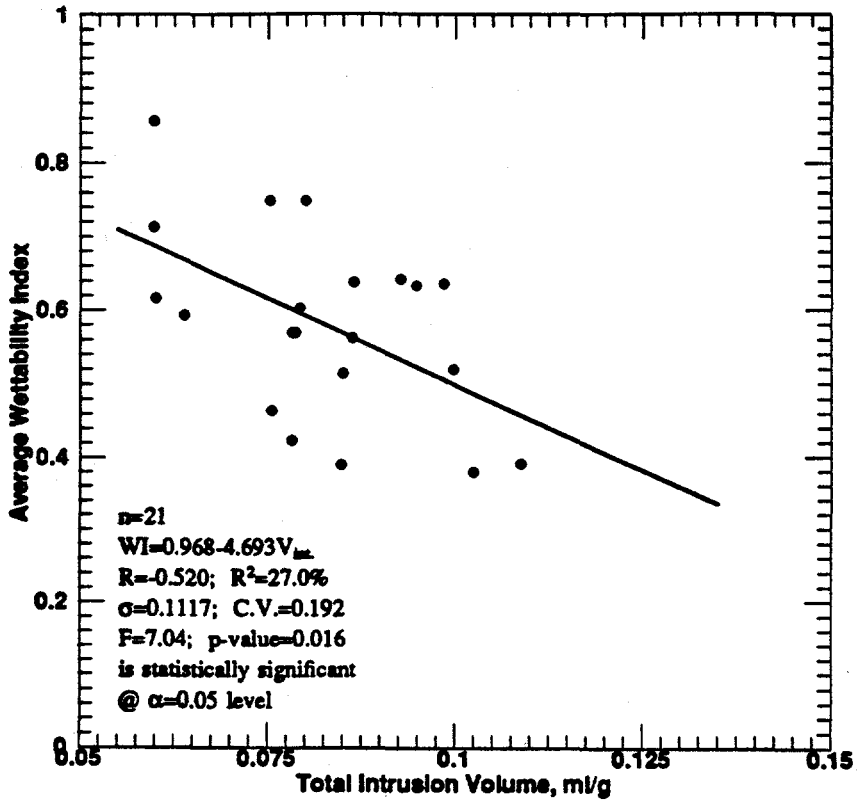

Fig. 5.102: Wettability Index vs. Total Intrusion Volume for Berea Sandstone Linear-Cores.

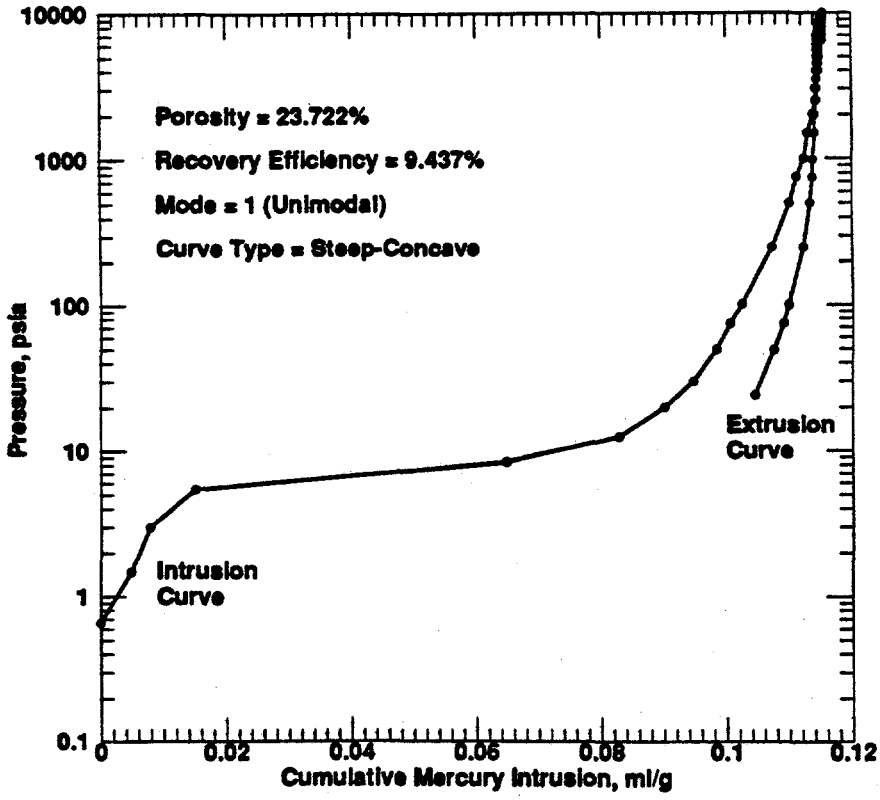

Fig. 5.103: Capillary Pressure vs. Cumulative Mercury Intrusion Curve for Berea Sandstone Linear-Core 2A - Plug 11.

measured, and because curve form is strongly correlated with recovery efficiency. According to Larson and Morrow (1981), variations in capillary-pressure curve shape reflect variation in pore structure. They further explained that geometrically similar porous media will have capillary pressure curves which are identical in shape and can be correlated by a factor which is equal or proportional to some microscopic length.

Figure 5.103 presents the capillary-pressure versus cumulative mercury intrusion/extrusion curve for plug 11 of sample core 2A. This figure shows that less energy is expended by the systems during extrusion than was gained during intrusion. Therefore, the sample is at a higher energy level at the completion of the cycle than at the beginning. The mode type of the curve is unimodal with steep-concave shape. This is further confirmed in Fig. 5.104, which is the plot of capillary pressure versus incremental mercury intrusion/extrusion curve for the same plug.

For most of the Berea sandstone core plugs investigated in this study, unimodal steep-concave capillary-pressure curve shapes were common. Steep-concave curves for the investigated samples correlate with low mercury recovery efficiencies (mean = 11%), high porosities (mean = 17%), moderate to large average pore diameters (mean = 5.2 μm), and low entry pressures. In the field, reservoir rocks exhibiting these types of behavior are not expected to perform well during primary production processes, but they are good candidates for undergoing enhanced recovery processes. The capillary-pressure versus cumulative pore area curve for the plug is presented in Fig. 5.105. Only the mercury intrusion data were used to plot Fig. 5.105.

Amthor et al. (1988) suggested that an ideal capillary-pressure curve (curve for an ideal reservoir) would have a moderate entry pressure (intermediate median throat size) but rapid intrusion over a small pressure range. Median throat size would be large enough so that porosity would be high, and small enough so that recovery would be good.

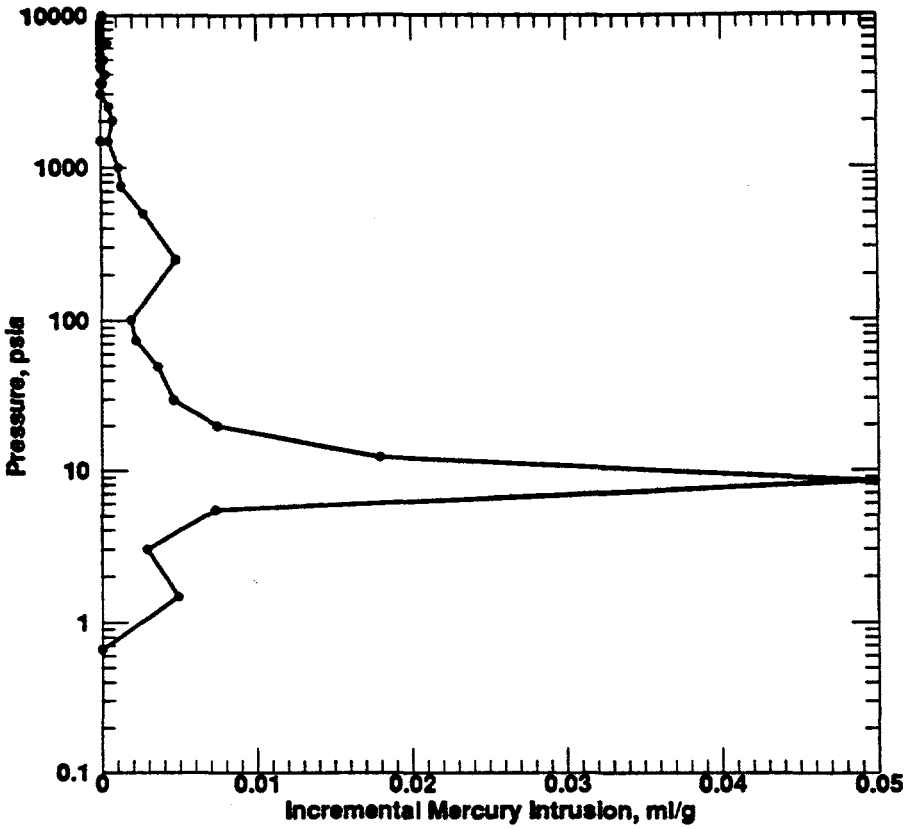

Fig. 5.104: Capillary Pressure vs. Incremental Mercury Intrusion Curve for Berea Sandstone Linear-Core 2A - Plug 11.

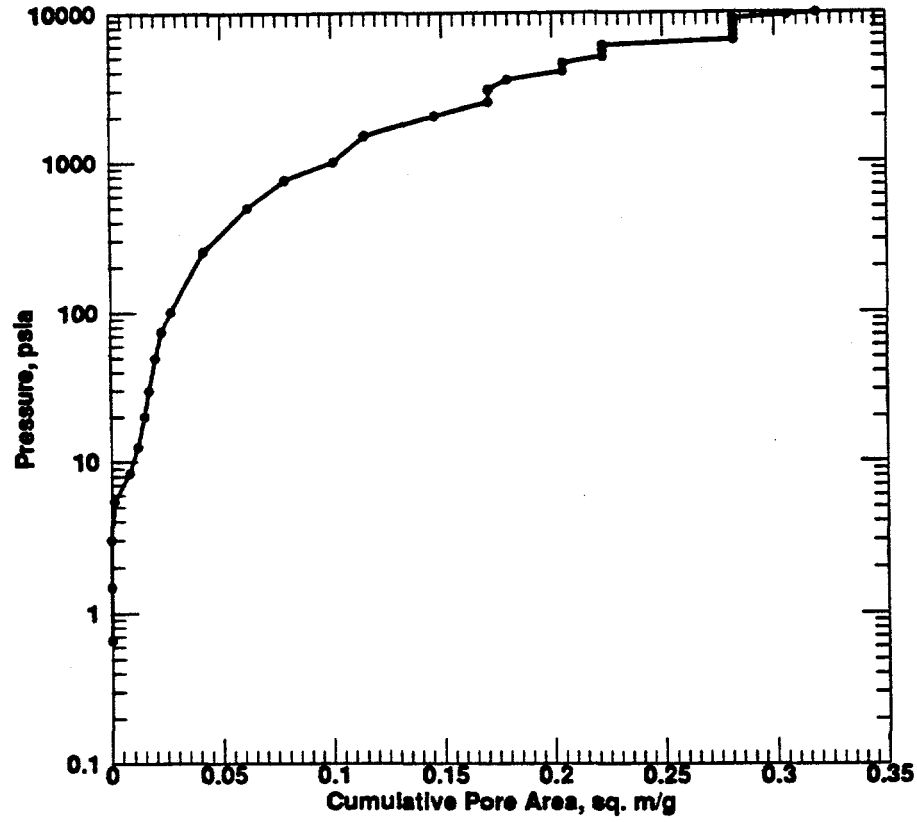

Fig. 5.105: Capillary Pressure vs. Cumulative Pore Area Curve for Berea Sandstone Linear-Core 2A - Plug 11.

5.4 Limestone Linear-Core Case

Sixteen sets of waterflooding displacement tests were conducted in Indiana limestone linear-core of varying lengths. Oil was displaced from the cores by brine at an overburden pressure of 500 psig and at a fixed temperature of 35°C. Brine was injected at rates varying from 1.23 to 1.48 cc/min, depending on the diameter and length of the core being tested. Similar to the sandstone case, the injection rate for each limestone core was determined using Eq. 2.1.

5.4.1 Introduction

The waterflood and wettability properties of the 16 Indiana limestone linear-cores are presented in Table 5.18. A detailed summary of the statistical description of the Indiana limestone experimental variables is shown in Table 5.19. The correlation matrix for the Indiana limestone waterflood properties is presented in Table 5.20. Regressed trend lines are provided on each of the plots for easy visualization of the influence of the various variables on one another.

5.4.2 Petrophysical Properties

The porosity, and permeability values measured using cores obtained from the same number cores indicated small variation. For all the Indiana limestone cores combined, the porosities varied from 14.1 to 16.2%, and the absolute permeabilities varied from 8.5 to 19.8 md. Compared to the sandstones data, the porosity and permeability data are lower for the limestones investigated. Petrophysical relationships or trends of limestone are of the same general type as observed for sandstones.

Figure 5.106 shows the plot of absolute permeability versus porosity for limestones. It shows a trend that as porosity increases, permeability increases. Pore structure is indicated in a qualitative way by the relation between porosity and permeability. As compared to

Table 5.18: Waterflood and Wettability Properties of the Indiana Limestone Linear-Cores

Core No.	S_{wi} (frac.)	WI	S_{or} @ B.T. (frac.)	S_{or} @ F.O. (frac.)	OR @ B.T. (% IOIP)	UOR @ F.O. (% IOIP)
9A	0.402	0.654	0.378	0.246	36.78	58.93
9B	0.454	0.650	0.256	0.188	53.09	65.65
10A	0.380	0.759	0.340	0.313	45.19	49.48
10B	0.520	0.692	0.270	0.243	43.75	49.42
11A	0.421	0.833	0.374	0.302	35.41	47.79
11B	0.440	0.766	0.355	0.296	36.63	47.18
12A	0.482	0.606	0.353	0.235	31.86	54.54
12B	0.451	0.712	0.289	0.238	47.39	56.54
13A	0.545	0.560	0.185	0.157	59.28	65.44
13B	0.391	0.788	0.414	0.316	32.00	48.21
14A	0.401	0.677	0.394	0.283	34.19	52.80
14B	0.432	0.715	0.418	0.288	26.40	49.29
15A	0.449	0.494	0.375	0.253	31.79	54.01
15B	0.371	0.669	0.409	0.330	34.98	47.60
16A	0.480	0.452	0.380	0.244	26.92	53.03
16B	0.437	0.723	0.458	0.278	18.64	50.61

Table 5.19: Statistical Description of the Waterflood and Wettability Variables for Indiana Limestone Linear-Cores

	OR @ B.T. (% IOIP)	UOR @ F.O. (%IOIP)	S_{or} @ B.T. (frac)	S_{or} @ F.O. (frac)	ϕ (frac)	k (md)	WI	$Ln_{w}\mu_{w}$	S_{wi} (frac)	N^{*}_{ca} (E-07)
Mean	37.14	53.16	0.353	0.263	0.151	12.62	0.672	5.015	0.441	7.064
Median	35.20	51.71	0.375	0.266	0.150	11.14	0.684	5.020	0.438	7.025
Min.	18.64	47.18	0.185	0.157	0.141	8.47	0.452	4.960	0.371	6.940
Max.	59.28	65.65	0.458	0.330	0.162	19.83	0.833	5.040	0.545	7.910
Q1	31.80	48.48	0.301	0.239	0.147	10.19	0.617	5.000	0.401	6.975
Q3	44.83	56.04	0.405	0.301	0.155	14.87	0.750	5.030	0.473	7.040
St. Dev.	10.39	5.91	0.071	0.047	0.006	3.35	0.103	0.020	0.049	0.229

Table 5.20: Correlation Matrix for the Waterflood and Wettability Properties for Indiana Limestone Linear-Cores

	ϕ	k	WI	S_{wi}	S_{or} @ B.T.	S_{or} @ F.O.	OR @ B.T.
k	0.496						
WI	0.188	-0.188					
S_{wi}	-0.050	0.166	-0.492				
S_{or} @ B.T.	-0.271	-0.605	0.219	-0.678			
S_{or} @ F.O.	-0.094	-0.581	0.575	-0.800	0.736		
OR @ B.T.	0.351	0.681	-0.023	0.361	-0.928	-0.579	
UOR @ F.O.	0.158	0.724	-0.493	0.474	-0.707	-0.677	0.628

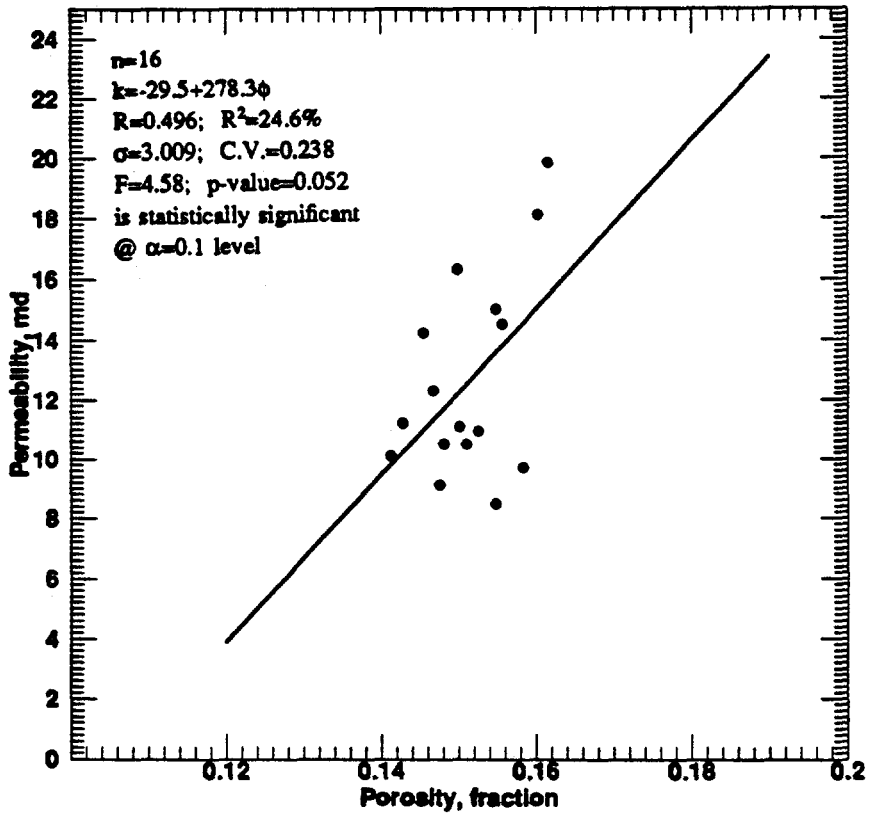

Fig. 5.106: Permeability vs. Porosity for Indiana Limestone Linear-Cores.

other carbonate rocks, the Indiana limestone data investigated in this study have high porosity and low permeability values. This type of reservoir rock suggests smaller pores and generally higher irreducible water saturation, as confirmed in Table 4.4 and later in the mercury porosimetry data analyses. The samples mean value for irreducible water saturation is 0.44 and that of the average pore diameter is 0.30 μm.

According to Wang et al. (1991), the relationship between porosity and permeability is only qualitative. For the same porosity, the permeability may differ by more than two orders of magnitude. They were of the opinion that an exact relationship between porosity and permeability is impossible to obtain for real rocks. They stated further that theoretically, a high porosity rock may have very low permeability if the pores are not well connected, and a low porosity rock may have high permeability if the pores are connected by fractures.

5.4.3 Waterflood Properties

Plots of the cumulative oil recovery in percent of initial oil-in-place versus cumulative brine injected in pore volume for the 16 core samples tested are presented in Figs. 5.107 through 5.110. Similar to the case of Berea sandstone core, the same numbered cores were taken from the same 3-ft. long core. The results of all the same numbered linear-core samples appeared to be similar. The production performance (producing water/oil ratio versus cumulative oil recovery in percent initial oil-in-place) for each of the 16 core samples are shown in Figs. 5.111 through 5.114. In all the tests, the water breakthrough point occurred at less than 0.3 pore volume of injected brine. As shown in Table 4.4, floodout occurred at various pore volumes of injected brine.

Furthermore, similar to the case for sandstone waterfloods, it is observed from Table 5.18 and Figs. 5.107 through 5.114 that in strongly water-wet floods, breakthrough occurs relatively late and very little oil is produced after water breakthrough, as shown for example

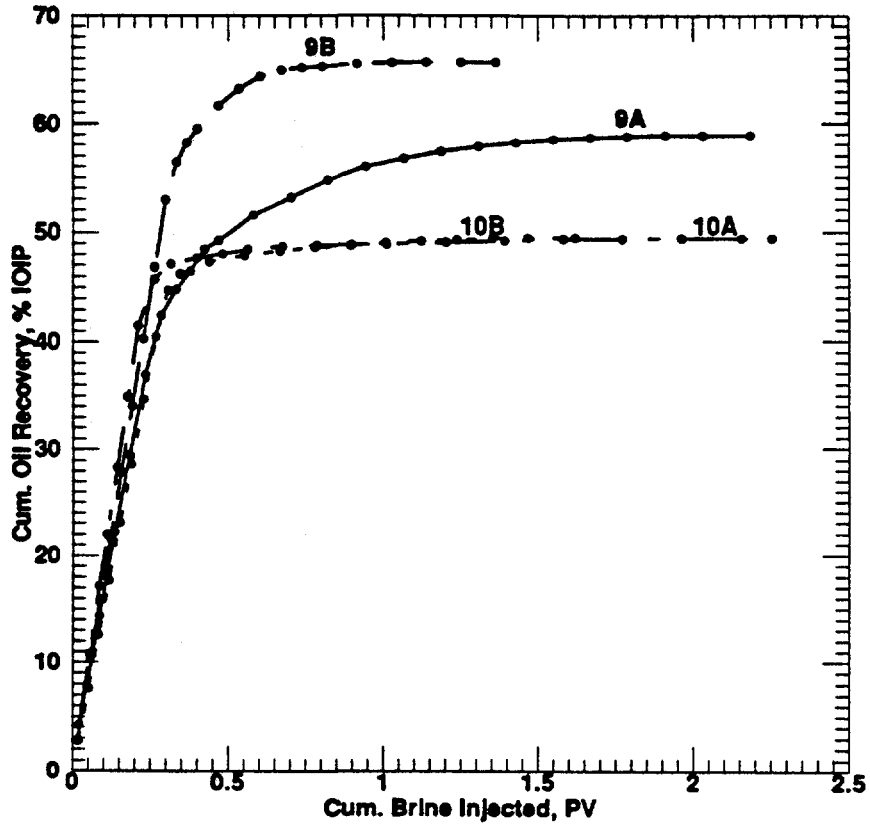

Fig. 5.107: Cumulative Oil Recovery vs. Cumulative Brine Injected for Indiana Limestone Linear-Core Samples 9A, 9B, 10A and 10B.

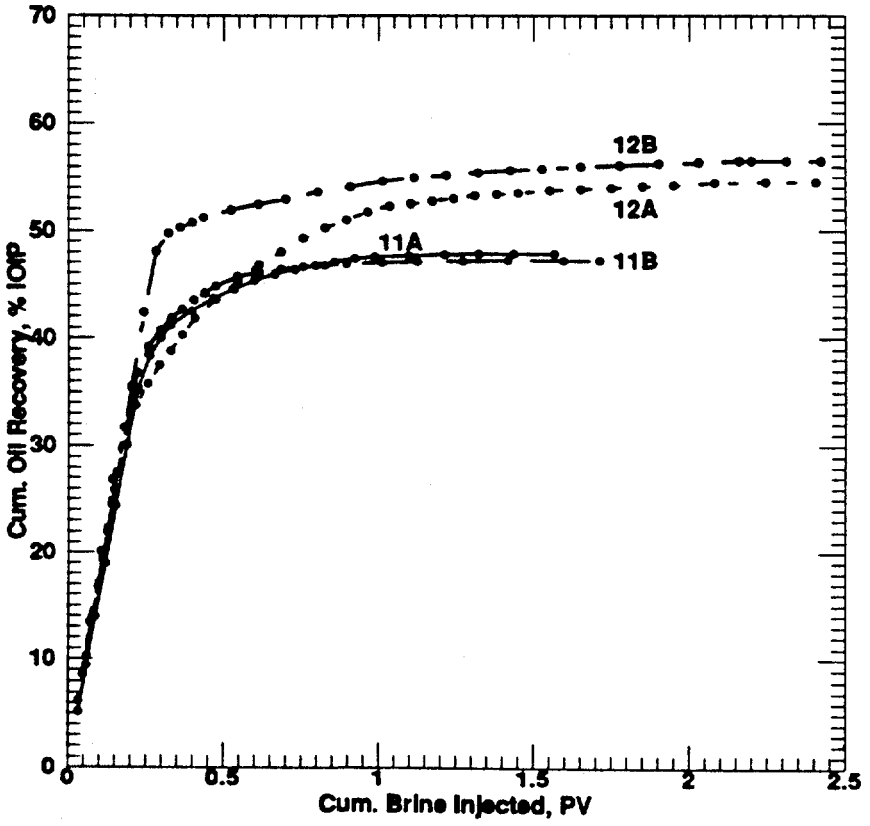

Fig. 5.108: Cumulative Oil Recovery vs. Cumulative Brine Injected for Indiana Limestone Linear-Core Samples 11A, 11B, 12A and 12B.

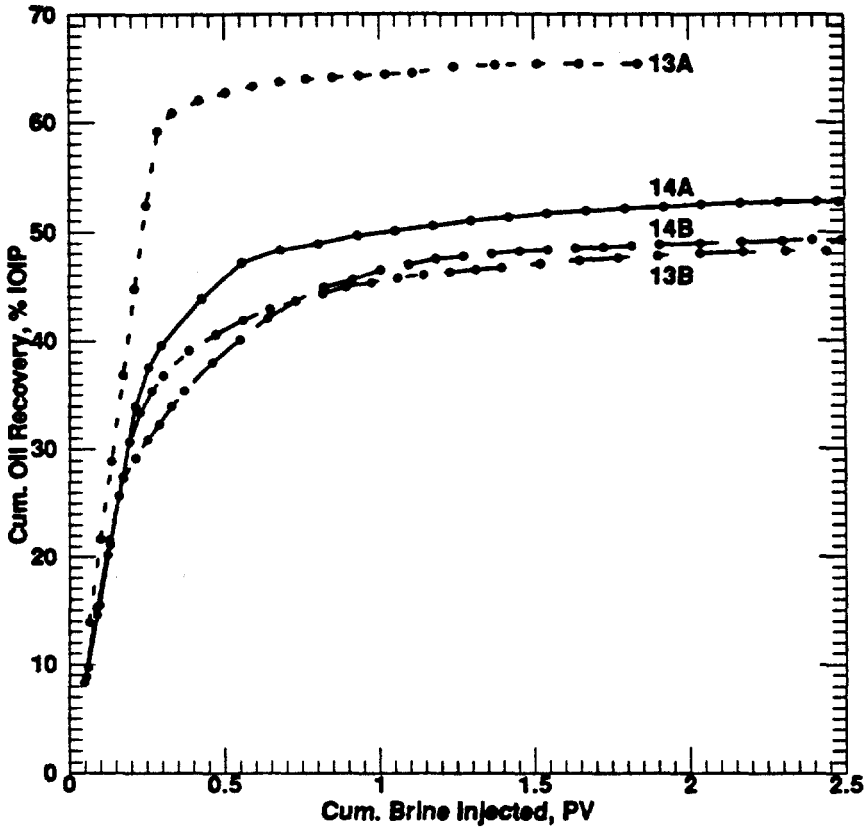

Fig. 5.109: Cumulative Oil Recovery vs. Cumulative Brine Injected for Indiana Limestone Linear-Core Samples 13A, 13B, 14A, 14B.

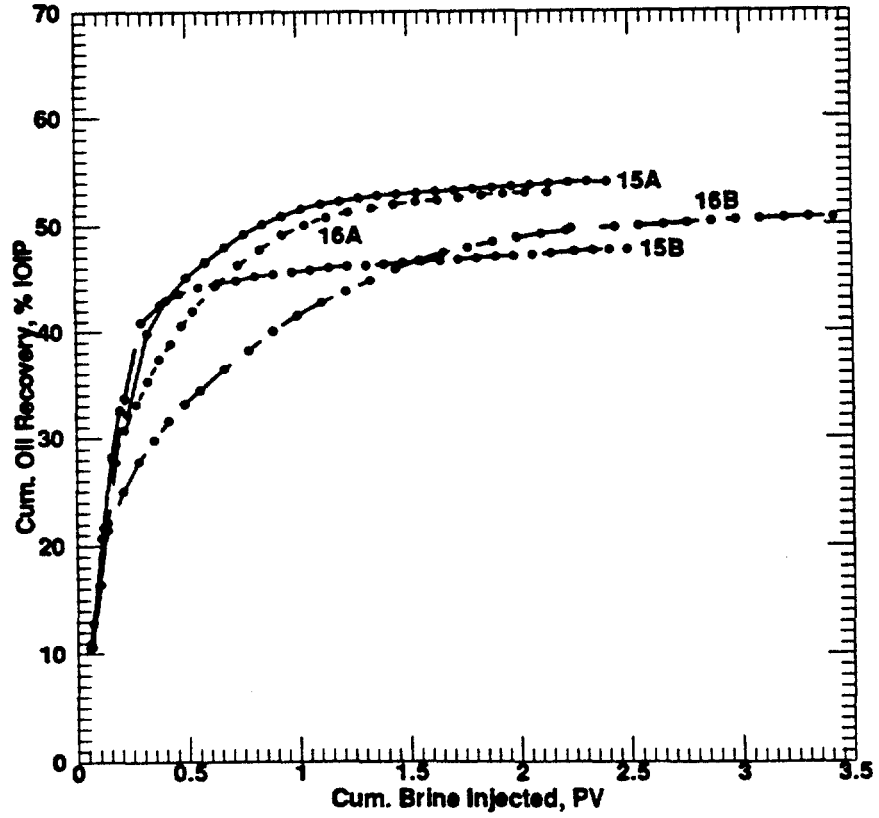

Fig. 5.110: Cumulative Oil Recovery vs. Cumulative Brine Injected for Indiana Limestone Linear-Core Samples 15A, 15B, 16A and 16B.

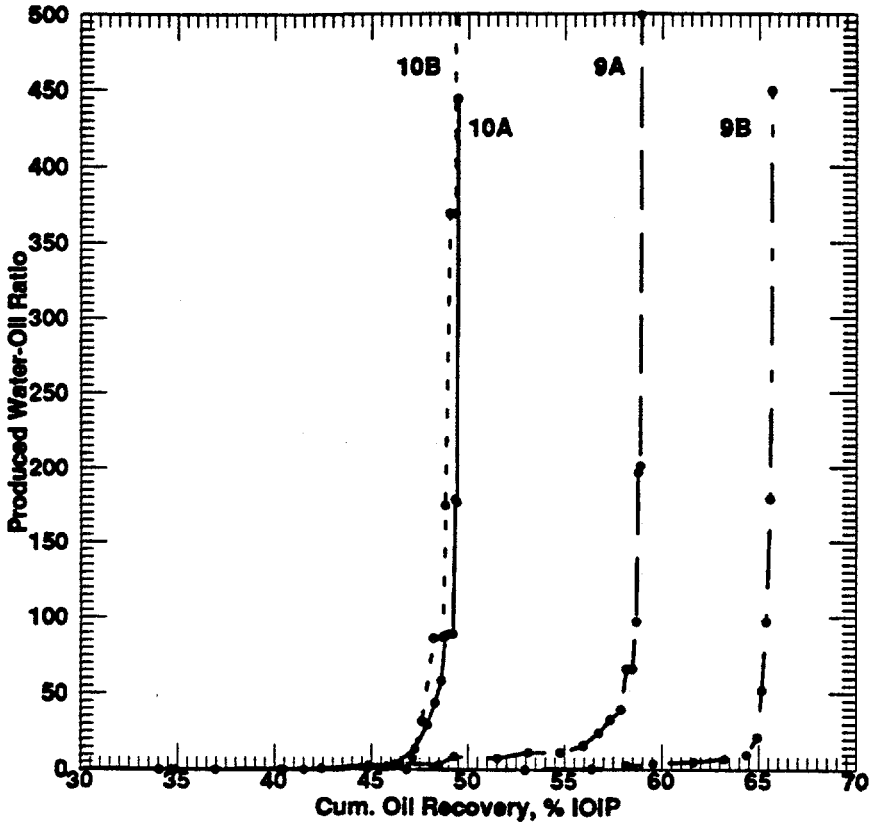

Fig. 5.111: Produced Water-Oil Ratio vs. Cumulative Oil Recovery for Indiana Limestone Linear-Core Samples 9A, 9B, 10A, and 10B.

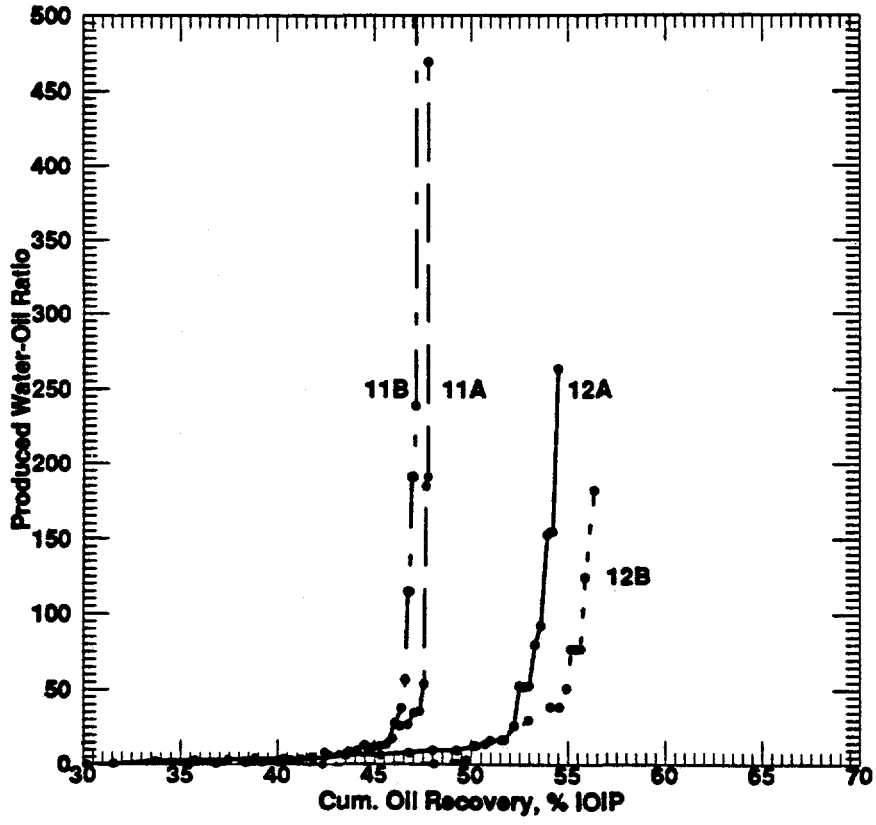

Fig. 5.112: Produced Water-Oil Ratio vs. Cumulative Oil Recovery for Indiana Limestone Linear-Core Samples 11A, 11B, 12A and 12B.

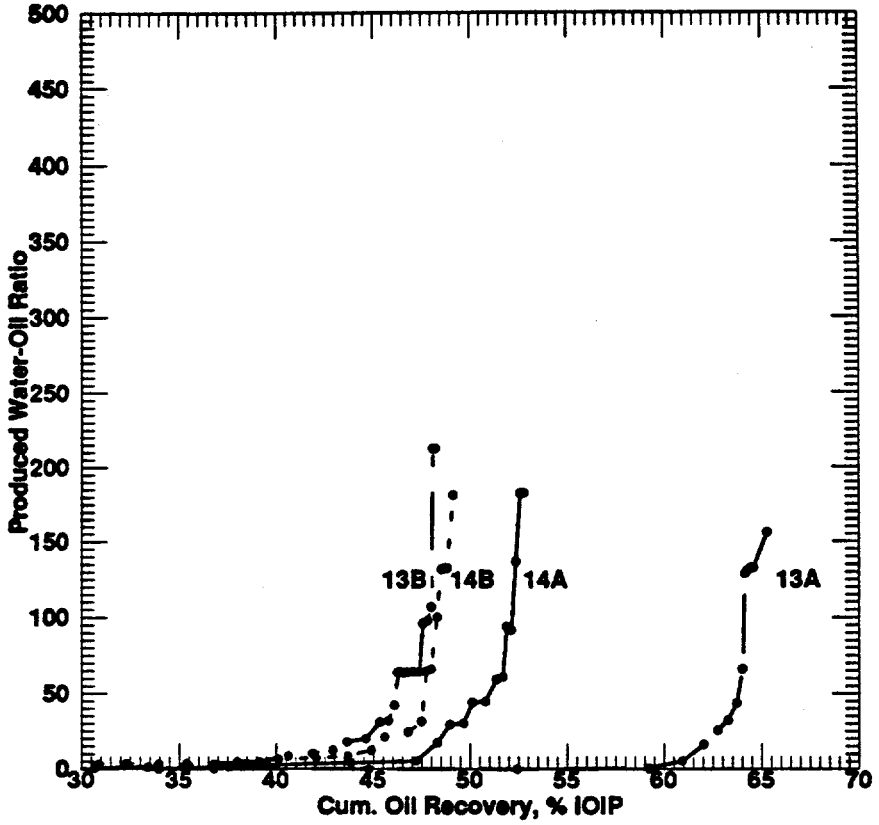

Fig. 5.113: Produced Water-Oil Ratio vs. Cumulative Oil Recovery for Indiana Limestone Linear-Core Samples 13A, 13B, 14A and 14B.

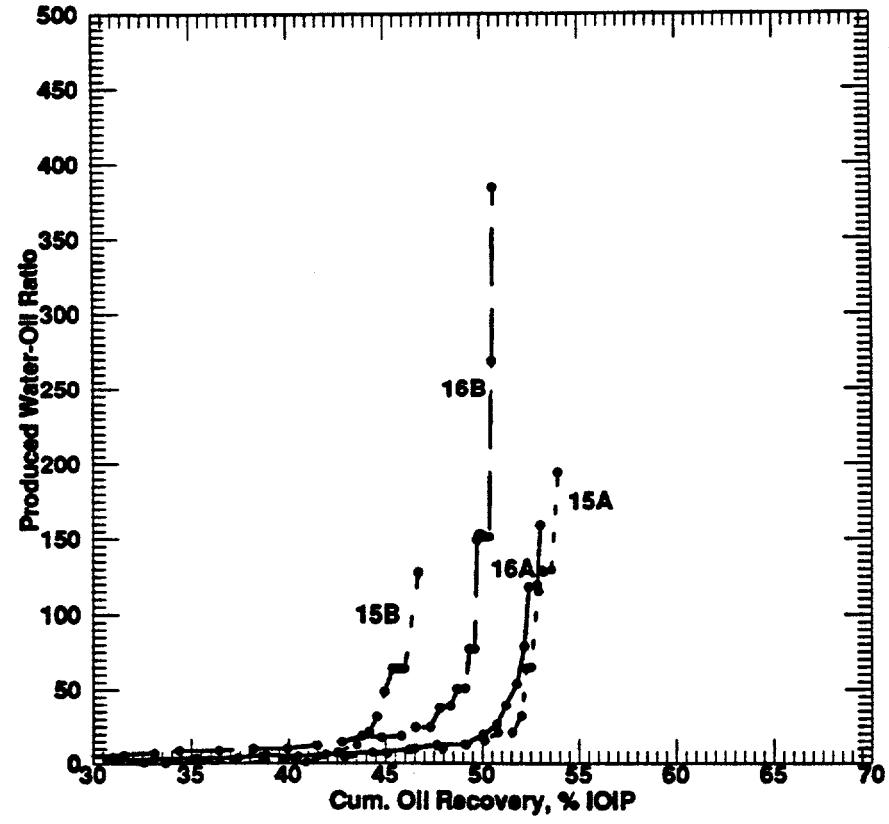

Fig. 5.114: Produced Water-Oil Ratio vs. Cumulative Oil Recovery for Indiana Limestone Linear-Core Samples 15A, 15B, 16A and 16B.

in the plots of Core Sample Nos. 10A, and 10B. Also, the water/oil ratio in strongly water-wet floods rises rapidly. However, in weakly water-wet floods, breakthrough occurs at an earlier time and the water rises gradually, as shown for example in the plots of Core Sample Nos. 14A through 16B.

Figure 5.115 shows residual oil saturation profiles at both the breakthrough and at floodout. The profiles of oil recovery at breakthrough and at floodout, are shown in Fig. 5.116. At breakthrough the residual oil saturation ranged from 0.185 to 0.458 and from 0.157 to 0.330 at floodout. The oil recovery at breakthrough values ranged from 18.6 to 59.3% IOIP and at floodout the ultimate oil recovery values ranged from 47.2 to 65.6% IOIP. The irreducible water saturation values ranged from 0.371 to 0.545, with a mean value of 0.441. The mean value for the irreducible water saturation of the investigated Indiana limestone cores are comparable to that of the investigated Berea sandstone cores.

Residual oil saturation versus irreducible water saturation at breakthrough and at floodout are plotted in Figs. 5.117 and 5.118, respectively. Oil recovery versus irreducible water saturation at breakthrough and at floodout are plotted in Figs. 5.119 and 5.120, respectively. These plots indicate that residual oil saturation is inversely related to irreducible water saturation, whereas, ultimate oil recovery at floodout is directly related to irreducible water saturation. The relationship of oil recovery at breakthrough with irreducible water saturation failed the significance test. The relationships between oil recovery and residual oil saturation at breakthrough and floodout are shown in Figs. 5.121 and 5.122, respectively. As expected, the plots show that oil recovery is inversely related to residual oil saturation, with coefficients of determination of more than 80% and strongly statistically significant at $\alpha = 0.001$ level.

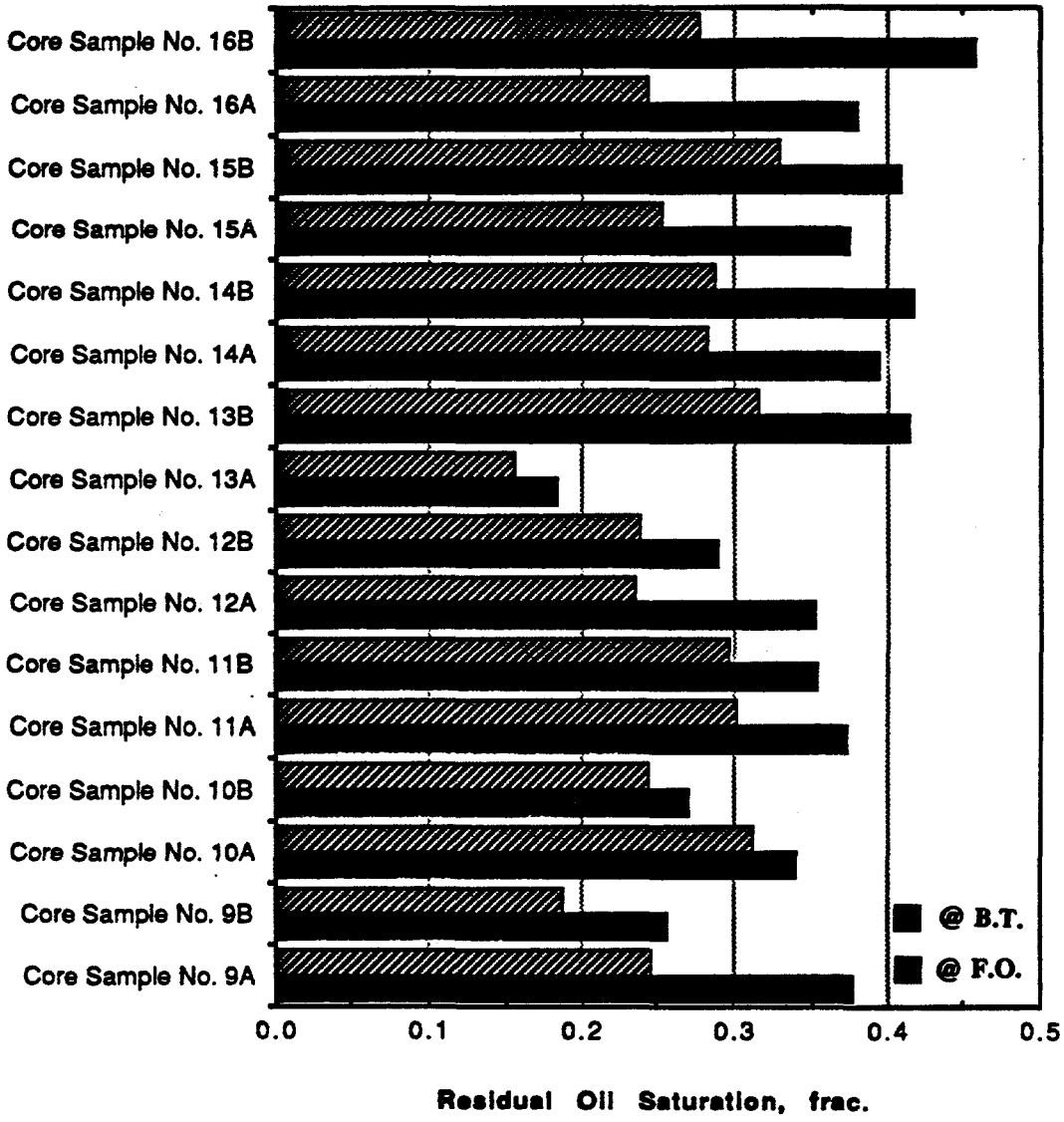

Fig. 5.115: Residual Oil Saturation Profiles at Breakthrough and Floodout for Indiana Limestone Linear-Cores.

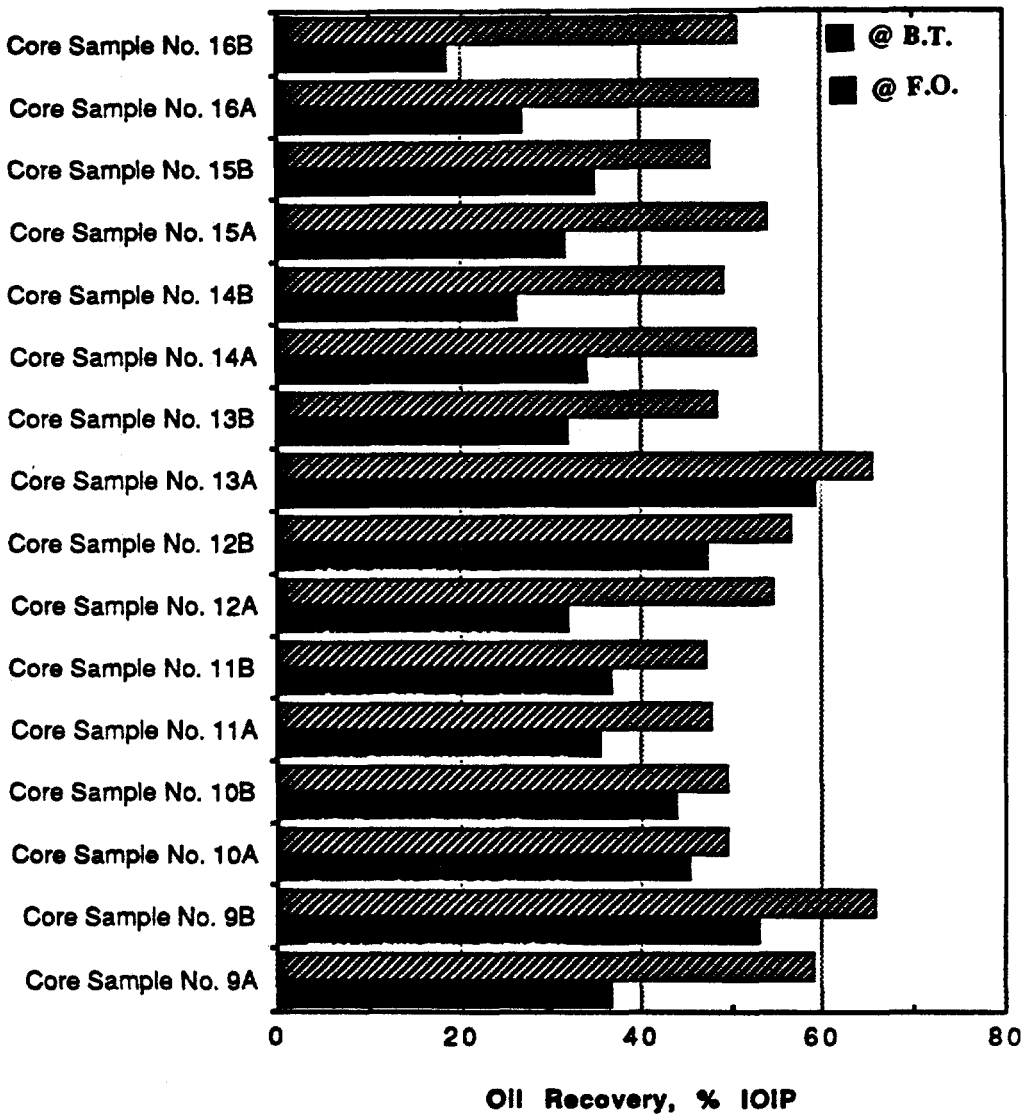

Fig. 5.116: Oil Recovery Profiles at Breakthrough and Floodout for Indiana Limestone Linear-Cores.

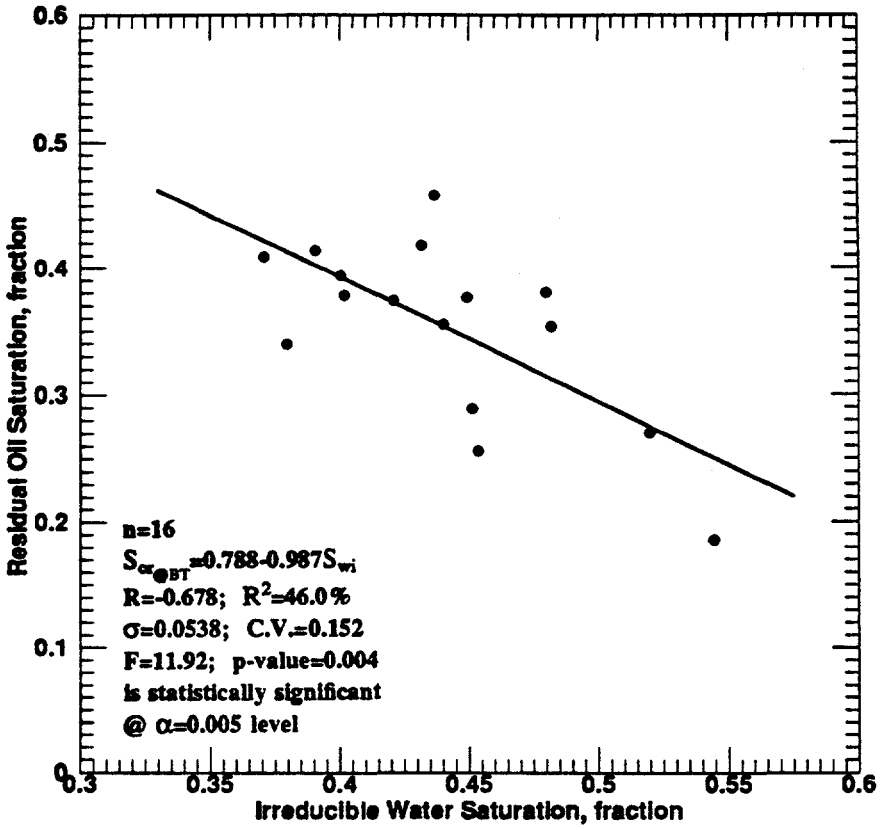

Fig. 5.117: Residual Oil Saturation vs. Irreducible Water Saturation for Indiana Limestone Linear-Cores at Breakthrough.

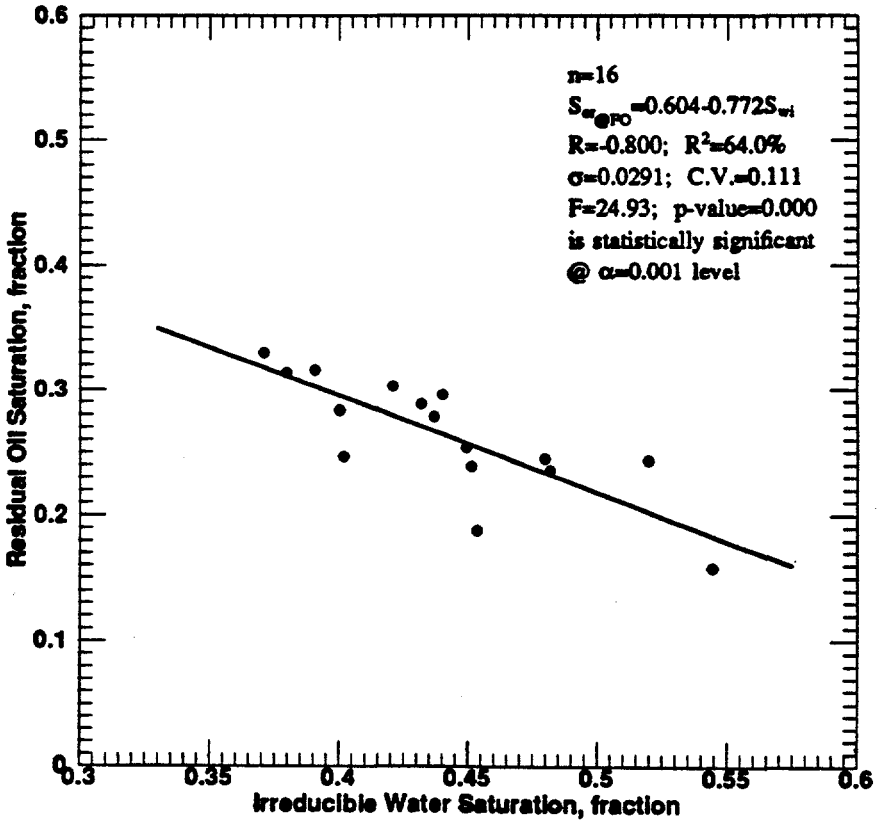

Fig. 5.118: Residual Oil Saturation vs. Irreducible Water Saturation for Indiana Limestone Linear-Cores at Floodout.

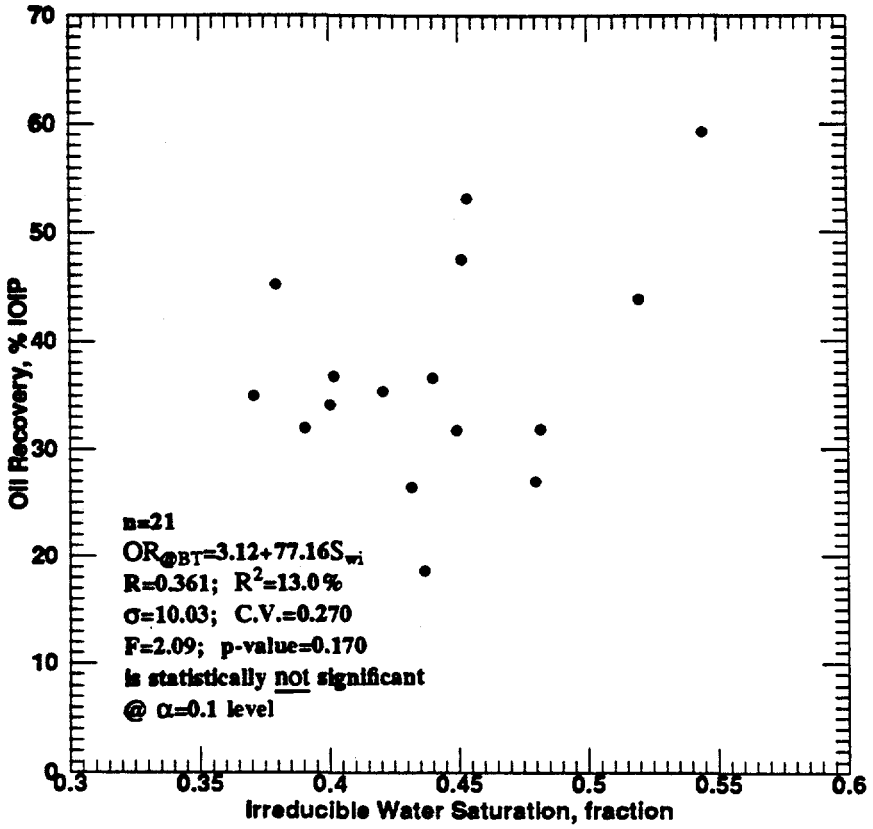

Fig. 5.119: Oil Recovery vs. Irreducible Water Saturation for Indiana Limestone Linear-Cores at Breakthrough.

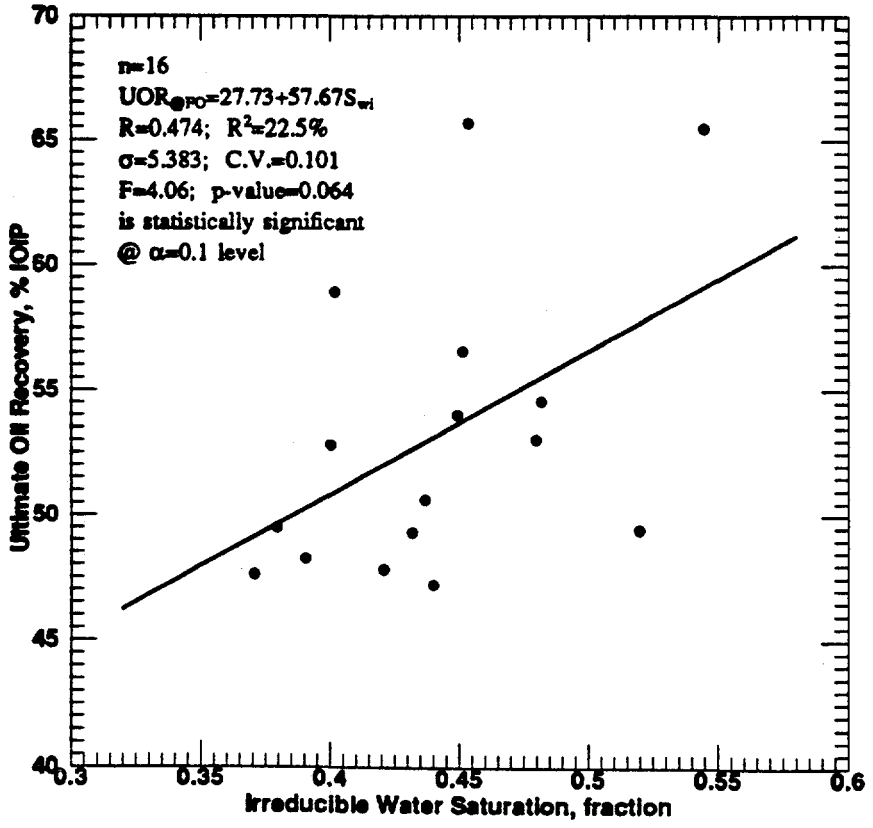

Fig. 5.120: Ultimate Oil Recovery vs. Irreducible Water Saturation for Indiana Limestone Linear-Cores at Floodout.

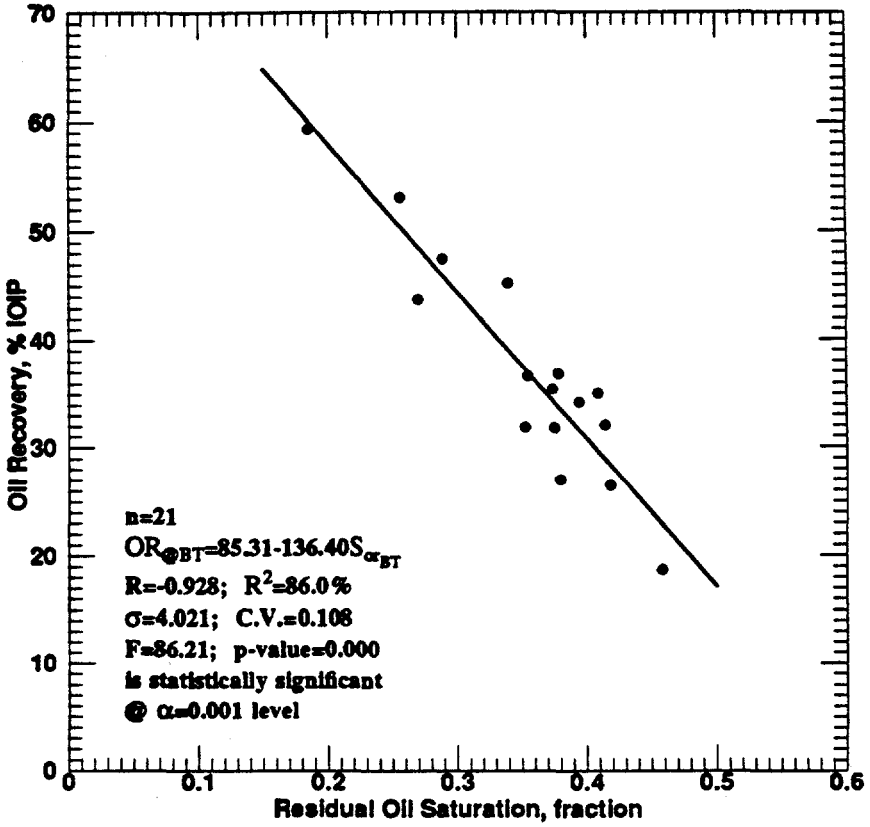

Fig. 5.121: Oil Recovery vs. Residual Oil Saturation for Indiana Limestone Linear-Cores at Breakthrough.

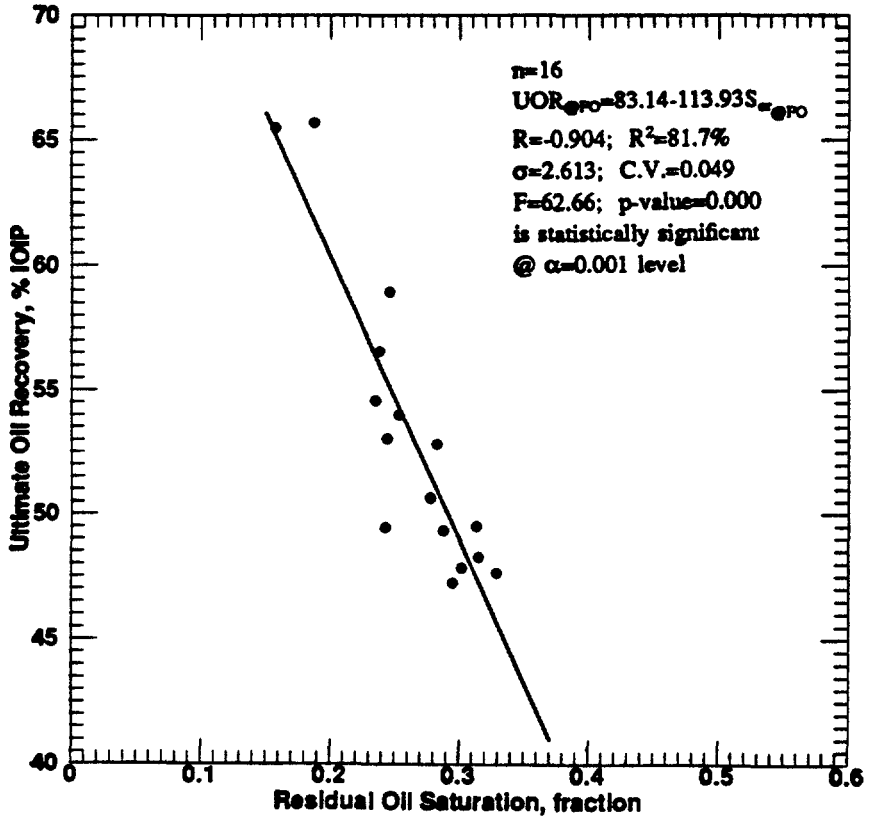

Fig. 5.122: Ultimate Oil Recovery vs. Residual Oil Saturation for Indiana Limestone Linear-Cores at Floodout.

5.4.3.1 Relation Between Waterflood and Petrophysical Properties

The relationships of petrophysical properties such as porosity, and permeability on the outcome of residual oil saturation and oil recovery from waterflooding were also investigated for limestones. As shown in Table 5.20, at breakthrough and at floodout, the relationships of permeability with residual oil saturation and oil recovery are statistically significant, since they have high correlation coefficient values. Further, at breakthrough and at floodout, the relationships of porosity with residual oil saturation and oil recovery, are found to be not statistically significant.

Permeability is inversely related to residual oil saturation at both the breakthrough and floodout. The permeability versus residual oil saturation relationship at breakthrough has a R^2 value of 48.4% and a R^2 value of 33.7% at floodout. For the case of permeability relationships with oil recovery at breakthrough and at floodout, they both showed directly related trends. Here, the relationship at breakthrough has a R^2 value of 55.8% and a R^2 value of 52.4% for ultimate oil recovery.

5.4.3.2 Scaling Coefficient and Capillary Number

The experimental design was properly scaled by keeping the scaling coefficient close to a value of 5.0 as presented in Table 4.4 for Indiana limestone linear-cores. The table also included the values of the capillary number which varied from $6.94*10^{-7}$ to $7.91*10^{-7}$, with a mean value of $7.06*10^{-7}$. The variation of these capillary number values is not as much as the variation of the values obtained for sandstone core samples. This was expected, since the length of the limestone cores used for the waterflood experiments were essentially the same, as shown in Table 4.4 for core sample Nos. 9A through 16A. Core sample No. 16B has the largest value of capillary number, due to its having the smallest length as compared to the other limestone core samples investigated.

5.4.4 Wettability Properties

From each of the waterflooded Indiana limestone linear-cores, 32 core plugs were extracted from along the flow path at an average interval of about 2.5 cm. The core plugs were perpendicular to the flood plane. Similar to the case of Berea sandstone core plug samples, during the process of the extraction, the distance of each core plug relative to the inlet face of the core was noted. For a given distance, two core plugs were obtained, one from the top and the other from the bottom of the core. An average value of the wettability index is obtained for a given distance. The distances are normalized by dividing the value of the measured distance relative to the core inlet by the total length of the core.

Figure 5.123 shows the distribution of wettability index per number of the limestone core plug samples. For all the 512 core plugs combined, wettability index varied from 0.30 to 1.00, with a mean value of 0.67. The plots of the wettability indices versus the normalized distances for each of the 16 cores are presented in Figs. 5.124 through 5.131. From the core plugs, an average value of wettability index was obtained for each of the cores. The mean average wettability index for all the 16 limestone cores combined was 0.67. The minimum and maximum values determined were 0.45 and 0.83, respectively. Based on these determinations, the limestone cores investigated in this study are classified as water-wet rocks.

5.4.4.1 Relation Between Wettability and Petrophysical Properties

The relationships of average wettability index with porosity, and permeability can also be established by the aid of the correlation coefficients earlier presented in Table 5.20. For limestones, average wettability index relationships with porosity, and permeability are both found to be not statistically significant at $\alpha = 0.1$ level.

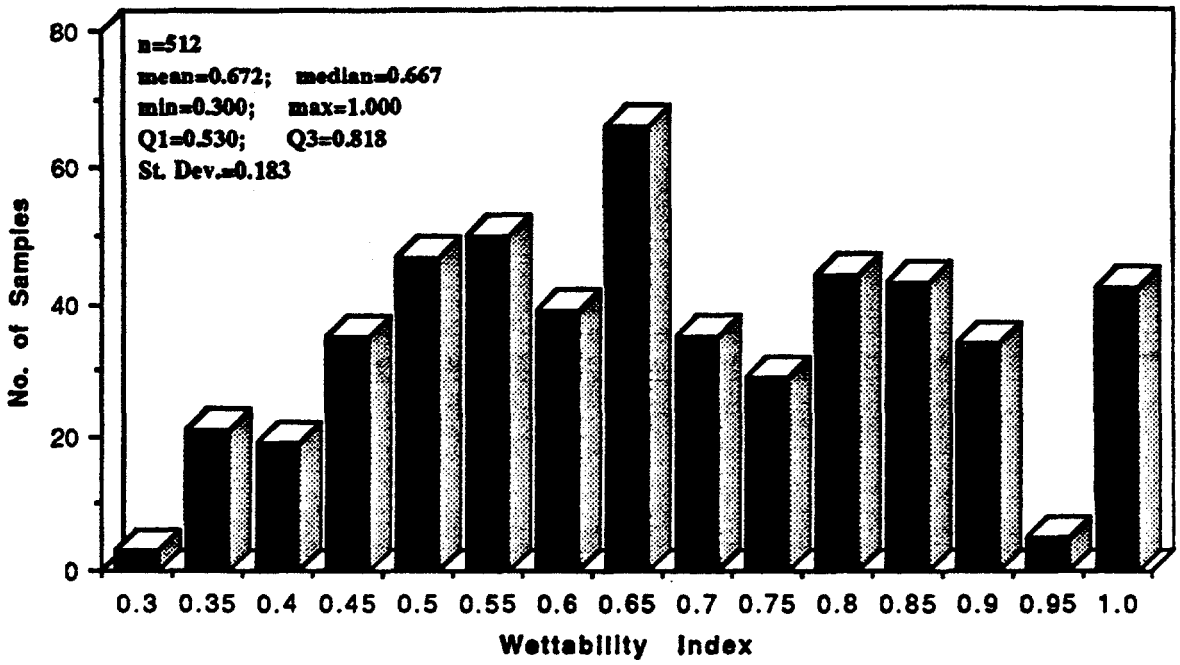

Fig. 5.123: Distribution of Wettability Index per Number of Indiana Limestone Linear-Cores Plugs.

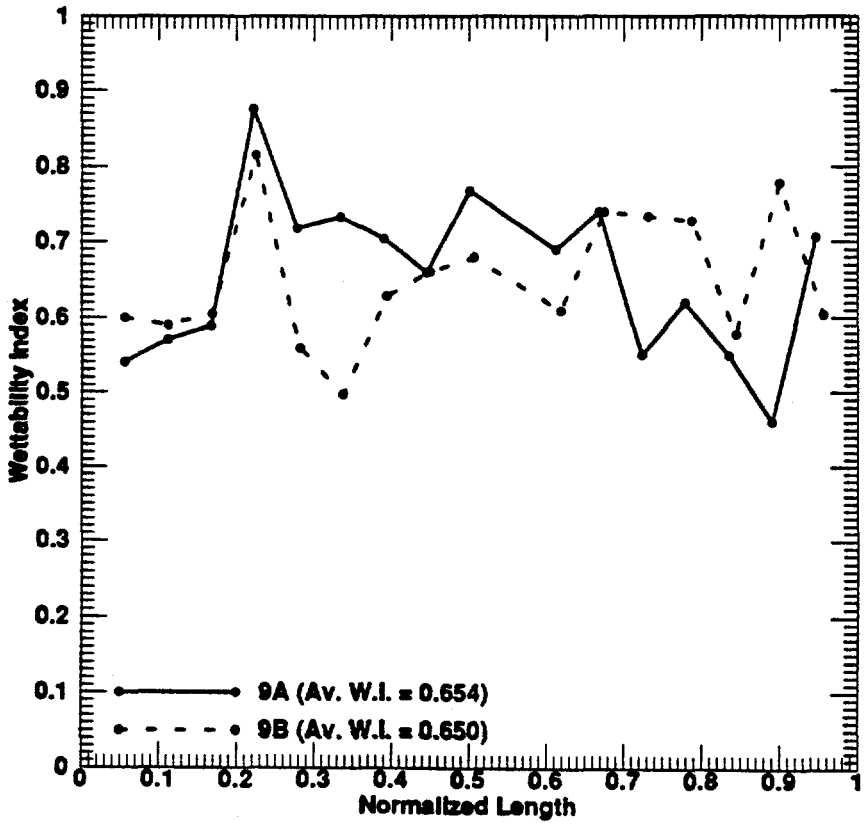

Fig. 5.124: Wettability Index vs. Normalized Length for Indiana Limestone Linear-Core Samples 9A and 9B.

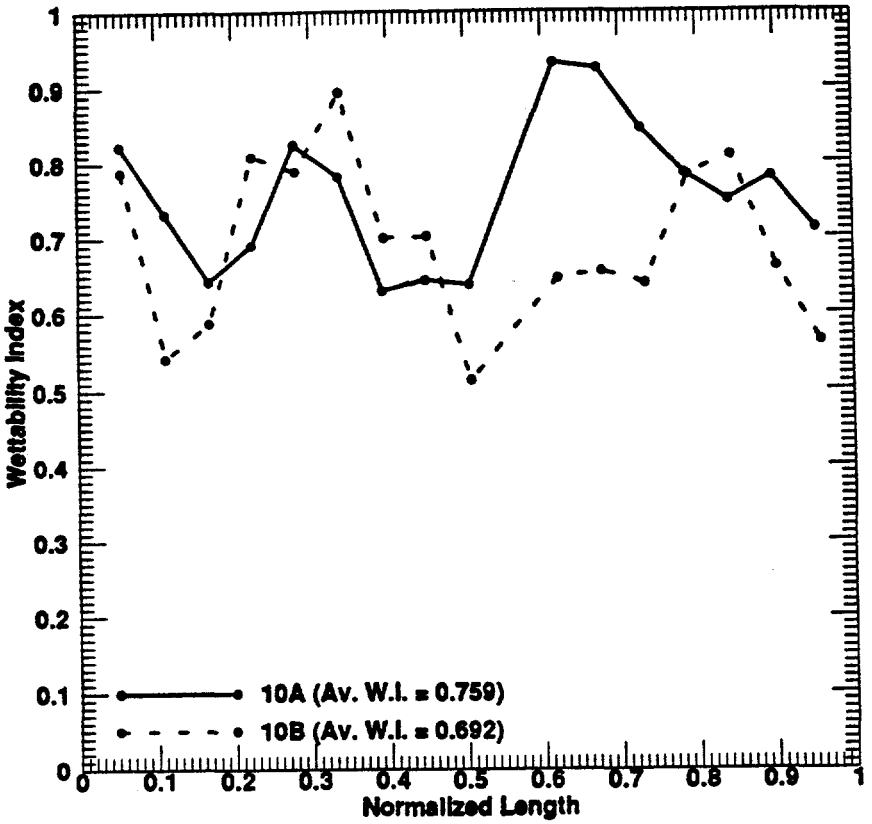

Fig. 5.125: Wettability Index vs. Normalized Length for Indiana Limestone Linear-Core Samples 10A and 10B.

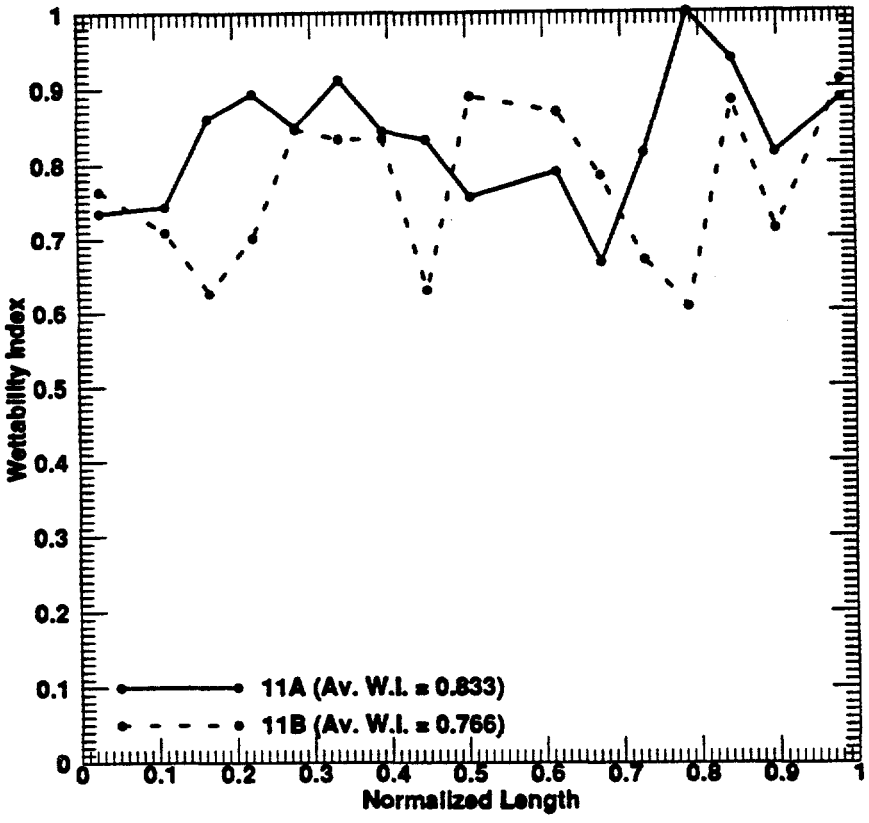

Fig. 5.126: Wettability Index vs. Normalized Length for Indiana Limestone Linear-Core Samples 11A and 11B.

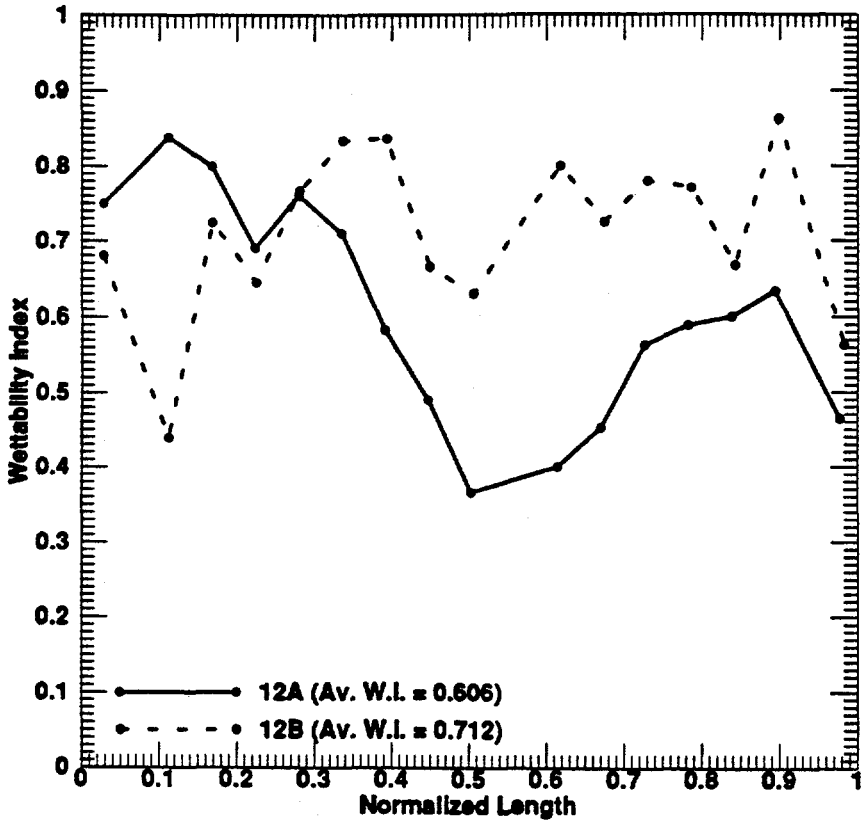

Fig. 5.127: Wettability Index vs. Normalized Length for Indiana Limestone Linear-Core Samples 12A and 12B.

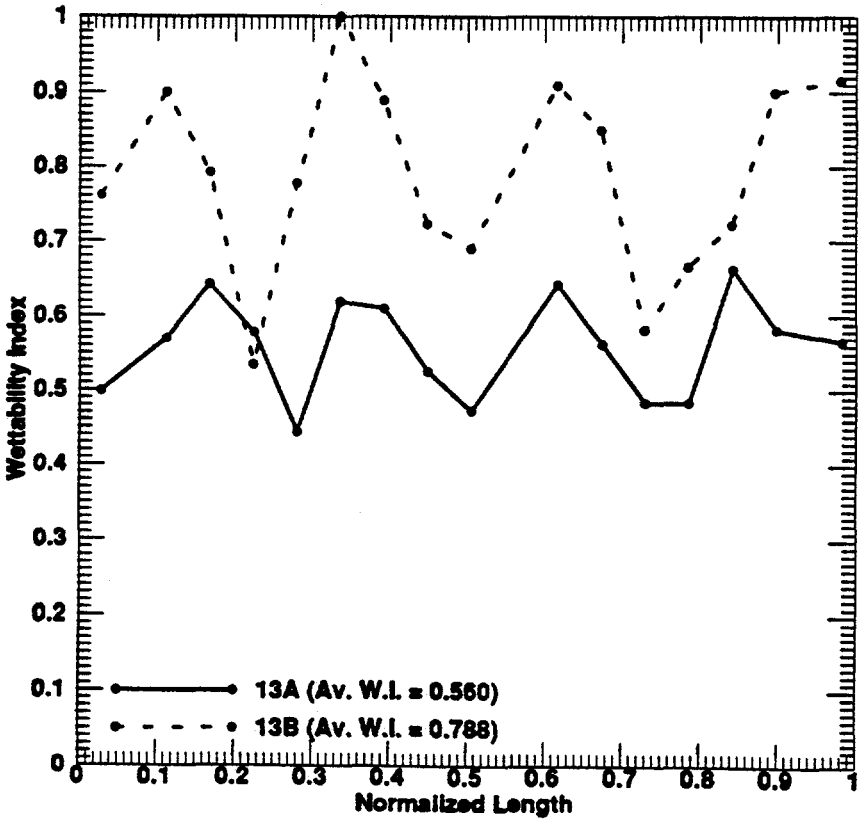

Fig. 5.128: Wettability Index vs. Normalized Length for Indiana Limestone Linear-Core Samples 13A and 13B.

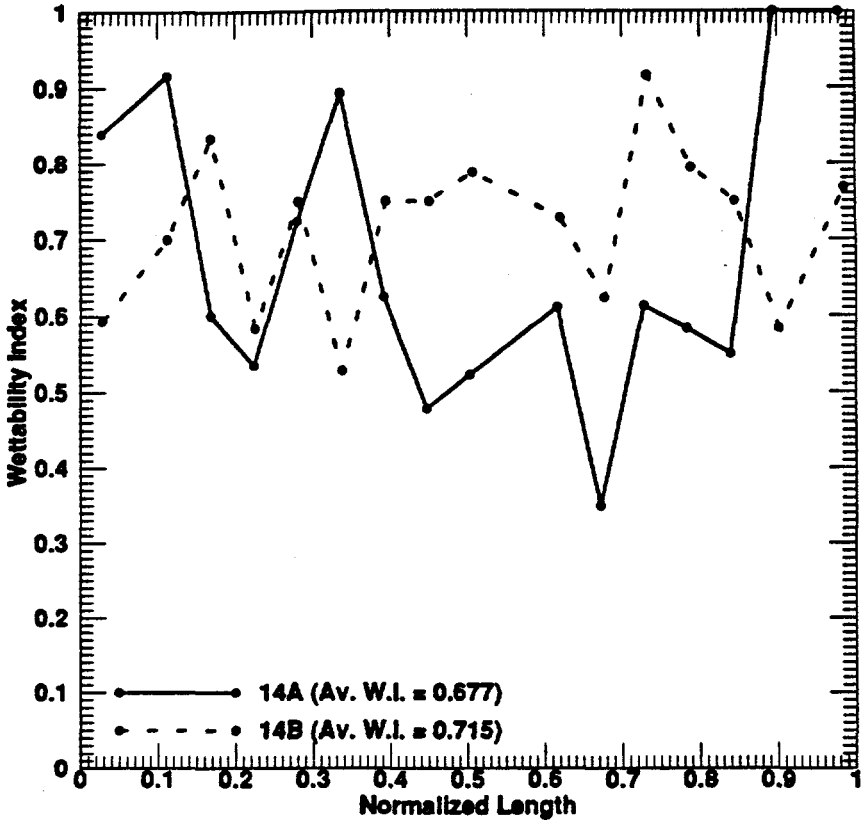

Fig. 5.129: Wettability Index vs. Normalized Length for Indiana Limestone Linear-Core Samples 14A and 14B.

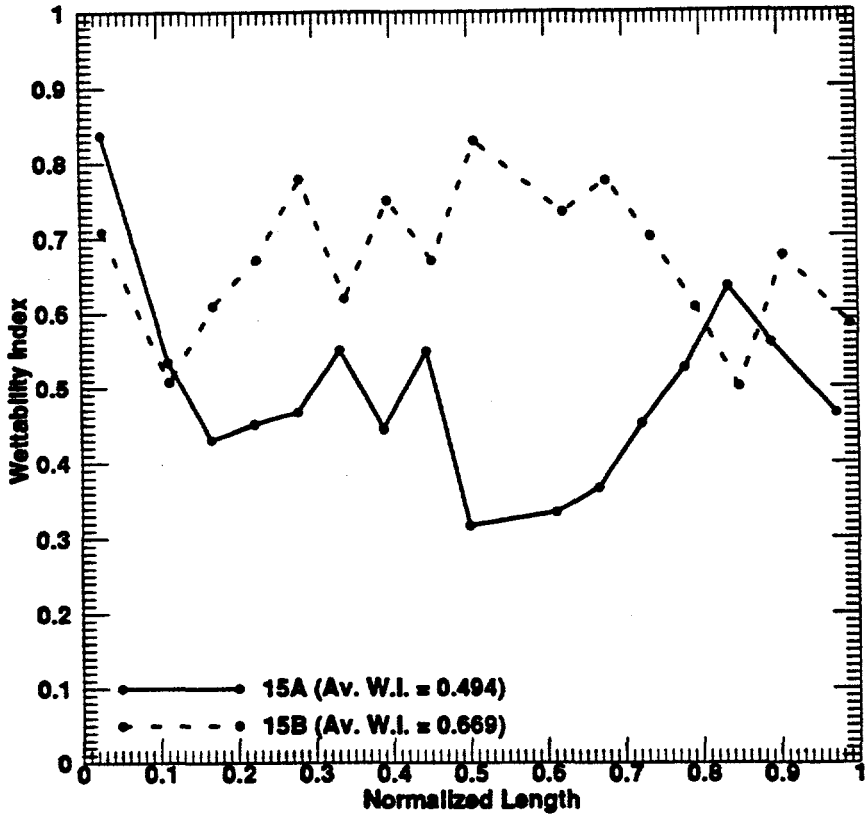

Fig. 5.130: Wettability Index vs. Normalized Length for Indiana Limestone Linear-Core Samples 15A and 15B.

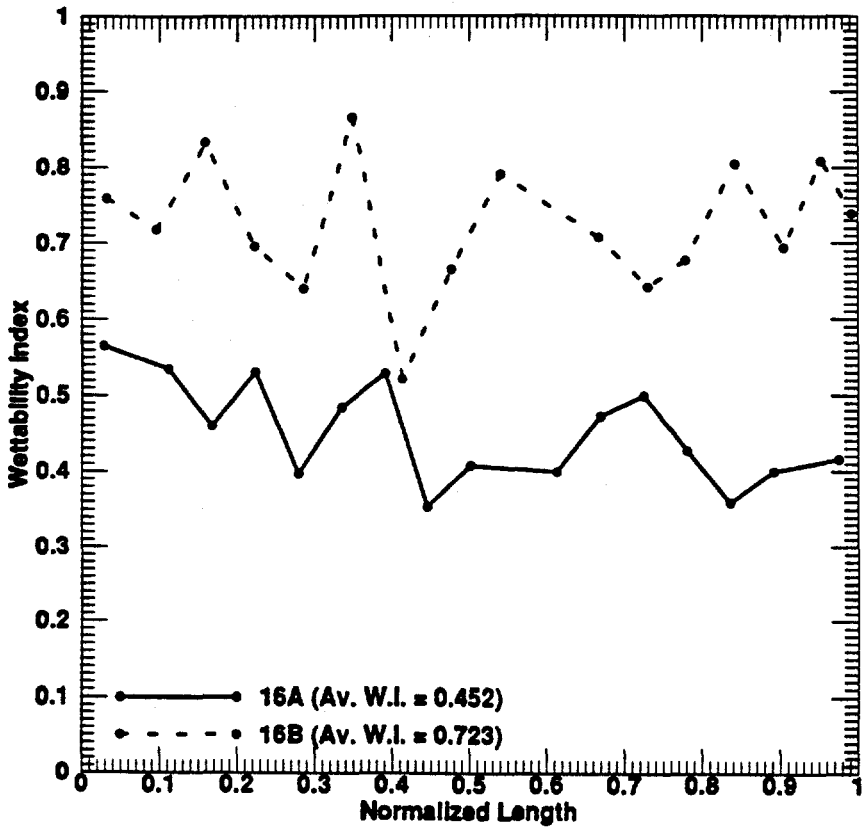

Fig. 5.131: Wettability Index vs. Normalized Length for Indiana Limestone Linear-Core Samples 16A and 16B.

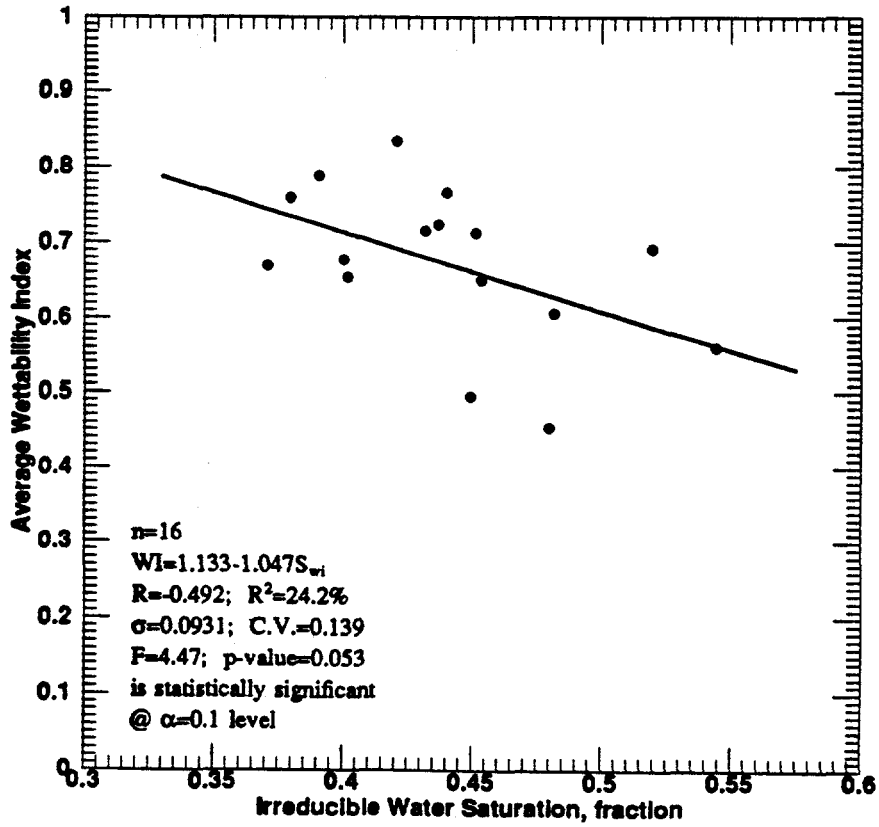

Fig. 5.132: Average Wettability Index vs. Irreducible Water Saturation for Indiana Limestone Linear-Cores.

5.4.4.2 Relation Between Wettability and Waterflood Properties

Figure 5.132 shows that average wettability index is inversely related to irreducible water saturation. The relationship is statistically significant at $\alpha = 0.1$ level. Figures 5.133 through 5.136 show the plots of residual oil saturation and oil recovery versus average wettability index at both the breakthrough and floodout. No relationships exist between residual oil saturation and oil recovery versus average wettability index at breakthrough, as shown in Figs. 5.133 and 5.135, respectively. Fig. 5.134 shows that residual oil saturation at floodout is directly related to average wettability index. As shown in Fig. 5.136 ultimate oil recovery at floodout is inversely related to average wettability index. Unlike the case of sandstones, it appears that limestone residual oil saturation at breakthrough is less sensitive to wettability than is residual oil saturation at floodout.

From these findings, one can deduce that for water-wet limestone rocks, as wettability index increases, residual oil saturation at floodout also increases and ultimate oil recovery at floodout by waterflood decreases. These findings are in agreement with the observation of Morrow (1990) and Jadhunandan and Morrow (1991), that oil recovery by waterflooding is optimum close to neutral wettability for water-wet systems.

5.4.5 Mercury Porosimetry Properties

A total of 512 core plugs were extracted from along the flow path of the 16 waterflooded Indiana limestone linear-cores. These extracted plugs are the same that were previously tested for wettability and later cleaned in readiness for the mercury porosimetry tests. After the completion of low-pressure and high-pressure runs, the plugs were discarded because of being contaminated with mercury.

Similar to the analysis on the wettability data, average values of mercury porosimetry properties were obtained for each of the core samples from the core plugs. These values are

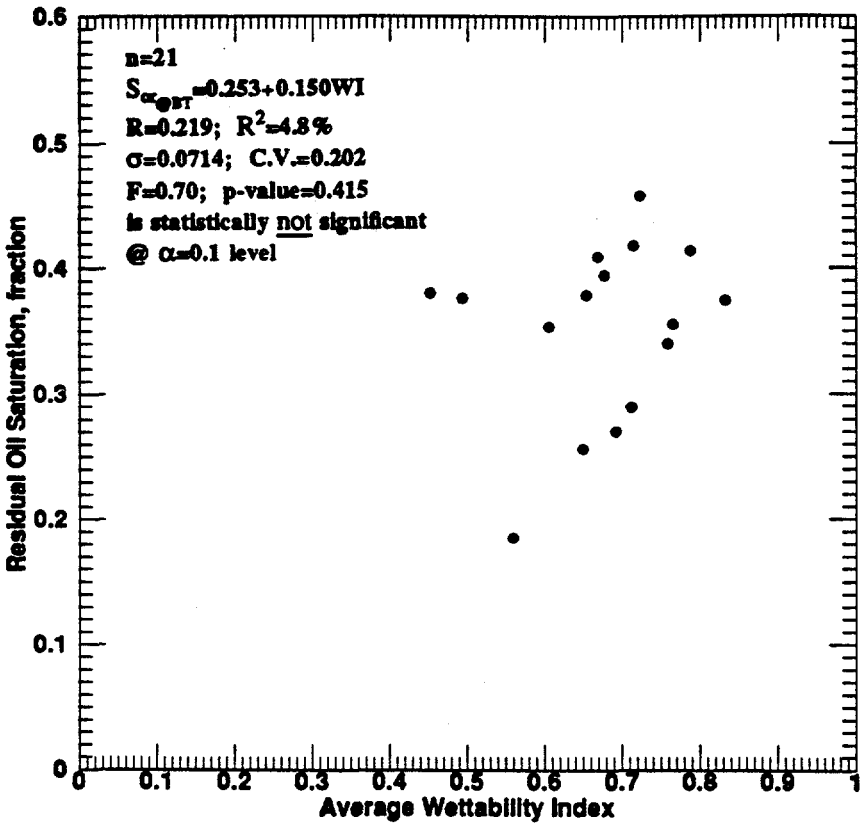

Fig. 5.133: Residual Oil Saturation vs. Average Wettability Index for Indiana Limestone Linear-Cores at Breakthrough.

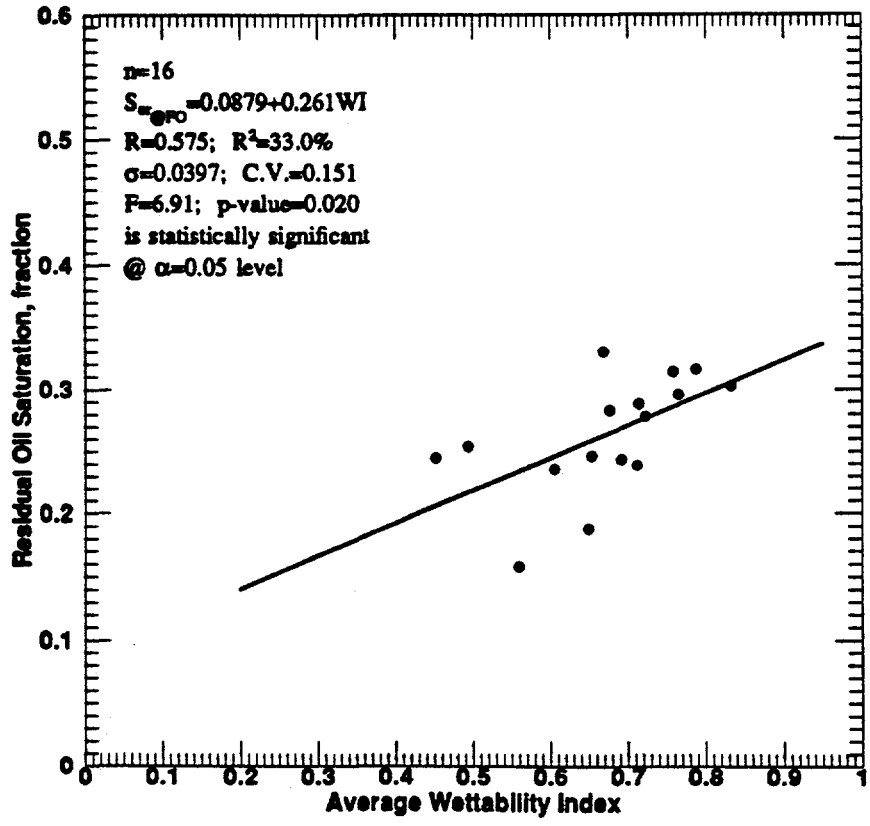

Fig. 5.134: Residual Oil Saturation vs. Average Wettability Index for Indiana Limestone Linear-Cores at Floodout.

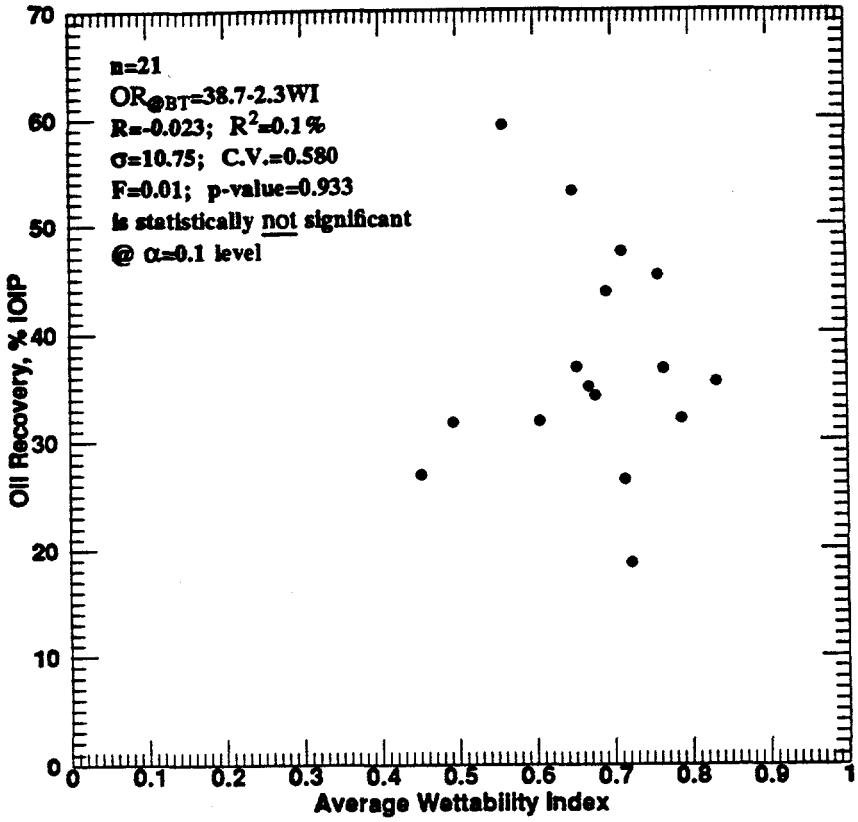

Fig. 5.135: Oil Recovery vs. Average Wettability Index for Indiana Limestone Linear-Cores at Breakthrough.

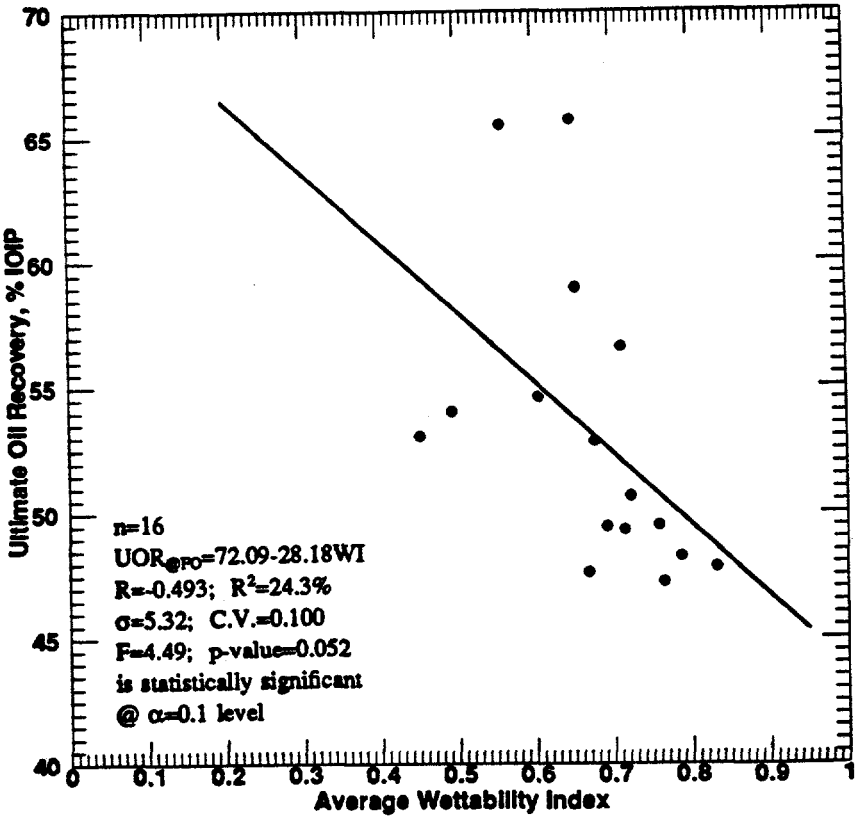

Fig. 5.136: Ultimate Oil Recovery vs. Average Wettability Index for Indiana Limestone Linear-Cores at Floodout.

presented in Table 5.21 for the types of mode, pore intrusion volumes, pore surface areas, pore specific surface areas, average pore diameters, apparent densities, mercury porosities, residual mercury saturations and mercury recovery efficiencies.

Table 5.22 shows the statistical description of the mercury porosimetry experimental data obtained. For all the linear-core samples combined, intrusion volumes varied from 0.06 to 0.08 ml/g, with an average of 0.07 ml/g; the surface areas varied from 0.83 to 1.06 m^2/g, with an average of 0.93 m^2/g; the specific surface area varied from $12.48*10^4$ to $16.45*10^4$ cm^2/cm^3, with an average of $13.94*10^4$ cm^2/cm^3; the average pore diameters varied from 0.26 to 0.35 μm, with an average of 0.30 μm; the apparent (skeletal) densities varied from 2.55 to 2.65 g/ml, with an average of 2.60 g/ml; the porosities varied from 13.8 to 16.2%, with an average of 14.6%; and the mercury recovery efficiencies varied from 33.9 to 44.1%, with an average value of 38.8%.

The limestone rocks investigated are considered to be very good reservoir rocks because they have both high mercury recovery efficiency and porosity values. According to Kopaska-Merkel and Friedman (1989), mercury recovery efficiency in mercury porosimetry is analogous to primary recovery of petroleum from natural reservoirs because both processes involve only simple pressure reduction. Hence, this type of rock with more than 25% mercury recovery efficiencies and fairly good porosities, would perform well during primary oil recovery period.

Figures 5.137 through 5.143 show the distributions of the various mercury porosimetry properties of the limestone core plug samples. The properties are total intrusion volume, surface area, specific surface area, average pore diameter, apparent (skeletal) density, mercury porosity, and mercury recovery efficiency, respectively. Figs. 5.137 and 5.142 show bimodal distributions for total intrusion volume and mercury porosity, respectively. For the distributions and subsequent analyses, only 329 out of the original 512 limestone

Table 5.21: Mercury Porosimetry Properties of the Indiana Limestone Linear-Cores

Core Sample No.	No. of Plugs	Type of Mode	$V_{int.}$ (ml/g)	SA (m^2/g)	S_o (cm^2/cm^3) (E+04)	$\bar{D}$ (μm)	ρ_g (g/ml)	ϕ_{Hg} (frac)	RE (frac)
9A	32	2	0.0688	0.987	14.346	0.279	2.625	0.153	0.388
9B	32	2	0.0738	1.030	13.957	0.309	2.649	0.162	0.375
10A	32	2	0.0644	0.830	12.888	0.313	2.622	0.144	0.339
10B	32	2	0.0673	0.936	13.908	0.291	2.606	0.144	0.375
11A	32	2	0.0678	0.853	12.581	0.335	2.603	0.150	0.386
11B	32	2	0.0635	0.892	14.047	0.273	2.588	0.141	0.423
12A	32	2	0.0693	0.865	12.482	0.299	2.551	0.138	0.379
12B	32	2	0.0668	0.860	12.874	0.312	2.619	0.149	0.352
13A	32	2	0.0766	0.970	12.663	0.350	2.616	0.155	0.339
13B	32	2	0.0691	0.958	13.864	0.289	2.622	0.145	0.387
14A	32	2	0.0645	1.061	16.450	0.260	2.587	0.143	0.424
14B	32	2	0.0635	0.935	14.724	0.273	2.589	0.141	0.417
15A	32	2	0.0633	0.914	14.439	0.279	2.571	0.140	0.382
15B	32	2	0.0660	0.834	12.636	0.317	2.604	0.146	0.357
16A	32	2	0.0614	0.953	15.521	0.299	2.589	0.144	0.437
16B	32	2	0.0674	1.056	15.668	0.263	2.593	0.149	0.441

Table 5.22: Statistical Description of the Mercury Porosimetry Experimental Variables for Indiana Limestone Linear-Cores

	$V_{int.}$ (ml/g)	SA (m^2/g)	S_o (cm^2/cc) (E+04)	$\bar{D}$ (μm)	ρ_g (g/ml)	ϕ_{Hg} (frac)	RE (frac)
Mean	0.0671	0.933	13.940	0.296	2.602	0.146	0.388
Median	0.0670	0.935	13.932	0.295	2.604	0.145	0.384
Min.	0.0614	0.830	12.482	0.260	2.551	0.138	0.339
Max.	0.0766	1.061	16.450	0.350	2.649	0.162	0.441
Q1	0.0637	0.861	12.716	0.274	2.588	0.142	0.362
Q3	0.0690	0.983	14.653	0.313	2.621	0.150	0.422
St. Dev.	0.0040	0.075	1.221	0.025	0.024	0.006	0.033

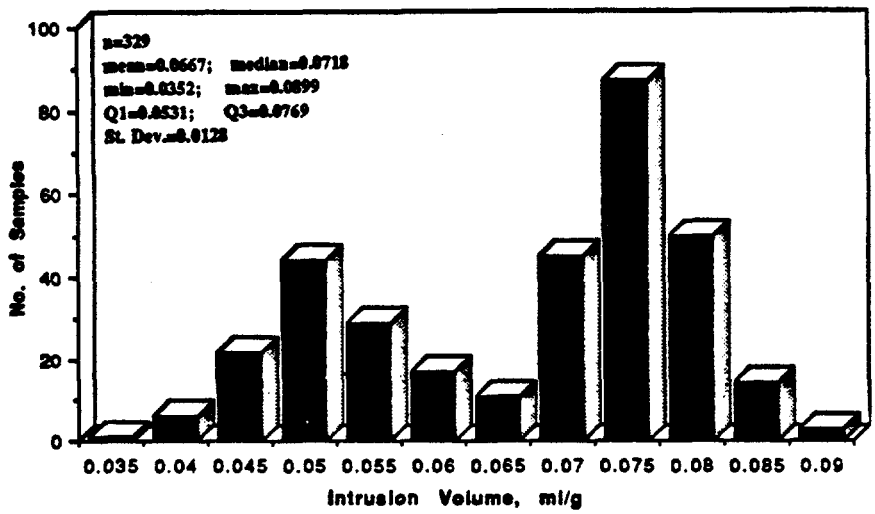

Fig. 5.137: Distribution of Total Intrusion Volume per Number of Indiana Limestone Linear-Cores Plugs.

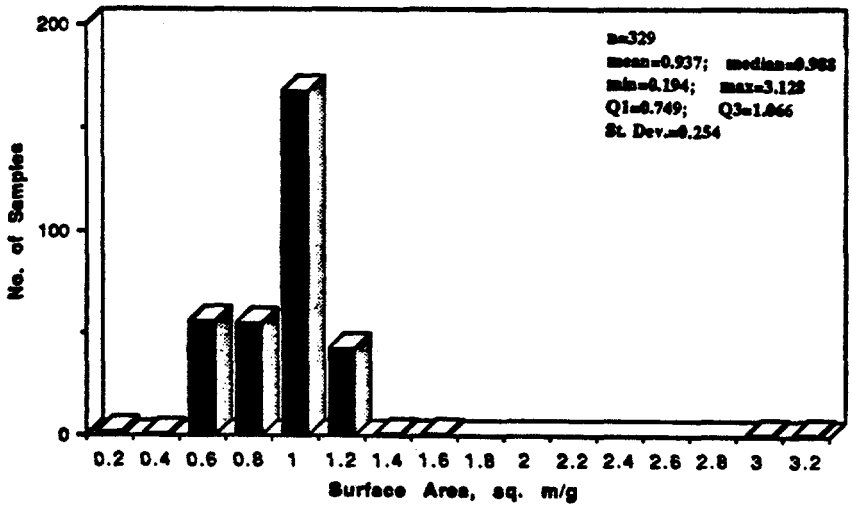

Fig. 5.138: Distribution of Surface Area per Number of Indiana Limestone Linear-Cores Plugs.

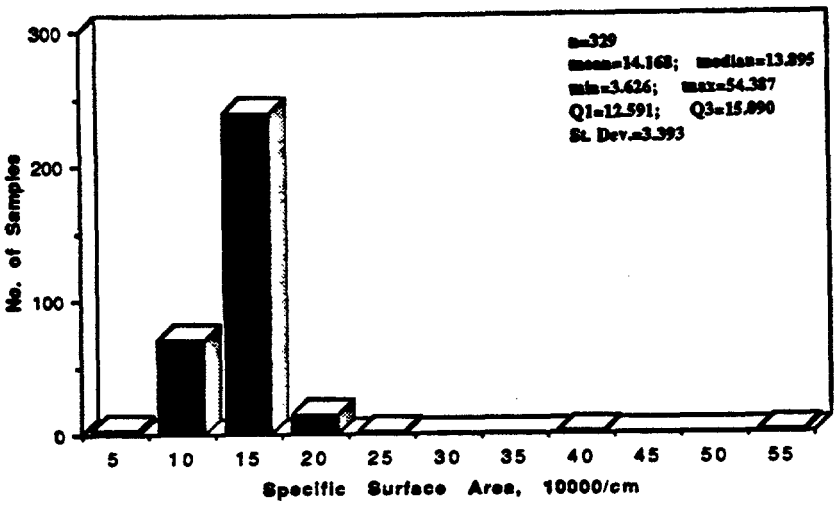

Fig. 5.139: Distribution of Specific Surface Area per Number of Indiana Limestone Linear-Cores Plugs.

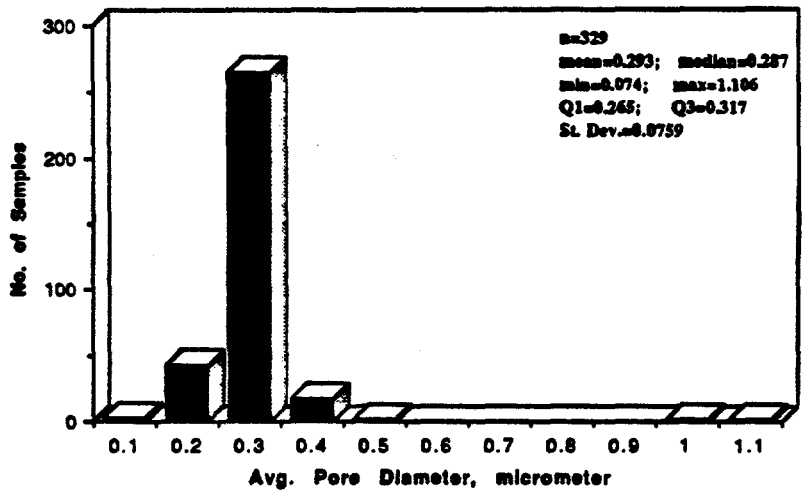

Fig. 5.140: Distribution of Average Pore Diameter per Number of Indiana Limestone Linear-Cores Plugs.

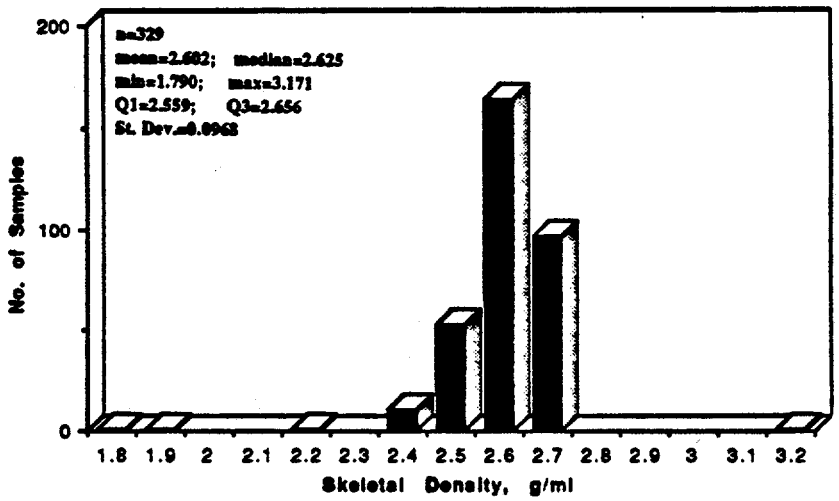

Fig. 5.141: Distribution of Apparent (Skeletal) Density per Number of Indiana Limestone Linear-Cores Plugs.

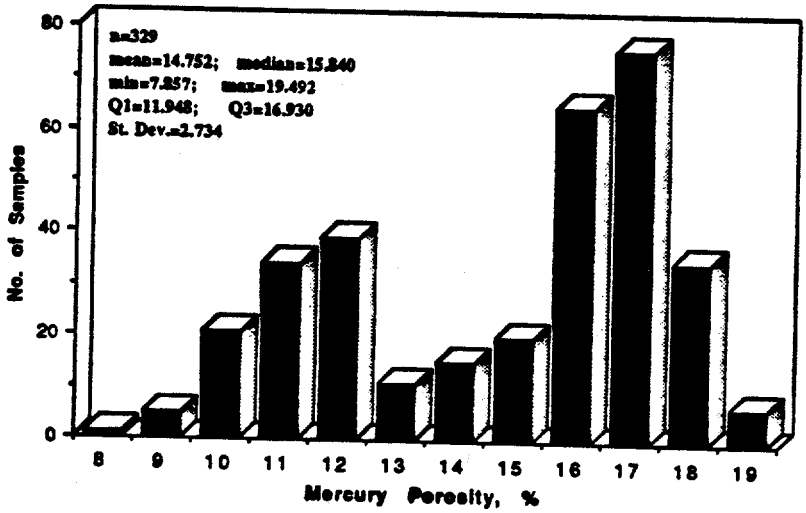

Fig. 5.142: Distribution of Mercury Porosity per Number of Indiana Limestone Linear-Cores Plugs.

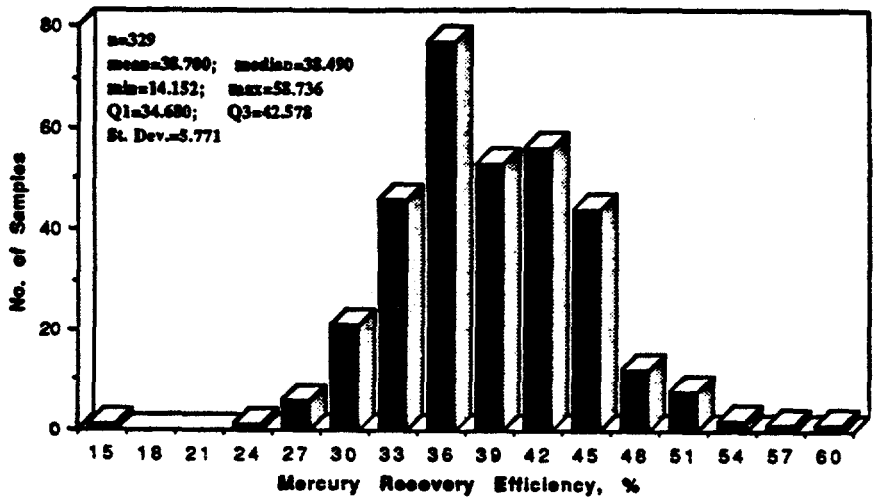

Fig. 5.143: Distribution of Mercury Recovery Efficiency per Number of Indiana Limestone Linear-Cores Plugs.

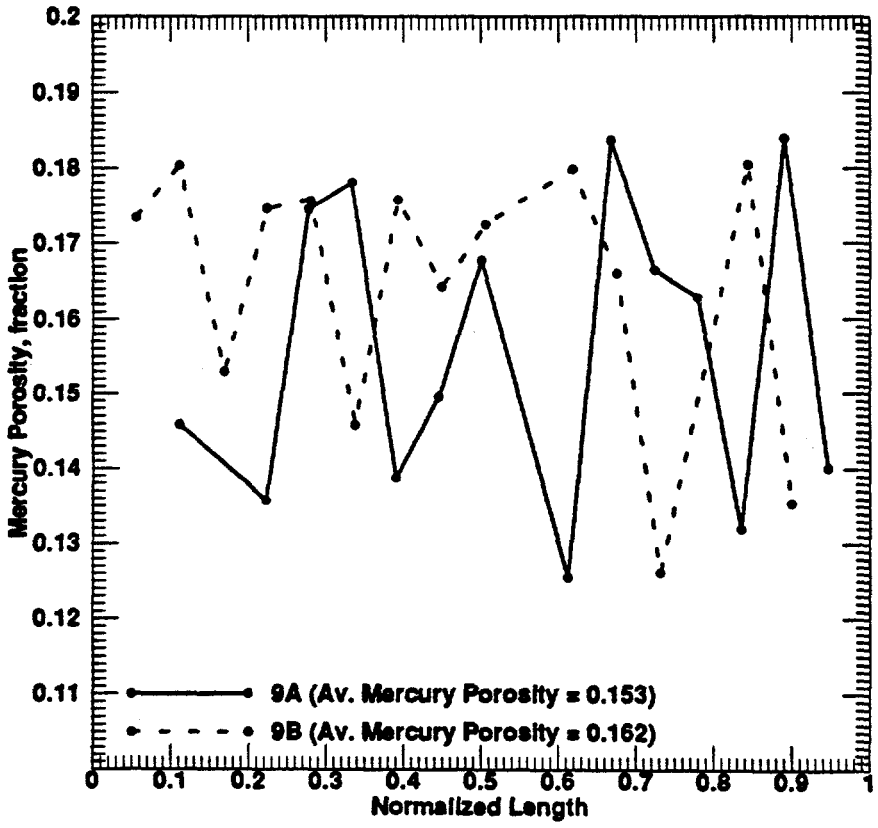

Fig. 5.144: Mercury Porosity vs. Normalized Length for Indiana Limestone Linear-Core Samples 9A and 9B.

core plugs were utilized, because of the removal of all the bad mercury porosimetry experimentally measured data.

The plots of the plugs mercury porosities versus the normalized distances for each of the 16 cores are presented in Figs. 5.144 through 5.151. Similar to the case of the wettability indices the exhibited trends are generally not constant. The reason for this is not fully understood, but might be related to the amount of microporosity within the fossil and oolite grains, and/or to the presence of clay fines in the core samples (Churcher et al., 1991).

The correlation matrix shown in Table 5.23 confirms the trends of Figs. 5.152 through 5.154. Figure 5.152 shows a good relationship between total intrusion volume and mercury porosity, with a R^2 value of about 52% and high F-test statistic value of 15.31. The relationship is statistically significant at $\alpha = 0.005$ level. Figure 5.153 shows that mercury recovery efficiency have inverse relationship with the average pore diameter. The relationship is strong and statistically significant at $\alpha = 0.001$ level. This is in agreement with the findings of Amthor et al. (1988), that for intermediate pore throat sizes, the mercury recovery efficiency are moderate for gently sloping bimodal systems. The mean values of this study's average pore throat diameter ($\overline{D} = 0.3$ μm) and mercury recovery efficiency (RE = 0.4), are within the range referred to by Amthor et al., in their findings as stated above.

Figure 5.154 shows that apparent (skeletal) density is directly related to total intrusion volume. The relationship is statistically significant at $\alpha = 0.1$ level. The relationship between mercury recovery efficiency and porosity was found not to be statistically significant, since the relationship has a low correlation coefficient value (R = -0.29), as shown in the correlation matrix of Table 5.23. Review of the literature also depicts that apparently no one consistent set of relationships exists between mercury recovery efficiency

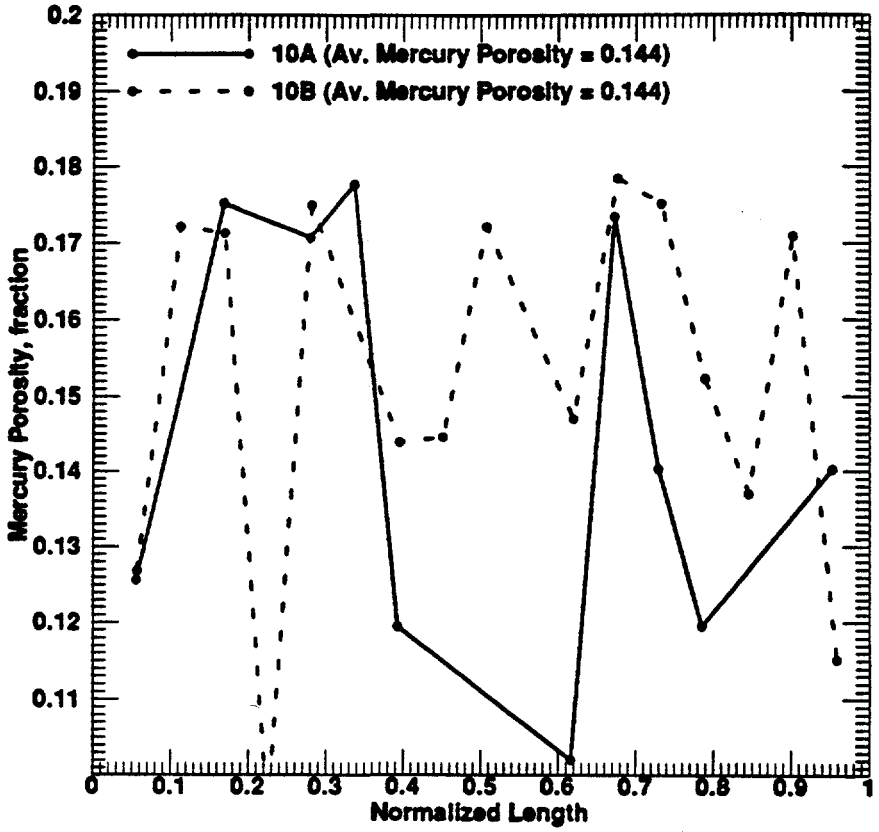

Fig. 5.145: Mercury Porosity vs. Normalized Length for Indiana Limestone Linear-Core Samples 10A and 10B.

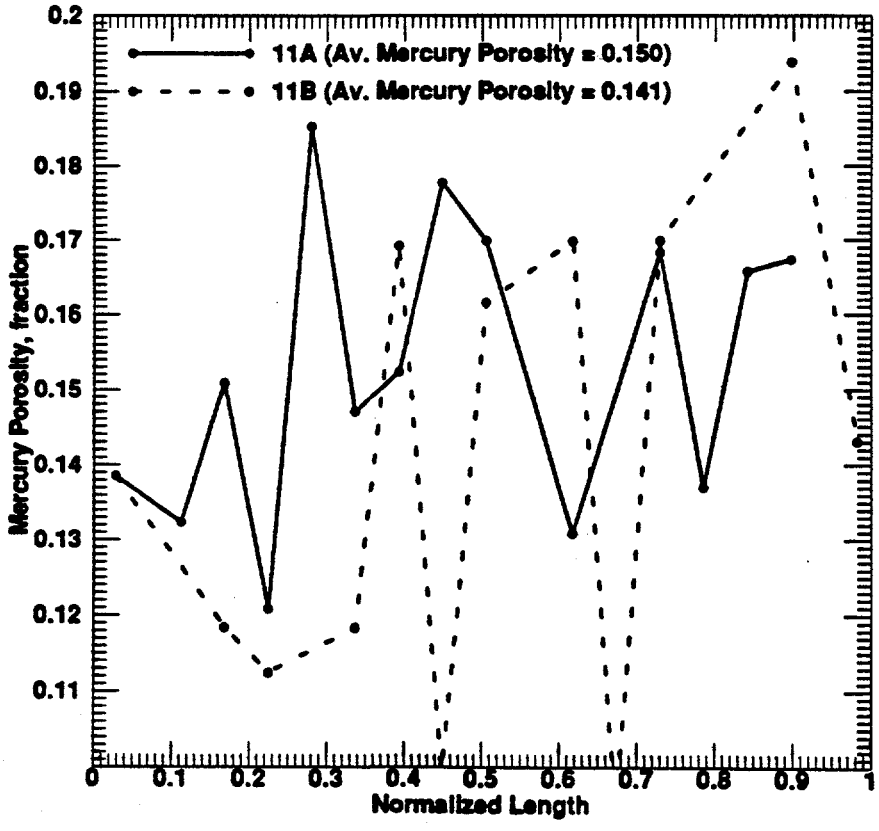

Fig. 5.146: Mercury Porosity vs. Normalized Length for Indiana Limestone Linear-Core Samples 11A and 11B.

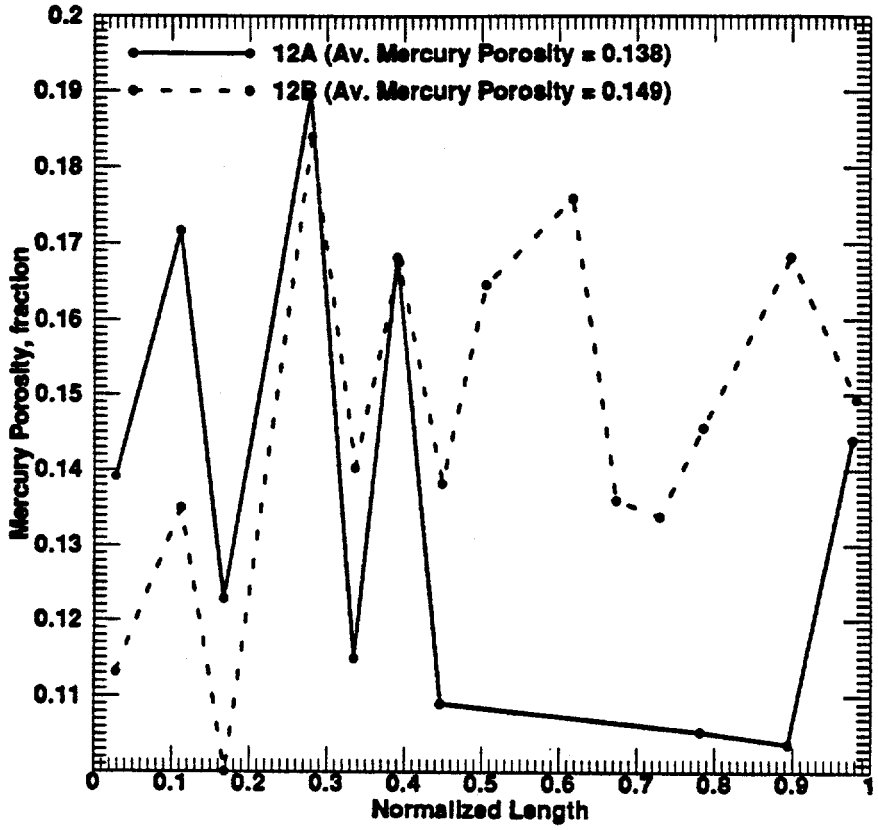

Fig. 5.147: Mercury Porosity vs. Normalized Length for Indiana Limestone Linear-Core Samples 12A and 12B.

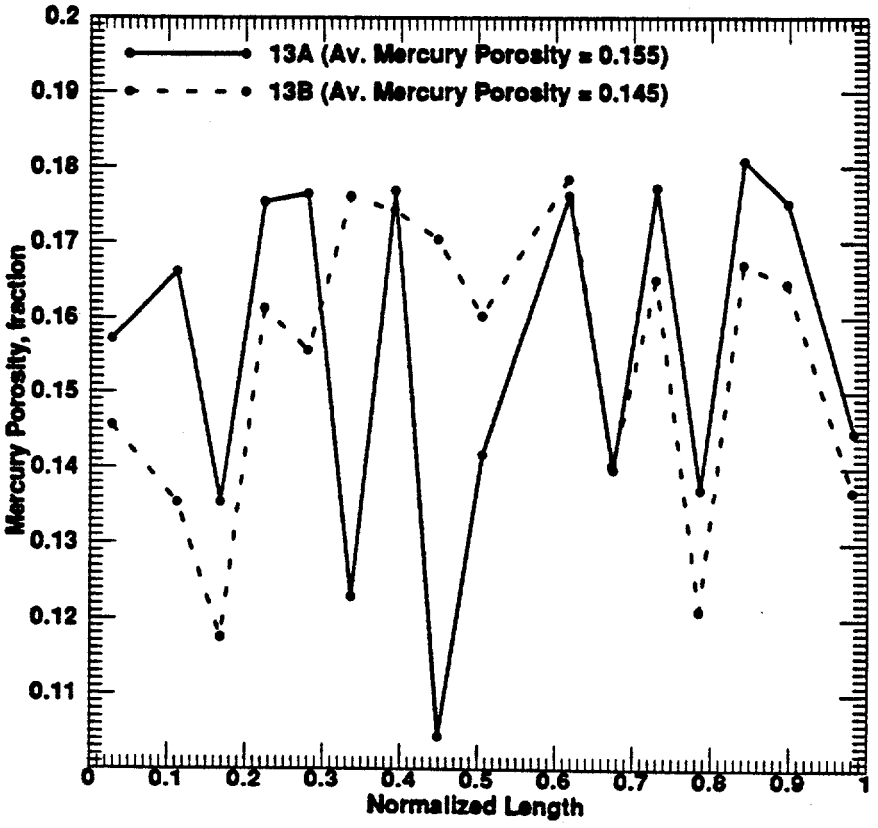

Fig. 5.148: Mercury Porosity vs. Normalized Length for Indiana Limestone Linear-Core Samples 13A and 13B.

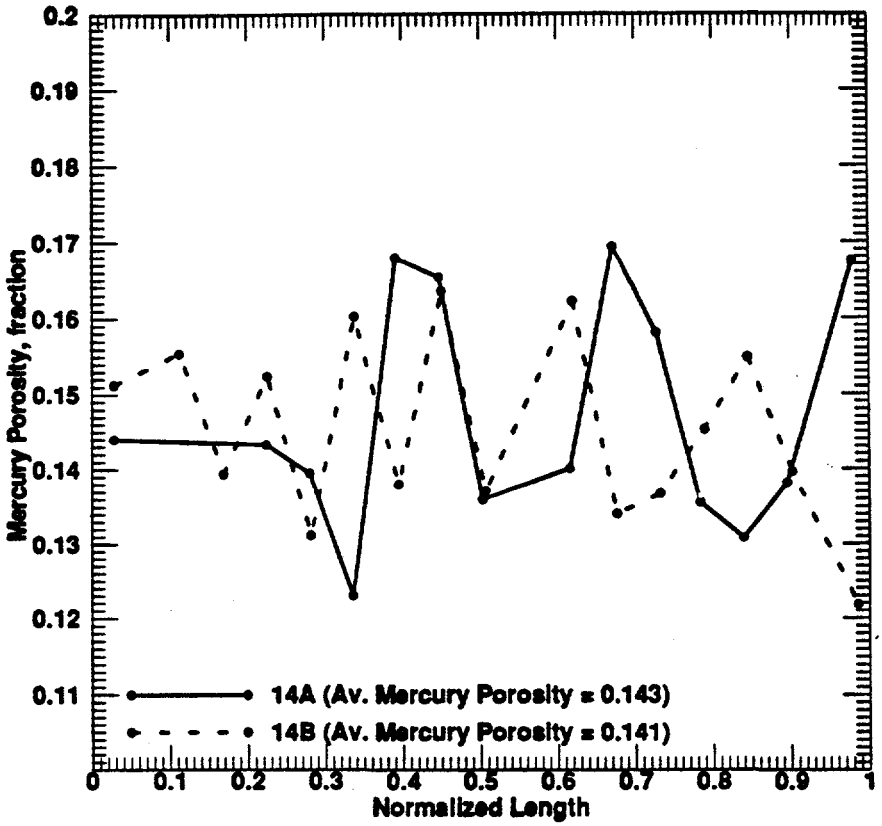

Fig. 5.149: Mercury Porosity vs. Normalized Length for Indiana Limestone Linear-Core Samples 14A and 14B.

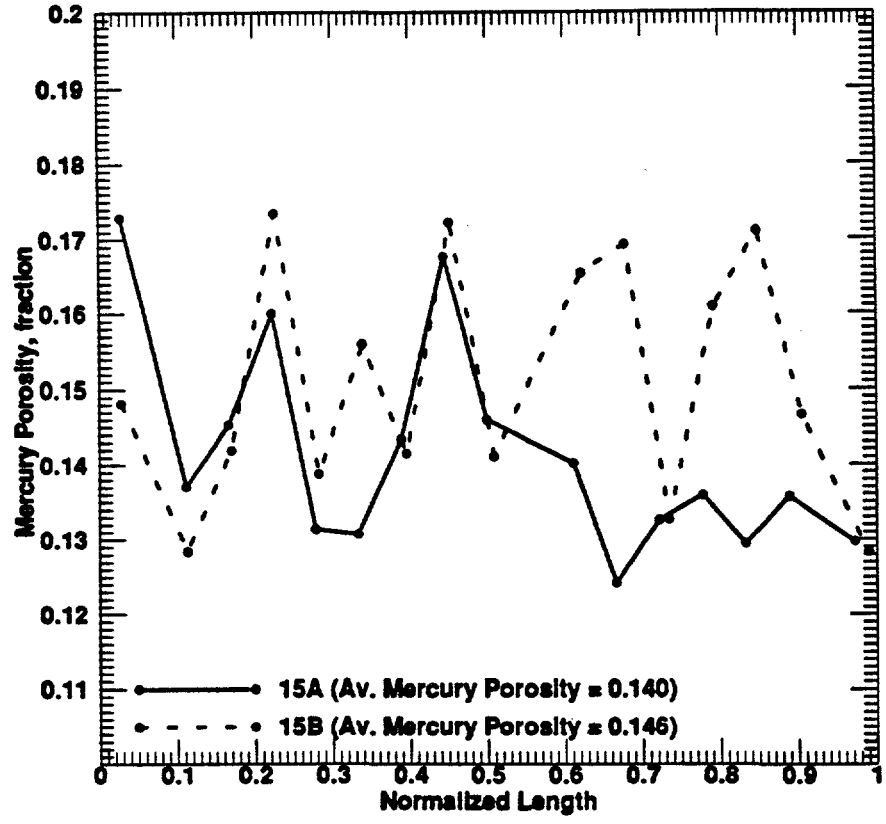

Fig. 5.150: Mercury Porosity vs. Normalized Length for Indiana Limestone Linear-Core Samples 15A and 15B.

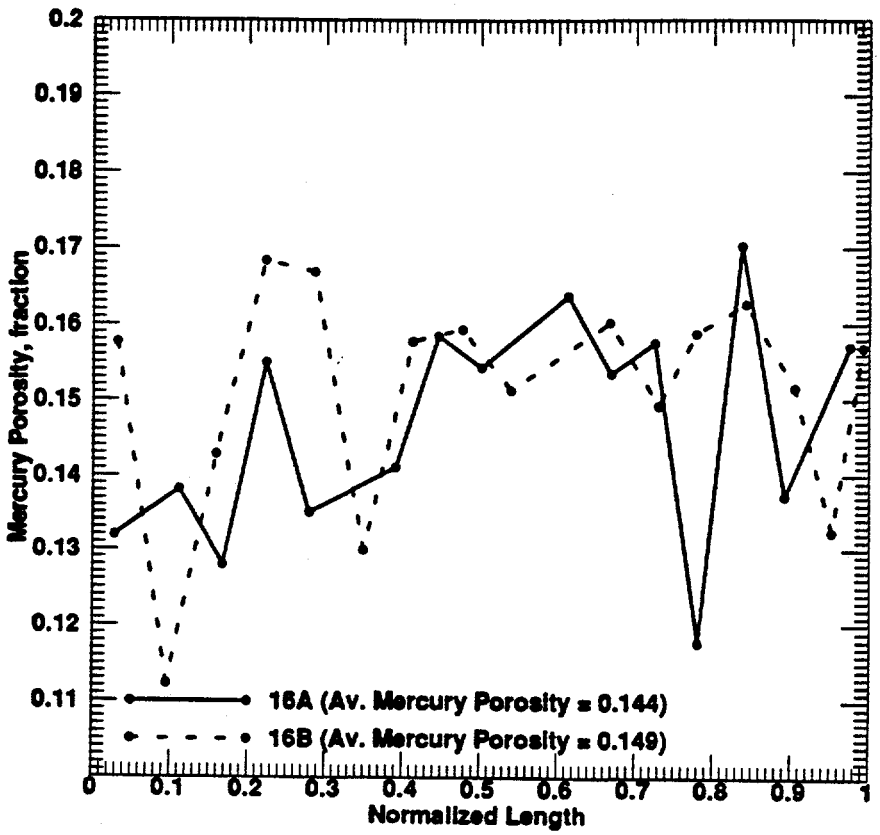

Fig. 5.151: Mercury Porosity vs. Normalized Length for Indiana Limestone Linear-Core Samples 16A and 16B.

Table 5.23: Correlation Matrix for the Mercury Porosimetry Properties for Indiana Limestone Linear-Cores

	$V_{int.}$	SA	S_o	$\bar{D}$	ρ_s	ϕ_{Hg}
SA	0.257					
S_o	-0.429	0.762				
$\bar{D}$	0.538	-0.472	-0.786			
ρ_s	0.482	0.170	-0.182	0.365		
ϕ_{Hg}	0.723	0.387	-0.133	0.436	0.813	
RE	-0.499	0.515	0.818	-0.734	-0.420	-0.291

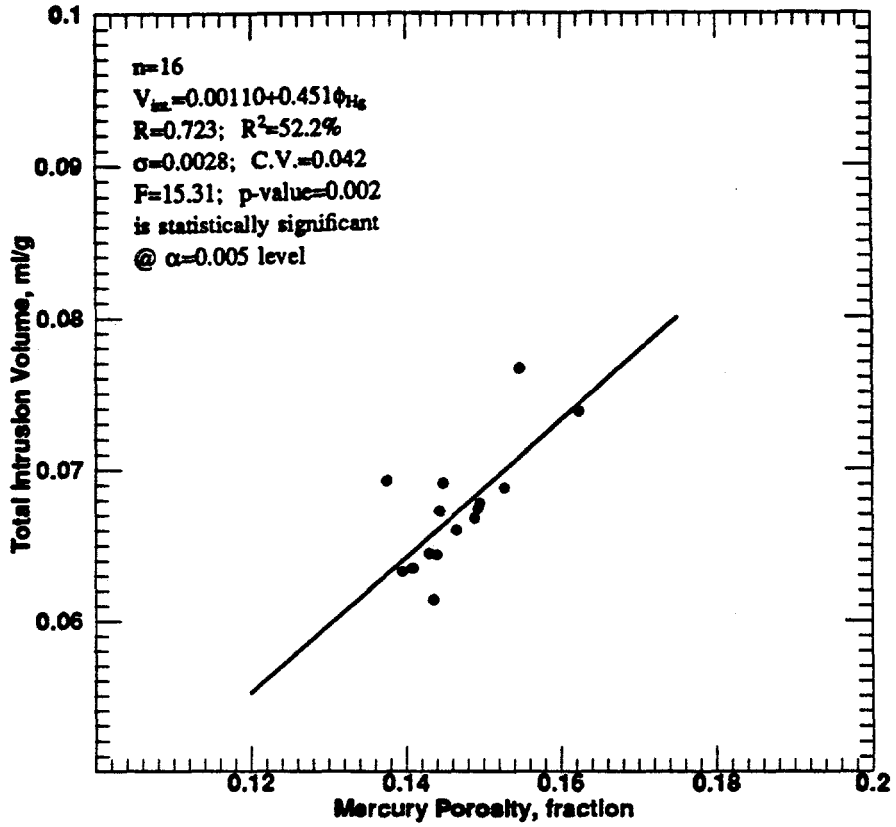

Fig. 5.152: Total Intrusion volume vs. Mercury Porosity for Indiana Limestone Linear-Cores.

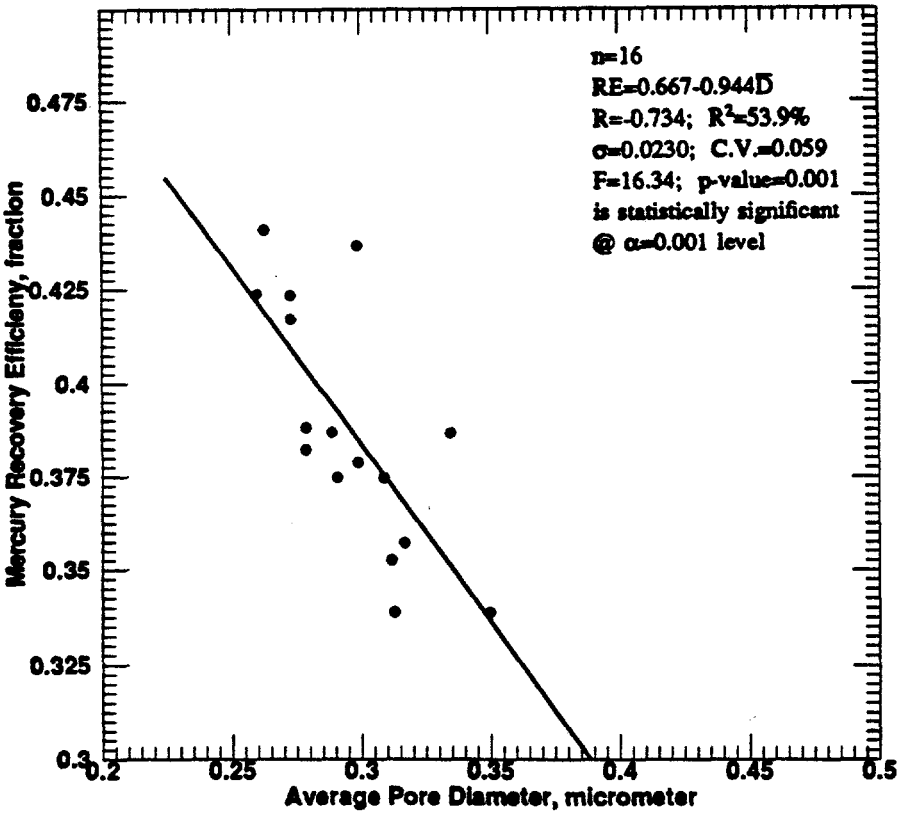

Fig. 5.153: Recovery Efficiency vs. Mercury Porosity for Indiana Limestone Linear-Cores.

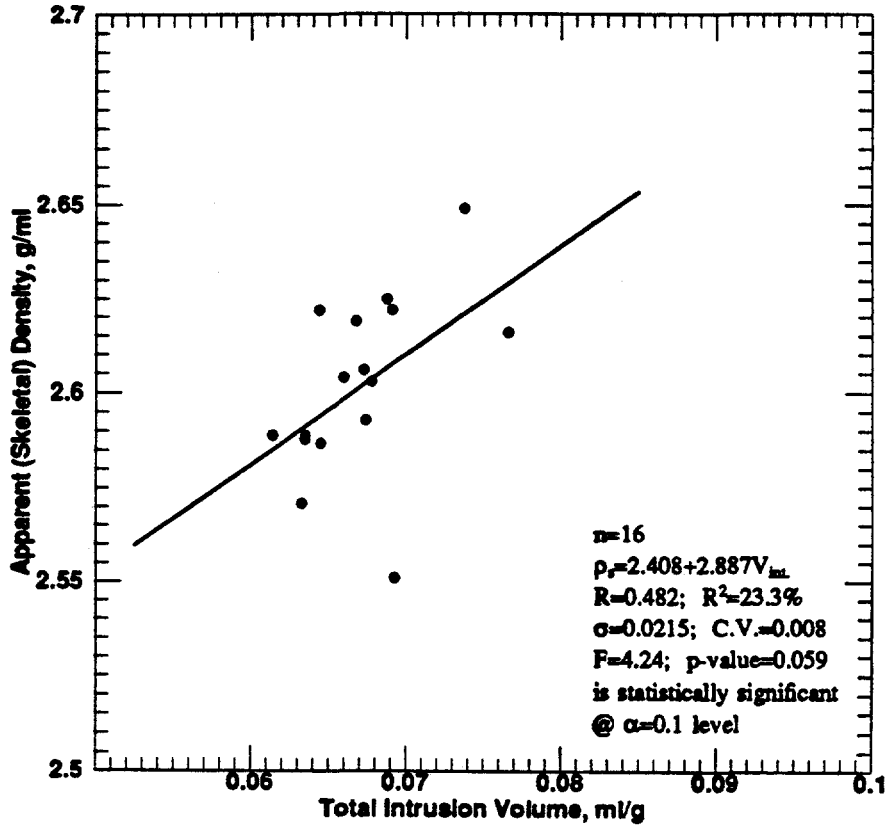

Fig. 5.154: Skeletal Density vs. Total Intrusion Volume for Indiana Limestone Linear-Cores.

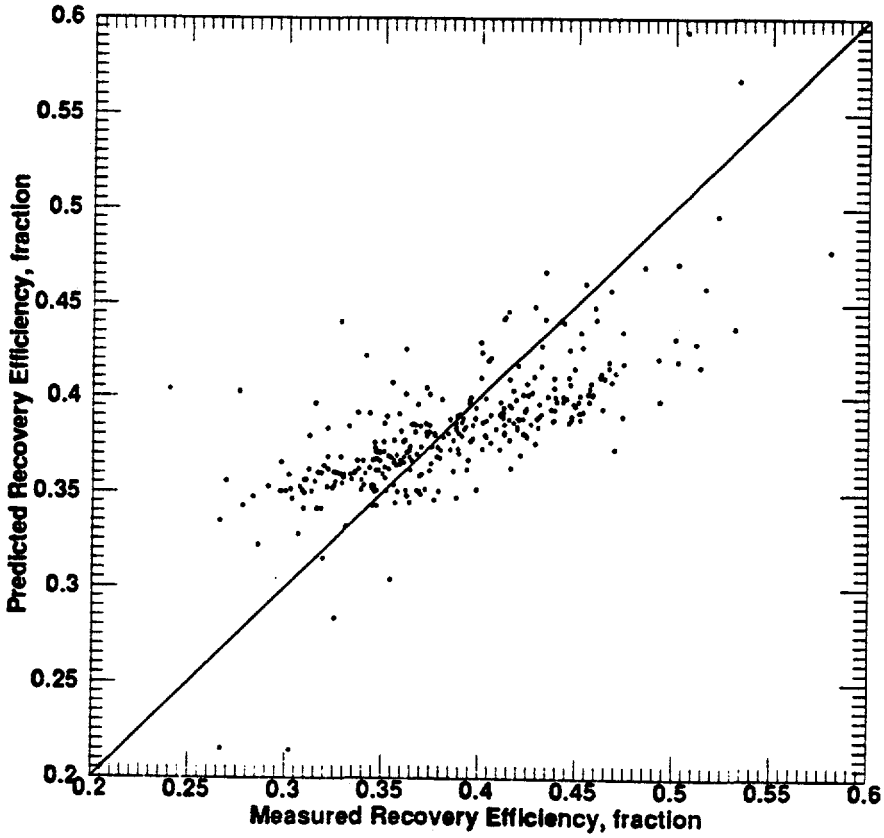

Fig. 5.155: Comparison of Measured Mercury Recovery Efficiency Values for Limestones with those Predicted by the New Correlation.

and porosity for carbonate rocks. An Inverse relationship was found by Amthor et al. (1988) and Kopaska-Merkel and Friedman (1989). Contrary to these findings, Wardlaw (1976), Ghosh and Friedman (1989), and Al-Fossail et al. (1991) found a direct relationship between mercury recovery efficiency and porosity of carbonate rock samples.

5.4.5.1 Mercury Recovery Efficiency Correlation

Using non-linear multiple regression analysis, a new correlation for estimating mercury recovery efficiency values for limestones is developed from 329 experimentally obtained mercury porosimetry data. Similar to the development in the case of sandstones, general form of the correlation for limestone is the same as earlier presented in Eq. 5.3.

By regressing the available mercury porosimetry data obtained from the 329 Indiana limestone core plug samples, the values of the coefficients were obtained. After the substitution of the values of the coefficients into Eq. 5.3, it results into the new correlation for estimating mercury recovery efficiency for limestones, as presented in Eq. 5.9:

$$RE = \frac{SA^{0.188}\,\phi_{Hg}}{3.53\,V_{int.}^{1.13}\,\overline{D}^{0.262}\,\rho_s^{1.20}} \tag{5.9}$$

The units of mercury recovery efficiency, RE, mercury porosity, ϕ_{Hg}, and the other variables in Eq. 5.9 are as defined in the nomenclature.

To test how good the correlation is, a crossplot to compare the predicted mercury recovery efficiency values using Eq. 5.9 with the measured values is shown in Fig. 5.155. Most of the plotted data points of this new correlation fall close to the 45° line, indicating its good degree of correlation. This new correlation has a standard deviation of 0.052, F-test statistic value of 375.0, and statistically significant with p-value of 0.000.

The plotted residuals versus measured mercury recovery efficiency for limestones is shown in Fig. 5.156. The trend of the scatter data points shows a directly increasing

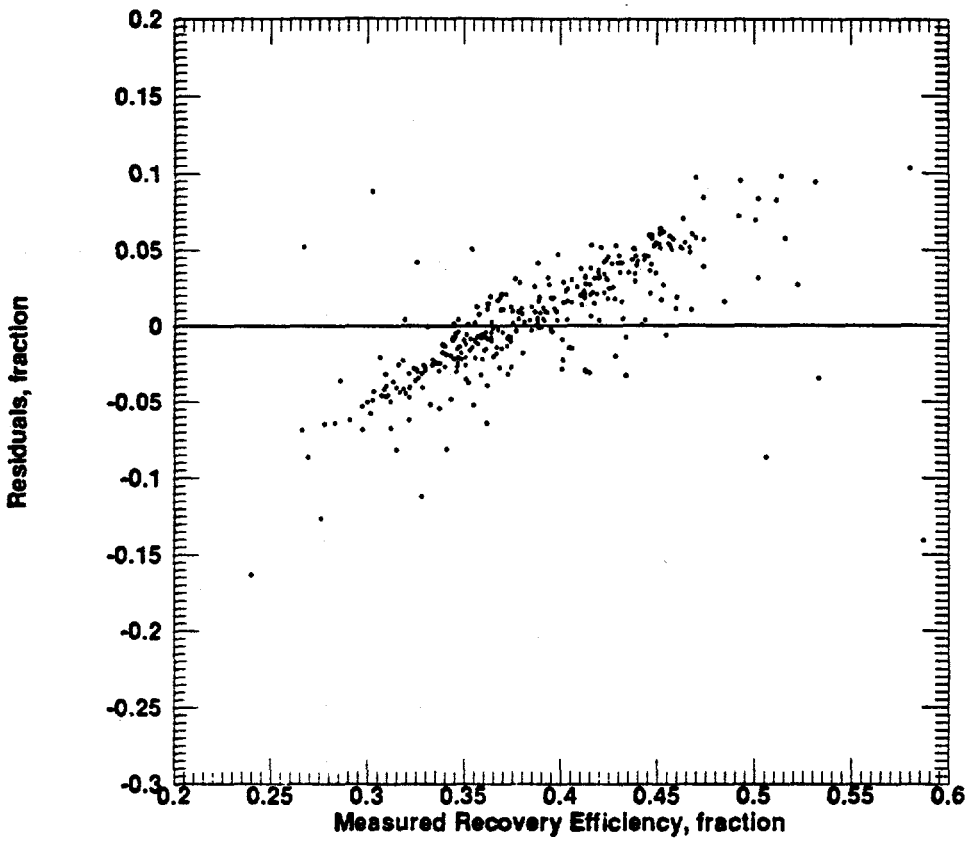

Fig. 5.156: Plotted Residuals Using the New Correlation vs. Measured Mercury Recovery Efficiency for Limestones.

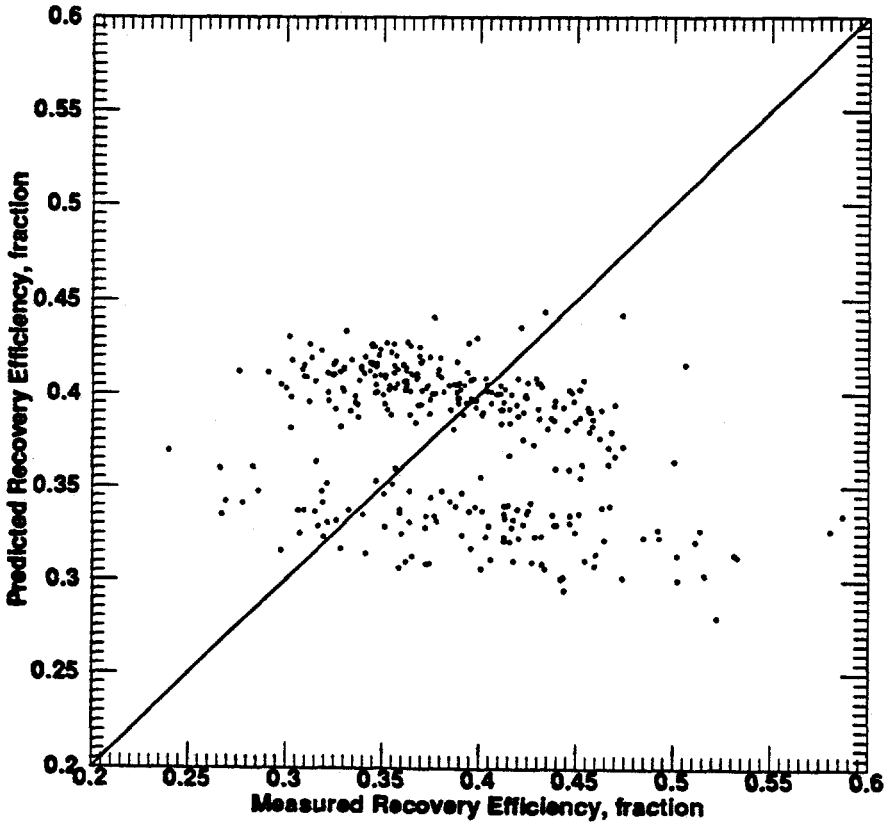

Fig. 5.157: Comparison of Measured Mercury Recovery Efficiency Values for Limestones with those Predicted by Al-Fossail et al. (1991) Correlation.

relation. The behavior of the plot suggests the addition of another independent variable to the correlation. One observation that can be drawn from this, is that an additional contribution to the dependent variable, mercury recovery efficiency, may be made by some property of the pore structure which was not measured in this study.

The predictive strength of the new correlation (Eq. 5.9) for estimating mercury recovery efficiency of limestones was compared with the correlation presented by Al-Fossail et al. (1991). The correlation by Al-Fossail et al. was developed using Saudi Arabian carbonate reservoir rocks. The correlation is given in Eq. 5.10 below:

$$RE = 16.876 + 1.4075\,\phi_{Hg} \tag{5.10}$$

In Eq. 5.10, mercury recovery efficiency, RE, and mercury porosity, ϕ_{Hg}, are both expressed as percentages.

The crossplot for comparing the predicted mercury recovery efficiency values using Eq. 5.10 with the measured values is shown in Fig. 5.157. Unlike the case of the new correlation, most of the plotted data points of Al-Fossail et al. correlation scatter widely along both sides of the 45° line, indicating that this correlation is not as good as the new correlation. This conclusion is further strengthened by the plot of Al-Fossail et al. correlation's residuals versus measured mercury recovery efficiency, which is shown in Fig. 5.158. The trend of the scatter data points is more directly related than that of Fig. 5.156. The behavior of this plot suggests the addition of more independent variables to the Al-Fossail et al. correlation, before its predictive capability could be improved.

5.4.5.2 Relation Between Porosimetry and Petrophysical Properties

Correlation matrices for the full models at breakthrough and floodout for limestones were investigated and presented in Tables 5.24 and 5.25, respectively. The agreement

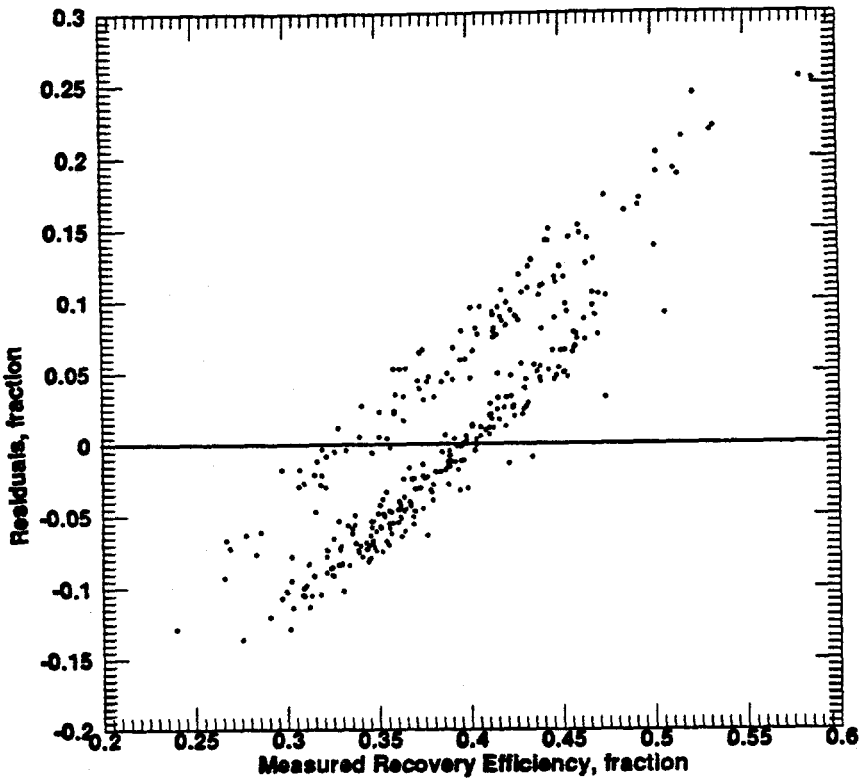

Fig. 5.158: Plotted Residuals Using Al-Fossail et al. (1991) Correlation vs. Measured Mercury Recovery Efficiency for Limestones.

Table 5.24: Correlation Matrix for the Full Model for Indiana Limestone Linear-Cores at Breakthrough

	ϕ brine	k	WI	S_{wi}	$V_{kst.}$	SA	S_s	$\bar{D}$	ρ_s	ϕ Hg	RE	S_{nw} @ B.T.
k	0.496											
WI	0.188	-0.188										
S_{wi}	-0.050	0.166	-0.492									
$V_{kst.}$	0.320	0.546	0.026	0.388								
SA	-0.126	0.155	-0.190	0.148	0.257							
S_s	-0.350	-0.230	-0.221	-0.096	-0.429	0.762						
$\bar{D}$	0.343	0.308	-0.037	0.280	0.538	-0.472	-0.786					
ρ_s	0.548	0.681	0.307	-0.164	0.482	0.170	-0.182	0.365				
ϕ_{Hg}	0.527	0.650	0.056	0.107	0.723	0.387	-0.133	0.436	0.813			
RE	-0.256	-0.572	-0.040	-0.081	-0.499	0.515	0.818	-0.734	-0.420	-0.291		
S_{nw} @ B.T.	-0.271	-0.605	0.219	-0.678	-0.628	0.054	0.458	-0.624	-0.403	-0.473	0.632	
OR @ B.T.	0.351	0.681	-0.023	0.361	0.637	-0.118	-0.513	0.661	0.603	0.565	-0.766	-0.928

Table 5.25: Correlation Matrix for the Full Model for Indiana Limestone Linear-Cores at Floodout

	ϕ brine	k	WI	S_{wi}	$V_{int.}$	SA	S_s	$\bar{D}$	ρ_s	ϕ Hg	RE	S_{or} @ F.O.
k	0.496											
WI	0.188	-0.188										
S_{wi}	-0.050	0.166	-0.492									
$V_{int.}$	0.320	0.546	0.026	0.388								
SA	-0.126	0.155	-0.190	0.148	0.257							
S_s	-0.350	-0.230	-0.221	-0.096	-0.429	0.762						
$\bar{D}$	0.343	0.308	-0.037	0.280	0.538	-0.472	-0.786					
ρ_s	0.548	0.681	0.307	-0.164	0.482	0.170	-0.182	0.365				
ϕ_{Hg}	0.527	0.650	0.056	0.107	0.723	0.387	-0.133	0.436	0.813			
RE	-0.256	-0.572	-0.040	-0.081	-0.499	0.515	0.818	-0.734	-0.420	-0.291		
S_{or} @ F.O.	-0.094	-0.581	0.575	-0.800	-0.640	-0.363	0.071	-0.323	-0.177	-0.507	0.238	
OR @ F.O.	0.158	0.724	-0.493	0.474	0.703	0.408	-0.079	0.337	0.386	0.682	-0.334	-0.904

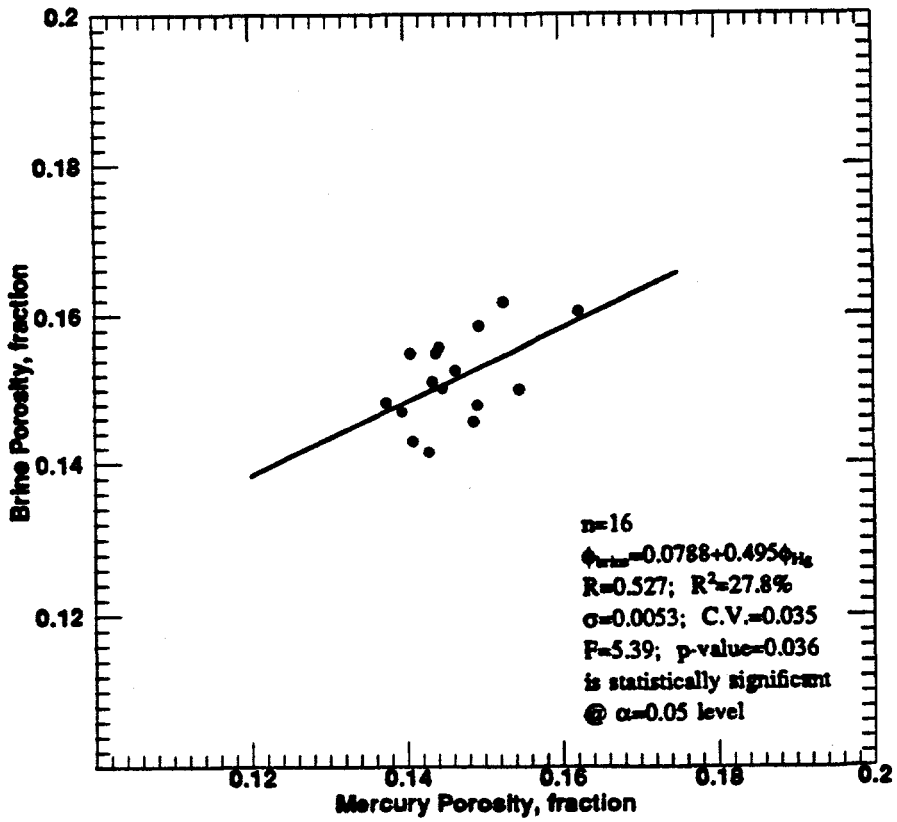

Fig. 5.159: Brine Porosity vs. Mercury Porosity for Indiana Limestone Linear-Cores.

between porosity values obtained using mercury porosimetry and those obtained from the corefloods were not as good as was expected, as shown in Fig. 5.159. It was observed that if a 45° degree line is drawn on the plot, 11 of the data points lie above the line and the other five are close to the 45° line. This finding implies that the brine porosities are larger than the mercury porosities. This is in agreement with what was observed for the case of sandstone core samples.

The relationship of brine permeability versus total intrusion volume is presented in Fig. 5.160. The relationship is direct with a standard deviation of 2.9 md, F-test statistic of 5.94, and statistically significant at $\alpha = 0.05$ level. The relationship of brine porosity with total intrusion volume failed the significance test, as show by its low correlation coefficient value in the correlation matrices presented in Tables 5.24 and 5.25. These tables are further employed to analyze the relationships of mercury porosimetry properties with brine porosity and brine permeability. Their relationships with surface area, specific surface area and average pore diameter, are not statistically significant. The specific surface area values of the limestone core samples investigated in this study, are considerably higher than those obtained for the sandstones ($12.48*10^4$ to $16.45*10^4$ versus $1.84*10^4$ to $8.58*10^4$ cm^2/cm^3). Brine porosity and brine permeability are directly related to apparent (skeletal) density. Brine permeability has is inversely related to mercury recovery efficiency. The relationship between brine porosity and mercury recovery efficiency is not statistically significant.

5.4.5.3 Relation Between Porosimetry and Waterflood Properties

The limestone's mercury porosimetry properties were individually related to the residual oil saturation and oil recovery at breakthrough and at floodout, as shown by their correlation coefficients in the correlation matrices of Tables 5.24 and 5.25, respectively. At breakthrough, unlike in the case of sandstones, all the relationships except those of surface area with residual oil saturation and oil recovery, were observed to be statistically

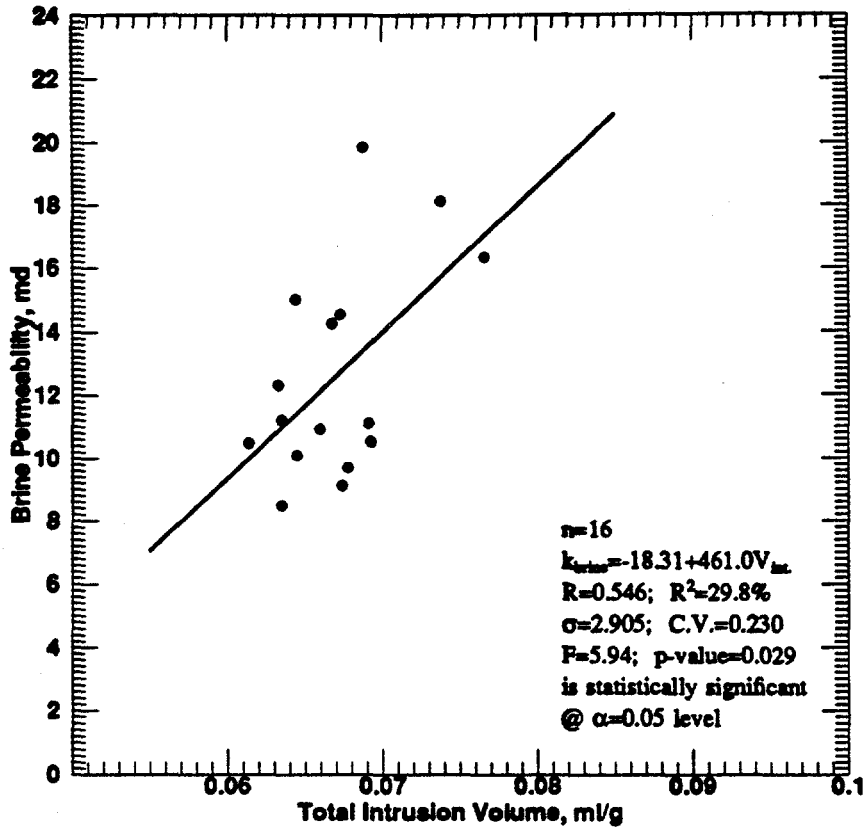

Fig. 5.160: Brine Permeability vs. Total Intrusion Volume for Indiana Limestone Linear-Cores.

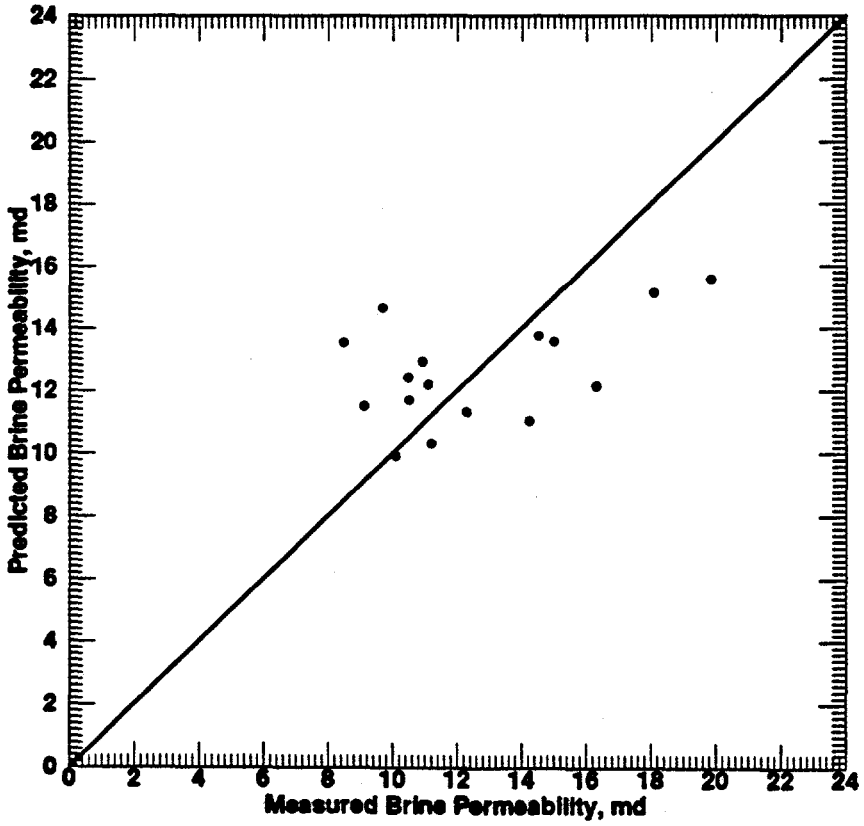

Fig. 5.161: Comparison of Measured Permeability Values for Limestones with those Predicted the New Correlation.

significant at $\alpha = 0.1$ level. At floodout, apart from the relationships of total intrusion volume and mercury porosity with residual oil saturation and oil recovery, the others failed the significance tests.

At both the breakthrough and floodout, the relationships of total intrusion volume with residual oil saturation are inverse and its relationships with oil recovery are direct. Residual oil saturation at breakthrough is directly related to specific surface area and mercury recovery efficiency, but inversely related to average pore diameter, apparent (skeletal) density, and mercury porosity. In the case of oil recovery at breakthrough, it is inversely related to specific surface area and mercury recovery efficiency, but directly related to average pore diameter, apparent (skeletal) density, and mercury porosity.

5.4.5.4 Permeability Correlation

Again, using non-linear multiple regression analysis, as in the case of mercury recovery efficiency, a new correlation for estimating permeability values for limestones using coreflood or mercury porosimetry measured data is developed. The development was initiated using the 16 limestone cores waterflood and mercury porosimetry experimentally obtained data. Similar to the sandstone case, the general form of the correlating equation is as earlier presented in Eq. 5.6.

To further improve the limestone permeability correlation, Eq. 5.6 was modified by multiplying the dependent variable by $(1-\phi)^2$, which implies that:

$$k(1-\phi)^2 = f(\phi, SA, S_s) \tag{5.11}$$

After applying multiple regression analysis methods on Eq. 5.11, the resulting developed correlation for estimating permeability is given as:

$$k = \frac{3.146 * 10^3 \phi^{2.98}}{SA^{0.0234} S_s^{0.0185} (1-\phi)^2} \tag{5.12}$$

In Eq. 5.12, permeability, k, is expressed in millidarcy and porosity, ϕ, is expressed as fraction. The other variables in the equation are as defined in the nomenclature.

To show how good the correlation is, a crossplot to compare the predicted brine permeability values using the new correlation, as presented in Eq. 5.12, with the measured values is shown in Fig. 5.161. The plotted data points deviate from the 45° line and not as good as would have been expected. Part of the scatter in the crossplot between predicted brine permeability and measured brine permeability may be artificial, caused by the inclusion of measurements from plugs with induced fractures, which were not easily noticeable by visual inspection of the plugs. The new correlation is statistically significant at $\alpha = 0.001$ level. The plotted residuals versus measured brine permeability values for limestones is shown in Fig. 5.162. The behavior of the plot suggests that porosity, surface area, and specific surface area were enough to develop a good correlation for permeability.

The predictive strength of the new correlation (Eq. 5.12) for estimating permeability of limestones was compared with the correlation presented in the study by Wang et al. (1991). The laboratory measured data obtained for this study were used for the comparison, due to the non-availability of independently measured data sets. The correlation by Wang et al. was developed using laboratory measured samples of 54 carbonates cores from 11 oil-producing reservoirs. The correlation is given in Eq. 5.13 below:

$$\ln k = 29.0585\,\phi - 1.6348 \qquad (5.13)$$

In Eq. 5.13, permeability, k, is in millidarcy and porosity, ϕ, is expressed as fraction.

The crossplot to compare the predicted permeability values using Eq. 5.13 with the measured values is shown in Fig. 5.163. Unlike the case of the new correlation, most of the plotted data points of Wang et al. correlation scatter widely along the upper part of the 45° line, indicating that this correlation mostly over-predicts. This conclusion is further

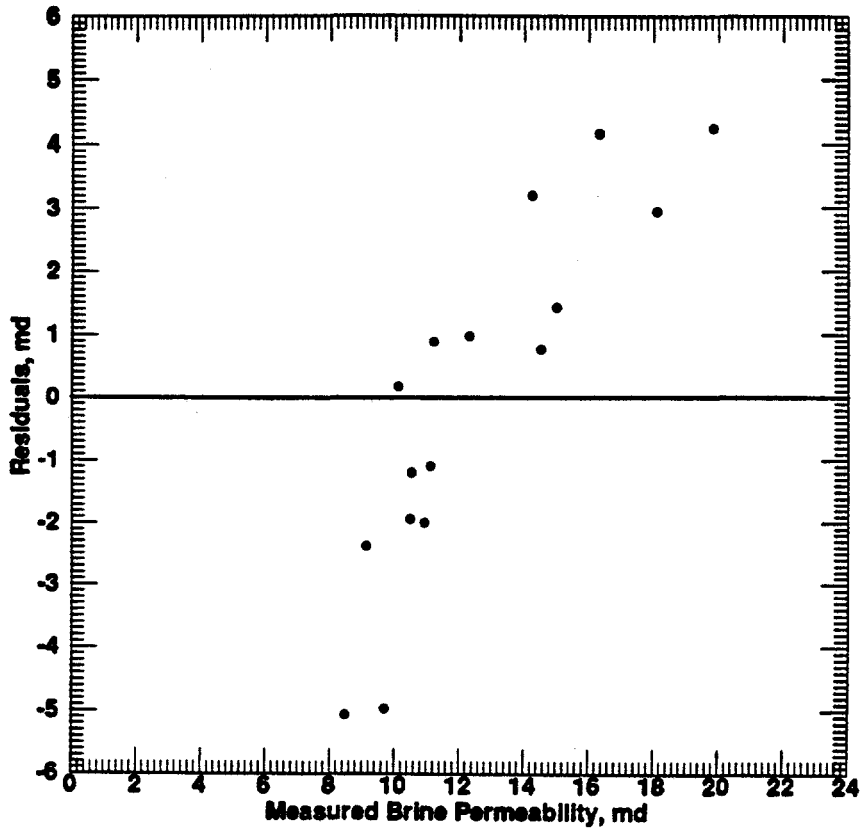

Fig. 5.162: Plotted Residuals the New Correlation vs. Measured Permeability for Limestones.

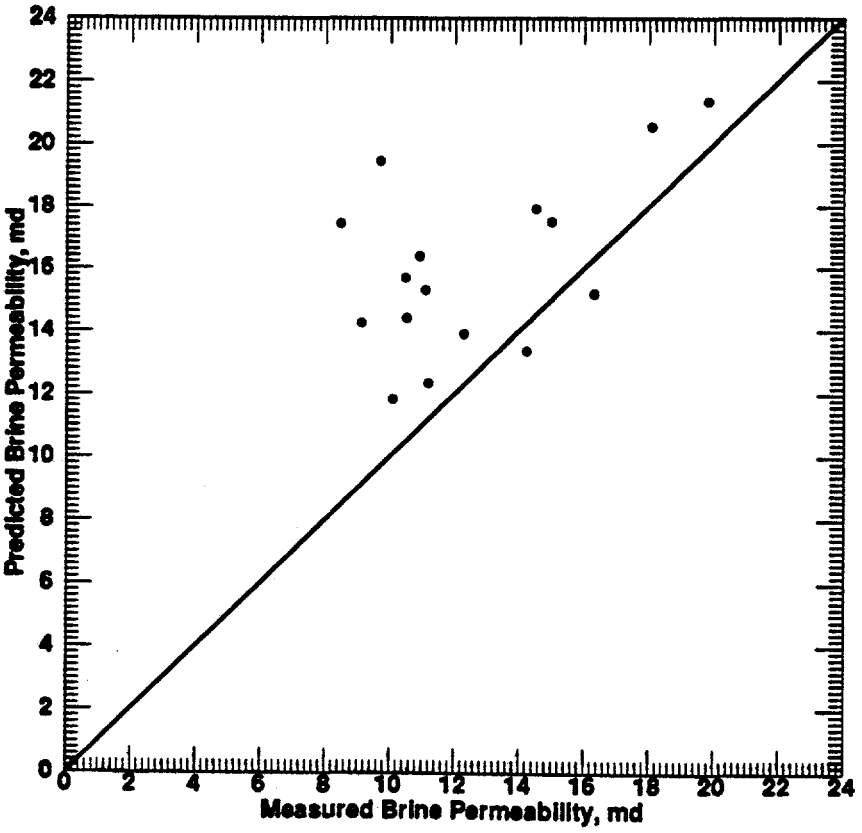

Fig. 5.163: Comparison of Measured Permeability Values for Limestones with those Predicted by Wang et al. (1991) Correlation.

strengthened by the plot of Wang et al. correlation's residuals versus measured permeability, which is shown in Fig. 5.164. The behavior of the scatter data points shows that it over-predicts and not as good as the scatter plots of Fig. 5.162. The behavior of the plot suggests the addition of more independent variables to the correlation of Wang et al., before its predictive capability could be improved.

Equation 5.12 was also used to estimate mercury permeability of the core plug samples. The resulting estimates of mercury permeability values for the 329 limestone core plug samples were plotted against the respective values of their measured mercury porosity values, as shown in Fig. 5.165. Again, similar to the sandstone case, the plotted data points fall very close to an exponential trend as expected for the relationship of porosity with permeability. Finally, the estimated average mercury permeability values were compared with the measured brine permeability values as shown in Fig. 5.166. Similar to the observation in Fig. 5.159, which is the plot of brine porosity versus mercury porosity, the comparison was not perfect.

5.4.5.5 Relation Between Porosimetry and Wettability Properties

The relationships of average wettability index with the various mercury porosimetry properties were investigated, as shown in the correlation matrices of Tables 5.24 and 5.25. All of the mercury porosimetry properties show relationships that are not statistically significant with average wettability index.

5.4.5.6 Shape of the Capillary Pressure Curve

Capillary-pressure curves reflect the capillary forces which govern the distribution of fluids in the porous system and influence the flow of fluids. The shapes of the capillary-pressure curves do not appear to be a unique function of either sandstones or limestones, but mainly reflect the pore size distribution in the rock. Figure 5.167 presents the

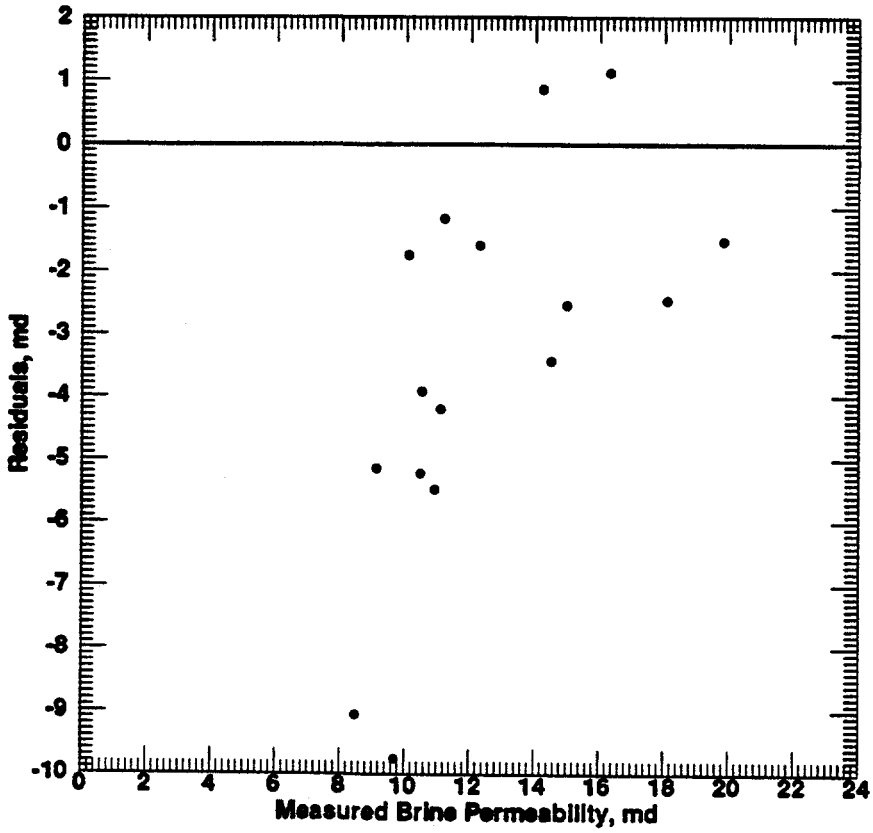

Fig. 5.164: Plotted Residuals Using Wang et al. (1991) Correlation vs. Measured Permeability for Limestones.

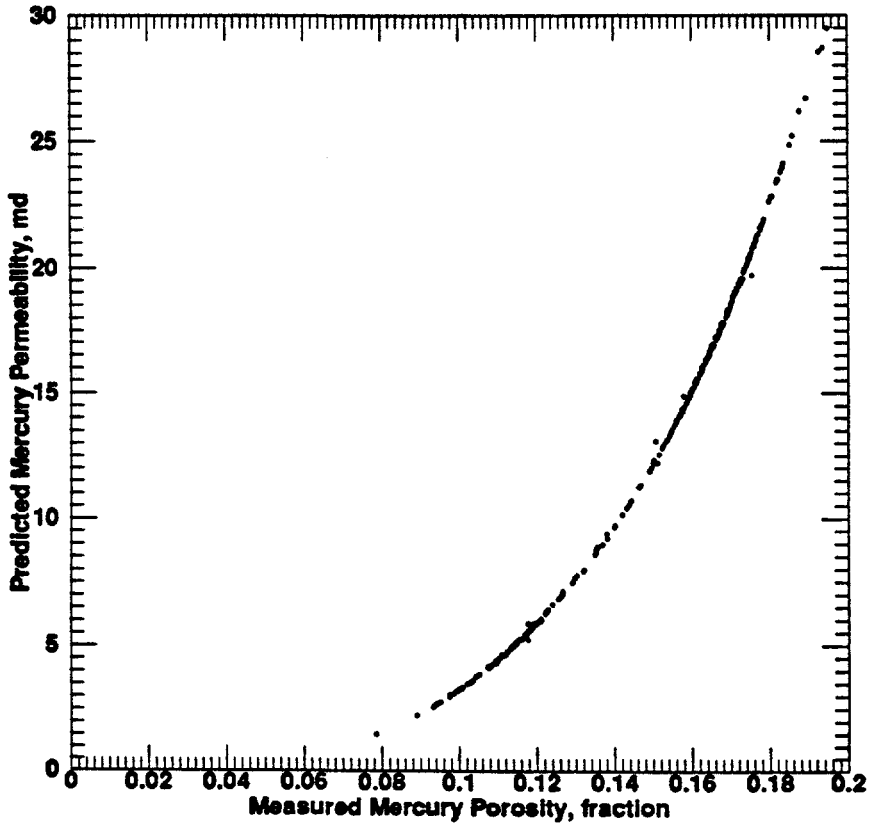

Fig. 5.165: Mercury Permeability for Limestones Predicted by Using the New Correlation vs. Measured Mercury Porosity.

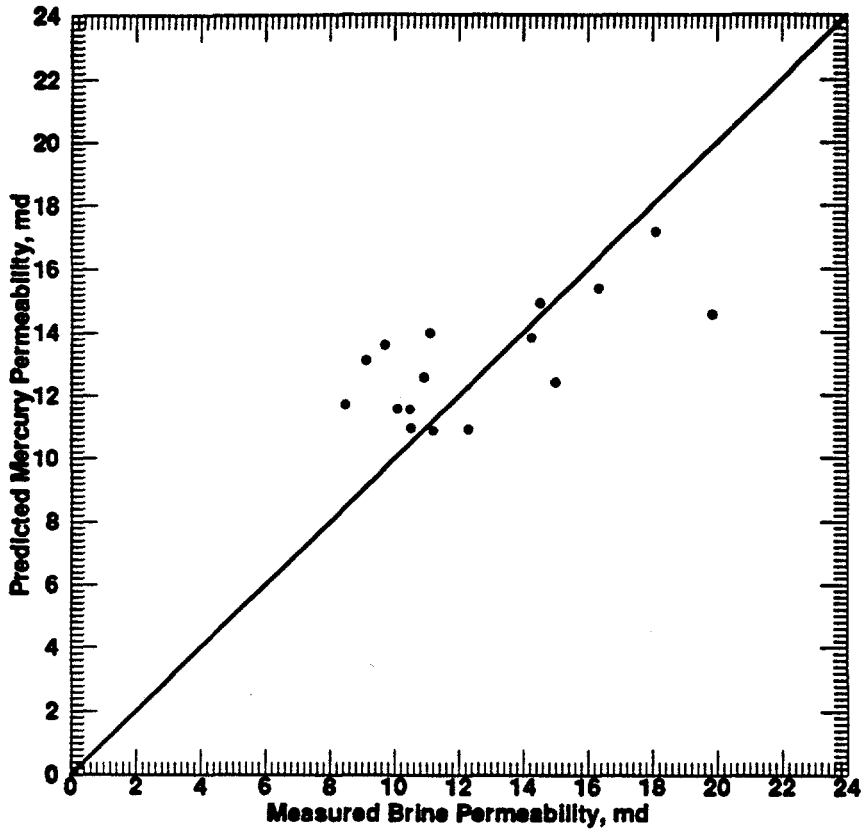

Fig. 5.166: Comparison of Measured Brine Permeability Values for Limestones with Mercury Permeability Predicted by the New Correlation.

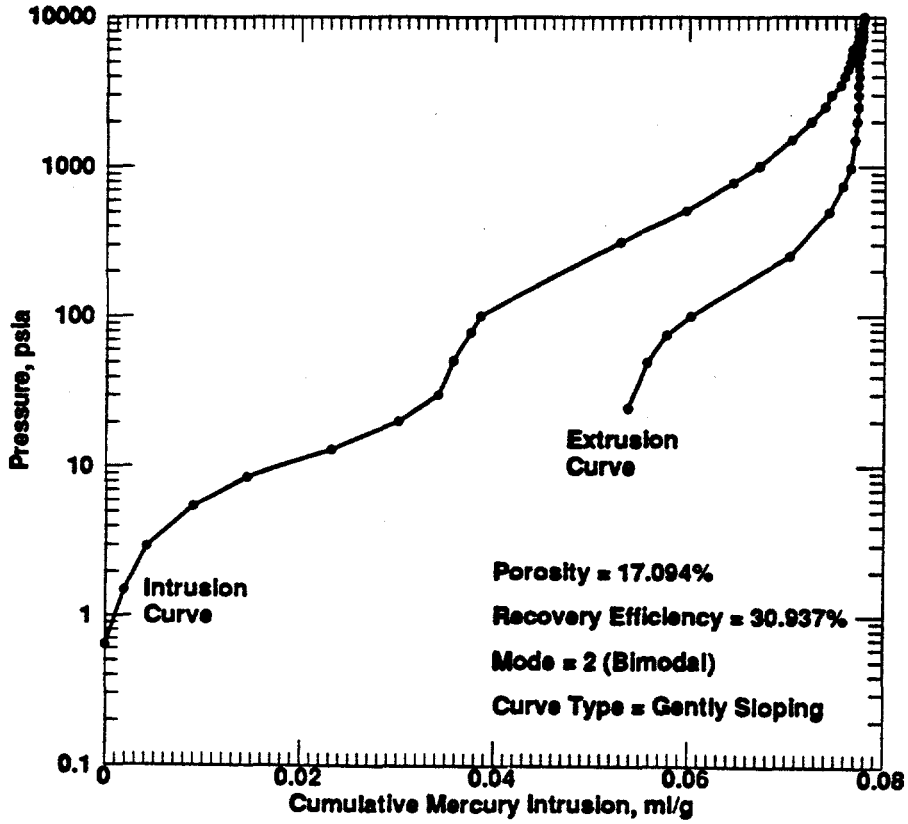

Fig. 5.167: Capillary Pressure vs. Cumulative Mercury Intrusion Curve for Indiana Limestone Linear-Core 2A - Plug 11.

capillary-pressure versus cumulative mercury intrusion/extrusion curve for plug 28 of linear-core sample 15B. Similar to most of the other Indiana limestone linear-core plug samples investigated in this study, the mode type of the curve is bimodal with gently-sloping shape. This is further confirmed in Fig. 5.168, which is the plot of capillary-pressure versus incremental mercury intrusion/extrusion curve for the same plug.

The existence of multiple modes is significant because it affects the overall non-wetting-phase recovery efficiency. For the investigated limestone samples, the gently slopping bimodal curves correlate with high mercury recovery efficiency (mean = 39%), high porosity (mean = 15%), intermediate average pore diameter (mean = 0.30 μm), and high entry pressures. The capillary-pressure versus cumulative pore area curve for the plug is presented in Fig. 5.169. Only the mercury intrusion data were used to plot Fig. 5.169.

Churcher et al. (1991) also observed bimodal capillary-pressure curve shapes in their studies using Indiana limestone core samples. They suggested that the bimodal pore throat size distributions in Indiana limestone samples may result from the distribution of the fine calcite crystals which line the pores and create microporosity. They were also of the opinion that it may also arise from the intra-particle porosity noted in some fragments and oolites.

In the report of their studies on the reservoir characterization of deeply-buried paleozoic carbonates from Oklahoma, Texas and New Mexico, Amthor et al. (1988) argued that the shapes of capillary-pressure curves are useful components of a formal classification of carbonate rocks. The simple empirical classification of capillary-pressure curves allows evaluation of potential reservoir rocks at a glance in terms of their petrophysical properties. They further postulated that steep-convex capillary-pressure curves indicate reservoir rocks with high recovery efficiencies, but low porosities and small throats, so that the production is likely to be economical only under high pressures (or thick oil columns) or from very large hydrocarbon pools. Conversely, steep-concave curves indicate porous reservoir rocks

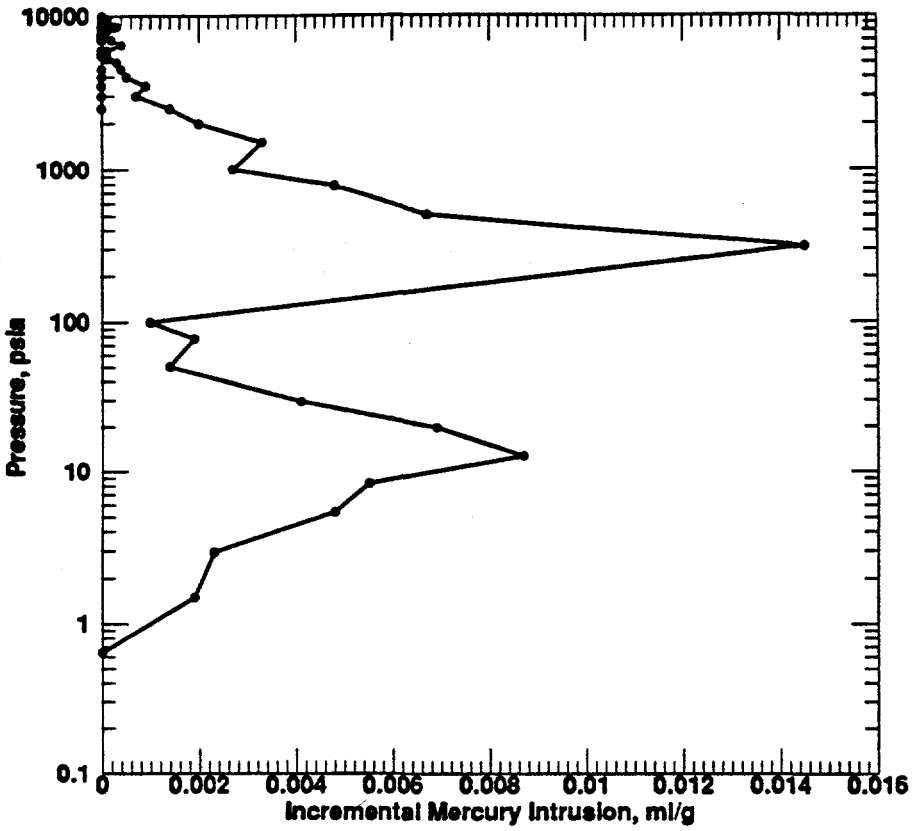

Fig. 5.168: Capillary Pressure vs. Incremental Mercury Intrusion Curve for Indiana Limestone Linear-Core 2A - Plug 11.

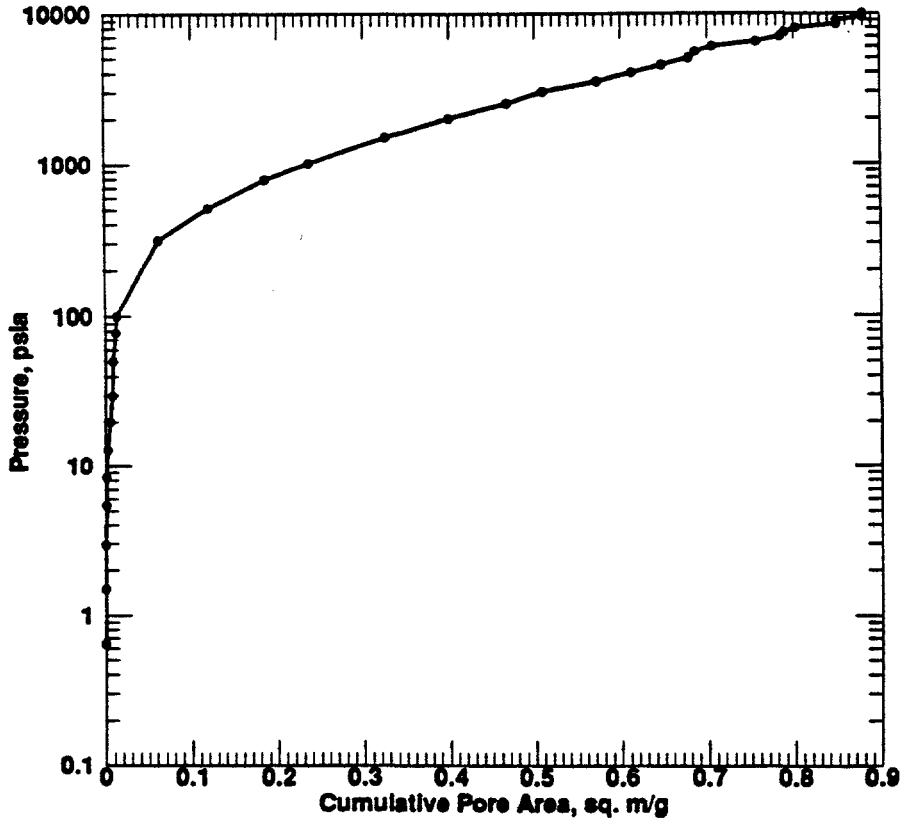

Fig. 5.169: Capillary Pressure vs. Cumulative Pore Area Curve for Indiana Limestone Linear-Core 2A - Plug 11.

with large throats but probably poor primary recovery efficiency. These reservoirs will be economical even at low pressures and with short oil columns and small total reserves, but will probably need enhanced recovery to produce a significant proportion of the reserves. They suggested that gently-sloping curves correspond to samples with moderate recovery efficiencies, intermediate median throat sizes, and variable porosities. Polymodal curves result from polymodal throat-size distribution, and exhibit variable recovery efficiencies and porosities.

Chapter 6

DEVELOPMENT OF THE EMPIRICAL MODELS

6.1 Introduction

Empirical models have been developed which relate residual oil saturation and oil recovery with rock-pore characteristics. The models for residual oil saturation and oil recovery are respectively given at two periods: at breakthrough and at floodout. Prior to the development the models, correlation matrix for the full models at breakthrough and at floodout were investigated and presented in the previous chapter. The tables also show the inter-relationships among the independent variables. On the basis of these analyses, the dependent variables, residual oil saturation and oil recovery at both the breakthrough and floodout periods, could be best represented as a function of the independent variables in linear terms or a minimum amount of interactions among the variables.

6.1.1 Building of the Regression Model

Multiple regression analysis is one of the most widely used of all statistical tools. The general linear regression model with normal error terms, simply in terms of dependent variable Y and X independent variables is defined as (Neter et al., 1990):

$$Y_i = \beta_0 + \beta_1 X_{i1} + \beta_2 X_{i2} + ... + \beta_{p-1} X_{i,p-1} + \varepsilon_i \qquad (6.1)$$

where:

$\beta_0, \beta_1, ..., \beta_{p-1}$ are parameters

$X_{i1}, ..., X_{i,p-1}$ are known constants

ε_i are the error term which should be normal and independent, with mean of 0 and constant variance of σ^2

$i = 1,.....,n$

A particular case of the general linear regression model (Eq. 6.1), is the polynomial regression. Considering the case of polynomial regression model with one independent variable:

$$Y_i = \beta_0 + \beta_1 X_i + \beta_2 X_i^2 + \varepsilon_i \tag{6.2}$$

Interaction effects can also be incorporated into Eq. 6.1. Considering the regression in two independent variables X_1 and X_2, the interaction effect is given as:

$$Y_i = \beta_0 + \beta_1 X_{i1} + \beta_2 X_{i2} + \beta_3 X_{i1} X_{i2} + \varepsilon_i \tag{6.3}$$

The regression model with transformed variables Y' and X'_k is called standardized regression model and it is given as follows (Neter et al., 1990):

$$Y'_i = \beta'_1 X'_{i1} + ... + \beta'_{p-1} X'_{i,p-1} + \varepsilon'_i \tag{6.4}$$

It can be shown that the new parameter $\beta'_1,.....,\beta'_{p-1}$ and the original parameters β_0, $\beta_1,.....,\beta_{p-1}$ in the ordinary linear regression model (Eq. 6.1) are related as follows:

$$\beta_k = \left[\frac{s_Y}{s_k} \right] \beta'_k \quad (k = 1,...,p-1) \tag{6.5}$$

s_Y and s_k are the respective standard deviations of the original and the standardized models. Hence, the resulting new transformed regression coefficients β'_k and the original regression coefficients β_k are related by simple scaling factors involving ratios of standard deviations.

Furthermore, in the process of trying to increase coefficient of correlations of the models, apart from the general linear regression, polynomial regression, interaction effects and transformation were applied on the independent variables before applying the designing scheme employed in this study. With this, the correlation coefficient and coefficient of determination were only slightly improved. For this reason, it was unnecessary to include some of the resulting transformed and interacting independent variables in the models for residual oil saturation and that of oil recovery. The interacting and transformed variables that were included in the development of the linear-core models are: product of porosity and irreducible water saturation (ϕS_{wi}), product of mercury porosity and specific surface area ($\phi_{Hg} S_s$), product of mercury porosity and mercury recovery efficiency (ϕ_{Hg}RE) and logarithm to base 10 of permeability (log k).

6.1.2 R_p^2 Criterion

The R_p^2 criterion calls for an examination of the coefficients of multiple determination, R^2 for all possible models. The number of parameters in a regression model is shown as a subscript of R^2. Therefore, R_p^2 indicates that there are p parameters, or p-1 predictor variables in the regression function on which R_p^2 is based. The reason for using the R_p^2 criterion is not to maximize R_p^2, but the intent is rather to find the point where adding more independent variables results in a very small increase in R_p^2.

6.1.3 C_p Criterion

This criterion is connected with the total mean squared error of the n fitted values for each subset regression model. Neter, et al. (1990) indicated that squared error concept involves a bias component and a random error component. The mean squared error pertains to the fitted values $\hat{Y}_i$ for the regression model employed. The C_p values for all possible regression models are plotted against the number of parameters, p, models with little bias

will tend to fall near the line, $C_p = p$. Models with substantial bias will tend to fall considerably above this line. C_p values below the line $C_p = p$ are interpreted as showing no bias; that is, they are below the line due to sampling error. In using the C_p criterion, one seeks to identify subsets of independent variables for which the C_p value is small and for which the C_p value is near p. Sets of independent variables with small C_p values have a small total mean squared error, and when the C_p value is also near p, the bias of the regression model is small.

6.1.4 Best Subsets Algorithms

For the development of the linear-core models, best subsets algorithms "BREG", which is available in MINITAB statistical computer software package (Ryan et al., 1985), was utilized. They are time-saving algorithms and they allow the best subsets according to a specified criteria to be identified, without requiring the fitting of all of the possible subset regression models. The algorithms also provide a number of "good" subsets for each possible number of independent variables in the model to give the investigator additional helpful information in making the final selection of the subset of variables to be employed in the regression model (Neter et al., 1990). It is worth noting that the best subsets algorithms are not good when the independent variables are very large. Under this condition, stepwise regression technique may need to be employed to assist in the selection of the independent variables.

Apart from the coefficient of determinations and standard deviations, the other selection criteria used are the C_p criteria and the adjusted coefficient of multiple determination (Adj. R-sq.). C_p criterion is concerned with the total mean squared error of the fitted values for each subset regression model. When there is no bias in the regression model with p-1 predictor variables, the expected value of C_p is approximately p. The

adjusted coefficient of multiple determination adjusts the coefficient of multiple determination R^2 by dividing each of the sum of the squares by its associated degree of freedom. It is suggested as a criterion which takes the number of parameters in the model into account through the degree of freedom (Neter et al., 1990; and Ryan et al., 1985). Adjusted coefficient of determination increases if and only if the mean square error increases.

To embark on the development of the linear-core models, the sets of data obtained for the sandstone and limestone samples were separated into common and uncommon rock/fluid properties. The common properties are porosity, absolute permeability, and irreducible water saturation. The uncommon properties used are wettability index, total intrusion volume, pore surface area, average pore diameter, apparent (skeletal) density, mercury porosity, and mercury recovery efficiency. Residual oil saturation is also included in all the oil recovery modeling building process. The models which are later presented in Eqs. 6.11 through 6.22 for sandstones and Eqs. 6.25 through 6.36 for limestones, are for common, uncommon and, for combination of both common and uncommon rock/fluid properties.

6.2 Sandstone Radial-Core Case

Summary statistics of variables to be used in the model are shown in Tables 5.1 for Berea sandstone radial-cores. The inter-correlations among the potential independent variables are shown in Table 6.1 for Berea sandstone radial-cores. Moreover, a schematic of the statistical data collection and design is presented in Fig. 6.1.

As indicated in Fig. 6.1, a data base was developed from waterflooding, wettability and porosimetry experiments. This data base was used to determine the functional relationships between ultimate oil recovery and rock properties investigated. These functional relationships were then incorporated into generalized stochastic models for predicting oil recovery by waterflooding. The developed stochastic models are used as

Table 6.1: Correlation Matrix for the Full Model for Berea Sandstone Radial-Cores

	SA	d	τ	ϕ	k	L	WI	S_{or}	S_{wi}	UOR
d	-0.609									
τ	-0.027	-0.052								
ϕ	-0.940	0.575	-0.021							
K	-0.910	0.514	-0.051	0.957						
L	0.753	-0.771	0.151	-0.724	-0.704					
WI	-0.418	0.081	0.705	0.299	0.346	-0.196				
S_{or}	-0.222	0.009	-0.277	0.142	-0.113	-0.146	-0.250			
S_{wi}	0.108	0.093	0.143	-0.011	0.042	0.103	0.153	-0.937		
UOR	0.437	-0.370	0.197	-0.450	-0.363	0.262	0.285	-0.767	0.563	1.000

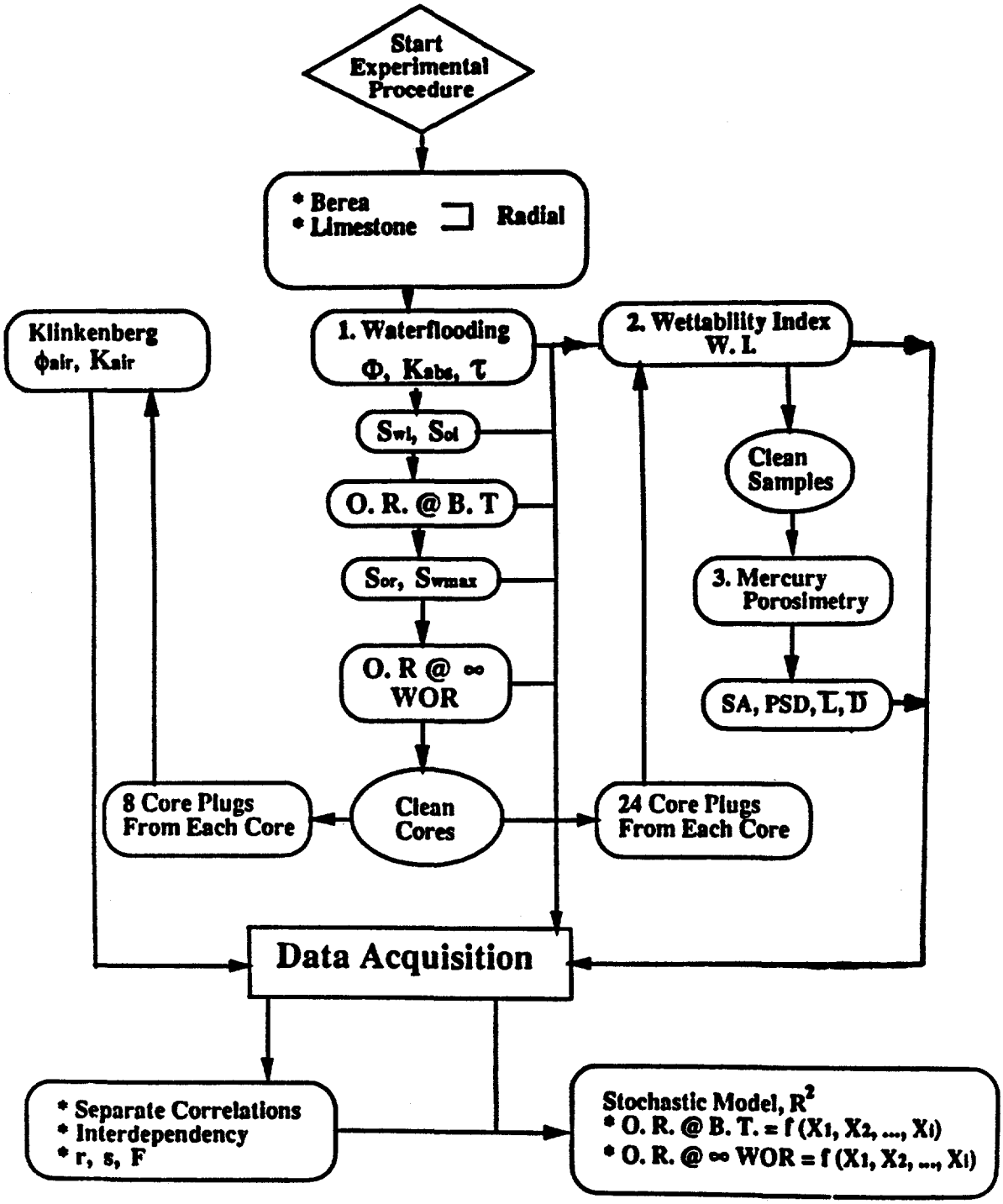

Fig. 6.1: Schematic Drawing of Statistical Data Collection and Design.

predictive tools in estimating oil recovery by waterflooding as a function of the rock properties of Berea sandstone and Indiana limestone radial-cores.

A first-order regression model relating the sandstone ultimate oil recovery, UOR, to all independent variables was fitted to the experimental data and presented in the following forms:

$$\begin{aligned} UOR = {} & 0.362 - 0.000064\,\tau + 0.000027\,k \\ & - 0.923\,\phi + 0.005\,SA - 0.0263\,d - 0.0183\,L \\ & + 0.375\,WI - 1.30\,S_{or} + 0.632\,S_{oi} \end{aligned} \tag{6.6}$$

Contrary to the specification in the nomenclature, the unit of ultimate oil recovery, UOR, in the sandstone and limestone radial-cores model developments, are in fraction.

The multiple regression model relating ultimate oil recovery to the independent variables of surface area, median pore-throat diameter, tortuosity, porosity, permeability, pore length, wettability index, residual and initial oil saturations, shows a good fit, with R^2 = 94.4%. The standard deviation of the model was determined to be 0.96% and the coefficient of correlation, R_N^2, between the ordered residuals and their respective values under normality, is high (98.3%). The high coefficient of correlation validates the linearity of the model and the assumption that, the error terms are normally distributed. Furthermore, a high value (18.65) of the F-test statistic indicates that there is a statistically significant regression of the independent variables on ultimate oil recovery, that is, the use of these nine variables significantly improves the prediction of ultimate oil recovery.

The normal probability plot of the residuals for the full model is presented in Fig. 6.2. Normal probability plots are used to test the residuals normality or departure from normality, identify outliers and test the model's linearity. In addition to the normal probability plot, the residual plot for this particular model is presented in Fig. 6.3. Residual

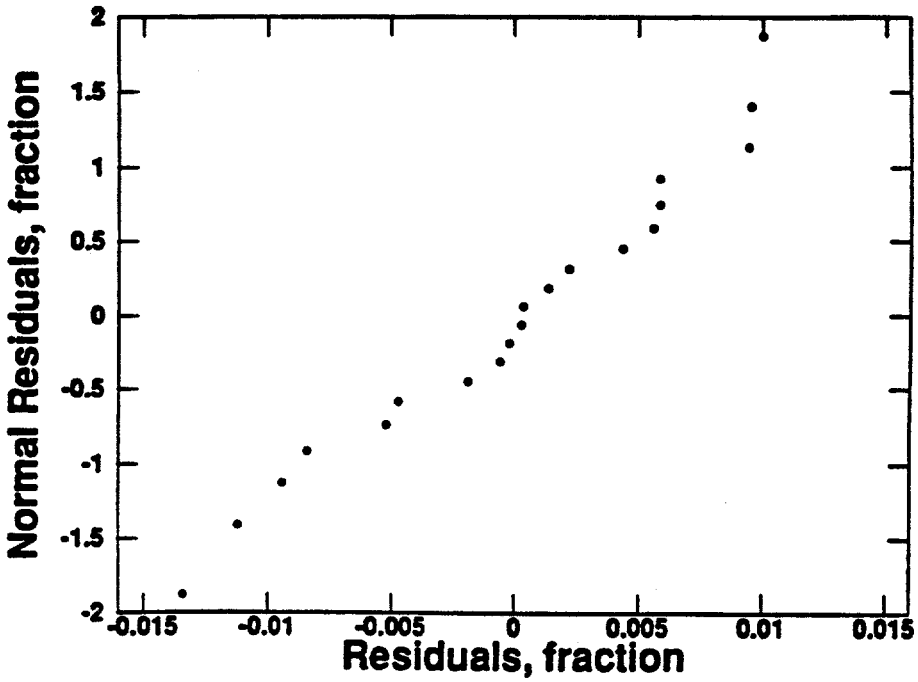

Fig. 6.2: Normal Probability Plot for the Full Model of the Berea Sandstone Radial-Core Case.

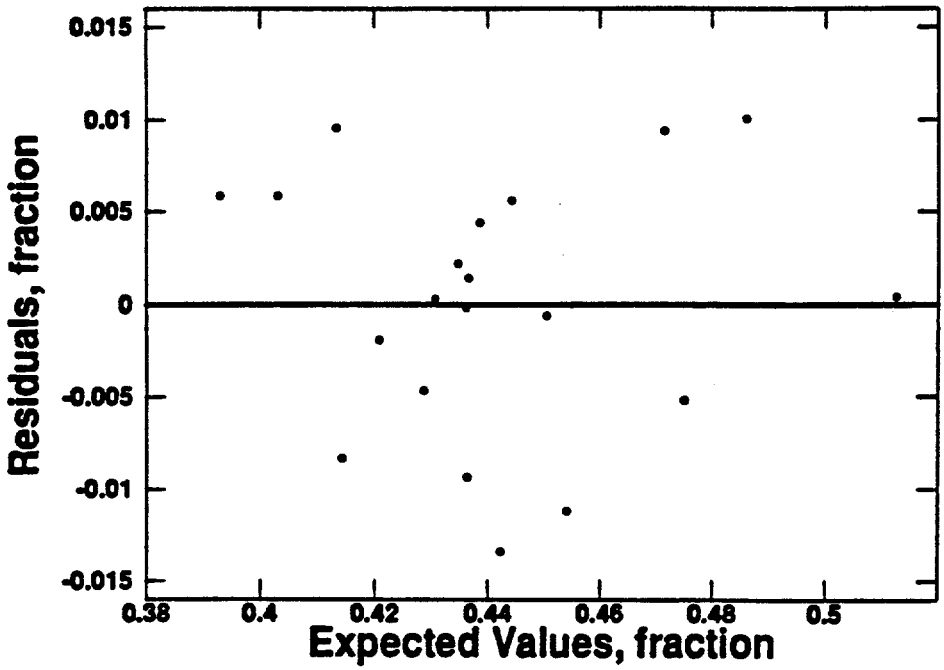

Fig. 6.3: Residual Plot vs. Expected Values for the Full Model of the Berea Sandstone Radial-Core Case.

plots test the possibility of error terms being correlated and also test the regression functions linearity. They are also used to validate the regression model's assumption that the error terms variability is constant. The coefficients of correlation between the ordered residuals and their respective values under normality are denoted by R_N^2. The values of these coefficients for the different tested models are presented in Table 6.2. Table 6.3, which is the table of alpha critical values, supports the conclusion that the error terms are normally distributed in that $R_N^2 = 0.984$ is greater than the coefficient of correlation at a probability level $\alpha = 0.01$, $R_N^2 = 0.929$, for $n = 20$.

Tables 6.2 and 6.3 and Figs. 6.2 and 6.3, representing residual and normal residual plots, indicate that most of the independent variables are linearly associated with the dependent variable. The residual oil saturation, shows the highest degree of correlation and tortuosity shows the lowest. Further, the correlation matrix on Table 6.1 shows the inter-correlations among the potential independent variables. This table indicates that surface area has a high pairwise correlation with pore-entry diameter and wettability index. On the basis of these analyses, the dependent variables in linear terms only. Moreover, analyses indicated that it was unnecessary to include the interaction terms since some of the independent variables such as surface area, has a high pairwise correlation with respect to other independent variables such as pore length and porosity. Table 6.4 shows the pairwise comparison of the different independent variables used in the full sandstone radial-flow model.

The R_p^2 values as a function of p, the number of parameters, are plotted in Fig. 6.4. The maximum R_p^2 value for the possible subsets of p-1 predictor variables, appears at the top of the graph for each p. These points are connected by dashed lines to show the impact of adding additional independent variables. Figure 6.4 indicates that little increase in maximum R_p^2 is realized after 6 variables are included in the model. In particular, the use of

Table 6.2: R_p^2, MSE_p, C_p and R_N^2 Values for the Investigated Regression Sandstone Radial-Core Models

Variables	p	df	SSE_p	R^2_p	MSE_p	C_p	R^2_N
S_{ei}	2	18	0.0112241	31.6	0.0006236	105.604	0.983
S_{er}	2	18	0.0067652	58.8	0.0003758	57.296	0.973
WI	2	18	0.0150823	8.1	0.0008379	147.405	0.978
L	2	18	0.0152882	6.9	0.0008493	149.636	0.924
K	2	18	0.0142500	13.2	0.0007917	138.388	0.930
ϕ	2	18	0.0130872	20.3	0.0007271	125.790	0.941
τ	2	18	0.0157821	3.9	0.0008768	154.987	0.957
d	2	18	0.0141766	13.7	0.0007876	137.593	0.927
SA	2	18	0.0132774	19.1	0.0007376	127.850	0.941
S_{er}, S_{ei}	3	17	0.0035314	78.5	0.0002077	24.260	0.783
τ, S_{er}	3	17	0.0067608	58.8	0.0003977	59.248	0.973
τ, S_{ei}	3	17	0.0109953	33.0	0.0006468	105.126	0.984
τ, S_{er}, S_{ei}	4	16	0.0029848	81.8	0.0001865	20.338	0.783
τ, WI, S_{er}	4	16	0.0064027	61.0	0.0004002	57.368	0.987
τ, WI, S_{ei}	4	16	0.0010540	35.8	0.0006588	102.198	0.990
WI, S_{er}, S_{ei}	4	16	0.0035299	78.5	0.0002206	26.244	0.783
τ, WI, S_{er}, S_{ei}	5	15	0.0026293	84.0	0.0001753	18.486	0.876
SA, d, τ, WI, S_{er}	6	14	0.0027859	83.0	0.0001990	22.183	0.967
SA, d, τ, WI, S_{ei}	6	14	0.0047629	71.0	0.0003402	43.602	0.981
SA, d, τ, S_{er}, S_{ei}	6	14	0.0020582	87.5	0.0001470	14.299	0.957
SA, d, WI, S_{er}, S_{ei}	6	14	0.0020506	84.7	0.0001790	19.148	0.943
SA, τ, WI, S_{er}, S_{ei}	6	14	0.0014184	91.4	0.0001013	7.367	0.988
d, τ, WI, S_{er}, S_{ei}	6	14	0.0014756	91.0	0.0001054	7.987	0.987
SA, d, τ, WI, S_{er}, S_{ei}	7	13	0.0011822	92.8	0.0000909	6.808	0.984
SA, d, τ, L, WI, S_{er}	7	13	0.0019949	87.9	0.0001535	15.613	0.978
SA, d, τ, L, WI, S_{ei}	7	13	0.0035260	78.8	0.0002712	32.201	0.983
SA, d, τ, L, S_{er}, S_{ei}	7	13	0.0018647	88.6	0.0001434	14.203	0.961
SA, d, L, WI, S_{er}, S_{ei}	7	13	0.0019240	88.4	0.0001471	14.719	0.971
SA, τ, L, WI, S_{er}, S_{ei}	7	13	0.0014135	91.4	0.0001087	9.314	0.975
d, τ, L, WI, S_{er}, S_{ei}	7	13	0.0014753	91.0	0.0001135	9.984	0.987
SA, d, τ, L, WI, S_{er}, S_{ei}	8	12	0.0010678	93.5	0.0000890	7.569	0.993
SA, d, τ, ϕ, K, L, WI, S_{er}	9	11	0.0014350	91.3	0.0001305	13.547	0.985
SA, d, τ, ϕ, K, L, WI, S_{ei}	9	11	0.0028059	82.9	0.0002551	28.400	0.970
SA, d, τ, ϕ, K, L, S_{er}, S_{ei}	9	11	0.0012183	92.6	0.0001108	11.199	0.965
SA, d, τ, ϕ, K, WI, S_{er}, S_{ei}	9	11	0.0010853	93.4	0.0000987	9.758	0.995
SA, d, τ, ϕ, L, WI, S_{er}, S_{ei}	9	11	0.0009537	94.2	0.0000867	8.333	0.992
SA, d, ϕ, K, L, WI, S_{er}, S_{ei}	9	11	0.0013351	91.9	0.0001214	12.465	0.984
SA, τ, ϕ, K, L, WI, S_{er}, S_{ei}	9	11	0.0013160	92.0	0.0001196	12.258	0.983
d, τ, ϕ, K, L, WI, S_{er}, S_{ei}	9	11	0.0009233	94.4	0.0000839	8.000	0.983
SA, d, τ, ϕ, K, L, WI, S_{er}, S_{ei}	10	10	0.0009231	94.4	0.0000923	10.000	0.983

Table 6.3: Table of Alpha Critical Values

	α				α		
N	.10	.05	.01	N	.10	.05	.01
4	.8951	.8734	.8318	30	.9707	.9639	.9490
5	.9033	.8804	.8320	40	.9767	.9715	.9597
10	.9347	.9180	.8804	50	.9807	.9764	.9664
15	.9506	.9383	.9110	60	.9835	.9799	.9710
20	.9600	.9503	.9290	75	.9865	.9835	.9757
25	.9662	.9582	.9408				

Table 6.4: Pairwise Comparison of the Different Independent Variables Used in the Sandstone Radial-Core Models

Variables	p	df	SSE_p	R^2_p	MSE_p	C_p
SA, d	2	18	0.0108006	37.1	0.006000	101.016
τ, SA	2	18	0.3759490	0.1	0.020886	-
τ, d	2	18	0.3751920	0.3	0.020844	-
τ, ϕ	2	18	0.0043970	0.0	0.002443	31.638
ϕ, d	2	18	0.0029460	33.0	0.000163	15.918
ϕ, SA	2	18	0.0005090	88.4	0.000028	-10.485
k, τ	2	18	0.6711450	0.3	0.037286	-
k, d	2	18	0.4953250	26.4	0.027518	-
k, SA	2	18	0.1161550	82.7	0.006453	-
L, k	2	18	1.5626	49.5	0.0868	-
L, ϕ	2	18	1.4719	52.5	0.0818	-
L, τ	2	18	3.0259	2.3	0.1681	-
L, d	2	18	1.2544	59.5	0.0897	-
L, SA	2	18	1.3386	56.8	0.0744	-
WI, L	2	18	0.011150	3.9	0.000619	104.802
SA, S_{wi}	2	18	0.025288	1.2	0.501405	257.976
d, S_{wi}	2	18	0.025366	0.9	0.001409	258.821
τ, S_{wi}	2	18	0.025067	2.0	0.001393	255.582
ϕ, S_{wi}	2	18	0.025584	0.0	0.001421	261.183
k, S_{wi}	2	18	0.025542	0.2	0.001419	260.728
L, S_{wi}	2	18	0.025315	1.1	0.001406	258.269
WI, S_{wi}	2	18	0.024986	2.3	0.001388	254.704
S_{wi}, S_w	2	18	0.003146	87.7	0.000125	18.084
d, S_w	2	18	0.021791	0.0	0.001211	220.089
τ, S_w	2	18	0.020115	7.7	0.001117	201.931
ϕ, S_w	2	18	0.021352	2.0	0.001186	215.333
k, S_w	2	18	0.021517	1.3	0.001195	217.120
L, S_w	2	18	0.021328	2.1	0.001185	215.072
SA, S_w	2	18	0.020717	4.9	0.001151	208.453
WI, S_w	2	18	0.020430	6.3	0.001135	205.343
WI, SA	2	18	0.009056	17.5	0.000531	87.646
WI, d	2	18	0.011520	0.7	0.000640	108.817
WI, τ	2	18	0.005835	49.4	0.000324	47.216
WI, ϕ	2	18	0.010560	8.9	0.000587	98.407
WI, k	2	18	0.010212	11.9	0.000567	94.640

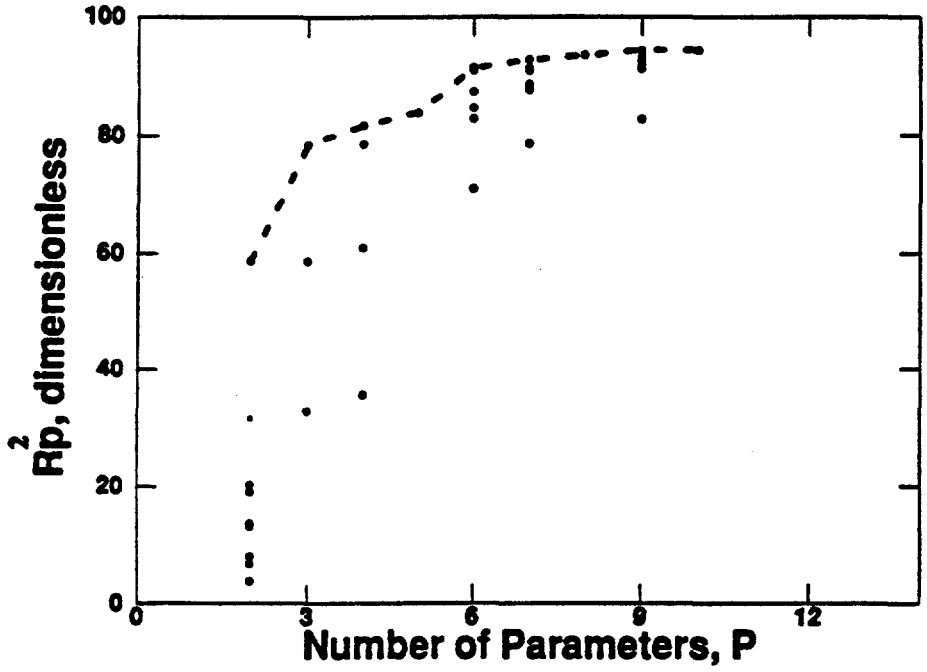

Fig. 6.4: R_p^2 Values vs. Number of Parameters for the Berea Sandstone Radial-Core Case.

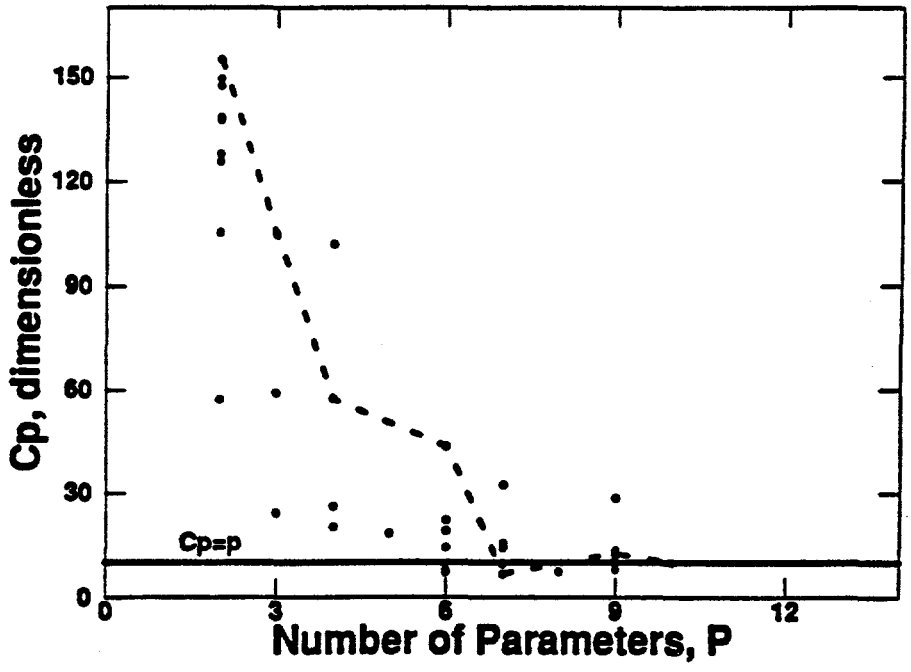

Fig. 6.5: C_p Values vs. Number of Parameters for the Berea Sandstone Radial-Core Case.

the subset containing SA, d, τ, WI, S_{or}, and S_{oi} in the regression model appears to be reasonable according to the R_p^2 criterion. Note that the variables ϕ, and k, which correlate most highly with the independent variables are not in this model. This indicates that SA, d, τ, WI, S_{or} and S_{oi} contained much of the information presented by ϕ and k, since porosity and permeability are highly correlated with these variables.

In Fig. 6.5, the C_p values for the selected models are plotted as a function of p, the number of parameters. As shown in Fig. 6.6, plotting C_p values against R_p^2 values suggested that the subset containing SA, d, τ, WI, S_{or}, and S_{oi} is a better choice than the full model. The model selected has a C_p value of 6.808, which falls below the line, $C_p = p$. Since the value of C_p is then small, the model's total mean square error is also small.

In an effort to reduce the number of independent variables involved in the model, various forms of reduced models were statistically analyzed (Boukadi, 1991). One of the reduced models is:

$$\begin{aligned} UOR &= 0.0052 + 0.252\ SA - 0.167\ d - 0.454\ \tau \\ &\quad + 0.464\ WI - 1.74\ S_{or} + 1.08\ S_{oi} \end{aligned} \tag{6.7}$$

The reduced model with six independent variables presented in Eq. (6.7) has a high coefficient of determination, R^2, value of 92.8%. The F-test statistic value of 27.92 indicates that the mean square for regression is 27.92 times greater than the mean square for error. The residual and normal residual plots for this particular model are presented in Figs. 6.7 and 6.8, respectively. Reference are made to Fig. 6.4, containing the plots of R_p^2 versus the number of parameters, Fig. 6.5, containing the plot of the C_p values versus the number of parameters, and Fig. 6.6, containing the plot of the C^p values versus R_p^2 values, respectively, and to Table 6.2. These lead to the conclusion that this model is the preferred model. This conclusion is predicated on the fact that this model uses essential variables, has a high

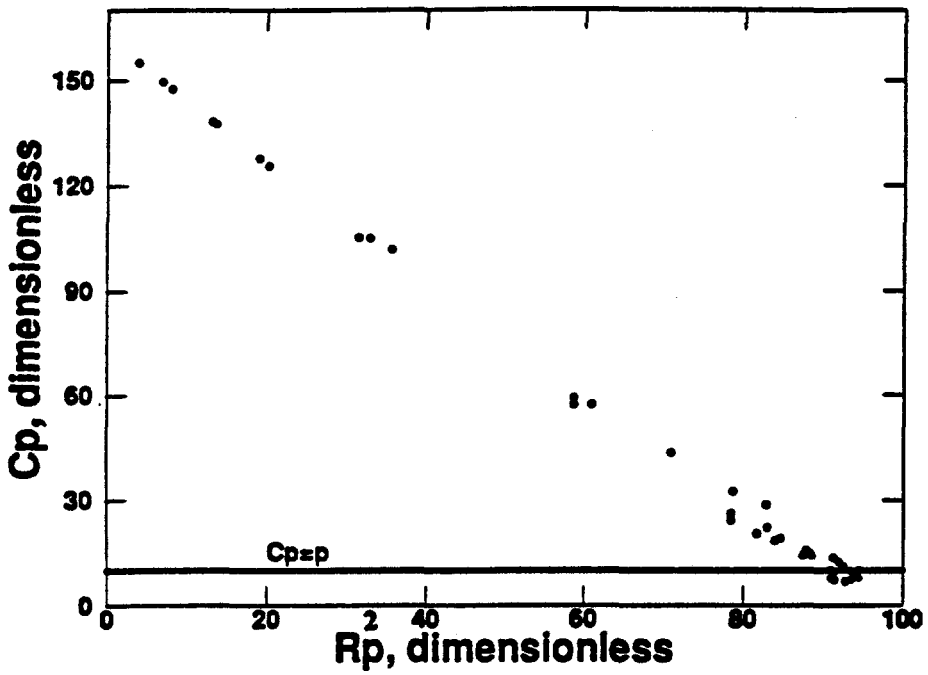

Fig. 6.6: C_p Values vs. R_p^2 Values for the Berea Sandstone Radial-Core Case.

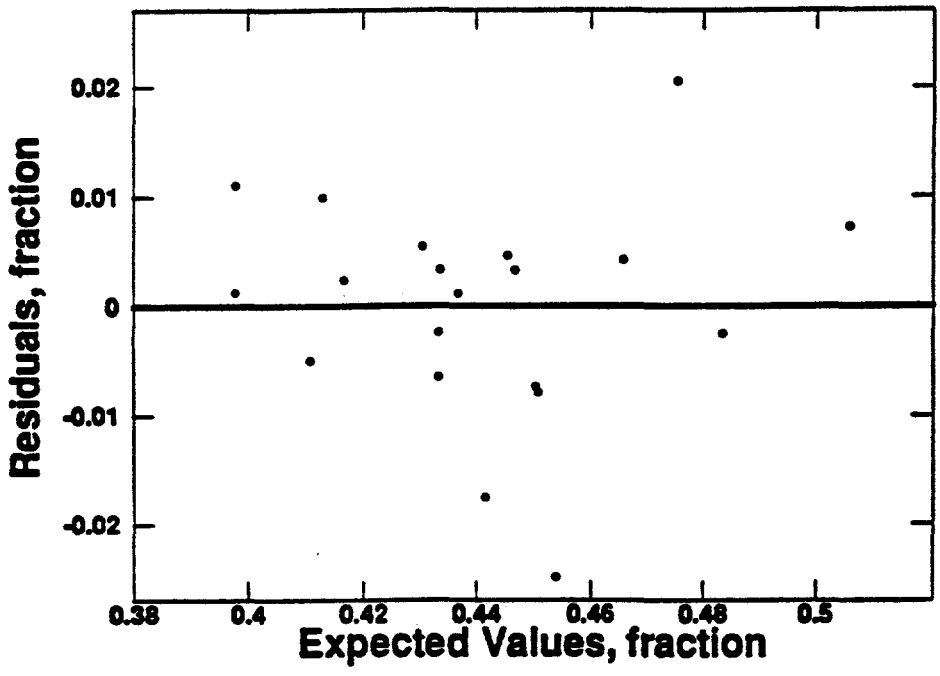

Fig. 6.7: Residual Plot vs. Expected Values for the Selected Normalized Model of the Berea Sandstone Radial-Core Case.

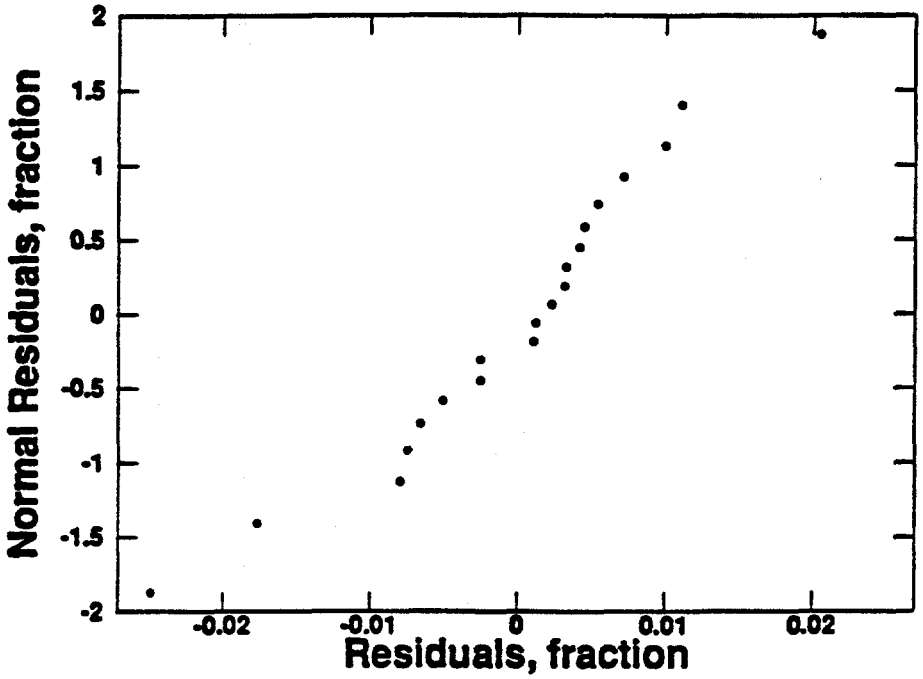

Fig. 6.8: Normal Probability Plot for the Selected Normalized Model of the Berea Sandstone Radial-Core Case.

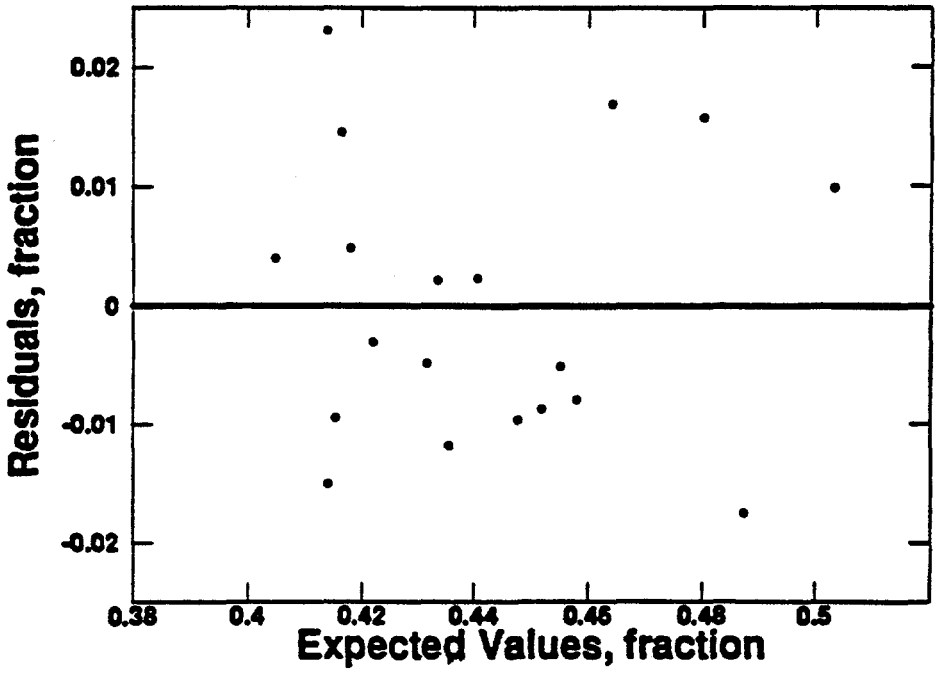

Fig. 6.9: Residual Plot vs. Expected Values for the Reduced Normalized Model of the Berea Sandstone Radial-Core Case.

coefficient of multiple determination, R^2 = 92.8%, uses fewer variables, has a low standard deviation, σ = 0.0754, and its first-order classification stands since the error terms are strongly normal, R_N^2 = 98.4%. As shown in Table 6.2, reducing the selected model resulted in higher values of C_p which leads to the conclusion that the bias in these models is large. Among the reduced models, the one below was selected:

$$\begin{aligned} UOR &= 0.0034 + 0.451\ SA - 0.166\ d - 0.412\ \tau \\ &\quad + 0.631\ WI - 0.636\ S_{or} \end{aligned} \tag{6.8}$$

As shown in Table 6.2, R_p^2, MSE_p, C_p and R_N^2 for the investigated regression models, the reduced model was selected based on the fact that it contains fewer variables, has a higher coefficient of multiple correlation and lower standard deviation as compared to the other reduced models. The residual and normal residual plots for this particular model are presented in Figs. 6.9 and 6.10, respectively. Reduction of the chosen model resulted in a higher standard error, σ = 0.1116, a lower R^2 of 83.0%, and a larger C_p of 22.183. This indicates a higher bias in the model. The residuals were less normal, R_N^2 = 96.7%, which leads to the conclusion that the first-order model classification is less powerful.

6.3 Limestone Radial-Core Case

Summary statistics of variables to be used in the model are shown in Tables 5.7 for Indiana limestone radial-cores. The inter-correlations among the potential independent variables are shown in Table 6.5 for Indiana limestone radial-cores. Residual plots for the full and reduced models are presented in figs. 6.11 and 6.12, respectively. The examination of these plots and the coefficients of correlations, R_N^2, between the ordered residuals and their respective values under normality as shown on Table 6.6, validate the assumption of the regression model that the error terms variability is constant and that the error terms are normally distributed.

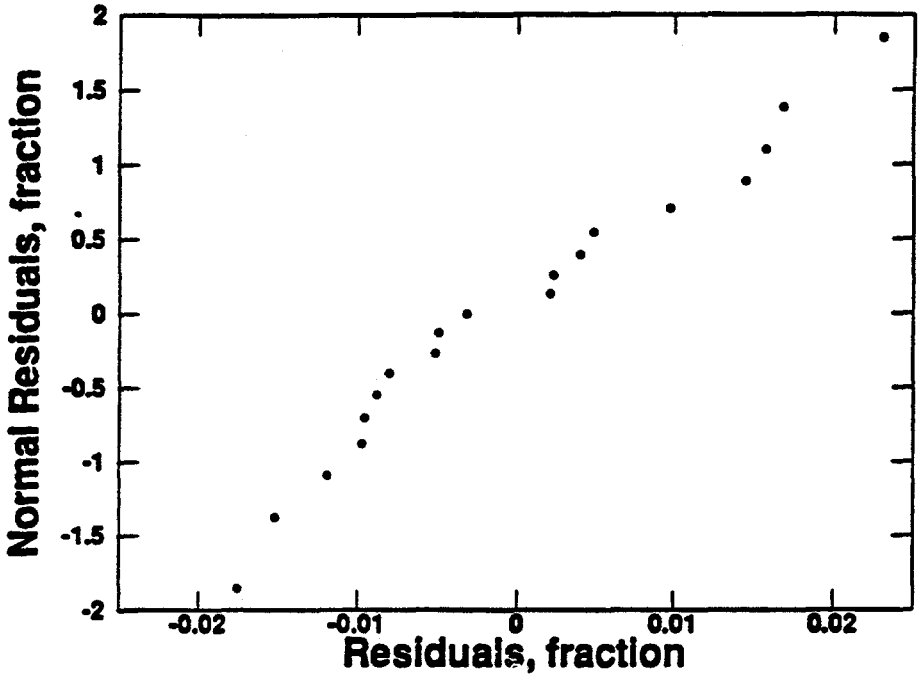

Fig. 6.10: Normal Probability Plot for the Reduced Normalized Model of the Berea Sandstone Radial-Core Case.

Table 6.5: Correlation Matrix for the Full Model for Indiana Limestone Radial-Cores

	ϕ	k	S_{oi}	S_{or}	WI	SA	d	UOR
k	0.899							
S_{oi}	-0.795	-0.776						
S_{or}	-0.415	-0.355	0.740					
WI	0.220	0.188	-0.165	0.035				
SA	0.415	0.337	-0.510	-0.384	0.012			
d	0.219	0.428	-0.329	-0.256	-0.028	-0.175		
UOR	-0.567	-0.625	0.409	-0.309	-0.263	-0.180	-0.156	1.000

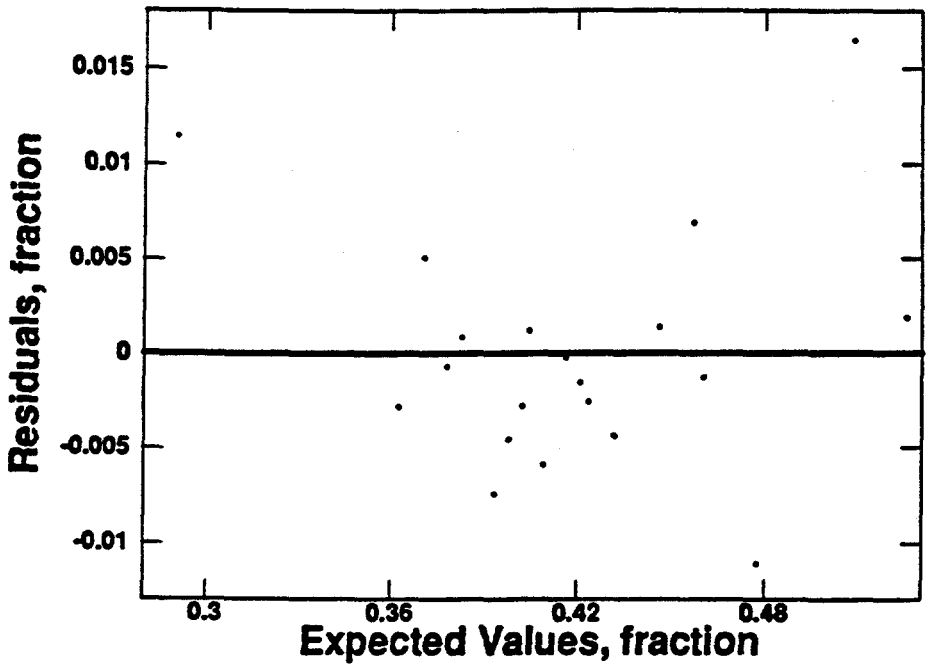

Fig. 6.11: Residual Plot vs. Expected Values for the Full Model of the Indiana Limestone Radial-Core Case.

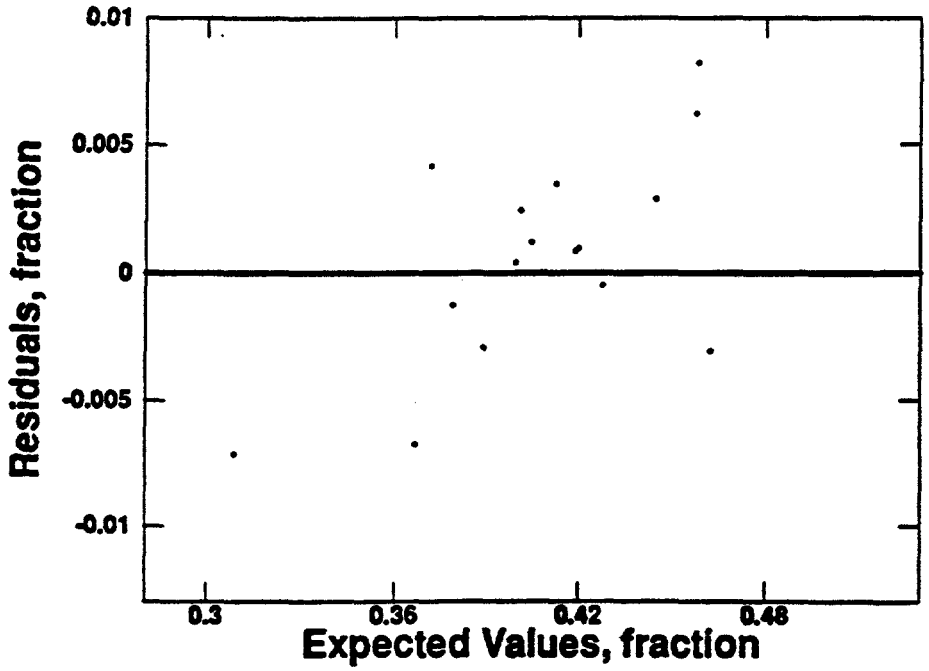

Fig. 6.12: Residual Plot vs. Expected Values for the Reduced Model of the Indiana Limestone Radial-Core Case.

Table 6.6: R_p^2, MSE_p, C_p and R_N^2 Values for the Investigated Regression Limestone Radial-Core Models

Variables	p	df	SSE_p	R^2_p	MSE_p	C_p	R^2_N
S_{oi}	2	18	0.045211	16.7	0.002512	755.519	0.977
S_{or}	2	18	0.049097	9.5	0.002728	821.833	0.988
WI	2	18	0.050520	6.9	0.002807	846.116	0.972
ϕ	2	18	0.036843	32.1	0.002047	612.720	0.966
d	2	18	0.052514	3.2	0.002917	880.144	0.971
SA	2	18	0.052942	2.4	0.002941	887.447	0.975
ϕS_{oi}	2	18	0.041697	23.2	0.002317	697.550	0.973
ϕS_{or}	2	18	0.020218	62.7	0.001123	329.017	0.965
S_{oi}, S_{or}	3	17	0.000387	99.3	0.000023	-7.396	0.983
ϕS_{oi}, ϕS_{or}	3	17	0.000864	98.4	0.000051	0.744	0.945
ϕS_{oi}, ϕS_{or}, SA	4	16	0.000810	98.5	0.000051	1.822	0.960
ϕS_{oi}, ϕS_{or}, d	4	16	0.000839	98.5	0.000052	2.317	0.961
ϕS_{oi}, ϕS_{or}, WI	4	16	0.000851	98.4	0.000053	2.522	0.945
ϕS_{oi}, ϕS_{or}, d, SA	5	15	0.000798	98.5	0.000053	3.618	0.962
ϕS_{oi}, ϕS_{or}, WI, d	5	15	0.000827	98.5	0.000055	4.113	0.960
ϕS_{oi}, ϕS_{or}, WI, SA	5	15	0.000793	98.5	0.000053	3.532	0.959
ϕS_{oi}, ϕS_{or}, WI, d, SA	6	14	0.000782	98.6	0.000056	-0.655	0.965
ϕS_{oi}, ϕS_{or}, k, WI, d, SA	7	13	0.000762	98.6	0.000059	6.998	0.990

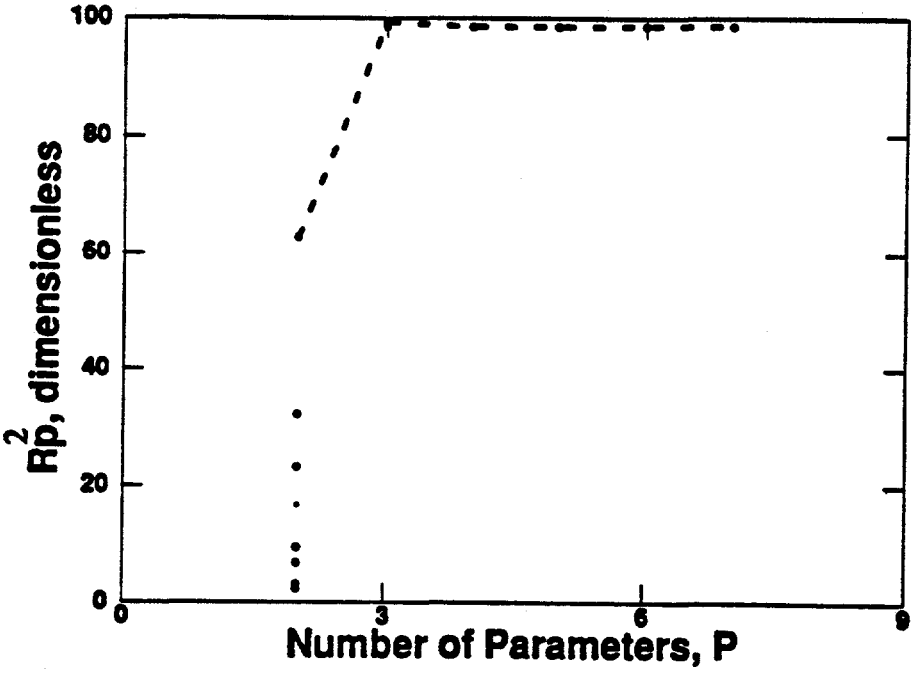

Fig. 6.13: R_p^2 Values vs. Number of Parameters for the Indiana Limestone Radial-Core Case.

Full model representation of the dependent variable, ultimate oil recovery, in terms of the independent variables such as surface area, SA, median pore-throat diameter, d, rock permeability, k, the product of the porosity and initial oil saturation, ϕS_{oi} , wettability index, WI, and the product of porosity and residual oil saturation, ϕS_{or} , indicates that:

$$\begin{aligned} UOR &= 0.350 - 0.000038\,k + 0.0226\,SA \\ &\quad - 0.0010\,d + 0.0467\,WI - 13.0\,\phi\,S_{or} \\ &\quad + 7.770\,\phi\,S_{oi} \end{aligned} \tag{6.9}$$

The model in Eq. (6.9) shows a good fit with R^2 value of 98.6%. This high coefficient of determination again validates the linearity of the model. Moreover, the F-test statistic value of 152.21 indicates that the regression is statically significant.

A reduced model illustration of the dependent variable, UOR, as a function of the initial and residual oil saturations results in:

$$UOR = 0.408 - 2.09\,S_{or} + 1.24\,S_{oi} \tag{6.10}$$

In the case of limestone rocks investigated, the effect of rock properties on oil recovery was ineffective as shown in Eq. (6.10). The reduced model shows a good fit with R^2 value of 99.3%. The F-test statistic value of 1183.37 indicates that the regression of UOR on S_{or} and S_{oi} is highly significant.

Figure 6.13 contains a plot of R_p^2 values as a function of the number of parameters, p. Reference to Table 6.6, and to Fig. 6.13, indicate that there is no increase in the values of R_p^2 after the incorporation of 2 independent variables in the model. Therefore, the use of the subset containing S_{oi} and S_{or} in the regression model is the most suitable approach according to the R_p^2 criterion.

Figure 6.14 contains a plot of C_p values as a function of the number of parameter, p.

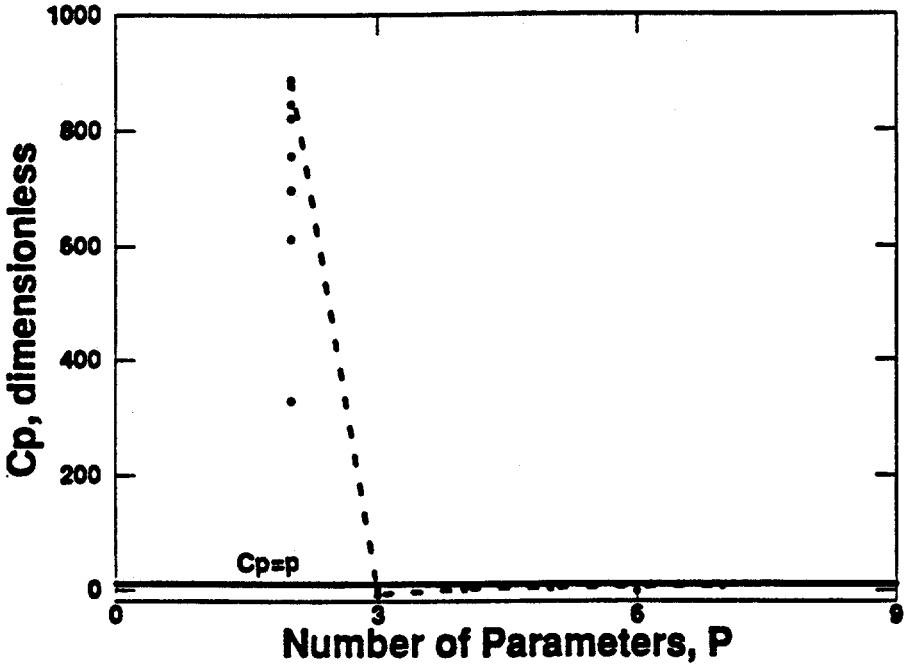

Fig. 6.14: C_p Values vs. Number of Parameters for the Indiana Limestone Radial-Core Case.

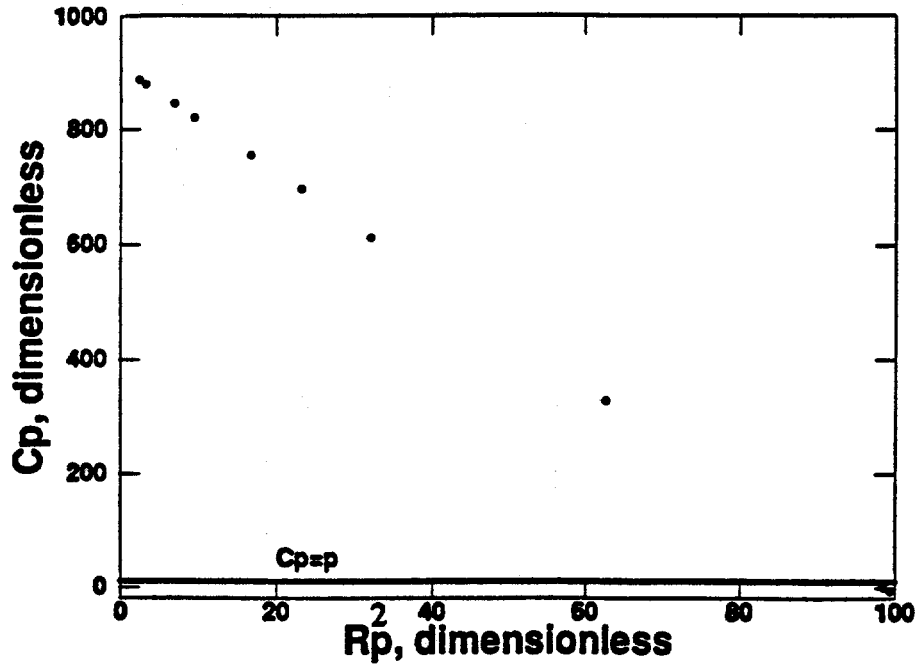

Fig. 6.15: C_p Values vs. R_p^2 Values for the Indiana Limestone Radial-Core Case.

Furthermore, Fig. 6.15 shows a plot of C_p values against R_p^2. As was the case for the Berea sandstone radial-core model, the C_p value of the model which was -7.396, falls below the line, $C_p = p$. This suggests that the selected model is associated with sampling error and shows no bias. Examination of Figs. 6.14 and 6.15 implies that the reduced model with the subset containing S_{oi} and S_{or} is a better model.

6.4 Sandstone Linear-Core Case

During the process of the building of the models, the results obtained using the linear independent variables alone needed to be improved further, in the case of the sandstone samples. For this reason, log k, ϕS_{wi}, ϕS_s and ϕRE terms were introduced into the models as part of the independent variables.

6.4.1 With Common Rock/Fluid Properties

The output for the best subsets algorithms for the development of models for predicting residual oil saturation and oil recovery at both breakthrough and floodout for sandstones, using the common rock/fluid properties alone, are shown in Tables 6.7 through 6.10. In these and the other tables presented in this chapter, the asterisk on one of the number of independent variables, shows the best subsets chosen, after taking the selection criteria into consideration. The units for all the variables in the various models are defined in the nomenclature. The developed models for sandstones using the common rock/fluid properties alone, are presented in Eqs. 6.11 through 6.14.

6.4.1.1 Residual Oil Saturation at Breakthrough

From Table 6.7, the final model developed for predicting residual oil saturation at breakthrough for sandstones, using rock/fluid properties alone, is given as:

Table 6.7: Best Subsets Regression for Residual Oil Saturation at Breakthrough for Sandstone Linear-Cores (Using Common Rock Properties)

Vars.	R-sq	Adj. R-sq	C_p	σ	ϕ	k	S_{wi}	ϕS_{wi}	logk
1	42.8	39.8	5.2	0.0623				x	
1	24.6	20.6	12.2	0.0715			x		
2	51.1	45.7	4.0	0.0592			x	x	
2	49.7	44.1	4.5	0.0600	x			x	
3	52.3	43.8	5.5	0.0602	x		x	x	
3	51.5	42.9	5.8	0.0607		x		x	x
4*	60.6	50.7	4.3	0.0564		x	x	x	x
4	56.5	45.6	5.9	0.0592	x	x		x	x
5	61.3	48.4	6.0	0.0577	x	x	x	x	x

Table 6.8: Best Subsets Regression for Residual Oil Saturation at Floodout for Sandstone Linear-Cores (Using Common Rock Properties)

Vars.	R-sq	Adj. R-sq	C_p	σ	ϕ	k	S_{wi}	ϕS_{wi}	logk
1	66.3	64.5	0.1	0.0401				x	
1	57.1	54.8	4.8	0.0453			x		
2*	69.7	66.3	0.4	0.0391		x	x		
2	68.9	65.5	0.7	0.0396			x		x
3	69.9	64.6	2.2	0.0401		x	x		x
3	69.7	64.3	2.4	0.0402		x	x	x	
4	70.2	62.7	4.1	0.0411	x	x	x		x
4	70.0	62.5	4.2	0.0412	x	x	x	x	
5	70.4	60.5	6.0	0.0423	x	x	x	x	x

Table 6.9: Best Subsets Regression for Oil Recovery at Breakthrough for Sandstone Linear-Cores (Using Common Rock Properties)

Vars.	R-sq	Adj. R-sq	C_p	σ	ϕ	k	S_{wi}	ϕS_{wi}	logk
1	29.9	26.2	11.4	16.077			x		
1	19.0	14.7	15.8	17.279	x				
2	50.4	44.9	5.1	13.890			x	x	
2	47.5	41.7	6.3	14.291	x		x		
3	52.7	44.4	6.1	13.956	x		x	x	
3	52.4	44.0	6.3	14.010			x	x	x
4*	61.8	52.3	4.5	12.924		x	x	x	x
4	54.8	43.5	7.3	14.063	x	x	x		x
5	63.0	50.6	6.0	13.151	x	x	x	x	x

Table 6.10: Best Subsets Regression for Ultimate Oil Recovery at Floodout for Sandstone Linear-Cores (Using Common Rock Properties)

Vars.	R-sq	Adj. R-sq	C_p	σ	ϕ	k	S_{wi}	ϕS_{wi}	logk
1	22.2	18.1	-0.2	9.342					x
1	21.2	17.1	0.0	9.399		x			
2*	29.3	21.4	0.3	9.149		x	x		
2	28.4	20.5	0.5	9.204			x		x
3	29.6	17.2	2.2	9.393		x	x	x	
3	29.4	17.0	2.3	9.406		x	x		x
4	30.4	13.0	4.0	9.625		x	x	x	x
4	29.9	12.4	4.1	9.660	x	x	x		x
5	30.6	7.4	6.0	9.930	x	x	x	x	x

$$S_{or_{@BT}} = -1.525 - 2.354 * 10^{-3} k + 0.770 S_{wi} - 4.316 \phi S_{wi} + 1.018 \log k \quad (6.11)$$

The R^2 for Eq. 6.11 is 60.6%, its adj.-R^2 is 50.7%, its C_p criterion value is 4.3 and its standard deviation is 0.056. Since the best subset chosen for this equation contains four independent variables, the number of parameters, p, which is the number of independent variables plus the constant term included in Eq. 6.11, is therefore equal to 5. This implies that the developed model is unbiased, since it has a C_p criterion value less than p.

6.4.1.2 Residual Oil Saturation at Floodout

The output for the best subsets algorithms for the development of model for predicting residual oil saturation at floodout for sandstones, using the common rock/fluid properties alone, is shown in Table 6.8. The final model developed is given as:

$$S_{or_{@FO}} = 0.345 - 2.789 * 10^{-4} k - 0.227 S_{wi} \quad (6.12)$$

The R^2 for Eq. 6.12 is 69.7%, its adj.-R^2 is 66.3%, its C_p criterion value is 0.4 and its standard deviation is 0.039. The developed model contains two independent variables, which implies that the model is unbiased.

6.4.1.3 Oil Recovery at Breakthrough

Table 6.9 shows the output for the best subsets algorithms for the development of model for predicting oil recovery at breakthrough for sandstones, using the common rock/fluid properties alone. The final model developed is given as:

$$OR_{@BT} = 550.6 + 0.557 k - 298.1 S_{wi} + 1147.4 \phi S_{wi} - 258.0 \log k \quad (6.13)$$

The R^2 for Eq. 6.13 is 61.8%, its adj.-R^2 is 52.3%, its C_p criterion value is 4.5 and its

standard deviation is 12.9. The developed model contains four independent variables, which implies that the model is unbiased.

6.4.1.4 Ultimate Oil Recovery at Floodout

Table 6.10 shows the output for the best subsets algorithms for the development of model for predicting ultimate oil recovery at floodout for sandstones, using the common rock/fluid properties alone. The final model developed is given as:

$$UOR = 59.3 - 0.0573\ k - 13.4\ S_{wi} \tag{6.14}$$

The R^2 for Eq. 6.14 is 29.3%, its adj.-R^2 is 21.4%, its C_p criterion value is 0.3 and its standard deviation is 9.15. The developed model contains two independent variables, which implies that the model is unbiased.

6.4.2 With Uncommon Rock/Fluid Properties

The output for the best subsets algorithms for the development of models for predicting residual oil saturation and oil recovery at both breakthrough and floodout for sandstones, using the uncommon rock/fluid properties alone, are shown in Tables 6.11 through 6.14. The developed models are presented in Eqs. 6.15 through 6.18.

6.4.2.1 Residual Oil Saturation at Breakthrough

From Table 6.11, the final model developed for predicting residual oil saturation at breakthrough for sandstones, using uncommon rock/fluid properties alone, is given as:

$$\begin{aligned} S_{or_{BT}} &= 2.397 - 58.25\ V_{int.} + 4.720\ SA - 0.936\ \rho_s \\ &\quad + 29.43\ \overline{D} - 2.367 * 10^{-4}\ \phi_{Hg}\ S_s + 4.593\ \phi_{Hg}\ RE \end{aligned} \tag{6.15}$$

The R^2 for Eq. 6.15 is 67.1%, its adj.-R^2 is 53.0%, its C_p criterion value is 5.0 and its

Table 6.11: Best Subsets Regression for Residual Oil Saturation at Breakthrough for Sandstone Linear-Cores (Using Uncommon Rock Properties)

Vars.	R-sq	Adj. R-sq	C_p	σ	WI	$V_{int.}$	SA	S_s	$\bar{D}$	ρ_s	ϕ_{Hg}	RE	$\phi_{Hg}S_s$	ϕ_{Hg}RE
1	19.7	15.4	12.2	0.0739	x									
1	17.7	13.4	12.9	0.0747		x								
2	41.8	35.3	6.2	0.0646			x						x	
2	38.1	31.3	7.5	0.0666	x		x							
3	55.7	47.9	3.1	0.0580		x				x	x			
3	53.3	45.1	4.0	0.0595		x		x			x			
4	60.4	50.4	3.4	0.0565		x		x		x	x			
4	60.3	50.4	3.4	0.0565		x				x	x		x	
5	63.1	50.7	4.4	0.0564		x				x	x		x	x
5	63.0	50.6	4.5	0.0564		x		x		x	x			x
6*	67.1	53.0	5.0	0.0550		x	x			x	x		x	x
6	67.0	52.8	5.0	0.0552		x	x			x	x	x	x	
7	69.4	52.9	6.1	0.0551		x	x	x		x	x		x	x
7	69.4	52.9	6.2	0.0551	x	x	x			x	x		x	x
8	70.9	51.5	7.6	0.0559	x	x	x	x		x	x		x	x
8	70.7	51.2	7.6	0.0561		x	x	x		x	x	x	x	x
9	71.9	49.0	9.2	0.0574		x	x	x	x	x	x	x	x	x
9	71.7	48.6	9.3	0.0576	x	x	x	x		x	x	x	x	x
10	72.5	45.0	11.0	0.0595	x	x	x	x	x	x	x	x	x	x

Table 6.12: Best Subsets Regression for Residual Oil Saturation at Floodout for Sandstone Linear-Cores (Using Uncommon Rock Properties)

Vars.	R-sq	Adj. R-sq	C_p	σ	WI	$V_{int.}$	SA	S_s	$\bar{D}$	ρ_s	ϕ_{Hg}	RE	$\phi_{Hg}S_s$	ϕ_{Hg}RE
1	19.4	15.2	38.0	0.0620						x				
1	12.2	7.6	42.9	0.0648	x									
2	32.2	24.6	31.3	0.0585						x				x
2	30.3	22.6	32.6	0.0593	x								x	
3	38.9	28.1	28.8	0.0572				x	x			x		
3	38.6	27.8	28.9	0.0573		x				x	x			
4	47.8	34.7	24.7	0.0544		x			x				x	x
4	47.3	34.1	25.0	0.0547		x	x		x					x
5	53.2	37.6	23.0	0.0532		x			x			x	x	x
5	53.0	37.4	23.1	0.0533		x	x		x			x		x
6	67.1	53.0	15.5	0.0462		x	x			x	x	x	x	
6	66.6	52.3	15.8	0.0465		x	x			x	x		x	x
7	74.2	60.3	12.6	0.0425		x	x	x		x	x		x	x
7	72.8	58.2	13.6	0.0436		x	x		x	x	x	x	x	
8	82.8	71.4	8.7	0.0361		x	x	x	x	x	x		x	x
8	78.6	64.3	11.6	0.0402		x	x	x	x	x	x	x	x	
9*	85.1	72.8	9.2	0.0351		x	x	x	x	x	x	x	x	x
9	83.7	70.3	10.2	0.0367	x	x	x	x	x	x	x		x	x
10	85.4	70.7	11.0	0.0365	x	x	x	x	x	x	x	x	x	x

Table 6.13: Best Subsets Regression for Oil Recovery at Breakthrough for Sandstone Linear-Cores (Using Uncommon Rock Properties)

Vars.	R-sq	Adj. R-sq	C_p	σ	WI	V_{kx}	SA	S_s	$\bar{D}$	ρ_s	ϕ_{Hg}	RE	$\phi_{Hg}S_s$	ϕ_{Hg}RE
1	40.6	37.5	6.7	14.80		x								
1	34.2	30.7	9.2	15.58							x			
2	60.1	55.6	0.9	12.46		x					x			
2	56.9	52.1	2.2	12.95			x						x	
3	63.0	56.5	1.7	12.35	x	x					x			
3	61.9	55.2	2.2	12.53		x	x						x	
4	65.7	57.1	2.7	12.26	x	x	x						x	
4	65.4	56.8	2.8	12.30	x		x				x		x	
5	69.1	58.8	3.3	12.01		x	x		x			x	x	
5	69.0	58.7	3.3	12.02			x		x		x	x	x	
6*	73.4	62.1	3.6	11.53			x	x	x		x		x	x
6	73.1	61.6	3.7	11.60		x	x	x	x				x	x
7	74.5	60.7	5.2	11.73	x		x	x	x		x		x	x
7	74.2	60.3	5.3	11.80	x	x	x	x	x				x	x
8	74.7	57.9	7.1	12.14	x		x	x	x	x	x		x	x
8	74.5	57.4	7.2	12.21	x	x	x	x	x		x		x	x
9	74.9	54.4	9.0	12.64	x	x	x	x	x	x	x		x	x
9	74.7	54.1	9.1	12.68	x		x	x	x	x	x	x	x	x
10	74.9	49.8	11.0	13.26	x	x	x	x	x	x	x	x	x	x

Table 6.14: Best Subsets Regression for Ultimate Oil Recovery at Floodout for Sandstone Linear-Cores (Using Uncommon Rock Properties)

Vars.	R-sq	Adj. R-sq	C_p	σ	WI	V_{kx}	SA	S_s	$\bar{D}$	ρ_s	ϕ_{Hg}	RE	$\phi_{Hg}S_s$	ϕ_{Hg}RE
1	57.5	55.3	-3.4	6.90		x								
1	54.2	51.8	-2.4	7.17							x			
2*	62.2	58.0	-2.9	6.69		x			x					
2	61.1	56.8	-2.6	6.79		x								x
3	63.6	57.2	-1.4	6.75		x						x		x
3	63.3	56.8	-1.3	6.78		x		x						x
4	65.7	57.1	-0.0	6.76		x	x					x		x
4	65.6	57.0	-0.0	6.76		x						x	x	x
5	67.5	56.6	1.4	6.80		x	x				x		x	x
5	67.2	56.2	1.5	6.83		x		x		x		x		x
6	68.1	54.4	3.2	6.97		x	x				x	x	x	x
6	67.7	53.8	3.3	7.01	x	x	x				x		x	x
7	68.5	51.5	5.1	7.19	x	x	x				x	x	x	x
7	68.2	51.2	5.1	7.21		x	x			x	x	x	x	x
8	68.6	47.7	7.0	7.46	x	x	x	x			x	x	x	x
8	68.5	47.6	7.0	7.47	x	x	x			x	x	x	x	x
9	68.6	43.0	9.0	7.79	x	x	x	x		x	x	x	x	x
9	68.6	43.0	9.0	7.79	x	x	x	x	x		x	x	x	x
10	68.7	37.3	11.0	8.17	x	x	x	x	x	x	x	x	x	x

standard deviation is 0.055. The developed model contains six independent variables, which implies that the model is unbiased. Statistically, this model is essentially the same as its counterpart that was previously developed using common rock/fluid properties alone, considering their standard deviation values.

6.4.2.2 Residual Oil Saturation at Floodout

From Table 6.12, the final model developed for predicting residual oil saturation at floodout for sandstones, using uncommon rock/fluid properties alone, is given as:

$$\begin{aligned} S_{or_{@FO}} &= 2.128 - 67.26\, V_{int.} + 11.48\, SA + 2.607 * 10^{-5}\, S_s \\ &\quad + 1.813 * 10^{-2}\, \overline{D} - 1.117\, \rho_s + 35.79\, \phi_{Hg} - 3.898\, RE \\ &\quad - 7.338 * 10^{-4}\, \phi_{Hg}\, S_s + 43.19\, \phi_{Hg}\, RE \end{aligned} \tag{6.16}$$

The R^2 for Eq. 6.16 is 85.1%, its adj.-R^2 is 72.8%, its C_p criterion value is 9.2 and its standard deviation is 0.035. The developed model contains nine independent variables, which implies that the model is unbiased. Statistically, this model is as good as its counterpart that was previously developed using common rock/fluid properties alone, considering their standard deviation values.

6.4.2.3 Oil Recovery at Breakthrough

Table 6.13 shows the output for the best subsets algorithms for the development of the model for predicting oil recovery at breakthrough for sandstones, using the uncommon rock/fluid properties alone. The final model developed is given as:

$$\begin{aligned} OR_{@BT} &= -138.5 + 1.515 * 10^{3}\, SA + 3.577 * 10^{-3}\, S_s + 4.344\, \overline{D} \\ &\quad + 740.8\, \phi_{Hg} - 9.794 * 10^{-2}\, \phi_{Hg}\, S_s + 2.926 * 10^{3}\, \phi_{Hg}\, RE \end{aligned} \tag{6.17}$$

The R^2 for Eq. 6.17 is 73.4%, its adj.-R^2 is 62.1%, its C_p criterion value is 3.6 and its standard deviation is 11.5. The developed model contains six independent variables, which

implies that the model is unbiased. Statistically, this model is slightly better than its counterpart that was previously developed using common rock/fluid properties alone, considering their standard deviation values.

6.4.2.4 Ultimate Oil Recovery At Floodout

From Table 6.14, the final model developed for predicting ultimate oil recovery at floodout for sandstones, using uncommon rock/fluid properties alone, is given as:

$$UOR = 10.62 + 597.9\ V_{int.} + 0.743\ \overline{D} \qquad (6.18)$$

The R^2 for Eq. 6.18 is 62.2%, its adj.-R^2 is 58.0%, its C_p criterion value is -2.9 and its standard deviation is 6.69. The developed model contains two independent variables, which implies that the model is unbiased. Statistically, this model is better than its counterpart that was previously developed using common rock/fluid properties alone.

6.4.3 With Both Common and Uncommon Rock/Fluid Properties

The output for the best subsets algorithms for the development of models for predicting residual oil saturation and oil recovery at both breakthrough and floodout for sandstones, using both the common and uncommon rock/fluid properties, are shown in Tables 6.15 through 6.18. The developed models are presented in Eqs. 6.19 through 6.22. Further, to avoid having both brine and mercury porosimetry measured porosities as variables in the same model, mercury porosity terms were substituted with brine porosity terms.

6.4.3.1 Residual Oil Saturation at Breakthrough

From Table 6.15, the final model developed for predicting residual oil saturation at breakthrough for sandstones, using the combined rock/fluid properties is given as:

Table 6.15: Best Subsets Regression for Residual Oil Saturation at Breakthrough for Sandstone Linear-Cores (Using Both Common and Uncommon Rock Properties)

Vars.	R-sq	Adj. R-sq	C_p	σ	ϕ	k	WI	S_{wi}	$V_{kn.}$	SA	S_o	$\bar{D}$	ρ_o	RE	ϕ S_{wi}	log k	ϕ S_o	ϕ RE
1	42.8	39.8	7.1	0.0623											x			
1	24.6	20.6	14.7	0.0716				x										
2	59.1	54.5	2.2	0.0542					x						x			
2	57.7	53.0	2.8	0.0551				x	x									
3	65.1	59.0	1.7	0.0515				x	x			x						
3	64.5	58.2	2.0	0.0519				x		x	x							
4	67.6	59.6	2.6	0.0511				x	x				x				x	
4	67.3	59.1	2.8	0.0513				x	x	x			x					
5	74.3	65.8	1.8	0.0470		x			x			x			x	x		
5	72.0	62.7	2.8	0.0490					x				x		x	x	x	
6	78.5	69.4	2.0	0.0445		x			x			x			x	x		x
6	78.4	69.1	2.1	0.0447		x			x			x		x	x	x		
7*	80.5	69.9	3.2	0.0440		x		x	x	x			x			x	x	
7	80.4	69.9	3.2	0.0440		x			x	x			x		x	x	x	
8	81.8	69.7	4.7	0.0442	x	x			x	x			x		x	x	x	
8	81.2	68.6	4.9	0.0450	x	x		x	x	x			x			x	x	
9	83.5	69.9	6.0	0.0440	x	x			x	x			x	x	x	x	x	
9	83.1	69.2	6.1	0.0446	x	x			x	x		x	x		x	x	x	
10	84.5	69.1	7.5	0.0446	x	x	x		x	x			x	x	x	x	x	
10	84.4	68.9	7.6	0.0448	x	x	x		x	x		x	x		x	x	x	
11	85.3	67.3	9.2	0.0459	x	x	x	x	x	x			x	x	x	x	x	
11	85.1	67.0	9.3	0.0462	x	x	x	x	x	x		x	x		x	x	x	
12	85.7	64.2	11.0	0.0480	x	x	x	x	x	x			x	x	x	x	x	x
12	85.3	63.3	11.2	0.0486	x	x	x	x	x	x		x	x	x	x	x	x	
13	85.7	59.3	13.0	0.0513	x	x	x	x	x	x	x		x	x	x	x	x	x
13	85.7	59.1	13.0	0.0513	x	x	x	x	x	x		x	x	x	x	x	x	x
14	85.7	52.5	15.0	0.0554	x	x	x	x	x	x	x	x	x	x	x	x	x	x

Table 6.16: Best Subsets Regression for Residual Oil Saturation at Floodout for Sandstone Linear-Cores (Using Both Common and Uncommon Rock Properties)

Vars.	R-sq	Adj. R-sq	C_p	σ	ϕ	k	WI	S_{wi}	$V_{int.}$	SA	S_o	$\bar{D}$	ρ_o	RE	ϕ S_{wi}	log k	ϕ S_o	ϕ RE
1	66.3	64.5	-0.4	0.0401											x			
1	57.1	54.8	4.2	0.0454				x										
2	78.0	75.5	-4.1	0.0333				x	x									
2	71.0	67.7	-0.7	0.0383					x						x			
3	80.0	76.4	-3.1	0.0327				x	x			x						
3	79.6	76.0	-3.0	0.0330				x	x									x
4	82.6	78.3	-2.4	0.0314				x	x		x							x
4	82.4	78.0	-2.3	0.0316				x	x								x	x
5	84.4	79.2	-1.3	0.0307				x	x	x					x		x	
5	83.1	77.4	-0.6	0.0320		x		x	x			x			x			
6*	85.5	79.3	0.1	0.0307		x		x	x	x					x		x	
6	85.1	78.7	0.4	0.0311				x	x	x					x	x	x	
7	85.9	78.4	1.9	0.0313		x		x	x	x					x	x	x	
7	85.7	78.0	2.0	0.0316		x		x	x	x			x		x		x	
8	86.4	77.4	3.7	0.0321				x	x	x		x	x		x		x	x
8	86.3	77.2	3.7	0.0322		x	x	x	x	x					x	x	x	
9	86.9	76.2	5.4	0.0329			x	x	x	x		x	x		x		x	x
9	86.8	76.1	5.5	0.0330		x		x	x	x			x	x	x		x	x
10	87.2	74.5	7.3	0.0340	x		x	x	x	x		x	x		x		x	x
10	87.1	74.2	7.4	0.0342		x		x	x	x			x	x	x	x	x	x
11	87.5	72.2	9.2	0.0356		x	x	x	x	x			x	x	x	x	x	x
11	87.5	72.1	9.2	0.0356	x	x	x	x	x	x		x	x		x		x	x
12	87.6	69.1	11.1	0.0375	x	x	x	x	x	x		x	x	x	x		x	x
12	87.6	69.0	11.1	0.0375	x	x	x	x	x	x			x	x	x	x	x	x
13	87.8	65.2	13.0	0.0397	x	x	x	x	x	x		x	x	x	x	x	x	x
13	87.7	64.8	13.1	0.0400	x	x	x	x	x	x	x	x	x		x	x	x	x
14	87.8	59.4	15.0	0.0429	x	x	x	x	x	x	x	x	x	x	x	x	x	x

Table 6.17: Best Subsets Regression for Oil Recovery at Breakthrough for Sandstone Linear-Cores (Using Both Common and Uncommon Rock Properties)

Vars.	R-sq	Adj. R-sq	C_p	σ	ϕ	k	WI	S_{wi}	$V_{int.}$	SA	S_o	$\bar{D}$	ρ_o	RE	ϕ S_{wi}	log k	ϕ S_o	ϕ RE
1	40.6	37.5	5.3	14.80					x									
1	29.9	26.2	9.3	16.08				x										
2	55.8	50.9	1.6	13.11				x	x									
2	53.0	47.7	2.7	13.53					x						x			
3	63.2	56.7	0.8	12.31				x	x			x						
3	61.7	54.9	1.4	12.56					x			x			x			
4	65.2	56.5	2.1	12.35			x	x	x			x						
4	64.6	55.7	2.3	12.45				x		x	x	x						
5	69.6	59.5	2.4	11.91		x		x							x	x		x
5	69.5	59.4	2.5	11.93		x		x	x			x				x		
6*	77.2	67.4	1.6	10.69		x		x	x			x			x	x		
6	75.2	64.6	2.3	11.14		x		x	x		x					x	x	
7	78.2	66.5	3.2	10.83	x	x		x	x			x			x	x		
7	78.0	66.1	3.3	10.89		x		x	x			x		x	x	x		
8	78.9	64.8	4.9	11.10	x	x		x	x			x		x	x	x		
8	78.9	64.8	4.9	11.11		x		x	x			x		x	x	x		x
9	81.8	66.9	5.9	10.77	x	x		x	x	x			x		x	x	x	
9	80.6	64.7	6.3	11.12		x		x	x			x	x	x	x	x		x
10	82.2	64.5	7.7	11.15	x	x		x	x	x			x	x	x	x	x	
10	82.2	64.4	7.7	11.16	x	x		x	x	x		x	x		x	x	x	
11	83.7	63.8	9.1	11.26	x	x		x	x	x			x	x	x	x	x	x
11	82.6	61.4	9.5	11.63	x	x	x	x	x	x		x	x		x	x	x	
12	83.9	59.8	11.0	11.86	x	x	x	x	x	x			x	x	x	x	x	x
12	83.7	59.3	11.1	11.94	x	x		x	x	x	x		x	x	x	x	x	x
13	84.0	54.4	13.0	12.64	x	x	x	x	x	x	x		x	x	x	x	x	x
13	83.9	54.1	13.0	12.68	x	x	x	x	x	x		x	x	x	x	x	x	x
14	84.0	46.8	15.0	13.65	x	x	x	x	x	x	x	x	x	x	x	x	x	x

Table 6.18: Best Subsets Regression for Ultimate Oil Recovery at Floodout for Sandstone Linear-Cores (Using Both Common and Uncommon Rock Properties)

Vars.	R-sq	Adj. R-sq	C_p	σ	ϕ	k	WI	S_{wi}	V_{lm}	SA	S_g	$\bar{D}$	ρ_g	RE	ϕ S_{wi}	log k	ϕ S_g	ϕ RE
1	57.5	55.3	-4.1	6.90					x									
1	22.2	18.1	6.6	9.34												x		
2	62.8	58.7	-3.7	6.64					x									x
2	62.2	58.0	-3.5	6.69					x			x						
3	66.6	60.7	-2.9	6.47	x				x			x						
3	65.8	59.7	-2.6	6.55					x		x							x
4	68.6	60.7	-1.5	6.49					x			x		x				x
4	68.1	60.1	-1.3	6.52	x				x	x							x	
5	71.7	62.3	-0.4	6.34	x				x	x			x				x	
5	71.0	61.4	-0.2	6.42					x				x	x			x	x
6	73.4	62.0	1.1	6.36	x				x	x	x		x				x	
6	73.1	61.5	1.2	6.40	x				x	x		x	x				x	
7	75.3	62.0	2.5	6.36	x				x	x	x	x	x				x	
7	74.8	61.3	2.6	6.42		x			x		x	x		x		x		x
8*	78.9	64.8	3.4	6.12	x	x			x	x			x	x			x	x
8	77.4	62.4	3.8	6.33	x				x	x			x	x		x	x	x
9	79.2	62.2	5.3	6.34	x	x			x	x	x		x	x			x	x
9	79.2	62.2	5.3	6.35	x	x	x		x	x			x	x			x	x
10	79.7	59.5	7.1	6.57	x	x	x		x	x			x	x		x	x	x
10	79.7	59.3	7.2	6.58	x	x		x	x	x			x	x	x		x	x
11	79.9	55.3	9.1	6.90	x	x	x		x	x	x		x	x		x	x	x
11	79.8	55.2	9.1	6.91	x	x		x	x	x			x	x	x	x	x	x
12	80.1	50.4	11.0	7.27	x	x	x	x	x	x			x	x	x	x	x	x
12	80.0	50.0	11.1	7.30	x	x	x		x	x	x		x	x	x	x	x	x
13	80.2	43.4	13.0	7.77	x	x	x	x	x	x	x		x	x	x	x	x	x
13	80.2	43.3	13.0	7.77	x	x	x	x	x	x		x	x	x	x	x	x	x
14	80.2	34.0	15.0	8.38	x	x	x	x	x	x	x	x	x	x	x	x	x	x

$$S_{or_{@BT}} = -2.389 - 2.112 * 10^{-3}\, k - 0.179\, S_{wi} - 8.14\, V_{int.} + 0.966\, SA + 0.626\, \rho_s + 1.015 \log k - 4.497 * 10^{-5}\, \phi\, S_s \quad (6.19)$$

The R^2 for Eq. 6.19 is 80.5%, its adj.-R^2 is 69.9%, its C_p criterion value is 3.2 and its standard deviation is 0.044. The developed model contains seven independent variables, which implies that the model is unbiased. Statistically, this model is slightly better than its other counterparts that were previously developed using the common rock/fluid properties alone and the uncommon rock/fluid properties alone.

6.4.3.2 Residual Oil Saturation At Floodout

From Table 6.16, the final model developed for predicting residual oil saturation at floodout for sandstones, using the combined rock/fluid properties is given as:

$$S_{or_{@FO}} = 0.808 - 1.930 * 10^{-4}\, k - 0.994\, S_{wi} - 5.594\, V_{int.} + 1.025\, SA + 3.594\, \phi\, S_{wi} - 4.015 * 10^{-5}\, \phi\, S_s \quad (6.20)$$

The R^2 for Eq. 6.20 is 85.5%, its adj.-R^2 is 79.3%, its C_p criterion value is 0.1 and its standard deviation is 0.0307. The developed model contains six independent variables, which implies that the model is unbiased. Statistically, this model is as good as its other previously developed counterparts, considering their standard deviation values.

6.4.3.3 Oil Recovery at Breakthrough

From Table 6.17, the final model developed for predicting oil recovery at breakthrough for sandstones, using the combined rock/fluid properties is given as:

$$OR_{@BT} = 526.2 + 0.620\, k - 221.3\, S_{wi} + 752.1\, V_{int.} + 2.014\, \overline{D} + 810.9\, \phi\, S_{wi} - 287.5 \log k \quad (6.21)$$

The R^2 for Eq. 6.21 is 77.2%, its adj.-R^2 is 67.4%, its C_p criterion value is 1.6 and its

standard deviation is 10.7. The developed model contains six independent variables, which implies that the model is unbiased. Statistically, this model is slightly better than its other previously developed counterparts, considering their standard deviation values.

6.4.3.4 Ultimate Oil Recovery At Floodout

From Table 6.18, the final model developed for predicting ultimate oil recovery at floodout for sandstones, using the combined rock/fluid properties is given as:

$$\begin{aligned} UOR &= 281.5 - 611.7\,\phi + 0.0826\,k + 2263.4\,V_{int.} - 484.3\,SA - 116.7\,\rho_s \\ &\quad + 563.4\,RE + 0.0182\,\phi\,S_s - 2597.0\,\phi\,RE \end{aligned} \qquad (6.22)$$

The R^2 for Eq. 6.22 is 78.9%, its adj.-R^2 is 64.8%, its C_p criterion value is 3.4 and its standard deviation is 6.12. The developed model contains eight independent variables, which implies that the model is unbiased. Statistically, this model is the best compared to its other previously developed counterparts.

6.4.4 Ranking of the Models

The statistical summary of the empirical models for Berea sandstone is shown in Table 6.19. This table also include the F-test statistic and the p-value for each of the developed sandstone models. Except for the ultimate oil recovery model at floodout using common rock/fluid properties, all the other oil recovery models are statistically significant at α = 0.005 level. The common rock/fluid properties ultimate oil recovery model is statistically significant at α = 0.05 level. For the residual oil saturation models, all of them except the residual oil saturation at breakthrough model using uncommon rock/fluid properties, are statistically significant at α = 0.005 level. The uncommon rock/fluid properties residual oil saturation at breakthrough model is statistically significant at α = 0.01 level. The ranking of the models is presented in Table 6.20, where "1st" stands for the

Table 6.19: Statistical Summary of the Empirical Models Developed for Sandstone Linear-Cores

Empirical Model For	Eqn. No.	No. Vars	R-sq	Adj. R-sq	C_p	σ	F test	P value
COMMON								
$S_{or_{@BT}}$	6.11	4	60.6	50.7	4.3	0.056	6.14	0.003
$S_{or_{@PO}}$	6.12	2	69.7	66.3	0.4	0.039	20.66	0.000
$OR_{@BT}$	6.13	4	61.8	52.3	4.5	12.924	6.48	0.003
$UOR_{@PO}$	6.14	2	29.3	21.4	0.3	9.149	3.73	0.044
UNCOMMON								
$S_{or_{@BT}}$	6.15	6	67.1	53.0	5.0	0.055	4.76	0.008
$S_{or_{@PO}}$	6.16	9	85.1	72.8	9.2	0.035	6.96	0.002
$OR_{@BT}$	6.17	6	73.4	62.1	3.6	11.526	6.45	0.002
$UOR_{@PO}$	6.18	2	62.2	58.0	-2.9	6.688	14.82	0.000
BOTH								
$S_{or_{@BT}}$	6.19	7	80.5	69.9	3.2	0.044	7.65	0.001
$S_{or_{@PO}}$	6.20	6	85.5	79.3	0.1	0.031	13.77	0.000
$OR_{@BT}$	6.21	6	77.2	67.4	1.6	10.687	7.89	0.001
$UOR_{@PO}$	6.22	8	78.9	64.8	3.4	6.120	5.61	0.004

Table 6.20: Ranking of the Empirical Models Developed for Sandstone Linear-Cores

Empirical Models For	COMMON	UNCOMMON	BOTH
$S_{or_{@BT}}$	3rd	2nd	1st
$S_{or_{@PO}}$	3rd	2nd	1st
$OR_{@BT}$	3rd	2nd	1st
$UOR_{@PO}$	3rd	2nd	1st

best model. If only one of the three types of models is to be chosen, the sandstone residual oil saturation and oil recovery by waterflooding are better predicted by the inclusion of both common and uncommon rock/fluid properties in the predictive models.

6.4.5 Validation of the Models

To test the validity of the sandstone models, crossplots to compare the predicted residual oil saturation and oil recovery values using Eqs. 6.19 through 6.22, with the measured values are plotted. The solid 45° lines in the plots represent a perfect correlation between the measured and predicted values. The plots of the residuals versus the measured values are also presented. For the case of the residuals plots, the horizontal line drawn on each of the plots represents the perfect correlation line. The crossplots and residuals plots for these newly developed models are shown in Figs. 6.16 through 6.23. For the four new sandstone models, most of the plotted data points fall close to the 45° line, indicating the high degree of predictive accuracy of the models. The behavior of the residuals plots, further suggest that the independent variables in the models were enough to define the various dependent variables.

Further, the newly developed sandstone ultimate oil recovery model (Eq. 6.22) was compared with three previously published models for predicting ultimate oil recovery that were developed from laboratory measured data. The models are those developed by Arnold and Crawford (1964), Donaldson et al. (1969), and Boukadi (1991), for sandstones. A critical review of the literature did not provide any previously published model developed from laboratory measured data to predict sandstone residual oil saturation at breakthrough or at floodout or to predict oil recovery at breakthrough.

Arnold and Crawford (1964) developed empirical models to show the analytical relation between the fluid and rock properties and oil recovery by waterflooding. They studied both consolidated and unconsolidated porous media. Their model for consolidated

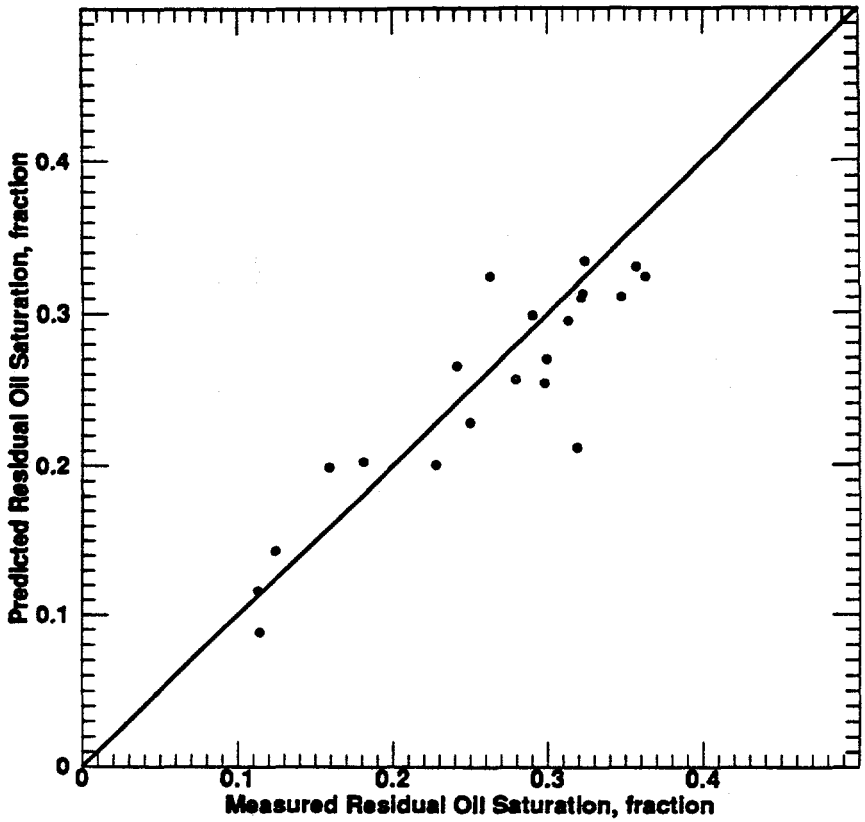

Fig. 6.16: Comparison of Measured Residual Oil Saturation at Breakthrough Values for Sandstones with those Predicted by the New Correlation (Eq. 6.19).

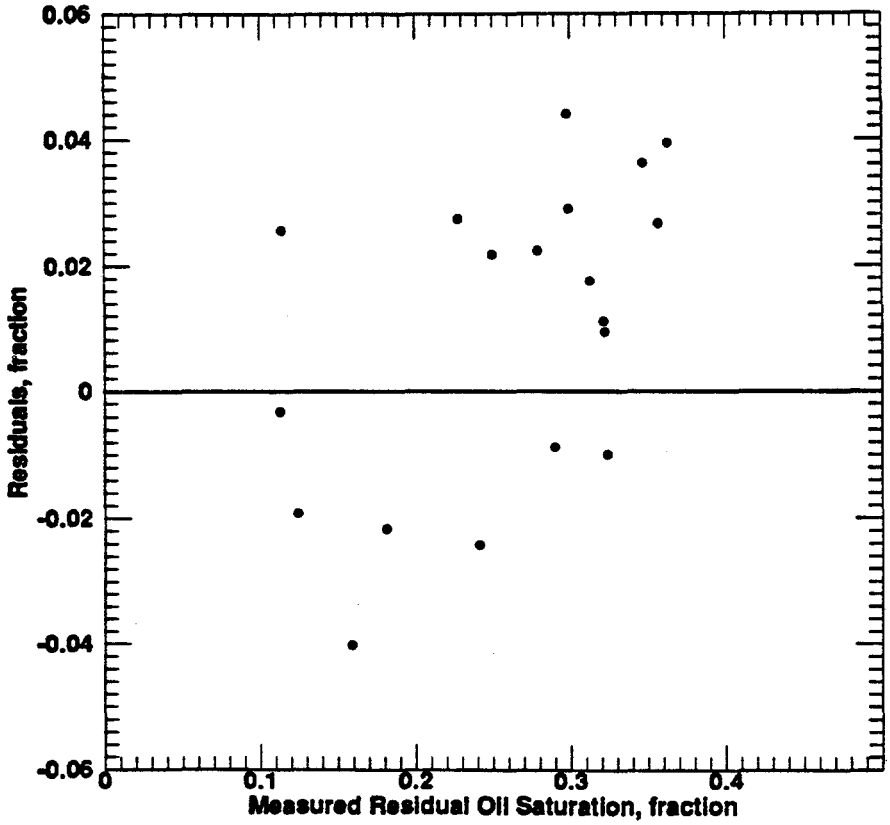

Fig. 6.17: Plotted Residuals Using the New Correlation (Eq. 6.19) vs. Measured Residual Oil Saturation at Breakthrough Values for Sandstones.

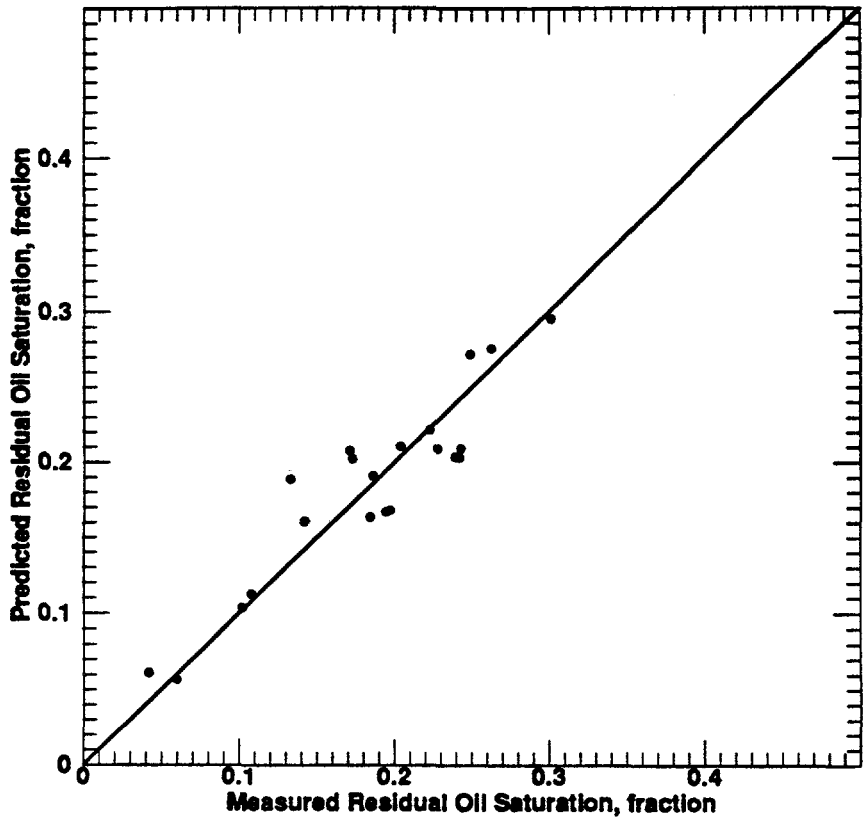

Fig. 6.18: Comparison of Measured Residual Oil Saturation at Floodout Values for Sandstones with those Predicted by the New Correlation (Eq. 6.20).

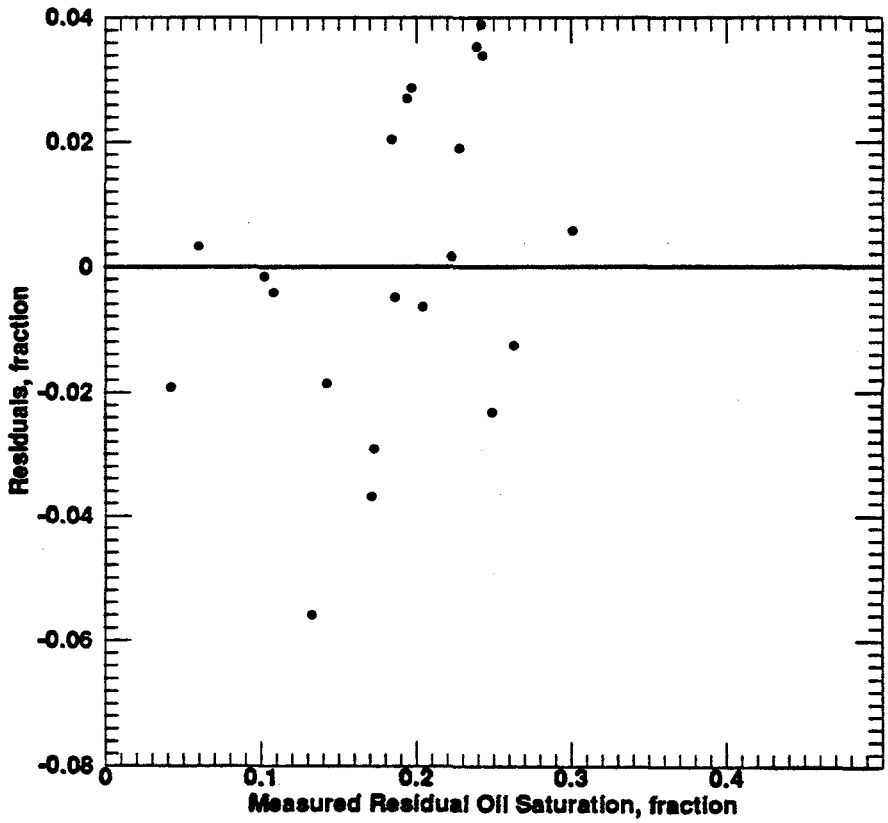

Fig. 6.19: Plotted Residuals Using the New Correlation (Eq. 6.20) vs. Measured Residual Oil Saturation at Floodout Values for Sandstones.

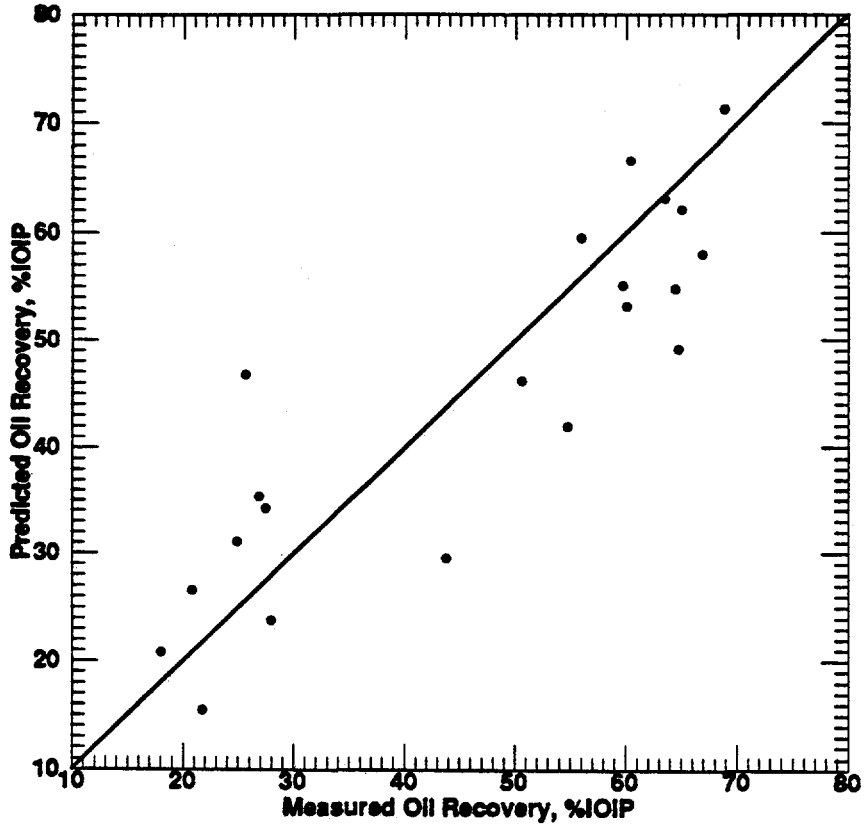

Fig. 6.20: Comparison of Measured Oil Recovery at Breakthrough Values for Sandstones with those Predicted by the New Correlation (Eq. 6.21).

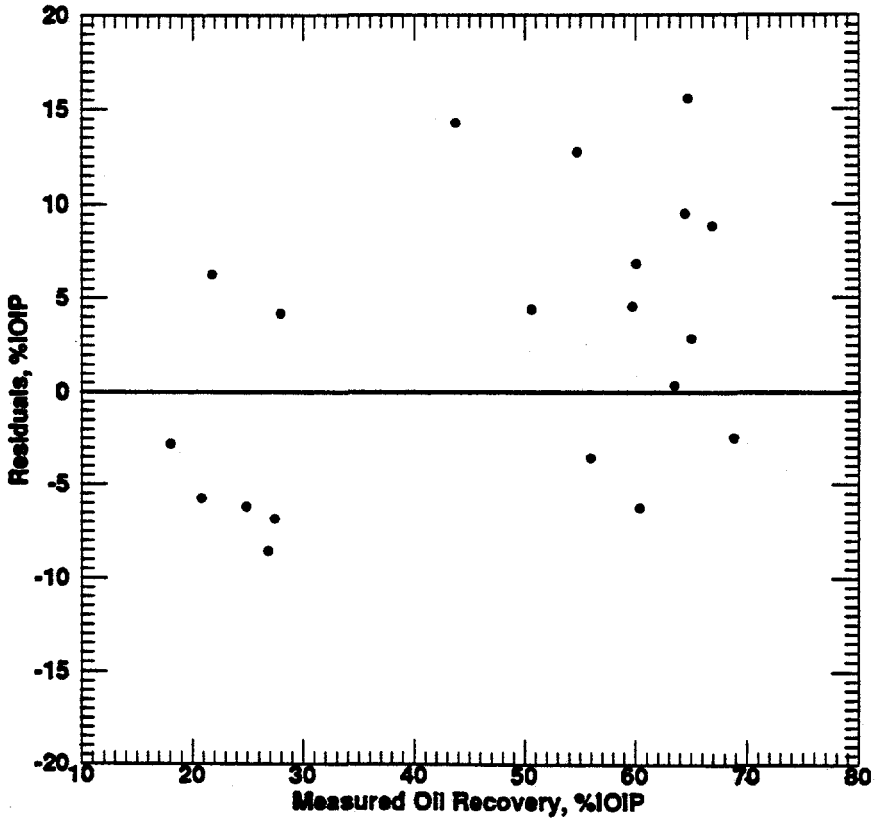

Fig. 6.21: Plotted Residuals Using the New Correlation (Eq. 6.21) vs. Measured Oil Recovery at Breakthrough Values for Sandstones.

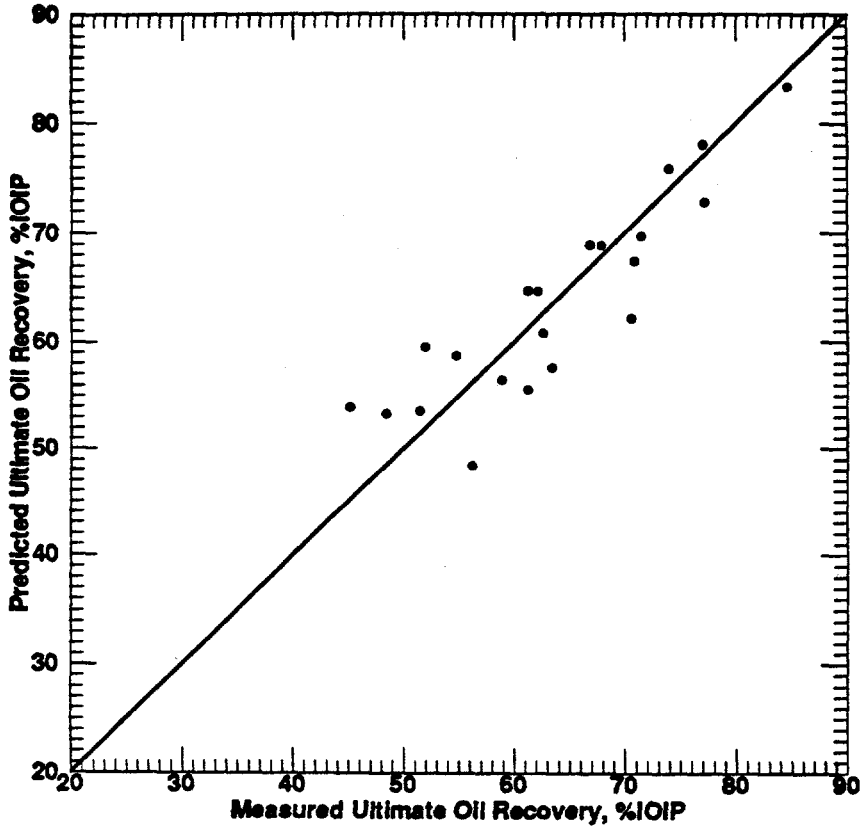

Fig. 6.22: Comparison of Measured Ultimate Oil Recovery at Floodout Values for Sandstones with those Predicted by the New Correlation (Eq. 6.22).

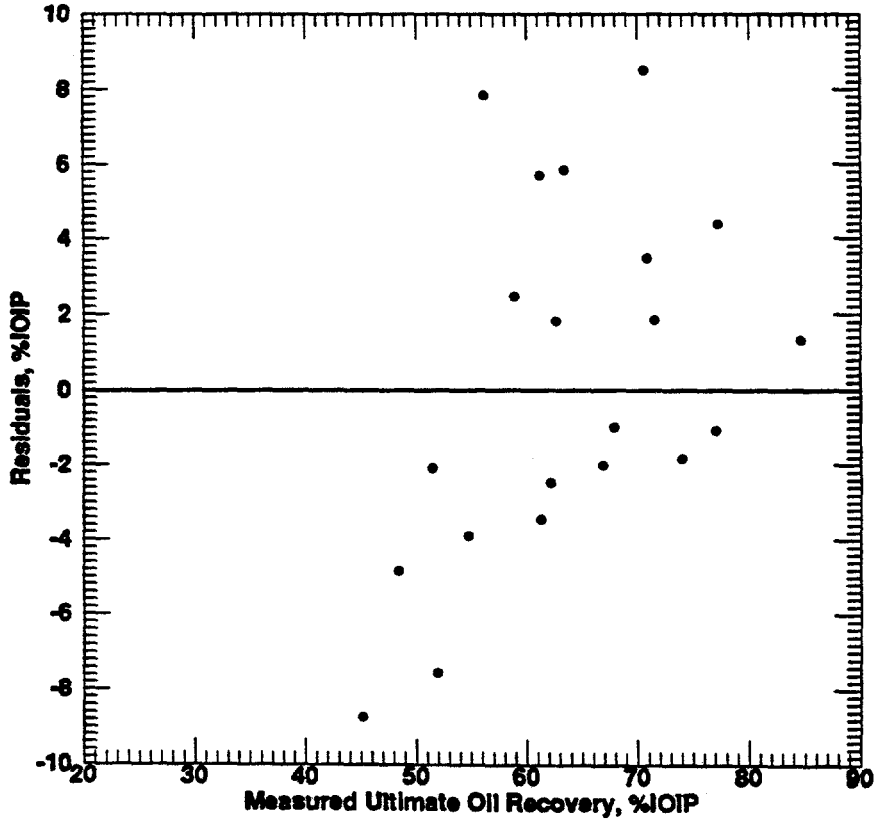

Fig. 6.23: Plotted Residuals Using the New Correlation (Eq. 6.22) vs. Measured Ultimate Oil Recovery at Floodout Values for Sandstones.

sands is given in Eq. 6.23 below:

$$\frac{1}{UOR} = 8.395 + 84.54\left(\frac{1}{k}\right) + 0.9823 \ln \mu_o + 0.1006\, \sigma_{ow} - 6.531\left(\frac{1}{S_{oi}}\right) + 2.651\left(\frac{1}{\phi}\right) + 0.7503\, F + 11.203\left(\frac{1}{k}\right)^2 - 0.1052\left(\ln \mu_o\right)^2 - 0.006168\, \sigma_{ow}^2 + 1.425\left(\frac{1}{S_{oi}}\right)^2 - 1.135\left(\frac{1}{\phi}\right)^2 - 0.01184\, F^2 \qquad (6.23)$$

In Eq. 6.23, ultimate oil recovery, UOR, is expressed as a fraction of the initial oil-in-place. The other variables in the equation are in the same units as shown in the nomenclature. The values of the formation resistivity factors can be estimated using the Humble (Lynch, 1962) relationship for estimating formation resistivity factors of granular systems like sandstones.

Donaldson et al. (1969) used laboratory measured data from outcrop cores of Torpedo sandstone, to develop models to predict ultimate oil recovery from waterflooding as a function of wettability index, permeability, porosity, oil viscosity, initial oil saturation, and interfacial tension. Among the four models they developed for sandstones, they recommended the use of the one given in Eq. 6.24 below:

$$UOR = 0.471 + 0.170\, WI + 0.130\, k - 0.158 \log\left(\mu_o\right) \qquad (6.24)$$

In Eq. 6.24, ultimate oil recovery, UOR, and the other variables in the equation are in the same units as shown in the nomenclature.

Boukadi (1991) models for sandstones were developed from laboratory measured radial core-flood data. Similar to the present study, the models made use of variables from wettability and mercury porosimetry properties. The model he recommended for predicting ultimate oil recovery for sandstones was earlier presented in Eq. 6.6. One of the differences between his models for predicting ultimate oil recovery and those proposed in this study, is

that his models included both initial oil saturation and residual oil saturation as independent variables. Oil recovery values can be routinely calculated with high degree of accuracy when the values of both the initial and residual oil saturations are known. It can then be argued that residual oil saturation should not be included as an independent variable in an empirical model for predicting oil recovery.

Due to non-availability of independent data, the crossplots and residual plots were developed using the experimentally measured data that were presented earlier. The crossplots and residuals plots for comparing the predicted ultimate oil recovery values using Eqs. 6.23 and 6.24, with the measured values are shown in Figs. 6.24 through 6.27. Unlike the case of the new model (Eq. 6.22), which is shown in Fig. 6.27, all of the plotted data points of the crossplot of Arnold and Crawford (1964) model, as shown in Fig. 6.24 and that of Donaldson et al. (1969) model, as shown in Fig. 6.26, scatter widely below the 45° line. These indicate that the models under-predict. This conclusion is further supported by the plot of the residuals of Arnold and Crawford model and that of Donaldson et al. model, versus the measured ultimate oil recovery values. These residual plots are shown in Figs. 6.23, 6.25, and 6.27, for the newly developed model, for Arnold and Crawford model, and for Donaldson et al. model, respectively. The plots of the scatter data points of Figs. 6.25 and 6.27, appear to follow a trend and that of Fig. 6.23 has no definite trend. The behavior of Figs. 6.25 and 6.27 suggest the need to add more independent variables to Arnold and Crawford model and to Donaldson et al. model, before their predictive capability could be enhanced.

The crossplot and residuals plot for Boukadi model are not shown, because it was noted that the differences between the values predicted by his model and the measured values of ultimate oil recovery for sandstones, occurred due to his definition of tortuosity. He defined tortuosity in terms of retention time in seconds, whereas the definition of

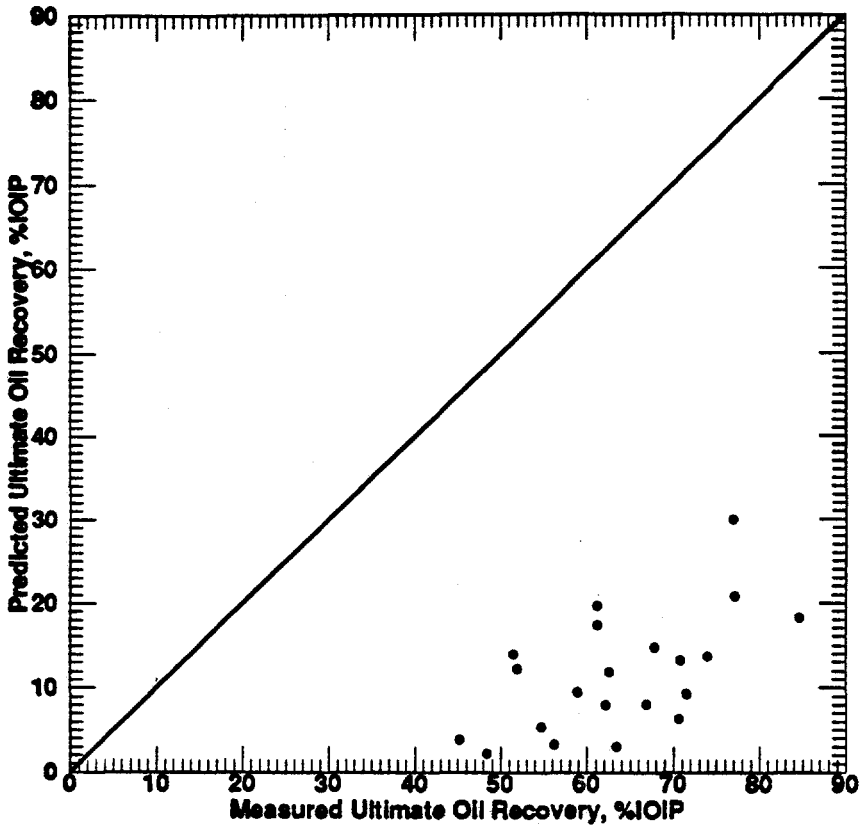

Fig. 6.24: Comparison of Measured Ultimate Oil Recovery at Floodout Values for Sandstones with those Predicted by Arnold and Crawford (1964) Correlation (Eq. 6.23).

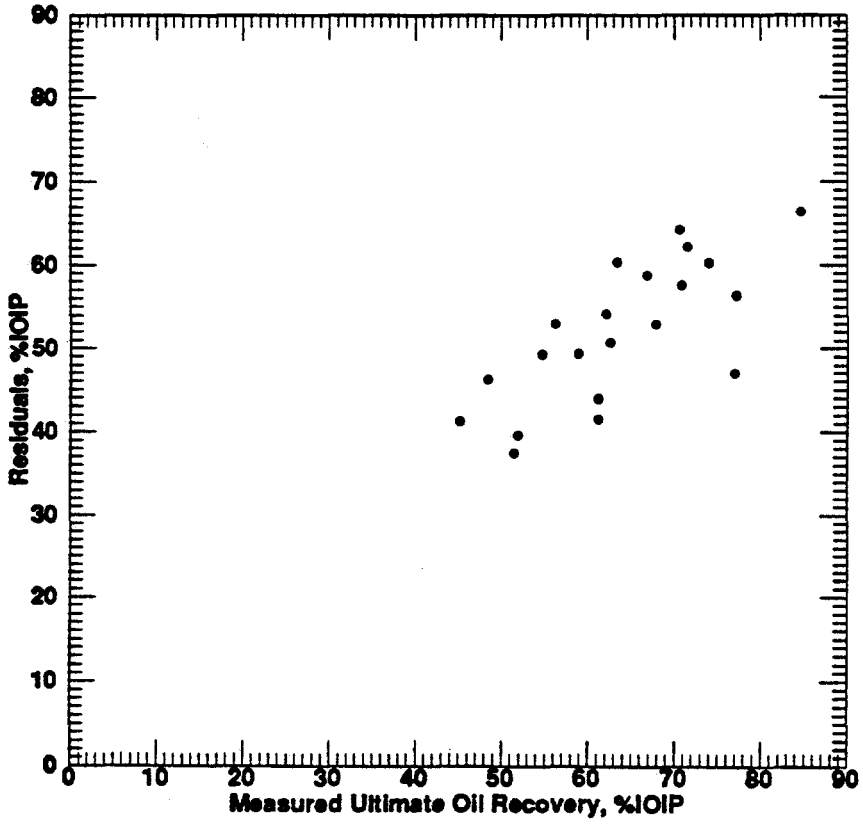

Fig. 6.25: Plotted Residuals Using Arnold and Crawford (1964) Correlation (Eq. 6.23) vs. Measured Ultimate Oil Recovery at Floodout Values for Sandstones.

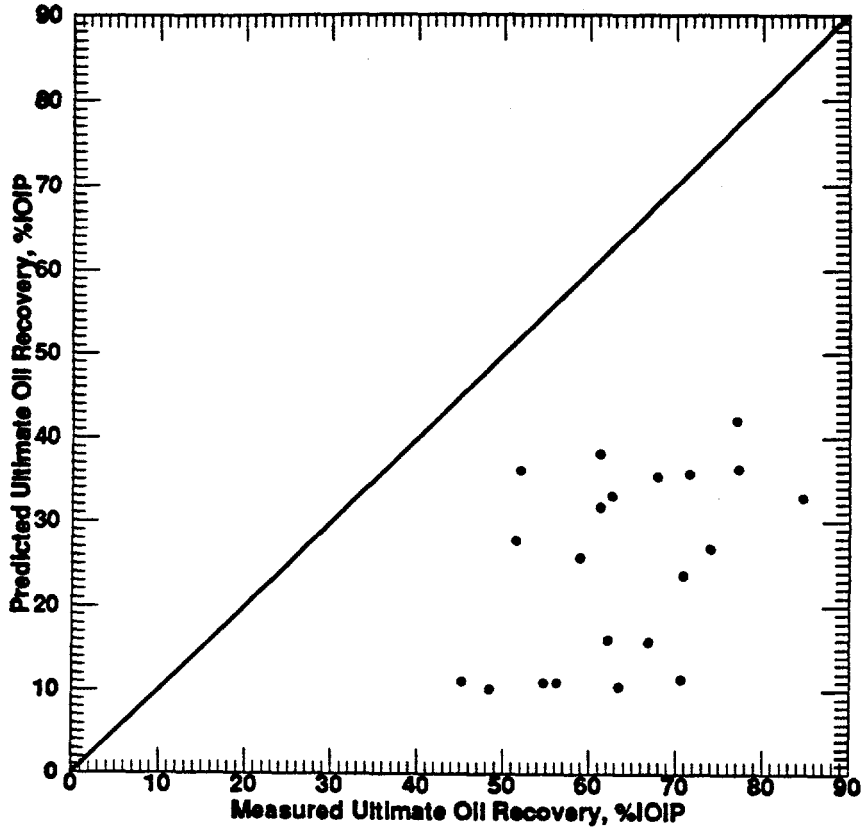

Fig. 6.26: Comparison of Measured Ultimate Oil Recovery at Floodout Values for Sandstones with those Predicted by Donaldson et al. (1969) Correlation (Eq. 6.24).

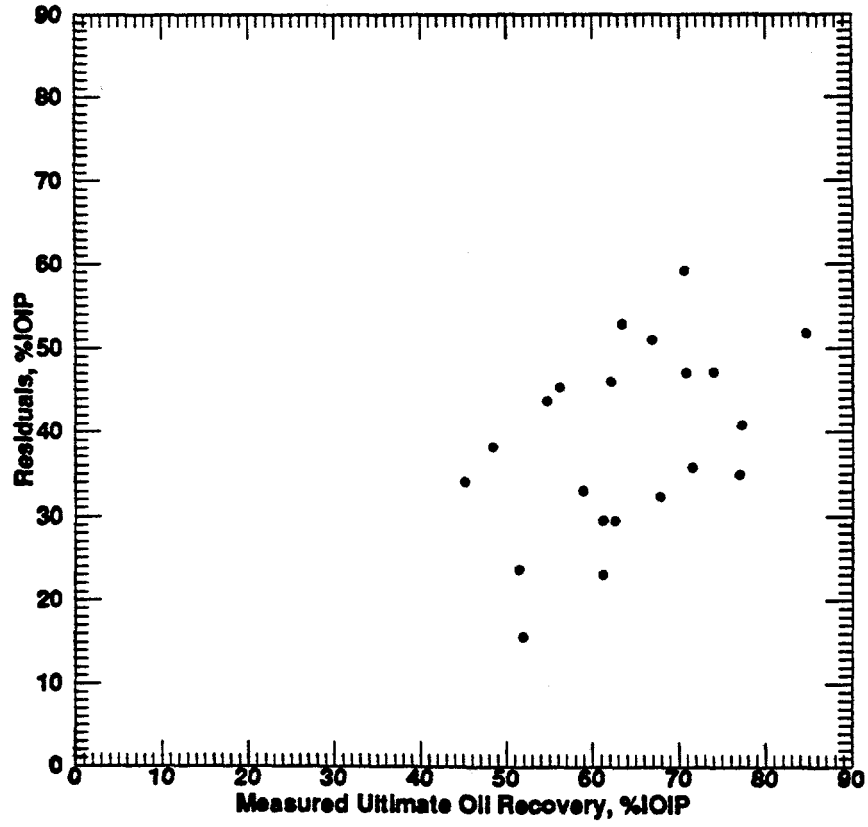

Fig. 6.27: Plotted Residuals Using Donaldson et al. (1969) Correlation (Eq. 6.24) vs. Measured Ultimate Oil Recovery at Floodout Values for Sandstones.

tortuosity as presented in the literature (Winsauer et al., 1952; Wyllie and Spangler, 1952; Amyx et al., 1960; and Given, 1986) is different.

6.5 Limestone Case

The development of the limestone models was initially started by employing similar independent variables as those used for the sandstone case. To further improve the models, log k, ϕS_{wi} and ϕRE terms were introduced into the models as part of the independent variables.

6.5.1 With Common Rock/Fluid Properties

The output for the best subsets algorithms for the development of models for predicting residual oil saturation and oil recovery at both breakthrough and floodout for limestones, using the common rock/fluid properties alone, are shown in Tables 6.21 through 6.24. The developed models are presented in Eqs. 6.25 through 6.28.

6.5.1.1 Residual Oil Saturation at Breakthrough

From Table 6.21, the final model developed for predicting residual oil saturation at breakthrough for limestones, using the common rock/fluid properties alone, is given as:

$$S_{or_{BT}} = 1.637 + 0.0298\ k - 5.578\ \phi\ S_{wi} - 1.183 \log k \qquad (6.25)$$

The R^2 for Eq. 6.25 is 74.3%, its adj.-R^2 is 67.9%, its C_p criterion value is 2.1 and its standard deviation is 0.040. The developed model contains three independent variables, which implies that the model is unbiased.

Table 6.21: Best Subsets Regression for Residual Oil Saturation at Breakthrough for Limestone Linear-Cores (Using Common Rock Properties)

Vars.	R-sq	Adj. R-sq	C_p	σ	ϕ	k	S_{wi}	ϕS_{wi}	logk
1	54.9	51.7	5.8	0.049				x	
1	46.0	42.1	9.3	0.054			x		
2	71.9	67.6	1.1	0.040			x		x
2	71.7	67.4	1.2	0.040				x	x
3*	74.3	67.9	2.1	0.040		x		x	x
3	72.8	66.0	2.7	0.041	x			x	x
4	74.3	65.0	4.1	0.042	x	x		x	x
4	74.3	65.0	4.1	0.042		x	x	x	x
5	74.6	62.0	6.0	0.044	x	x	x	x	x

Table 6.22: Best Subsets Regression for Residual Oil Saturation at Floodout for Limestone Linear-Cores (Using Common Rock Properties)

Vars.	R-sq	Adj. R-sq	C_p	σ	ϕ	k	S_{wi}	ϕS_{wi}	logk
1	64.0	61.5	23.8	0.029			x		
1	63.5	60.8	24.4	0.029				x	
2	84.6	82.3	5.3	0.020		x	x		
2	83.2	80.6	6.7	0.021			x		x
3	86.0	82.5	6.0	0.020		x	x	x	
3	85.9	82.4	6.0	0.020	x	x	x		
4*	90.0	86.3	4.0	0.017		x	x	x	x
4	89.9	86.3	4.0	0.017	x	x	x		x
5	90.0	84.9	6.0	0.018	x	x	x	x	x

Table 6.23: Best Subsets Regression for Oil Recovery at Breakthrough for Limestone Linear-Cores (Using Common Rock Properties)

Vars.	R-sq	Adj. R-sq	C_p	σ	ϕ	k	S_{wi}	ϕS_{wi}	logk
1	48.6	45.0	0.1	7.71					x
1	46.4	42.5	0.7	7.88		x			
2*	55.0	48.1	0.6	7.48				x	x
2	54.2	47.2	0.8	7.55			x		x
3	56.3	45.4	2.3	7.68		x		x	x
3	55.1	43.8	2.6	7.79			x	x	x
4	57.1	41.6	4.1	7.94		x	x	x	x
4	57.0	41.4	4.2	7.96	x	x		x	x
5	57.7	36.5	6.0	8.28	x	x	x	x	x

Table 6.24: Best Subsets Regression for Ultimate Oil Recovery at Floodout for Limestone Linear-Cores (Using Common Rock Properties)

Vars.	R-sq	Adj. R-sq	C_p	σ	ϕ	k	S_{wi}	ϕS_{wi}	logk
1	52.5	49.1	8.0	4.2147		x			
1	50.5	47.0	8.9	4.3004					x
2	65.3	60.0	4.6	3.7352		x	x		
2	62.7	57.0	5.7	3.8753			x		x
3	68.7	60.9	5.2	3.6929		x	x	x	
3	68.5	60.6	5.3	3.7053	x	x	x		
4*	76.2	67.6	4.0	3.3641		x	x	x	x
4	76.0	67.3	4.1	3.3787	x	x	x		x
5	76.3	64.4	6.0	3.5236	x	x	x	x	x

6.5.1.2 Residual Oil Saturation at Floodout

From Table 6.22, the final model developed for predicting residual oil saturation at floodout for limestones, using the common rock/fluid properties alone, is given as:

$$S_{or_{@ro}} = 0.080 - 3.694 * 10^{-2} k - 1.452 S_{wi} + 4.930 \phi S_{wi} + 0.884 \log k \quad (6.26)$$

The R^2 for Eq. 6.26 is 90.0%, its adj.-R^2 is 86.3%, its C_p criterion value is 4.0 and its standard deviation is 0.017. The developed model contains four independent variables, which implies that the model is unbiased.

6.5.1.3 Oil Recovery at Breakthrough

From Table 6.23, the final model developed for predicting oil recovery at breakthrough for limestones, using the common rock/fluid properties alone, is given as:

$$OR_{@BT} = -50.14 + 360.9 \phi S_{wi} + 58.12 \log k \quad (6.27)$$

The R^2 for Eq. 6.27 is 55.0%, its adj.-R^2 is 48.1%, its C_p criterion value is 0.6 and its standard deviation is 7.48. The developed model contains two independent variables, which implies that the model is unbiased.

6.5.1.4 Ultimate Oil Recovery at Floodout

From Table 6.24, the final model developed for predicting ultimate oil recovery at floodout for limestones, using the common rock/fluid properties alone, is given as:

$$UOR = 117.9 + 6.475 k + 184.1 S_{wi} - 918.0 \phi S_{wi} - 152.9 \log k \quad (6.28)$$

The R^2 for Eq. 6.28 is 76.2%, its adj.-R^2 is 67.6%, its C_p criterion value is 4.0 and its

standard deviation is 3.36. The developed model contains four independent variables, which implies that the model is unbiased.

6.5.2 With Uncommon Rock/Fluid Properties

The output for the best subsets algorithms for the development of models for predicting residual oil saturation and oil recovery at both breakthrough and floodout for limestones, using the uncommon rock/fluid properties alone, are shown in Tables 6.25 through 6.28. The developed models are presented in Eqs. 6.29 through 6.32.

6.5.2.1 Residual Oil Saturation at Breakthrough

From Table 6.25, the final model developed for predicting residual oil saturation at breakthrough for limestones, using the uncommon rock/fluid properties alone, is given as:

$$S_{or_{@BT}} = 13.99 - 96.31\ \phi_{Hg} - 34.60\ RE + 244.7\ \phi_{Hg}\ RE \qquad (6.29)$$

The R^2 for Eq. 6.29 is 70.7%, its adj.-R^2 is 63.3%, its C_p criterion value is -1.1 and its standard deviation is 0.043. The developed model contains three independent variables, which implies that the model is unbiased. Statistically, this model is as good as its counterpart that was previously developed using common rock/fluid properties alone, considering their standard deviation values.

6.5.2.2 Residual Oil Saturation at Floodout

From Table 6.26, the final model developed for predicting residual oil saturation at floodout for limestones, using the uncommon rock/fluid properties alone, is given as:

$$S_{or_{@FO}} = 0.602 + 0.268\ WI - 7.741\ V_{int.} \qquad (6.30)$$

The R^2 for Eq. 6.30 is 75.9%, its adj.-R^2 is 72.2%, its C_p criterion value is -0.7 and its

Table 6.25: Best Subsets Regression for Residual Oil Saturation at Breakthrough for Limestone Linear-Cores (Using Uncommon Rock Properties)

Vars.	R-sq	Adj. R-sq	C_p	σ	WI	$V_{int.}$	SA	S_s	$\bar{D}$	ρ_s	ϕ_{Hg}	RE	ϕ_{Hg}RE
1	40.0	35.7	2.1	0.0567								x	
1	39.5	35.2	2.2	0.0569		x							
2	53.0	45.8	1.0	0.0520		x						x	
2	51.0	43.5	1.5	0.0531		x			x				
3*	70.7	63.3	-1.1	0.0428							x	x	x
3	59.1	48.9	1.6	0.0505	x	x						x	
4	72.3	62.3	0.5	0.0434	x						x	x	x
4	72.1	62.0	0.5	0.0436		x					x	x	x
5	73.9	60.8	2.1	0.0442	x	x					x	x	x
5	73.2	59.7	2.3	0.0448			x			x	x	x	x
6	74.0	56.6	4.1	0.0465	x		x	x			x	x	x
6	73.9	56.6	4.1	0.0466	x	x	x				x	x	x
7	74.0	51.2	6.1	0.0494	x	x	x	x			x	x	x
7	74.0	51.2	6.1	0.0494	x		x	x	x		x	x	x
8	74.3	44.9	8.0	0.0524	x	x	x	x	x		x	x	x
8	74.0	44.3	8.1	0.0528	x	x	x	x		x	x	x	x
9	74.4	36.0	10.0	0.0565	x	x	x	x	x	x	x	x	x

Table 6.26: Best Subsets Regression for Residual Oil Saturation at Floodout for Limestone Linear-Cores (Using Uncommon Rock Properties)

Vars.	R-sq	Adj. R-sq	C_p	σ	WI	$V_{int.}$	SA	S_s	$\bar{D}$	ρ_s	ϕ_{Hg}	RE	ϕ_{Hg}RE
1	40.9	36.7	7.6	0.0373		x							
1	33.0	28.2	10.2	0.0397	x								
2*	75.9	72.2	-2.0	0.0247	x	x							
2	62.2	56.4	2.5	0.0309	x							x	
3	76.8	71.0	-0.3	0.0252	x	x						x	
3	76.8	71.0	-0.3	0.0252	x	x							x
4	77.3	69.0	1.5	0.0261	x	x				x		x	
4	77.2	68.9	1.5	0.0261	x	x						x	x	
5	79.7	69.6	2.7	0.0258	x	x						x	x	x
5	77.9	66.9	3.3	0.0270	x	x	x	x				x		
6	81.5	69.1	4.1	0.0261	x	x	x	x	x			x		
6	80.5	67.5	4.5	0.0267	x	x			x			x	x	x
7	81.7	65.7	6.1	0.0274	x	x	x	x	x			x		x
7	81.7	65.7	6.1	0.0274	x	x	x	x	x			x	x	
8	81.8	61.0	8.0	0.0293	x	x	x	x	x	x		x		x
8	81.8	61.0	8.0	0.0293	x	x	x	x	x	x		x	x	
9	81.9	54.7	10.0	0.0315	x	x	x	x	x	x		x	x	x

Table 6.27: Best Subsets Regression for Oil Recovery at Breakthrough for Limestone Linear-Cores (Using Uncommon Rock Properties)

Vars.	R-sq	Adj. R-sq	C_p	σ	WI	$V_{int.}$	SA	S_o	$\bar{D}$	ρ_o	ϕ_{Hg}	RE	ϕ_{Hg}RE
1	58.6	55.6	9.9	6.92								x	
1	43.7	39.6	17.8	8.07					x				
2	72.8	68.7	4.4	5.82							x		x
2	71.4	67.0	5.1	5.97							x	x	
3	86.8	83.5	-1.0	4.23							x	x	x
3	74.4	68.0	5.5	5.88			x				x		x
4*	88.0	83.6	0.4	4.21					x		x	x	x
4	87.6	83.1	0.5	4.27				x			x	x	x
5	88.3	82.5	2.2	4.34	x			x			x	x	x
5	88.1	82.2	2.3	4.38	x				x		x	x	x
6	88.5	80.8	4.1	4.55	x			x	x		x	x	x
6	88.4	80.7	4.1	4.56		x	x	x			x	x	x
7	88.6	78.6	6.0	4.81	x	x	x	x			x	x	x
7	88.6	78.6	6.0	4.81		x	x	x	x		x	x	x
8	88.6	75.6	8.0	5.13	x	x	x	x	x		x	x	x
8	88.6	75.6	8.0	5.14	x	x	x	x		x	x	x	x
9	88.7	71.6	10.0	5.53	x	x	x	x	x	x	x	x	x

Table 6.28: Best Subsets Regression for Ultimate Oil Recovery at Floodout for Limestone Linear-Cores (Using Uncommon Rock Properties)

Vars.	R-sq	Adj. R-sq	C_p	σ	WI	$V_{int.}$	SA	S_o	$\bar{D}$	ρ_o	ϕ_{Hg}	RE	ϕ_{Hg}RE
1	49.4	45.8	30.1	4.35		x							
1	46.5	42.7	32.6	4.47							x		
2	75.6	71.8	10.4	3.14	x	x							
2	74.8	70.9	11.0	3.19	x						x		
3	83.4	79.2	5.9	2.69	x	x					x		
3	81.3	76.6	7.6	2.85	x	x				x			
4	84.4	78.8	7.0	2.72	x	x			x		x		
4	83.6	77.6	7.7	2.79	x	x		x			x		
5	86.3	79.5	7.4	2.67	x	x			x		x		x
5	86.2	79.2	7.5	2.69	x	x			x		x	x	
6	89.1	81.9	7.1	2.51	x	x			x		x	x	x
6	88.7	81.2	7.4	2.56	x	x	x	x	x		x		
7*	92.6	86.1	6.2	2.20	x	x	x	x	x			x	x
7	92.3	85.6	6.4	2.24	x	x	x	x	x		x	x	
8	92.8	84.5	8.0	2.32	x	x	x	x	x	x		x	x
8	92.7	84.4	8.1	2.33	x	x	x	x	x		x	x	x
9	92.8	82.0	10.0	2.51	x	x	x	x	x	x	x	x	x

standard deviation is 0.025. The developed model contains two independent variables, which implies that the model is unbiased. Statistically, this model is not as good as its counterpart that was previously developed using common rock/fluid properties alone.

6.5.2.3 Oil Recovery at Breakthrough

From Table 6.27, the final model developed for predicting oil recovery at breakthrough for limestones, using the uncommon rock/fluid properties alone, is given as:

$$OR_{@BT} = -1792.4 - 73.68\,\overline{D} + 1.331 * 10^{4}\,\phi_{Hg} + 4619.0\,RE - 3.329 * 10^{4}\,\phi_{Hg}\,RE \quad (6.31)$$

The R^2 for Eq. 6.31 is 88.0%, its adj.-R^2 is 83.6%, its C_p criterion value is 0.4 and its standard deviation is 4.21. The developed model contains four independent variables, which implies that the model is unbiased. This model is statistically better than its counterpart that was previously developed using common rock/fluid properties alone.

6.5.2.4 Ultimate Oil Recovery at Floodout

From Table 6.28, the final model developed for predicting ultimate oil recovery at floodout for limestones, using the uncommon rock/fluid properties alone, is given as:

$$UOR = -896.8 - 19.03\,WI + 1.702 * 10^{4}\,V_{int.} - 1242.6\,SA + 7.877 * 10^{-3}\,S_s - 299.3\,\overline{D} - 495.0\,RE + 2882.8\,\phi_{Hg}\,RE \quad (6.32)$$

The R^2 for Eq. 6.32 is 92.6%, its adj.-R^2 is 86.1%, its C_p criterion value is 6.2 and its standard deviation is 2.20. The developed model contains seven independent variables, which implies that the model is unbiased. Statistically, this model is better than its counterpart that was previously developed using common rock/fluid properties alone.

6.5.3 With Both Common and Uncommon Rock/Fluid Properties

The output for the best subsets algorithms for the development of models for predicting residual oil saturation and oil recovery at both breakthrough and floodout for limestones, using both the common and uncommon rock/fluid properties, are shown in Tables 6.29 through 6.32. The developed models are presented in Eqs. 6.33 through 6.36. Further, to avoid having both brine and mercury porosimetry measured porosities as variables in the same model, mercury porosity terms were substituted with brine porosity terms.

6.5.3.1 Residual Oil Saturation at Breakthrough

From Table 6.29, the final model developed for predicting residual oil saturation at breakthrough for limestones, using both the common and uncommon rock/fluid properties, is given as:

$$\begin{aligned} S_{or_{@BT}} = & -11.21 + 67.84\,\phi - 0.117\,k + 21.36\,S_{wi} \\ & + 5.974\,V_{int.} - 0.963\,\overline{D} - 0.497\,\rho_s \\ & + 1.661\,RE - 147.4\,\phi\,S_{wi} + 3.432\log k \end{aligned} \qquad (6.33)$$

The R^2 for Eq. 6.33 is 97.1%, its adj.-R^2 is 92.7%, its C_p criterion value is 6.4 and its standard deviation is 0.019. The developed model contains nine independent variables, which implies that the model is unbiased. This model is the best, compared to its other previously developed counterparts.

6.5.3.2 Residual Oil Saturation at Floodout

From Table 6.30, the final model developed for predicting residual oil saturation at floodout for limestones, using both the common and uncommon rock/fluid properties, is given as:

Table 6.29: Best Subsets Regression for Residual Oil Saturation at Breakthrough for Limestone Linear-Cores (Using Both Common and Uncommon Rock Properties)

Vars.	R-sq	Adj. R-sq	C_p	σ	ϕ	k	WI	S_{wi}	$V_{kst.}$	SA	S_s	$\bar{D}$	ρ_g	RE	ϕS_{wi}	log k	ϕRE
1	54.9	51.7	24.3	0.0491											x		
1	46.0	42.1	31.6	0.0538				x									
2	82.3	79.6	4.3	0.0319										x	x		
2	79.5	76.4	6.5	0.0343				x						x			
3	88.6	85.8	1.2	0.0266									x		x		x
3	88.3	85.4	1.4	0.0270				x					x	x			
4	88.8	84.7	3.0	0.0276							x		x		x		x
4	88.7	84.6	3.1	0.0277					x				x		x		x
5	90.2	85.3	3.9	0.0271		x							x		x	x	x
5	89.4	84.2	4.5	0.0281		x		x					x	x		x	
6	91.7	86.2	4.7	0.0263		x			x				x		x	x	x
6	91.4	85.7	4.9	0.0268	x	x		x						x	x	x	
7	93.9	88.6	4.9	0.0239	x	x		x		x		x			x	x	
7	93.6	88.0	5.2	0.0245	x	x		x				x		x	x	x	
8	96.5	92.5	4.8	0.0194	x	x		x	x			x		x	x	x	
8	96.3	92.1	5.0	0.0199	x	x		x	x			x			x	x	x
9*	97.1	92.7	6.4	0.0191	x	x		x	x			x	x	x	x	x	
9	97.0	92.5	6.4	0.0194	x	x		x	x			x	x		x	x	x
10	97.4	92.2	8.1	0.0197	x	x		x	x	x	x		x		x	x	x
10	97.4	92.2	8.1	0.0197	x	x		x	x	x	x		x	x	x	x	
11	97.5	90.6	10.0	0.0216	x	x		x	x	x	x	x	x	x	x	x	
11	97.5	90.5	10.0	0.0217	x	x		x	x	x	x	x	x		x	x	x
12	97.5	87.6	12.0	0.0249	x	x	x	x	x	x	x	x	x	x	x	x	
12	97.5	87.6	12.0	0.0249	x	x	x	x	x	x	x	x	x		x	x	x
13	97.5	81.4	14.0	0.0305	x	x	x	x	x	x	x	x	x	x	x	x	x

Table 6.30: Best Subsets Regression for Residual Oil Saturation at Floodout for Limestone Linear-Cores (Using Both Common and Uncommon Rock Properties)

Vars.	R-sq	Adj. R-sq	C_p	σ	ϕ	k	WI	S_{wi}	$V_{im.}$	SA	S_g	$\bar{D}$	ρ_g	RE	ϕS_{wi}	log k	ϕRE
1	64.0	61.5	17.4	0.0291				x									
1	63.5	60.8	17.8	0.0293											x		
2	84.6	82.3	2.5	0.0197		x		x									
2	83.2	80.6	3.7	0.0206				x								x	
3	88.2	85.2	1.7	0.0180		x		x		x							
3	87.6	84.5	2.1	0.0184				x		x						x	
4	91.7	88.6	0.8	0.0158		x	x	x	x								
4	91.0	87.7	1.4	0.0165			x	x	x							x	
5	93.4	90.0	1.4	0.0148		x	x	x	x					x			
5	93.2	89.7	1.6	0.0150		x	x	x	x		x						
6*	95.2	92.0	1.9	0.0133	x	x	x		x						x	x	
6	95.1	91.8	2.0	0.0134	x	x	x	x	x							x	
7	95.5	91.6	3.6	0.0136	x	x	x		x			x			x	x	
7	95.5	91.6	3.7	0.0136	x	x	x		x				x		x	x	
8	96.1	91.6	5.2	0.0136	x	x	x	x	x			x			x	x	
8	95.8	91.0	5.4	0.0140	x	x	x		x			x			x	x	x
9	96.4	90.9	7.0	0.0141	x	x	x		x	x	x	x			x	x	
9	96.3	90.6	7.1	0.0143	x	x	x	x	x	x	x	x				x	
10	96.9	90.6	8.6	0.0144	x	x	x	x	x	x	x	x			x	x	
10	96.6	89.8	8.8	0.0150	x	x	x	x		x	x	x			x	x	x
11	97.3	89.8	10.2	0.0149	x	x	x	x	x	x	x	x			x	x	x
11	97.3	89.8	10.2	0.0150	x	x	x	x	x	x	x	x		x	x	x	
12	97.4	86.8	12.2	0.0170	x	x	x	x	x	x	x	x	x		x	x	x
12	97.3	86.6	12.2	0.0172	x	x	x	x	x	x	x	x	x	x	x	x	
13	97.6	81.6	14.0	0.0201	x	x	x	x	x	x	x	x	x	x	x	x	x

Table 6.31: Best Subsets Regression for Oil Recovery at Breakthrough for Limestone Linear-Cores (Using Both Common and Uncommon Rock Properties)

Vars.	R-sq	Adj. R-sq	C_p	σ	ϕ	k	WI	S_{wi}	$V_{int.}$	SA	S_s	$\bar{D}$	ρ_s	RE	ϕS_{wi}	log k	ϕRE
1	58.6	55.6	20.3	6.92										x			
1	48.6	45.0	28.0	7.71												x	
2	70.7	66.2	12.8	6.04										x	x		
2	69.0	64.3	14.1	6.21						x				x			
3	82.4	77.9	5.8	4.88				x					x	x			
3	81.9	77.3	6.1	4.95									x		x		x
4	82.8	76.5	7.4	5.03				x					x		x		x
4	82.8	76.5	7.4	5.04				x			x		x	x			
5	86.6	79.9	6.4	4.65		x							x		x	x	x
5	84.9	77.4	7.8	4.94		x		x					x			x	x
6	88.7	81.2	6.8	4.51		x			x				x		x	x	x
6	88.4	80.6	7.1	4.58		x		x			x		x	x		x	
7	91.8	84.7	6.4	4.07	x	x		x				x		x	x	x	
7	91.5	84.1	6.6	4.14	x	x		x				x			x	x	x
8	95.2	89.7	5.7	3.33	x	x		x	x			x		x	x	x	
8	95.0	89.2	5.9	3.42	x	x		x	x			x			x	x	x
9	96.4	90.9	6.8	3.13	x	x		x	x			x	x	x	x	x	
9	96.3	90.7	6.9	3.17	x	x		x	x			x	x		x	x	x
10*	97.4	92.1	8.1	2.92	x	x		x	x	x	x		x		x	x	x
10	97.4	92.1	8.1	2.92	x	x		x	x	x	x		x	x	x	x	
11	97.4	90.3	10.0	3.23	x	x		x	x	x	x	x	x	x	x	x	
11	97.4	90.3	10.0	3.24	x	x	x	x	x	x	x		x		x	x	x
12	97.4	87.2	12.0	3.72	x	x	x	x	x	x	x	x	x	x	x	x	
12	97.4	87.1	12.0	3.73	x	x	x	x	x	x	x	x	x		x	x	x
13	97.4	80.8	14.0	4.56	x	x	x	x	x	x	x	x	x	x	x	x	x

Table 6.32: Best Subsets Regression for Ultimate Oil Recovery at Floodout for Limestone Linear-Cores (Using Both Common and Uncommon Rock Properties)

Vars.	R-sq	Adj. R-sq	C_p	σ	ϕ	k	WI	S_{wi}	$V_{shr.}$	SA	S_g	$\bar{D}$	ρ_g	RE	ϕS_{wi}	log k	ϕRE
1	52.5	49.1	8.0	4.21		x											
1	50.5	47.0	8.8	4.30												x	
2	75.6	71.8	0.3	3.14			x		x								
2	66.0	60.7	4.3	3.70		x			x								
3	84.1	80.1	-1.3	2.63		x	x		x								
3	83.0	78.7	-0.9	2.72			x		x							x	
4	86.2	81.2	-0.2	2.56		x	x		x		x						
4	86.2	81.1	-0.2	2.57		x	x		x	x							
5	90.4	85.5	0.0	2.25	x	x	x		x							x	
5	88.3	82.4	0.9	2.47	x	x	x		x								x
6*	91.9	86.4	1.4	2.17	x	x	x		x			x				x	
6	91.3	85.5	1.6	2.25	x	x	x		x				x			x	
7	92.6	86.1	3.1	2.20	x	x	x			x	x	x				x	
7	92.5	86.0	3.1	2.21	x	x	x		x			x	x			x	
8	93.5	86.1	4.7	2.20	x	x	x	x	x			x			x	x	
8	92.9	84.8	5.0	2.30	x	x	x		x	x	x	x				x	
9	93.7	84.2	6.7	2.35	x	x	x	x		x	x	x			x	x	
9	93.6	84.0	6.7	2.36	x	x	x	x	x			x			x	x	x
10	94.6	83.9	8.3	2.37	x	x	x	x	x	x	x	x			x	x	
10	94.1	82.3	8.5	2.49	x	x	x	x		x	x	x			x	x	x
11	95.1	81.6	10.1	2.54	x	x	x	x	x	x	x	x			x	x	x
11	95.1	81.5	10.1	2.54	x	x	x	x	x	x	x	x		x	x	x	
12	95.1	75.6	12.0	2.91	x	x	x	x	x	x	x	x		x	x	x	x
12	95.1	75.5	12.1	2.92	x	x	x	x	x	x	x	x	x		x	x	x
13	95.2	64.3	14.0	3.53	x	x	x	x	x	x	x	x	x	x	x	x	x

$$S_{or_{@ro}} = -0.293 + 3.114\,\phi - 3.057 * 10^{-2}\,k + 0.113\,WI - 3.185\,V_{int.} - 3.370\,\phi\,S_{wi} + 0.766 \log k \quad (6.34)$$

The R^2 for Eq. 6.34 is 95.2%, its adj.-R^2 is 92.0%, its C_p criterion value is 1.9 and its standard deviation is 0.013. The developed model contains six independent variables, which implies that the model is unbiased. This model is as good as the model developed using common rock/fluid properties alone and better than that developed using uncommon rock/fluid properties alone.

6.5.3.3 Oil Recovery at Breakthrough

From Table 6.31, the final model developed for predicting oil recovery at breakthrough for limestones, using both the common and uncommon rock/fluid properties, is given as:

$$OR_{@BT} = 857.7 - 9925.0\,\phi + 18.91\,k - 3527.0\,S_{wi} + 1.045 * 10^{4}\,V_{int.} - 823.1\,SA + 5.297 * 10^{-3}\,S_s + 188.3\,\rho_s + 2.374 * 10^{4}\,\phi\,S_{wi} - 567.8 \log k - 2203.1\,\phi\,RE \quad (6.35)$$

The R^2 for Eq. 6.35 is 97.4%, its adj.-R^2 is 92.1%, its C_p criterion value is 8.1 and its standard deviation is 2.92. The developed model contains ten independent variables, which implies that the model is unbiased. This model is the best, compared to its other previously developed counterparts.

6.5.3.4 Ultimate Oil Recovery at Floodout

From Table 6.32, the final model developed for predicting ultimate oil recovery at floodout for limestones, using both the common and uncommon rock/fluid properties, is given as:

$$UOR = 190.9 - 428.8\,\phi + 6.972\,k - 21.81\,WI + 568.7\,V_{int.} + 46.86\,\overline{D} - 182.3 \log k \quad (6.36)$$

The R^2 for Eq. 6.36 is 91.9%, its adj.-R^2 is 86.4%, its C_p criterion value is 1.4 and its standard deviation is 2.17. The developed model contains six independent variables, which implies that the model is unbiased. This model is as good as the model developed using uncommon rock/fluid properties and better than the model developed using common rock/fluid properties.

6.5.4 Ranking of the Models

For the Indiana limestones, the statistical summary of the developed models is shown in Table 6.33. Except for the residual oil saturation at breakthrough model using uncommon rock/fluid properties alone, that is statistically significant at $\alpha = 0.005$ level, all the other developed limestone residual oil saturation models are significant at $\alpha = 0.001$ level. For the case of the developed limestone oil recovery models, except for the oil recovery at breakthrough model using common rock/fluid properties alone, that is statistically significant at $\alpha = 0.01$ level, all the other developed models are significant at $\alpha = 0.005$ level. Furthermore, similar to the previous observation in the case of the sandstone models, the ranking of the models as presented in Table 6.34 shows that the predictions of residual oil saturation and oil recovery at both breakthrough and at floodout are best achieved with the inclusion of both common and uncommon rock/fluid data into the limestone models.

6.5.5 Validation of the Models

To test the validity of the limestone models, crossplots to compare the predicted residual oil saturation and oil recovery values using the best of the developed models as presented in Tables 6.33 and 6.34, with the measured values are plotted. The solid 45° lines in the plots represent perfect correlation between the measured and predicted values. The

Table 6.33: Statistical Summary of the Empirical Models Developed for Limestone Linear-Cores

Empirical Model For	Eqn. No.	No. Vars	R-sq	Adj. R-sq	C_p	σ	F test	P value
COMMON								
$S_{or@BT}$	6.25	3	74.3	67.9	2.1	0.040	11.56	0.001
$S_{or@PO}$	6.26	4	90.0	86.3	4.0	0.017	24.61	0.000
$OR_{@BT}$	6.27	2	55.0	48.1	0.6	7.48	7.49	0.006
$UOR_{@PO}$	6.28	4	72.6	67.6	4.0	3.36	8.81	0.002
UNCOMMON								
$S_{or@BT}$	6.29	3	70.7	63.3	-1.1	0.043	9.64	0.002
$S_{or@PO}$	6.30	2	75.9	72.2	-2.0	0.025	20.43	0.000
$OR_{@BT}$	6.31	4	88.0	83.6	0.4	4.213	20.07	0.000
$UOR_{@PO}$	6.32	7	92.6	86.1	6.2	2.200	14.30	0.001
BOTH								
$S_{or@BT}$	6.33	9	97.1	92.7	6.4	0.019	22.08	0.001
$S_{or@PO}$	6.34	6	95.2	92.0	1.9	0.013	29.58	0.000
$OR_{@BT}$	6.35	10	97.4	92.1	8.1	2.920	18.50	0.002
$UOR_{@PO}$	6.36	6	91.9	86.4	1.4	2.174	16.95	0.000

Table 6.34: Ranking of the Empirical Models Developed for Limestone Linear-Cores

Empirical Models For	COMMON	UNCOMMON	BOTH
$S_{or@BT}$	2nd	3rd	1st
$S_{or@PO}$	2nd	3rd	1st
$OR_{@BT}$	3rd	2nd	1st
$UOR_{@PO}$	3rd	2nd	1st

plots of the residuals versus the measured values are also presented. For the case of the residuals plots, the horizontal line drawn on each of the plots represents the perfect correlation line. The crossplots and residual plots for these newly developed models are shown in Figs. 6.28 through 6.35. For the four new limestone models, most of the plotted data points fall very close to the 45° line, indicating the high degree of predictive accuracy of the models. The behavior of the residual plots, further suggest that the independent variables in the models were enough to define the various dependent variables.

Further, the best of the newly developed limestone ultimate oil recovery models (Eq. 6.36) was compared with Boukadi's (1991) model for predicting limestone ultimate oil recovery from laboratory measured data. The model Boukadi recommended for predicting ultimate oil recovery of waterflooded limestones was earlier presented in Eq. 6.10. To use Eq. 6.10, ultimate oil recovery, UOR, is expressed as fraction of initial oil-in-place. A critical review of the literature did not provide any previously published model developed from laboratory measured data to predict limestones residual oil saturation at breakthrough or at floodout or to predict oil recovery at breakthrough.

The crossplot and residual plot for comparing the predicted ultimate oil recovery values using Eq. 6.10, with the measured values are shown in Figs. 6.36 and 6.37. Unlike the case of the new model (Eq. 6.36), which is shown in Fig. 6.34, most of the plotted data points of the crossplot of Boukadi (1991) model, as shown in Fig. 6.36, scatter slightly above the 45° line. This indicates that Boukadi model over-predicts and that its predictive strength is good, but not as good as the newly developed model. The plots of the residuals versus measured ultimate oil recovery for the newly developed model and that of Boukadi, are shown in Figs. 6.35 and 6.37, respectively. Ignoring the data point above perfect correlation line, the plot of the scatter data points of Fig. 6.37, appears to follow a trend. The plot of the scatter data points of Fig. 6.35 has no definite trend. The behavior of Fig.

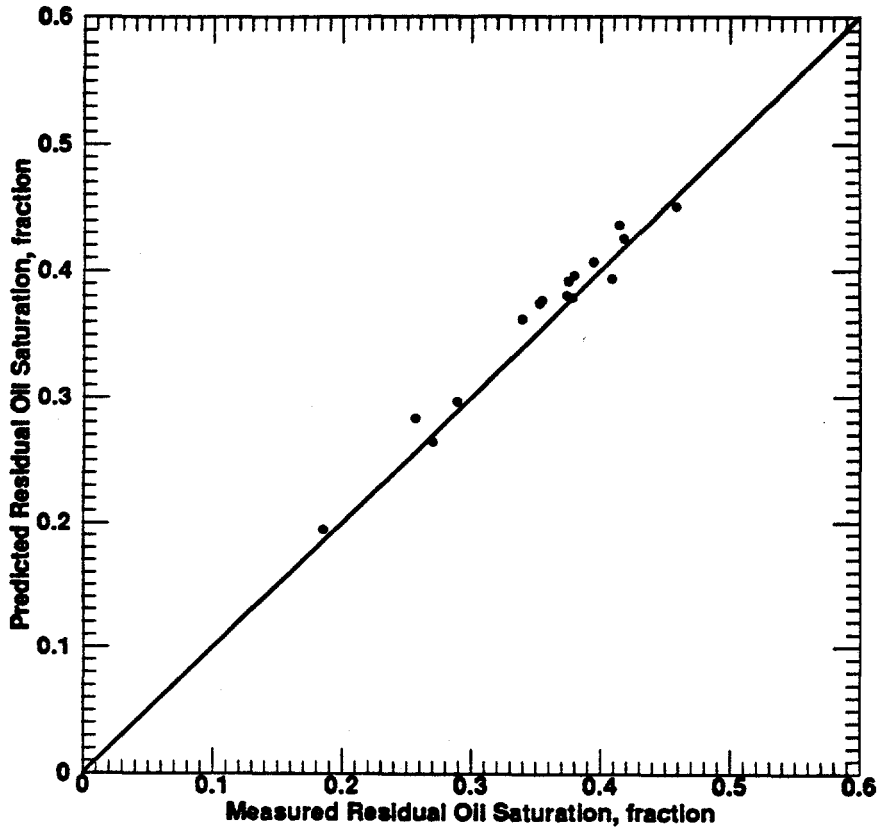

Fig. 6.28: Comparison of Measured Residual Oil Saturation at Breakthrough Values for Limestones with those Predicted by the New Correlation (Eq. 6.33).

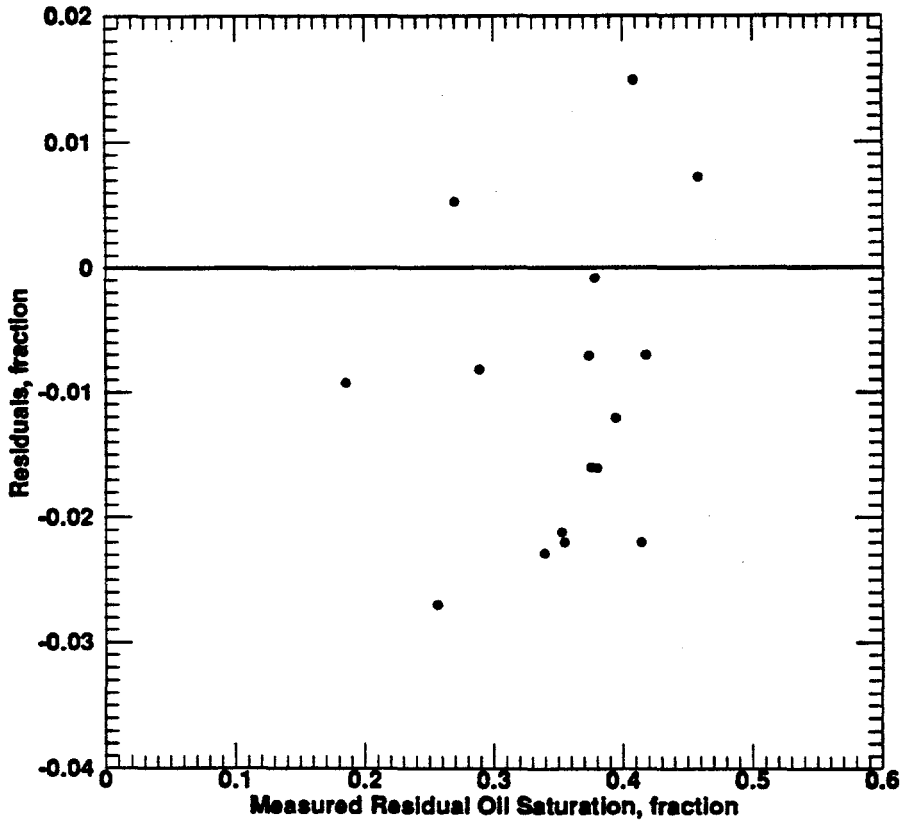

Fig. 6.29: Plotted Residuals Using the New Correlation (Eq. 6.33) vs. Measured Residual Oil Saturation at Breakthrough Values for Limestones.

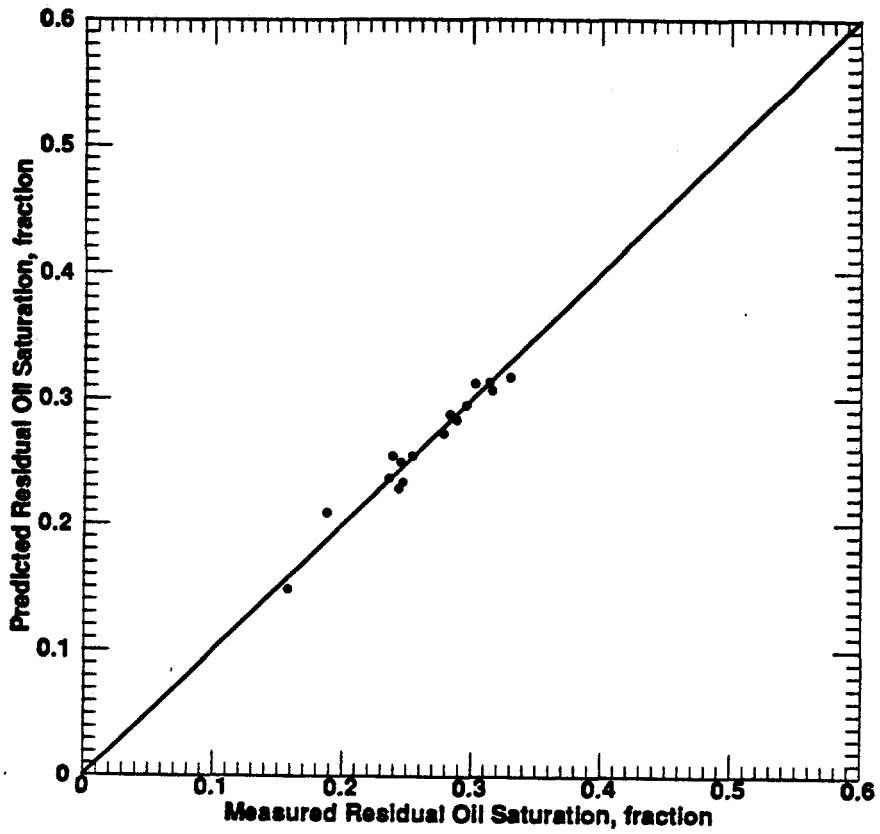

Fig. 6.30: Comparison of Measured Residual Oil Saturation at Floodout Values for Limestones with those Predicted by the New Correlation (Eq. 6.34).

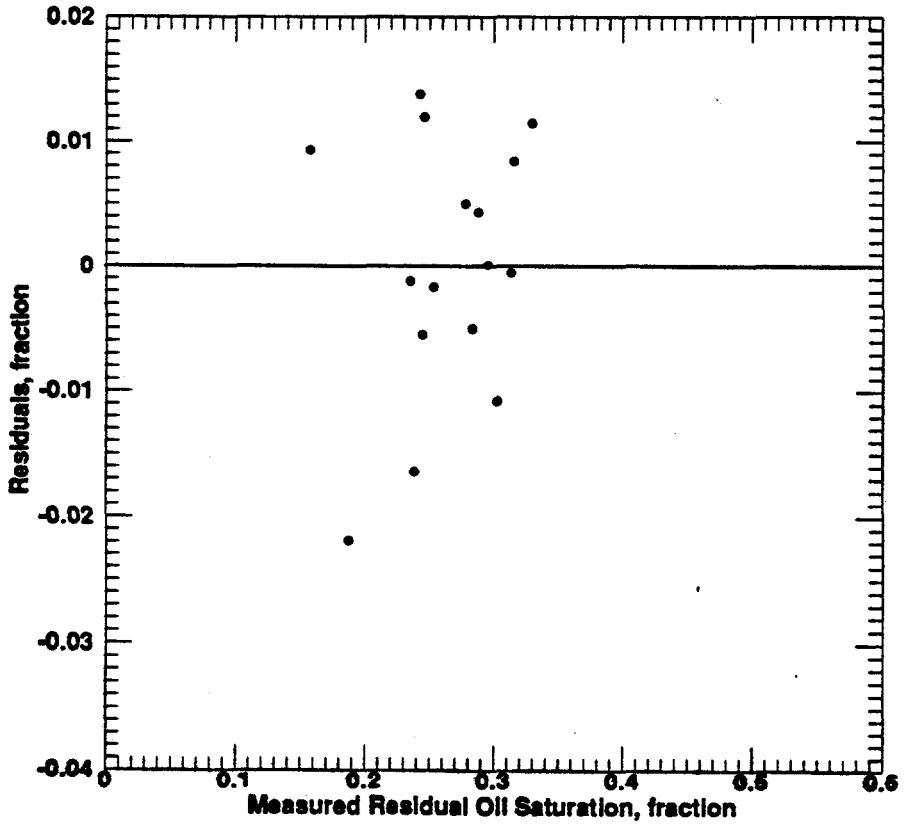

Fig. 6.31 Plotted Residuals Using the New Correlation (Eq. 6.34) vs. Measured Residual Oil Saturation at Floodout Values for Limestones.

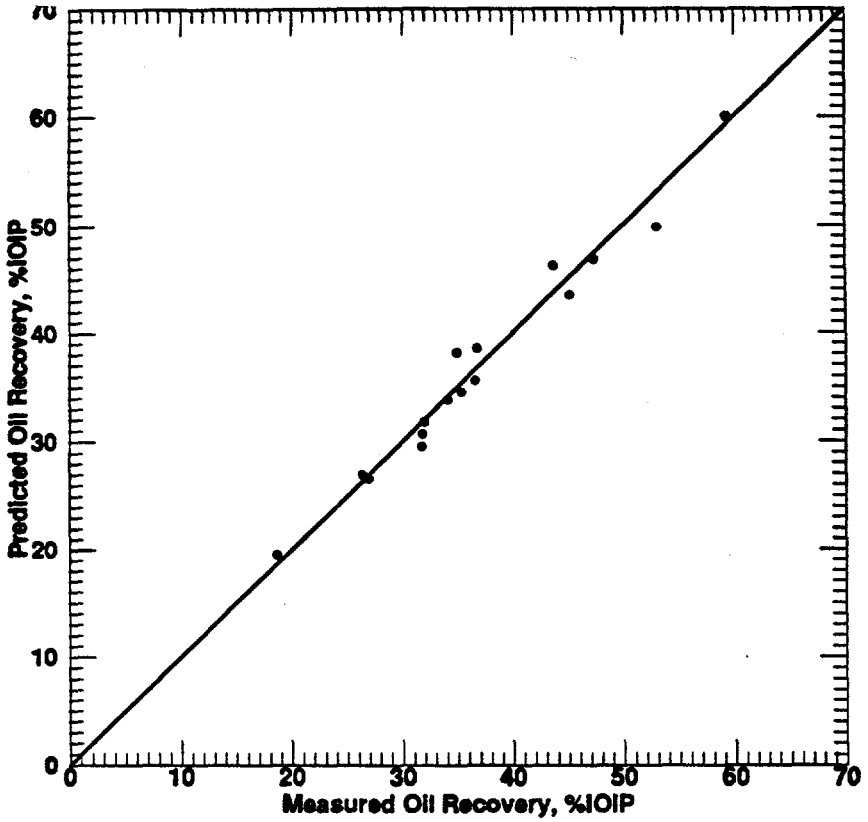

Fig. 6.32: Comparison of Measured Oil Recovery at Breakthrough Values for Limestones with those Predicted by the New Correlation (Eq. 6.35).

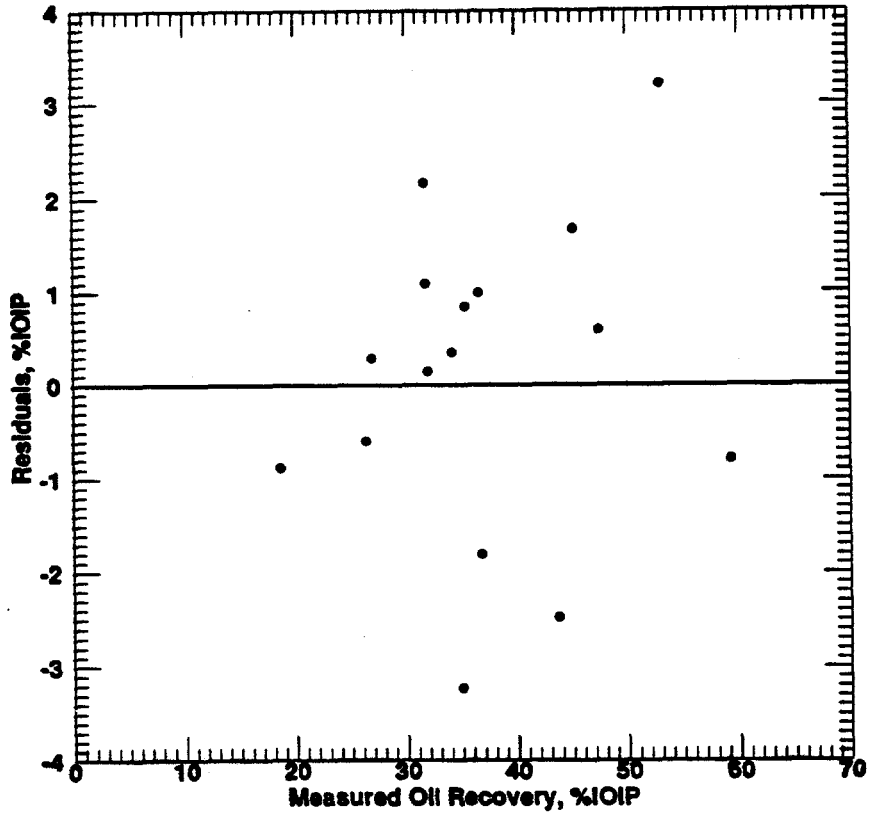

Fig. 6.33: Plotted Residuals Using the New Correlation (Eq. 6.35) vs. Measured Oil Recovery at Breakthrough Values for Limestones.

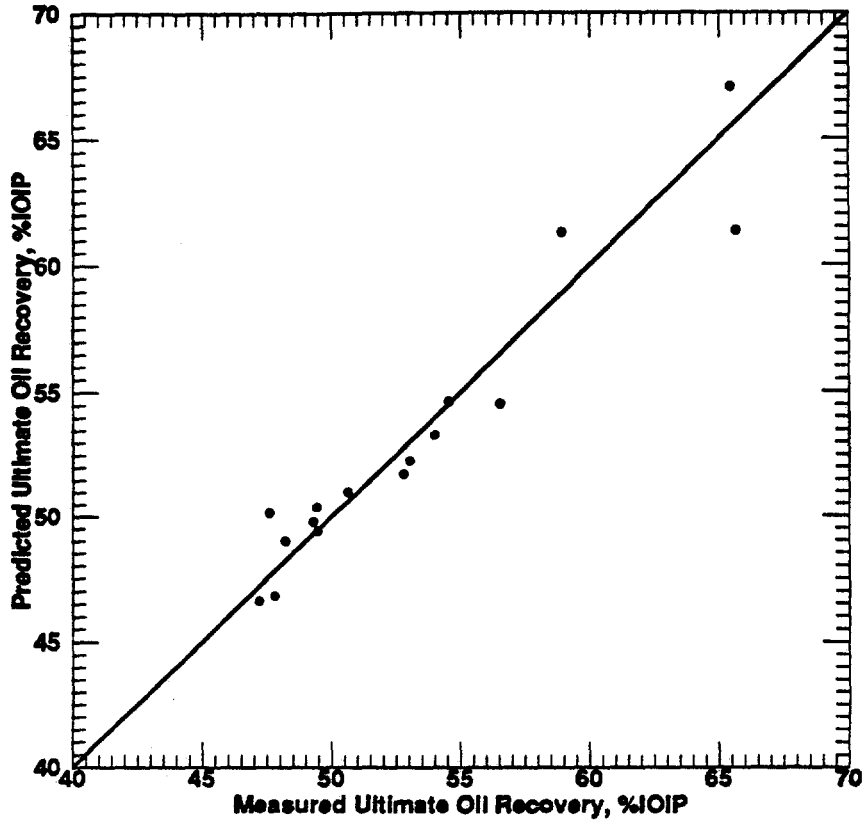

Fig. 6.34: Comparison of Measured Ultimate Oil Recovery at Floodout Values for Limestones with those Predicted by the New Correlation (Eq. 6.36).

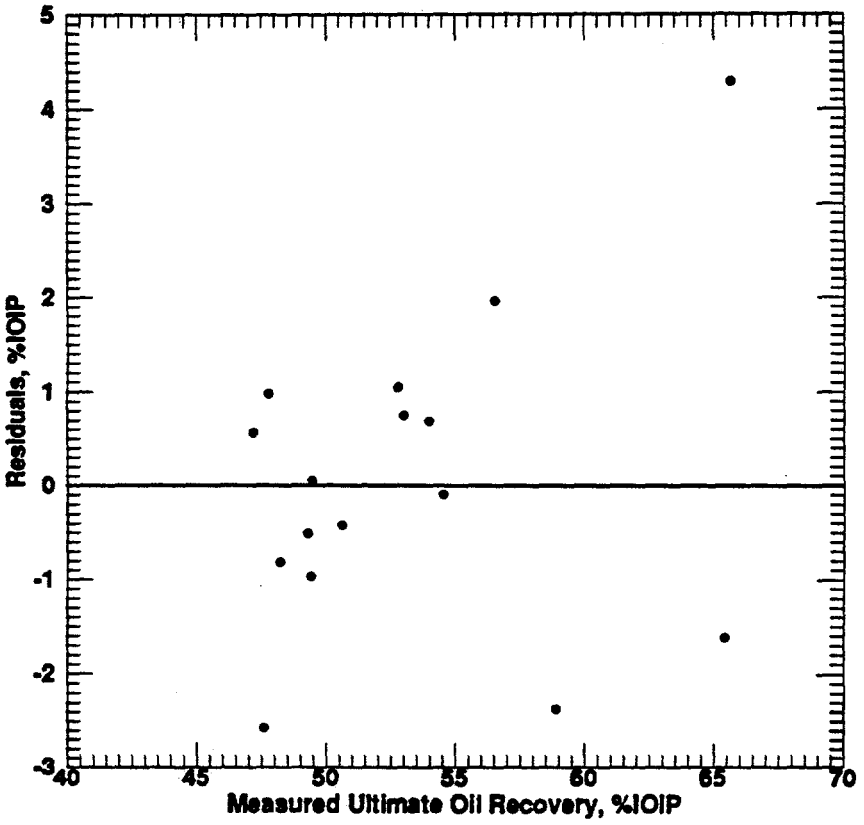

Fig. 6.35: Plotted Residuals Using the New Correlation (Eq. 6.36) vs. Measured Ultimate Oil Recovery at Floodout Values for Limestones.

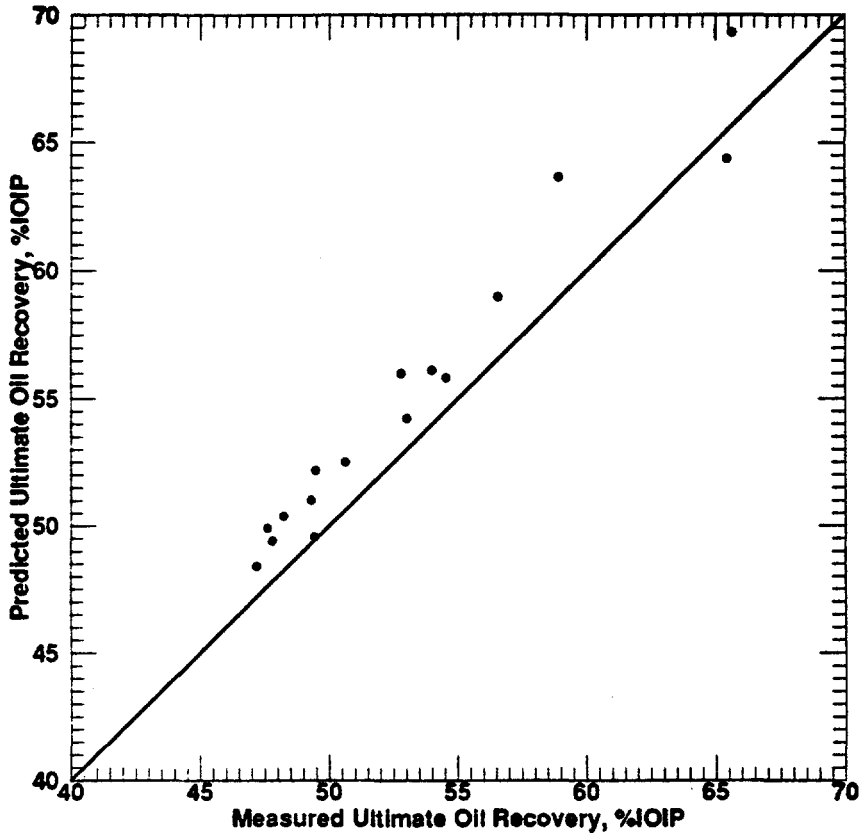

Fig. 6.36: Comparison of Measured Ultimate Oil Recovery at Floodout Values for Limestones with those Predicted by Boukadi (1991) Correlation (Eq. 6.10).

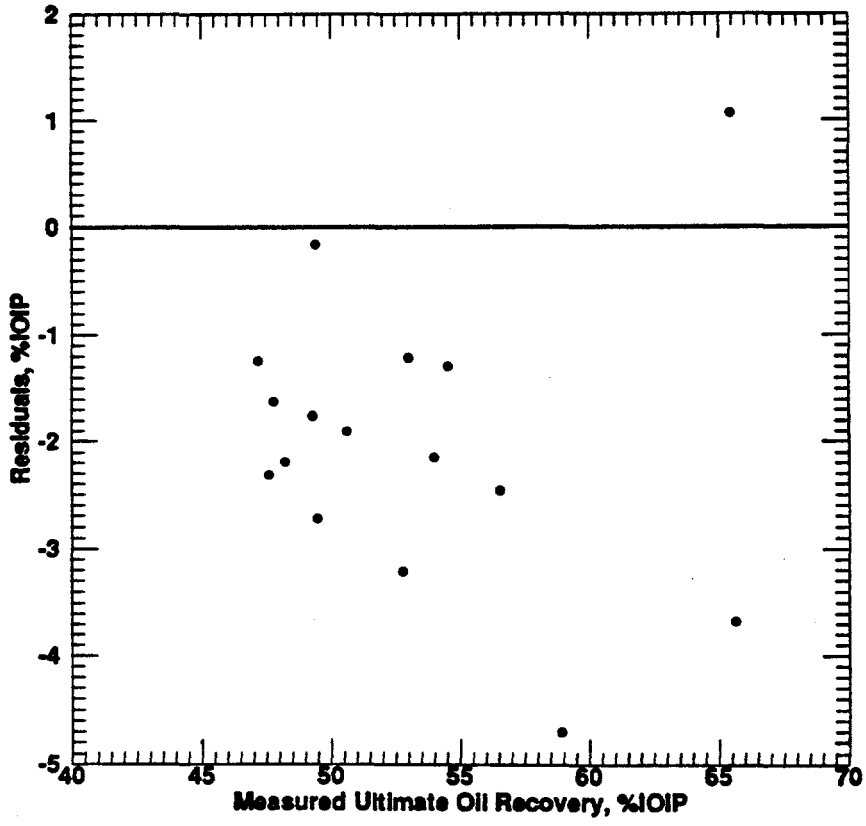

Fig. 6.37: Plotted Residuals Using Boukadi (1991) Correlation (Eq. 6.10) vs. Measured Ultimate Oil Recovery at Floodout Values for Limestones.

6.35 suggests the need to add more independent variables to Boukadi's model in order to further improve its predictive strength. Furthermore, as explained earlier, residual oil saturation should not have been included in his empirically developed models.

Chapter 7

SUMMARY AND CONCLUSIONS

The motivation for this study arose from the need to assist reservoir engineers, explorationists, and other multi-phase flow in porous media practitioners, to find a better and simple to use tool for estimating residual oil saturation and oil recovery, during primary or enhanced recovery period. To embark on this task, some important but not fully investigated rock-pore properties of various types of oil bearing rocks were investigated. These properties include: wettability, tortuosity, pore size distribution, pore surface area, specific surface area, pore diameter, apparent (skeletal) density, mercury porosimetry measured porosity, and mercury recovery efficiency.

To accomplish the above stated objective, radial and linear flow experimental investigations were performed, using Berea sandstone and Indiana limestone cores. For the radial flow cases, 20 sandstone radial-cores and 20 limestone radial-cores were utilized for the waterflood experiments. The study also included wettability and mercury porosimetry tests on 480 sandstone core plugs and 480 limestone core plugs, extracted from the waterflooded radial-cores. For the linear flow cases, well stabilized laboratory waterflood experiments were performed on 21 sandstone linear-cores and 16 limestone linear-cores. The stabilized flooding conditions were achieved by performing the waterflooding tests under an imposed scaling coefficient of approximately 5.0 cm^2.cp/min, regardless of the core length. For wettability and mercury porosimetry tests, 580 sandstone core plugs and 512 limestone core plugs were extracted from the waterflooded linear-cores. The data obtained from the different laboratory experiments were statistically analyzed and later-on compared to each other, to investigate the inter-relationships among various properties of sandstone and limestone reservoir rocks. Further, to assist in providing good initial estimates of reservoir

descriptions used in reservoir simulators to predict primary and enhanced recovery performance, new empirically derived mercury recovery efficiency and permeability correlations were proposed for sandstones and limestones.

To aid in the predictions of residual oil saturations and oil recoveries at breakthrough and at floodout, empirical models were developed for sandstones and limestones. In the case of the linear flow investigations, for each reservoir rock type, 12 models were developed. Separate models were developed using common rock/fluid properties, another sets were developed using uncommon rock/fluid properties, and finally both types of rock/fluid properties were combined to develop other sets of empirical models.

The following conclusions are deduced from this study:

1. Waterfloods in the investigated sandstone and limestone core samples, performed at stabilized conditions, have confirmed qualitatively the results of previous investigations. The trends of the relationships depicted by the investigated cores petrophysical and waterflood properties are similar to those in the literature.

2. The sandstone and limestone cores investigated were all found to be water-wet, with ultimate oil recovery by waterflooding appearing to be optimum at average wettability index values close to neutral wettability.

3. Pore-size distribution and median pore-throat size affect rock tortuosity expressed in terms of the wetting phase retention time in a water-wet medium.

4. Average rock pore length has a minimal or no effect on oil recovery by waterflooding. This is mainly due to the fact that in such waterflooding experiments, like the radial-core experiments, where capillary forces are the dominant forces, recovery is

controlled primarily by rock surface area and particularly median pore-throat diameter, rather than pore length. Further, tortuosity appears to be affected by median pore length.

5. The sandstone radial-cores investigated were characterized by steep-convex unimodal capillary pressure curves with median pore-throat sizes varying from 10 μm to 25 μm. Steep-convex unimodal, bimodal and polymodal capillary pressure and incremental intrusion curves are characteristic of the limestone radial-cores.

6. The sandstone linear-cores investigated were all found to exhibit steep-concave unimodal capillary-pressure curve shapes, while the limestone linear-cores exhibited gently-sloping bimodal capillary-pressure curve shapes. Unlike the limestones, these sandstones would not perform well during primary oil production period, but are good candidates for enhanced oil recovery methods.

7. Framework grains as well as the induced secondary porosity had no apparent effect on total porosity. Different proportions of framework grains did not affect the total porosity.

8. The amounts of clay matrix in sandstone cores affect the rock total porosity. Higher amounts of clay matrix lower the total porosity.

9. Due to the effect of high capillary forces in the sandstone cores, residual oil saturations were affected by total porosity. A low porosity permits a piston-like displacement and therefore lower levels of residual oil saturations. By contrast, higher porosities will result in higher residual oil saturations. This phenomenon is due to high

aspect ratios (ratio of pore-body to pore-throat diameters) associated with the high porosity systems.

10. High surface areas are associated with less porous systems. Tighter cores contain a significant number of shale streaks. Higher surface areas reflect the expansion of clay minerals in the tighter formations. Therefore, the abundance of shale content in the sandstone matrix results in higher rock surface areas. The presence of large amounts of cement, carbonate and quartz overgrowth increases the rock surface areas of the sandstone rocks.

11. New empirical correlations that can be easily programmed for computer application have been developed to estimate mercury recovery efficiency and permeability for sandstones and limestones. The permeability correlations can also be employed as a tool to estimate mercury porosimetry derived permeability values.

12. It was shown that besides porosity, total mercury intrusion volume, pore surface area, average pore diameter and apparent (skeletal) density are important factors for mercury recovery efficiency estimations. Further, besides porosity, pore surface area and specific surface area are important factors for permeability estimations.

13. For the case of the radial flow investigations, the standardized regression model selected, based on a subset of the variables, predicted oil recovery by waterflooding with a standard deviation of 7%. The fact that in this model, C_p is slightly lower than p is the result of random variation in the C_p estimate. The full model which involves 10 parameters predicted oil recovery with a standard deviation of 1%.

14. For the case of the linear flow investigations, new empirical models have been

developed for sandstones and limestones, to predict residual oil saturation and oil recovery at breakthrough and at floodout, using common, uncommon, and combination of both the common and uncommon laboratory measured rock/fluid properties.

15. All the 24 new linear-core models for sandstones and limestones are strongly statistically significant, but if only one sets of models are to be chosen, the ones developed using the combination of both common and uncommon rock/fluid properties are recommended.

16. Comparisons of measured laboratory ultimate oil recovery with the predicted values from the Arnold and Crawford (1964), Donaldson et al. (1969), Boukadi (1991), and the newly developed ultimate oil recovery linear-core models, indicate that the new models predict the most accurate results. However, the Boukadi's model for predicting limestones ultimate oil recovery has comparable accuracy, with the newly developed ultimate oil recovery model for limestones. These are biased comparisons, because they were based on data sets obtained from this study.

BIBLIOGRAPHY

Abrams, A.: "The Influence of Fluid Viscosity, Interfacial Tension, and Flow Velocity on Residual Oil Saturation Left by Waterflood," paper No. SPE 5050 presented at the 49th Annual Fall Meeting of the SPE, Houston, TX., Oct. 6-9, 1974.

Albright, J.C.: "Use of Well Logs to Characterize Fluid Flow in the Maljamar CO_2 Pilot," *JPT*, (Aug. 1986), 883-890.

Al-Fossail, K.A., Saner, S., Asar, H.K., and Hossain, M.: "Factor Affecting Mercury Capillary Pressure Behavior of Saudi Arabian Carbonate Reservoir Rocks," paper No. SPE 21434 presented at the 1991 SPE Middle East Oil Show, Bahrain, Nov. 16-19, 815-820.

Amaefule, J.O., and Handy, L.L.: "The Effects of Interfacial Tensions on Relative Oil/Water Permeabilities of Consolidated Porous Media," *SPEJ*, (June 1982), 371-381.

Amott, E.: "Observations Relating to the Wettability of Porous Rock," *AIME Trans.*, (1959), **216**, 156-162.

Amthor, J.E., Kopaska-Merkel, D.C., and Friedman, G.M.: "Reservoir Characterization, Porosity, and Recovery Efficiency of Deeply-Buried Paleozoic Carbonates: Examples From Oklahoma, Texas and New Mexico," *Carbonates and Evaporites*, (1988), **3**, No. 1, 33-52.

Amyx, J.W., Bass, D.M. Jr., and Whiting, R.L.: Petroleum Reservoir Engineering, 610 pp., McGraw-Hill Book Co., New York, NY., 1960.

Andersen, M.A., Thomas, D.C., and Teeters, D.C.: "A New Device for Determining Wetting Preference of Crude Oil/Brine/Solid Systems," *The Log Analyst*, (Sept.-Oct., 1989), 372-381.

Anderson, W.G.: "Wettability Literature Survey - Part 1: Rock/Oil/Brine Interactions and the Effects of Core Handling on Wettability," *JPT*, (Oct. 1986a), 1125-1144.

Anderson, W.G.: "Wettability Literature Survey - Part 2: Wettability Measurement," *JPT*, (Nov. 1986b), 1246-1262.

Anderson, W.G.: "Wettability Literature Survey - Part 3: The Effects of Wettability on the Electrical Properties of Porous Media," *JPT*, (Dec. 1986c), 1371-1378.

Anderson, W.G.: "Wettability Literature Survey - Part 4: Effects of Wettability on Capillary Pressure," *JPT*, (Oct. 1987a), 1283-1300.

Anderson, W.G.: "Wettability Literature Survey - Part 5: The Effects of Wettability on Relative Permeability," *JPT*, (Nov. 1987b), 1453-1468.

Anderson, W.G.: "Wettability Literature Survey - Part 6: The Effects of Wettability on Waterflooding," *JPT*, (Dec. 1987c), 1605-1622.

Archie, G.E.: "The Electrical Resistivity Log as an Aid in Determining Some Reservoir Characteristics," *AIME Trans.*, (1942), **146**, 54-61.

Archie, G.E.: "Classification of Carbonate Reservoir Rocks and Petrophysical Considerations," *AAPG Bull.*, (Feb. 1952), **36**, No. 2, 278-298.

Arcia, E. M., and Civan, F.: "Characterization of Formation damage by Particulate Processes," *J. Cand. Pet. Tech.*, (Mar. 1992), **31**, No. 3, 27-33.

Arnold, M.D., and Crawford, P.B.: "An empirical Equation Relating Oil and Rock Properties to Waterflood Recoveries, paper No. SPE 847, (Aug. 1964), 43-52.

Aschenbrenner, B.C., and Achauer, C.W.: "Minimum Conditions for Migration of Oil in Water-Wet Carbonate Rocks," *AAPG Bull.*, (Feb. 1960), **44**, No. 2, 235-243.

Aschenbrenner, B.C., and Chilingar, G.V.: "Teodorovich's Method for Determining Permeability From Pore-Space Characteristics of Carbonate Rocks," *AAPG Bull.*, (Feb. 1960), **44**, No. 2, 1421-1424.

Baker, P.A., and Kastner, M.: "Constrains on the Formation of Sedimentary Dolomite," *Science*, (July 10,1981), **213**, 214-216.

Ballin, P.R., Journel, A.G., and Aziz, K.: "Prediction of Uncertainty in Reservoir Performance Forecast," *J. of Can. Pet. Tech.*, (April 1992), **31**, No. 4, 52-62.

Barthel, R.: "The Effect of Large-Scale Heterogeneities on the Performance of Waterdrive Reservoirs," paper No. SPE 22697 presented at the 66th Annual Tech. Conference and Exhibition of the SPE, Dallas, TX., Oct. 6-9, 1991.

Batycky, J.P., McCaffery, F.G., Hodgins, P.K., and Fisher, D.B.: "Interpreting Capillary Pressure and Rock Wetting Characteristics from Unsteady-State Displacement Measurements," paper No. SPE 9403 presented at the 55th. Annual Fall Tech. Conf. and Exhibition of the SPE, Dallas, TX., (Sept. 21-24, 1980), 1-15.

Bear, J.: Dynamics of Fluids in Porous Media, 764 pp., American Elsevier Publishing Co., Inc., New York, NY., 1972.

Bell, W.K., Van Brakel, J., and Heertjes, P.M.: "Mercury Penetration and Retraction Hysteresis in Closely Packed Spheres," *Powder Tech.*, (1981), **29**, 75-88.

Bennion, D.W., and Griffiths, J.C.: "A Stochastic Model for Predicting Variations in Reservoir Rock Properties," *SPEJ*, (Mar. 1966), 9-16.

Bernard, G.G.: "Effect of Floodwater Salinity on Recovery of Oil from Cores Containing Clays," *Producers Monthly*, (June 1968), 2-5.

Bloch, S.: "Empirical Prediction of Porosity and Permeability in Sandstones," *AAPG Bull.*, (July 1991), **75**, No. 7, 1145-1160.

Bobek, J.E., Mattax, C.C., and Denekas, M.O.: "Reservoir Rock Wettability - Its Significance and Evaluation," *AIME Trans.*, (1958), **213**, 155-160.

Boneau, D.F., and Clampitt, P.L.: "A Surfactant System for the Oil-Wet Sandstone of the North Burbank Unit," *JPT*, (May 1977), 501-506.

Boon, J.A.: "Chemistry in Enhanced Oil Recovery - An Overview," *J. of Can. Pet. Tech.*, (Jan.-Feb. 1984), 59-65.

Borner, F.D., and Schon, J.H.: "A Relation between the Quadrature Component of Electrical Conductivity and the Specific Surface Area of Sedimentary Rocks," *The Log Analyst*, (Sept.-Oct., 1991), 612-613.

Boukadi, F.B.H.: "An Experimental and Theoretical Study to Relate Uncommon Rock/Fluid Properties to Oil Recovery," Ph.D. Dissertation, The Pennsylvania State University, University Park, PA., (Dec. 1991), 238pp.

Boukadi, F.B., Watson, R.W., and Owolabi, O.O.: "The influence of Reservoir Skeletal Properties on Ultimate Oil Recovery in Radial-Core Waterfloods,"paper No. CIM 92-55 in the proceeding of the 43rd Annual Technical Meeting of the Petroleum Society of CIM, Calgary, Alberta, Canada, June 7-10, 1992.

Breston, J.N., and Hughes, R.V.: "Relation Between Pressure and Recovery in Long Core Water Floods," *AIME Trans.*, (April 1949), 100-110.

Briggs, P., et al.: "Trends in Reservoir Management," *Schlumberger Oilfield Review*, (Jan. 1992), 8-24.

Brown, R.: "Although Extremely Powerful, Polynomial Curve Fitting Springs Hidden Surprises," *Personal Eng. & Instrumentation News*, (April 1990), 57-61.

Brown, R.: "Graphical Approach to Curve Fitting Uncovers Analysis Pitfalls," *Personal Eng. & Instrumentation News*, (Dec. 1989), 51-54.

Brown, C.E., and Neustadter, E.L.: "The Wettability of Oil/Water/Silica Systems With Reference to Oil Recovery," *J. of Can. Pet. Tech.*, (July-Sept. 1980), 100-110.

Buckley, S.E., and Leverett, M.C.: "Mechanism of Fluid Displacement in Sands," *AIME Trans.*, (1942), **146**, 107-116.

Buckley, J.S., Takamura, K., and Morrow, N.R.: "Influence of Electrical Surface Charges on the Wetting Properties of Crude Oils," *SPERE*, (Aug. 1989), 332-340.

Bulnes, A.C., and Fitting, R.U. Jr.: "An Introductory Discussion of the Reservoir Performance of Limestone Formations," *AIME Trans.*, (1945), **160**, 179-201.

Burdine, N.T.: "Relative Permeability Calculations from Pore Size Distribution Data," *AIME Trans.*, (1953), **198**, 71-78.

Burdine, N.T., Gournay, L.S., and Reichertz, P.P.: "Pore Size Distribution of Petroleum Reservoir Rocks," *Pet. Trans. AIME*, (1950), **189**, 195-204.

Candido, A., and Wardlaw, N.C.: "Reservoir Geology of the Carmopolis Oil Field," *Bull. Can. Petr. Geol.*, (Dec. 1985), **33**, No. 4, 379-395.

Carlile, R.E.: "Recovery, Recovery Fraction and Residual Oil Saturation Correlations For Sandstone, Water-Drive Reservoirs," Ph.D. Dissertation, Texas A & M Univ., (Jan. 1964), 56pp.

Carlson, M.R., and Andrews, R.J.: "A Dodsland-Hoosier Viking Waterflood Prediction," *J. of Can. Pet. Tech.*, (Jan. 1992), **31**, No. 1, 45-52.

Chang, M.M., Maerefat, N.L., Tomutsa, L., and Honarpour, M.M.: "Evaluation and Comparison of Residual Oil Saturation Determination Techniques," *SPEFE*, (March 1988), 251-262.

Chatzis, I., and Dullien, F.A.L.: "Mercury Porosimetry Curves of Sandstones. Mechanisms of Mercury Penetration and Withdrawal," *Powder Tech.*, (1981), **29**, 117-125.

Chatzis, I., and Morrow, N.R.: "Correlation of Capillary Number Relationships for Sandstone," *SPEJ*, (Oct. 1984), 555-562.

Chatzis, I., Morrow, N.R., and Lim, H.T.: "Magnitude and Detailed Structure of Residual Oil Saturation," *SPEJ*, (April 1983), 311-326.

Chilingarian, G.V., Chang, J., and Bagrintseva, K.I.: "Empirical Expression of Permeability in Terms of Porosity, Specific Surface Area, and Residual Water Saturation of Carbonate Rocks," *J. Pet. Sci. and Eng.*, (1990), **4**, 317-322.

Chilingarian, G.V., McClain, S., and Yen, T.F.: "Note on Carbonate Reservoir Rocks, No. 6: Determination of Porosity of Some Dolomitized Carbonate Rocks from Matrix Density of Drill Chips and Grains," *Energy Sources*, (1987), **9**, 67-70.

Chilingarian, G.V., and Yen, T.F.: "Note on Carbonate Reservoir Rocks, No. 5: Interrelationships Among Various Properties of Carbonates," *Energy Sources*, (1987), **9**, 51-65.

Choho, T., Pelce, V., Fasanino, G., and Picard, M.: "A New Method for Capillary Pressure and Relative Permeability Curve Matching for Gas/Water Flow," paper No. SPE 19812 presented at the 64th. Annual Tech. Conf. of the SPE, San Antonio, TX., (Oct. 8-11, 1989), 409-416.

Chopra, A.K., Stein, M.H., and Ader, J.C.: "Development of Reservoir Descriptions to Aid in Design of EOR Projects," *SPERE*, (May 1989), 143-150.

Choquette, P.W., and Lloyd, C.P.: "Geological Nomenclature and Classification of Porosity in Sedimentary Carbonates," *AAPG Bull.*, (Feb. 1970), **54**, No. 2, 207-250.

Christiansen, R.L.: "Geometric Concerns for Accurate Measurement of Capillary Pressure Relationships with Centrifuge Methods," *SPEFE*, (Dec. 1992), 311-314.

Chuanmao, L., and Friedman, G.M.: "Petrophysical Analysis of Modern Reef Rocks,"*Carbonates and Evaporites*, (1992), **7**, No. 1, 11-20.

Churcher, P.L., French, P.R., Shaw, J.C., and Schramm, L.L.: "Rock Properties of Berea Sandstone, Baker Dolomite, and Indiana Limestone," paper No. SPE 21044 presented at the 1991 SPE International Symposium on Oilfield Chemistry, Anaheim, CA., Feb. 20-22.

Ciccarone, M., and Warren, N.: "Thickness Trends and Structure of Berea Sandstone (Mississippian) in Washington County, Ohio," abstract in *AAPG Bull.*, (1985) **69**, No. 2, 244-245.

Collins, R.E., and Crawford, P.B.: "Calculations of Unsteady-State Gas Flow Through Porous Media, Corrected for Klinkenberg Effect," *AIME Trans.*, (1953), **198**, 339-340.

Coogan, A.H., and Heath, L.L.: "Berea Sandstone Gas Reservoirs in Portage County, Ohio," abstract in *AAPG Bull.*, (1984) **68**, No. 12, 1918.

Corbett, P.W.M., and Jensen, J.L.: "Variation of Reservoir Statistics According to Sample Spacing and Measurement Type for Some Intervals in the Lower Brent Group," *The Log Analyst*, (Jan. - Feb., 1992), 22-41.

Coretest Systems, Inc.: Operators Manual - Core Flood System, Mountain View, CA., Aug. 1, 1988.

Correa, A.C., Pande, K.K., Ramey, H.J. Jr., and Brigham, W.E.: "Computation and Interpretation of Miscible Displacement Performance in Heterogeneous Porous Media," *SPERE*, (Feb. 1990), 69-78.

Corvi, P., et al.: "Reservoir Characterization Using Expert Knowledge, Data and Statistics," *Schlumberger Oilfield Review*, (Jan. 1992), 25-39.

Craig, F.F.: The Reservoir Engineering Aspects of Waterflooding, 141 pp., SPE Monograph, Dallas, TX., 3,, 1971.

Craze, R.C.: "Performance of Limestone Reservoir," *AIME Trans.*, (1950), **189**, 287-294.

Craze, R.C., and Buckley, S.E.: "A Factual Analysis of the Effect of Well Spacing on Oil Recovery," *Drill. and Prod. Prac.*, (1945), 144-159.

Cuiec, L.: "Rock/Crude-Oil Interactions and Wettability: An Attempt to Understand Their Interrelation," paper No. SPE 13211 presented at the 59th Annual SPE Tech. Conf. and Exhibition, Houston, TX., Sept. 16-19, 1984.

Cuiec, L.: "Wettability and Oil Reservoirs," *North Sea Oil & Gas Reservoir*, The Norwegian Inst. of Tech., (Graham and Trotman, 1987), 193-207.

Cuiec, L., Longeron, D., and Pacsirszky, J.: "On the Necessity of Respecting Reservoir Conditions in Laboratory Displacement Studies," paper No. SPE 7785 presented at the Middle East Oil Tech Conf. of the SPE, Manama, Bahrain, Mar. 25-29, 1979.

Dake, L.P.: Fundamentals of Reservoir Engineering, 443 pp., Elsevier Scientific Publishing Co., New York, NY., 1978.

Davies, G.W., Gamble, I.J.A., and Heaviside, J.: "Field Wide Variations in Residual Oil Saturation in a North Sea Sandstone Reservoir," paper No. SPE 19851 presented at the 64th. Annual Tech. Conf. and Exhibition of the SPE, San Antonio, TX., (Oct. 8-11, 1989), 859-868.

Dimitrakopoulos, R.: "Stochastic Modelling of Space Dependent Reservoir-Rock Properties," *J. of Can. Pet. Tech.*, (July-Aug. 1991), **30**, No. 4, 43-51.

Dixon, J.R., and Marek, B.F.: "The Effect of Bimodal Pore Size Distribution on Electrical Properties of Some Middle Eastern Limestones," paper SPE No. 20601 presented at the 1991 SPE Middle East Oil Show, Bahrain, Nov. 16-19, 11-18.

Doctor, P.G., and Nelson, R.W.: "Geostatistical Estimation of Parameters for Hydrologic Transport Modelling," *Math. Geol.*, (1981), **13**, No. 5, 415-427.

Donaldson, E.C., Thomas, R.D., and Lorenz, P.B.: "Wettability Determination and Its Effect on Recovery Efficiency," *SPEJ*, (Mar. 1969), 13-20.

Dullien, F.A.L.: "New Network Permeability Model of Porous Media," *AIChE J.*, (March 1975), **21**, No. 2, 299-307.

Dullien, F.A.L., Allsop, H.A., MacDonald, I.F. and Chatzis, I.: "Wettability and Immiscible Displacement in Pembina Cardium Sandstone," *J. of Can. Pet. Tech.*, (July-Aug. 1990), 63-74.

Dullien, F.A.L., and Dhawan, G.K.: "Bivariate Pore-Size Distributions of Some Sandstones," *J. Colloid and Interface Sci.*, (July 1975), **52**, No. 1, 129-135.

Dullien, F.A.L., and Dhawan, G.K.: "Characterization of Pore Structure by a Combination of Quantitative Photomicrography and Mercury Porosimetry," *J. of Colloid and Interface Sci.*, (May 1974), **47**, No. 2, 337-349.

Du Prey, E.L.: "Gravity and Capillarity Effects on Imbibition in Porous Media," *SPEJ*, (June 1978), 195-206.

Dutton, S.P., and Diggs, T.N.: "Evolution of Porosity and Permeability in the Lower Cretaceous Travis Peak Formation, East Texas," *AAPG Bull.*, (Feb. 1992), **76**, No. 2, 252-269.

Dyer, S., and Farouq Ali, S.M.: "Mechanistic Aspects and Chemistry of Immiscible Carbon Dioxide Flooding," paper presented at the Annual Meeting of the AIChE, Chicago, Illinois (Nov. 11-16, 1990).

Edmondson, T.A.: "Effect of Temperature on Waterflooding," *J. of Can. Pet. Tech.*, (Oct.-Dec., 1965), 236-242.

Ehrlich, R., Kennedy, S.K., Crabtree, S.J., and Cannon, R.L.: "Petrographic Image Analysis, I. Analysis of Reservoir Pore Complexes," *J. Sed. Petrology*, (Dec. 1984), **54**, No. 4, 1365-1378.

Ehrlich, R., Tracht, J.H., and Kaye, S.E.: "Laboratory and Field Study of the Effect of Mobile Water on CO_2-Flood Residual Oil Saturation," *JPT*, (Oct. 1984), 1797-1809.

Etnyre, L.M.: "Statistical Detection of Hydrocarbons from Well Logs," paper presented at the SPWLA Twenty-Third Annual Logging Symposium, July 6-9, 1982.

Etnyre, L.M.: "Practical Application of Weighted Least Squares Methods to Formation Evaluation - Part II: Evaluating the Uncertainty in Least Squares Results," *The Log Analyst*, (May-June, 1984), 11-20.

Etris, E.L., Brumfield, D.S., Ehrlich, R., and Crabtree, S.J. Jr.: "Relations Between Pores, Throats and Permeability: A petrographical/Physical Analysis of Some Carbonate Grainstones and Packstones," *Carbonates and Evaporites*, (1988), **3**, No. 1, 17-32.

Farouq Ali, S.M., and Colmont, G.J.: "Appraisal of Micellar Flooding, Carbon Dioxide and Surfactant Flooding Projects," paper No. SPE 6624 presented at the 1977 SPE Eastern Regional Meeting, Pittsburgh, PA., Oct. 27-28.

Fassi-Fihri, O., Robin, M., and Rosenberg, E.: "Wettability Studies at the Pore Level: A New Approach by the Use of Cryo-Scanning Electron Microscopy," paper SPE No. 22596 presented at the 66th Annual Tech. Conference and Exhibition of the SPE, Dallas, TX., Oct. 6-9, 1991.

Fassihi, M.R.: "New Correlations for Calculation of Vertical Coverage and Areal Sweep Efficiency," *SPERE*, (Nov. 1986), 604-606.

Fatt, I.: "The Effect of Overburden Pressure on Relative Permeability," *AIME Trans.*, (1953), **198**, 325-326.

Fatt, I: "The Network Model of Porous Media I. - Capillary Pressure Characteristics," *AIME Trans.*, (1956), **207**, 144-159.

Fishlock, T.P., Smith, R.A., Soper, B.M., and Wood, R.W.: "Experimental Studies on the Waterflood Residual Gas Saturation and Its Production by Blowdown," *SPERE*, (May 1988), 387-394.

Fleureau, J.M.: "Wettability of Reservoir Core Samples," *SPEFE*, (June 1992), 132-138.

Fookes, P.G., and Hawkins, A.B.: "Limestone Weathering: Its Engineering Significance and a Proposed Classification Scheme," *Quarterly J. of Eng. Geol., London*, (1988), **21**, 7-31.

French, R.L., Brimhall, R.M., and Wu, C.H.: "A Statistical and Economic Analysis of Incremental Waterflood Infill Drilling Recoveries in West Texas Carbonate Reservoirs," paper No. SPE 22624 presented at the 66th Annual Tech. Conference and Exhibition of the SPE, Dallas, TX., Oct. 6-9, 1991.

Frimodig, J.P., Reese, N.A., and Williams, C.A.: "Carbon Dioxide Flooding Evaluation of High-Pour-Point, Paraffinic Red Wash Reservoir Oil," *SPEJ*, (Aug. 1983), 587-594.

Fulcher, R.A. Jr.: "Effect of the Capillary Number and its Constituents on Two-Phase Relative Permeabilities," Ph.D Dissertation, The Pennsylvania State University, University Park, PA., (Aug. 1982), 170pp.

Garboczi, E.J.: "Mercury Porosimetry and Effective Networks for Permeability Calculations in Porous Materials," *Powder Tech.* (1991), **67**, 121-125.

Gardner, K.L.: "Impregnation Technique Using Colored Epoxy to Define Porosity in Petrographic Thin Sections," *Can. J. Earth Sci.*, (1980), **17**, 1104-1107.

Ghosh, S.K., Urschell, S.F., and Friedman, G.M.: "Substitution of Simulated Well Cuttings for Core Plugs in the Petrophysical Analysis of Dolostones: Permian San Andres Formation, Texas," *Carbonates and Evaporites*, (1987), **2**, 95-100.

Ghosh, S.K., and Friedman, G.M.: "Petrophysics of a Dolostone Reservoir: San Andres Formation (Permian), West Texas," *Carbonates and Evaporites*, (1989), **4**, No. 1, 45-117.

Goodlett, O.G., Honarpour, M.M., Carroll, H.B., and Sarathi, P.S.: "Screening for EOR-1: Lab Evaluation Requires Appropriate Techniques," *Oil & Gas J.*, (June 23, 1986), 47-54.

Givens, W.W.: "Formation Factor, Resistivity Index, and Related Equations, Based Upon a Conductive Rock Matrix Model (CRMM)," paper presented at the SPWLA Twenty-Seventh Annual Logging Symposium, June 9-13, 1986.

Good, R.J., and Mikhail, R.S.: "The Contact Angle in Mercury Intrusion Porosimetry," *Powder Tech.*, (1981), **29**, 53-62.

Grape, S.G., Poston, S.W., and Osoba, J.S.: "Imbibition Flooding with CO_2-Enriched Water," paper No. 9018 presented at the 1990 Society of Core Analysts Conference, Dallas, TX., Aug. 15-16.

Graue, A., Kolltvelt, K., Llen, J. R., and Skauge, A.: "Imaging Fluid Saturation Development in Long-Core Flood Displacements," *SPEFE*, (Dec. 1990), 406-412.

Guerrero, E.T.: Practical Reservoir Engineering, 266 pp., The Petroleum Publishing Co., Tulsa, OK., 1968.

Guthrie, R.K., and Greenberger, M.H.: "The Use of Multiple-Correlation Analyses for Interpreting Petroleum-Engineering Data," *Drill. and Prod. Prac.*, (1955), 130-137.

Haldorsen, H.H., and Damsleth, E.: "Stochastic Modeling," *JPT*, (April 1990), 404-412.

Hassler, G.L., and Brunner, E.: "Measurement of Capillary Pressures in Small Core Samples," *AIME Trans.*, (1945), **160**, 114-123.

Hawkins, J.T.: "Comparison of Three Methods of Relative Permeability Measurement," *The Log Analyst*, (Sept.-Oct., 1989), 363-371.

Hawthorne, R.G.: "A model of Fluid Displacement in Multilayer Porous Media Including Capillary Pressure Effects Between Layers," paper No. SPE 5126 presented at the 49th. Annual Fall Meeting of the SPE, Houston, TX., Oct. 6-9, 1974.

Heaviside, J., and Black, C.J.J.: "Fundamentals of Relative Permeability: Experimental and Theoretical Considerations," paper No. SPE 12173 presented at the 1983 SPE Annual Fall Meeting, Dallas, Tx., Oct. 5-8.

Heaviside, J., Brown, C.E., and Gamble, I.J.A.: "Relative Permeability for Intermediate Wettability Reservoirs," paper No. SPE 16968 presented at the 1987 Annual Fall Meeting, Dallas, Tx., Sept. 27-30.

Henderson, G.D., Danesh, A.S., and Peden, J.M.: "Waterflooding of Gas-Condensate Fluids in Cores Above and Below the Dewpoint," paper No. SPE 22636 presented at the 66th Annual Tech. Conference and Exhibition of the SPE, Dallas, TX., Oct. 6-9, 1991.

Henley, D.H., Owen, W.W., and Craig, F.F. Jr.: "A Scaled Model Study of Bottom-Water Drives," paper No. SPE 1539-G presented at the 35th. Annual Fall Meeting of the SPE, Denver, CO., Oct. 2-5, 1960.

Hillebrand, L.B., and Coogan, A.H.: "Berea Sandstone Reservoirs in Ashland and Medina Counties, Ohio," abstract in *AAPG Bull.*, (1984), **68**, No. 12, 1920.

Hillebrand, L.B., and Coogan, A.H.: "Evaluating Berea Sandstone Reservoirs in Eastern Ashland County, Ohio," abstract in *AAPG Bull.*, (1986), **70**, No. 8, 1067.

Hjelmeland, O.S., and Larrondo, L.E.: "Experimental Investigation of the Effects of Temperature, Pressure, and Crude Oil Composition on Interfacial Properties," *SPERE*, (July 1986), 321-328.

Honarpour, M.M., Burchfield, T.E., and Linville, B.: "Reservoir Characterization Can Help Recovery Efficiency," *The American Oil & Gas Reporter*, (Sept. 1989), **32**, No. 9.

Honarpour, M., Koederitz, L., and Harvey, A. H.: Relative Permeability of Petroleum Reservoirs, 143 pp., CRC Press, Inc., Boca Raton, FL., 1986.

Honarpour, M., Maloney, D., Suzuki, S., and Tomutsa, L.: "Investigation of Cycle Dependent Centrifuge Capillary Pressure and Wettability Index Behavior for Water-Wet High Permeability Sandstones," paper No. 9006 presented at the 1990 Society of Core Analysts Conference, Dallas, TX., Aug. 15-16.

Hove, A., Ringen, J.K., and Read, P.A.: "Visualization of Laboratory Core Floods with the Aid of Computerized Tomography of X-Rays," paper No. SPE 13654 presented at the SPE California Regional Meeting, Bakersfield, CA., Mar. 27-29, 1985.

Howard, J.J.: "Porosimetry Measurement of Shale Fabric and its Relationship to Illite/Smectite Diagenesis," *The Clays and Clay Minerals*, (1991), **39**, No. 4, 355-361.

Huang, E.T.S., and Holm, L.W.: "Effect of WAG Injection and Rock Wettability on Oil Recovery During CO_2 Flooding," *SPERE*, (Feb. 1988), 119-129.

Hubbert, M.K.: "Darcy's Law and the Field Equations of the Flow of Underground Fluids," *AIME Trans.*, (1956), **207**, 222-239.

Huh, D.G., Cochrane, T.D., and Kovarik, F.S.: "The Effect of Microscopic Heterogeneity on CO_2-Foam Mobility: Part 1 - Mechanistic Study," *JPT*, (Aug. 1989), 872-879.

Hurlbut, C.S., Jr.: Manual of Mineralogy, John Wiley and Sons, Inc., New York (1942), 282-311.

Interstate Oil Compact Commission: Improved Oil Recovery, 363 pp., Interstate Oil Compact Commission, Oklahoma City, OK., 1983.

Isaaks, E.H., and Srivastava, R.M.: An Introduction to Applied Geostatistic, 561 pp., Oxford Univ. Press, New York, 1989.

Jackson, D.S.: "Petrology, Porosity, and Permeability of Berea Sandstone (Mississippian), Perry Township, Ashland County, Ohio," abstract in *AAPG Bull.*, (1985), **69**, No. 9, 1438.

Jadhunandan, P.P., and Morrow, N.R.: "Effect of Wettability on Waterflood Recovery for Crude-Oil/Brine/Rock Systems," paper No. SPE 22597 presented at the 66th Annual Tech. Conference and Exhibition of the SPE, Dallas, TX., Oct. 6-9, 1991a.

Jadhunandan, P.P., and Morrow, N.R.: "Spontaneous Imbibition of Water by Crude Oil/Brine/Rock Systems," *In Situ*, (1991b), **15**, No. 4, 319-345.

Jasti, J., Jesion, G., and Feldkamp, L.: "Microscopic Imaging of Porous-Media Using X-Ray Computer Tomography," paper No. SPE 20495 presented at the 65th Annual Technical Conference and Exhibition of the SPE, New Orleans, LA., (Sept. 23-26, 1990), 269-276.

Jennings, H.Y.: "Surface Properties of Natural and Synthetic Porous Media," *Prod. Monthly*, (1957), **21**, No. 5, 20.

Jha, K.N., and Chakma, A.: "Nitrogen Injection with Horizontal Wells for Enhancing Heavy-Oil Recovery: 2D and 3D Model Studies," paper No. SPE 23029 presented at the SPE Asia-Pacific Conference, Perth, Western Australia, Nov. 4-7, 1991.

Jia, D., Buckley, J.S., and Morrow, N.R.: "Control of Core Wettability with Crude Oil," paper No. SPE 21041 presented at the 1991 SPE International Symposium on Oilfield Chemistry, Anaheim, CA., Feb. 20-22.

Johnson, N., and Van Wingen, N.: "Recent Laboratory Investigations of Water Flooding in California," *AIME Trans.*, (1953), **198**, 219-224.

Journel, A.G.: "Geostatistics for Reservoir Characterization," paper No. SPE 20750 presented at the 1990 SPE Annual Conference, New Orleans, LA., (Sept. 23-26, 1990), 353-358.

Journel, A.G., and Alabert, F.G.: "New Method for Reservoir Mapping," *JPT*, (Feb. 1990), 212-218.

Kamath, J.: "Evaluation of Accuracy of Estimating Air Permeability From Mercury-

Injection Data," *SPEFE*, (Dec. 1992), 304-310.

Kazemi, H.: "Determination of Waterflood Residual Oil Saturation From Routine Core Analysis," *JPT*, (Jan. 1977), 31-32.

Keelan, D.K.: "Automated Core Measurement System for Enhanced Core Data at Overburden Conditions," paper No. SPE 15185 presented at the 1986 Rocky Mountain Regional Meeting of the SPE, Billings, MT., May 19-21.

Keller, G.V.: "Effect of Wettability on the Electrical Resistivity of Sand," *Oil and Gas J.*, (Jan. 1953), **31**, No. 4, 62-65.

Keller, W.O., and Morse, R.A.: "Some Examples of Fluid Flow Mechanism in Limestone Reservoirs," *AIME Trans.*, (Aug. 1949), 224-234.

Kelton, F.C.: "Analysis of Fractured Limestone Cores," *AIME Trans.*, (1950), **189**, 225-234.

Kimber, K.D., Farouq Ali, S.M., and Puttagunta, V.R.: "New Scaling Criteria and their Relative Merits for Steam Recovery Experiments," *J. of Can. Pet. Tech.*, (July-Aug. 1988), 86-94.

Kimbler, O.K., and Caudle, B.H.: "New Technique for Study of Fluid Flow," *Oil & Gas J.*, (1957), **85**, 85-88.

Kloubek, J.: "Hysteresis in Porosimetry," *Powder Tech.*, (1981a), **29**, 63-73.

Kloubek, J.: "A New Method for the Investigation of Porous Structures Using Mercury Porosimetry," *Powder Tech.*, (1981b), **29**, 89-97.

Knight, R., and Nur, A.: "The Effect of Level of Water Saturation on the Dielectric Constant of Sandstones," *Proc.*, 1984 SPWLA Annual Logging Symposium, June 10-13.

Kopaska-Merkel, D.C., and Amthor, J.E.: "Very High-Pressure Mercury Porosimetry as a Tool in Reservoir Characterization," *Carbonates and Evaporites*, (1988), **3**, No. 1, 53-63.

Kopaska-Merkel, D.C., and Friedman, G.M.: "Petrofacies Analysis of Carbonate Rocks: Example from Lower Paleozoic Hunton Group of Oklahoma and Texas," *AAPG Bull.*, (Nov. 1989a), **73**, No. 11, 1289-1306.

Kopaska-Merkel, D.C., and Friedman, G.M.: "Supplementary Data for Petrofacies Analysis of Carbonate Rocks: Example from the Lower Paleozoic Hunton Group of Oklahoma and Texas," *Carbonates and Evaporites*, (1989b), **4**, No. 2, 243-245.

Kremesec, V.J., and Treiber, L.E.: "Effect of System Wettability on Oil Displacement by Micellar Flooding," paper No. SPE 6001 presented at the 51st. Annual Fall Tech. Conf. and Exhibition of the SPE, New Orleans, La., Oct. 3-6, 1976.

Kyte, J.R., and Rapoport, L.A.: "Linear Waterflood Behavior and End Effects in Water-Wet Porous Media," *AIME Trans.*, (1958), **213**, 423-426.

Kyte, J.R., Stanclift, R.J. Jr., Stephan, S.C. Jr., and Rapoport, L.A.: "Mechanism of Water Flooding in the Presence of Free Gas," *AIME Trans.*, (1956), **207**, 215-221.

Lai, F.S.Y., MacDonald, I.F., Dullien, F.A.L., and Chatzis, I.: "A Study of the Applicability of the Independent Domain Model of Hysteresis to Capillary Pressure Hysteresis in Sandstone Samples," *J. of Colloid and Interface Sci.*, (Dec. 1981), **84**, No. 2, 362-378.

Lake, L.W., Schmidt, R.L., and Venuto, P.B.: "A Niche for Enhanced Oil Recovery in the 1990s," *Schlumberger Oilfield Review*, (Jan. 1992), 55-61.

Lane, A., Shah, N., and Conner, W.C., Jr.: "Measurement of the Morphology of High-Surface-Area Solids: Porosimetry as a Percolation Process," *J. of Colloid and Interface Sci.*, (Jan. 1986), **109**, No. 1, 235-242.

Larson, I.G., and Morrow, N.R.: "Effects of Sample Size on Capillary Pressures in Porous Media," *Powder Tech.*, (1981), **30**, 123-138.

Latil, M.: Enhanced Oil Recovery, 236 pp., Editions Technip, Paris, 1980.

Law, J.: "A Statistical Approach to the Interstitial Heterogeneity of Sand Reservoirs," *AIME Trans.*, (1944), **155**, 202-222.

Lee, J.E., Niven, R.G., Cochrane, J.T.H., and Richardson, J.G.: "The Effect of Rate on Recovery for Canadian Carbonate Reservoirs," paper No. SPE 5128 presented at the 49th. Annual Fall Meeting of the SPE, Houston, TX., Oct. 6-9, 1974.

Leverett, M.C.: "Capillary Behavior in Porous Solids," *AIME Trans.*, (1941), **152**, 152-168.

Levine, J.S.: "Displacement Experiments in a Consolidated Porous System," *AIME Trans.*, (1954), **201**, 57-66.

Li, Y., and Wardlaw, N.C.: "Mechanisms of Nonwetting Phase Trapping during Imbibition at Slow Rates," *J. of Colloid and Interface Sci.*, (Feb. 1986a), **109**, No. 2, 473-486.

Li, Y., and Wardlaw, N.C.: "The Influence of Wettability and Critical Pore-Throat Size Ratio on Snap-off," *J. of Colloid and Interface Sci.*, (Feb. 1986b), **109**, No. 2, 461-472.

Lin, E.C., and Huang, E.T.S.: "The Effect of Rock Wettability on Water Blocking During Miscible Displacement," *SPERE*, (May 1990), 205-212.

Lowell, S., and Shields, J.E.: "Equivalency of Mercury Porosimetry and Gas Adsorption," *Powder Tech.*, (1981a), **29**, 225-231.

Lowell, S., and Shields, J.E.: "Pore Spectra from Continuous Scan Mercury Porosimetry," *Powder Tech.*, (1981b), **29**, 201-204.

Lowell, S., and Shields, J.E.: Powder Surface Area and Porosity, 2nd Ed., Chapman and Hall, New York, 1981c.

Lynch, E.J.: Formation Evaluation, Harper & Row, New York, 1962.

Ma, S., Morrow, N.R.: "Effect of Firing on Petrophysical Properties of Berea Sandstone," paper No. SPE 21045 presented at the 1991 SPE International Symposium on Oilfield Chemistry, Anaheim, CA., Feb. 20-22.

Ma, S., Jiang, M., and Morrow, N.R.: "Correlation of Capillary Pressure Relationships and Calculations of Permeability," paper No. SPE 22685 presented at the 66th Annual Tech. Conference and Exhibition of the SPE, Dallas, TX., Oct. 6-9, 1991.

Marek, B.F., Hartman, K.J., and McDonald, A.E.: "Three-Phase Relative Permeability of Limestones Having Bimodal Pore-Size Distribution," paper No. SPE 21374 presented at the 1991 SPE Middle East Oil Show, Bahrain, Nov. 16-19, 333-344.

Marsden, S.S.: "Wettability: The Elusive Key to Waterflooding," *Petroleum Engineer*, (April 1965), 82-87.

Matheron, G.: "Principles of Geostatistics," *Econ. Geol.*, (1963), **58**, 1246-1266.

Matiisen, A., and Atwater, J.E.: "An Overview of Computer-Enhanced Analyses of Core Data," *J. of Can. Pet. Tech.*, (May-June), 57-62.

Mattax, C.C., and Kyte, J.R.: "Ever See a Water Flood?," a reprint from the *Oil & Gas J.*, (Oct. 16, 1961), 6pp.

Mayer, E.H., Earlougher, R.C. Sr., Spivak, A., and Costa, A.: "Analysis of Heavy-Oil Immiscible CO_2 Tertiary Coreflood Data," *SPERE*, (Feb. 1988), 69-75.

Melas, F.F., and Friedman, G.M.: "Petrophysical Characteristics of the Jurassic Smackover Formation, Jay Field, Conecuh Embayment, Alabama and Florida," *AAPG Bull.*, (Jan. 1992), **76**, No. 1, 81-100.

Melrose, J.C., and Brandner, C.F.: "Role of Capillary Forces in Determining Microscopic Displacement Efficiency for Oil Recovery by Waterflooding," *The J. Can. Pet.*

Tech., (Oct.-Dec., 1974), 54-62.

Metwally, M.: "Recovery Mechanisms: Fireflooding a High-Gravity Crude in a Waterflooded Sandstone Reservoir, Countess Field, Alberta," paper No. SPE 21536 presented at the 1991 SPE International Thermal Operations Symposium, Bakersfield, CA., Feb. 7-8.

Micromeritics: Instruction Manual - Autopore II 9220, Norcross, GA., Oct. 9, 1987.

Mikkelsen, M., Schele, A., Rong, O., and de Boer, E.T.: "Abnormal Permeability Behavior of a North Sea Sandstone Reservoir," paper No. SPE 22600 presented at the 66th Annual Tech. Conference and Exhibition of the SPE, Dallas, TX., Oct. 6-9, 1991.

Miller, M.A., and Ramey, H.J. Jr.: "Effect of Temperature on Oil/Water Relative Permeabilities of Unconsolidated and Consolidated Sands," *SPEJ*, (Dec. 1985), 945-953.

Mohanty, K.K., Davis, H.T., and Scriven, L.E.: "Physics of Oil Entrapment in Water-Wet Rock," *SPERE*, (Feb. 1987), 113-128.

Mohanty, K.K., and Miller, A.E.: "Factors Influencing Unsteady Relative Permeability of a Mixed-Wet Reservoir Rock," paper No. SPE 18292 presented at the 1988 Annual Fall Meeting, Houston, TX., Oct. 2-5.

Moore, J.: "Laboratory Determined Electric Logging Parameters of Bradford Third Sand," *Producers Monthly*, (Mar. 25, 1958), 30-39.

Moore, T.F. and Slobod, R.L.: "The Effect of Viscosity and Capillarity on the Displacement of Oil by Water," *Producers Monthly*, (Aug. 1956), 20-30.

Morgan, J.T., and Gordon, D.T.: "Influence of Pore Geometry on Water-Oil Relative Permeability," *JPT*, (Oct. 1970), 1199-1208.

Morris, E.E., and Wieland, D.R.: "A Microscopic Study of the Effect of Variable Wettability Conditions on Immiscible Fluid Displacement," paper No. SPE 704 presented at the 38th. Annual Fall Meeting of the SPE, New Orleans, LA., (Oct. 6-9, 1963), 703-706.

Morrow, N.R.: "Irreducible Wetting-Phase Saturations in Porous Media," *Chem. Eng. Sci.*, (1970), **25**, 1799-1815.

Morrow, N.R.: "Wettability and its Effect on Oil Recovery," *JPT*, (Dec. 1990), 1476-1484.

Morrow, N.R., Cram, P.J., and McCaffery, F.G.: "Displacement Studies in Dolomite with Wettability Control by Octanoic Acid," paper No. SPE 3993 presented at the 1972

Annual Fall Meeting of the SPE, San Antonio, TX., Oct. 8-11.

Moscou, L., and Lub, S.: "Practical Use of Mercury Porosimetry in the Study of Porous Solids," *Powder Tech.*, (1981), **29**, 45-52.

Mukaida, K.: "Density Measurements of Small Porous Particles by Mercury Porosimetry," *Powder Tech.*, (1981), **29**, 99-107.

Mungan, N.: "Certain Wettability Effects in Laboratory Waterfloods," *JPT*, (Feb. 1966), 247-252.

Neter, J., Wasserman, W., and Kutner, M.H.: Applied Linear Statistical Models, 1181 pp., 3rd. Ed., Irwin, Boston, MA., 1990.

O'Meara, D.J. Jr., Hirasaki, G.J., and Rohan, J.A.: "Centrifuge Measurements of Capillary Pressure: Part 1 - Outflow Boundary Condition," paper No. SPE 18296 presented at the 63rd. Annual Tech. Confr. and Exhibition of the SPE, Houston, TX., (Oct. 2-5, 1988), 349-362.

Omoregie, Z.S.: "Factors Affecting the Equivalency of Different Capillary Pressure Measurement Techniques," *SPEFE*, (Mar. 1988), 147-155.

Ormiston, R.M., and Luce, M.C.: "Surface Processing of Carbon Dioxide in EOR Projects," *JPT*, (Aug. 1986), 823-828.

Orr, C. Jr.: "Application of Mercury Penetration to Materials Analysis," *Powder Tech.*, (1969/70), **3**, 117-123.

Owens, W.W., and Archer, D.L.: "The Effect of Rock Wettability on Oil Water Relative Permeability Relations," *JPT*, (July 1971), 873-878.

Owolabi, O.O.: "Empirical Modeling of the Microscopic Rock-Pore Characteristics in Sandstone Linear Cores to Residual Oil Saturation and Oil Recovery by Waterflood," in the proceeding of papers submitted for the 1992 Mobil sponsored student paper contest - Ph.D Division.

Owolabi, O.O.: "Relating Uncommon Rock/Fluid Properties to Oil Recovery for Various Types of Oil Bearing Rocks: Experimental and Empirical Studies," Ph.D. Dissertation, The Pennsylvania State University, University Park, PA., (May 1993), 412pp.

Owolabi, O.O., and Watson, R.W.: "The Influence of Mercury Porosimetry Properties, Tortuosity, Porosity and Wettability on Sandstone Waterflood Residual Oil Saturation," paper in the proceeding of the Eighth Wyoming EOR Symposium, Casper, Wy., May 20-21,1992.

Pathak, P., Davis, H.T., and Scriven, L.E.: "Dependence of Residual Non-Wetting Liquid

on Pore Topology," paper No. SPE 11016 presented at the 57th Annual Meeting of the SPE, New Orleans, LA., Sept. 1982.

Patton, J.B.: "Petrology of the Salem Limestone (Indiana Building Stone)," abstract in *Econ. Geol.*, (1953), **48**, No. 4, 331.

Pickell, J.J., Swanson, B.F., and Hickman, W.B.: "Application of Air-Mercury and Oil-Air Capillary Pressure Data in the Study of Pore Structure and Fluid Distribution," *SPEJ*, (Mar. 1966), 55-61.

Pittman, E.D.: "Relationship of Porosity and Permeability to Various Parameters Derived from Mercury Injection-Capillary Pressure Curves for Sandstone," *AAPG Bull.*, (Feb. 1992), **76**, No. 2, 191-198.

Pugh, V.J., Thomas, D.C., and Gupta, S.P.: "Correlations of Liquid and Air Permeabilities for Use in Reservoir Engineering Studies," *The Log Analyst*, (Sept.-Oct. 1991), 493-497.

Purcell, W.R.: "Capillary Pressures - Their Measurement Using Mercury and the Calculation of Permeability Therefrom," *AIME Trans.*, (Feb. 1949), **186**, 39-48.

Raffensperger, J.P., and Ferrell, R.E., Jr.: "An Empirical Model of Intrinsic Permeability in Reactive Clay-Bearing Sands," *Water Resources Research*, (Nov. 1991), **27**, No. 11, 2835-2844.

Rajan, R.R.: "Theoretically Correct Analytical Solution for Calculating Capillary Pressure-Saturation from Centrifuge Experiments," paper presented at the SPWLA 27th Annual Logging Symposium, June 9-13, 1986.

Rajani, B.B.: "A Simple Model for Describing Variation of Permeability with Porosity for Unconsolidated Sands," *In Situ*, (1988) **12**, No. 3, 209-226.

Rao, D.N., Girard, Marcel, and Sayegh, S.G.: "The Influence of Reservoir Wettability on Waterflood and Miscible flood performance," *J. Can. Pet. Tech.*, (June 1992), **31**, No. 6, 47-55.

Rapoport, L.A., and Leas, W.J.: "Properties of Linear Waterfloods," *AIME Trans.*, (1953), **198**, *139-148*.

Rathmell, J.J., Braun, P.H., and Perkins, T.K.: "Reservoir Waterflood Residual Oil Saturation from Laboratory Tests," *JPT*, (Feb. 1973), 175-185.

Raza, S.H., Treiber, L.E., and Archer, D.L.: "Wettability of Reservoir Rocks and Its Evaluation," *Producers Monthly*, (April 1968), 2-7.

Reedy, G.K.: "Accurate Residual Oil Saturation Measurement Using a Modified Log-Inject-Log Procedure," *Proc.*, 1984 SPWLA Annual Logging Symposium, June 10.

Reverberi, G., Feraiolo, G., and Peloso, A.: *Ann. Chim.*, (1966), **56**, No. 1552.

Ritter, L.C., and Drake, R.L.: "Pore-Size Distribution in Porous Materials," *Ind. Eng. Chem. Anal. Ed.*, (Dec. 1945), **17**, No. 12, 782

Rojas, G., and Farouq Ali, S.M.: "Scaled Model Studies of Carbon Dioxide/Brine Injection Strategies for Heavy Oil Recovery from Thin Formations," *J. of Can. Pet. Tech.*, (Jan.-Feb. 1986), 85-94.

Rollins, J.B., Holditch, S.A., and Lee, W.J.: "Characterizing Average Permeability in Oil and Gas Formations," paper No. SPE 19793 presented at the 64th Annual Tech. Conference and Exhibition of the SPE, San Antonio, TX, Oct. 8-11, 1989.

Roof, J.G.: "Snap-Off of Oil Droplets in Water-Wet Pores," *SPEJ*, (Mar. 1970), 85-90.

Rose, W., and Channapragada, R.: "Microscopic Aspects of Capillary Imbibition," paper No. SPE 1549-G presented at the 35th. Annual Fall Meeting of the SPE, Denver, CO., Oct. 2-5, 1960.

Rose, W., and Wyllie, M.R.J.: "A Note on the Theoretical Description of Wetting Liquid Relative Permeability Data," *AIME Trans.*, (Dec. 1949), 329.

Ross, G.D., Todd, A.C., Tweedie, J.A., and Will, A.G.S.: "The Dissolution Effects of CO_2-Brine Systems on the Permeability of U.K. and North Sea Calcareous Sandstones," paper No. SPE/DOE 10685 presented at the 1982 Third Joint SPE/DOE Symposium on EOR, Tulsa, OK., April 4-7.

Ruth, D., and Wong, S.: "Calculation of Capillary Pressure Curves from Data Obtained by the Centrifuge Method," paper No. 8802 presented at the 1988 Soc. Core Analysts (SCA) Conference.

Ruth, D., and Wong, S.: "Centrifuge Capillary Pressure Curves," *J. of Can. Pet. Tech.*, (May-June 1990), 67-72.

Ruzyla, K.: "Characterization of Pore Space by Quantitative Image Analysis," *SPEFE*, (Aug. 1986), 389-398.

Ruzyla, K., and Friedman, G.M.: "Geological Heterogeneities Important to Future Enhanced Recovery in Carbonate Reservoirs of Upper Ordovician Red River Formation at Cabin Creek Field, Montana," *SPEJ*, (June 1982), 429-444.

Ryan, B.F., Joiner, B.L., and Ryan, T.A. Jr.: Minitab Handbook, 379 pp., 2nd. Ed., Duxbury Press, Boston, MA., 1985.

Salathiel, R.A.: "Oil Recovery by Surface Film Drainage in Mixed-Wettability Rocks," *JPT*, (Oct. 1973), 1216-1224.

Saller, A.H., Van Horn, D., Miller, J.A., and Guy, T.: "Reservoir Geology of Devonian Carbonates and Chert - Implications for Tertiary Recovery, Dollarhide Field, Andrews County, Texas," *AAPG Bull.*, (Jan. 1991), **75**, No. 1, 86-107.

Sattler, A.R.: "Multiwell Experiment Core Analysis - An Overview of the Core Analysis of a Low-Permeability Sandstone Reservoir," *The Core Analyst*, (Sept.-Oct., 1991), 498-510.

Sayegh, S.G., Krause, F.F., Girard, M., and DeBree, C.: "Rock/Fluid Interactions of Carbonated Brines in a Sandstone Reservoir: Pembina Cardium, Alberta, Canada," *SPEFE*, (Dec. 1990), 399-405.

Schmidt, V., McDonald, D.A., and Platt, R.L.: "Pore Geometry and Reservoir Aspects of Secondary Porosity in Sandstones," *Bull. Can. Pet. Geol.*, (May 1977), **25**, No. 2, 271-290.

Schneider, F.N., and Owens, W.W.: "Sandstone and Carbonate Two- and Three-Phase Relative Permeability Characteristics," *SPEJ*, (Mar. 1970), 75-84.

Schenk, C.J., and Richardson, R.W.: "Recognition of Interstitial Anhydrite Dissolution: A Cause of Secondary Porosity, San Andres Limestone, New Mexico, and Upper Minnelusa Formation, Wyoming," *AAPG Bull.*, (July 1985), **69**, No. 7, 1064-1076.

Schwartz, D.E.: "Scanning Electron Microscope-Cold Stage: Viewing Fluid Saturated Reservoir Rock," paper No. SPE 9248 presented at the 1980 Annual Fall Meeting of the SPE, Dallas, Tx., Sept. 21-24.

Selley, R.C.: Elements of Petroleum Geology, pp. 219-275, W.H. Freeman & Co., New York, NY., 1985.

Shakoor, A., and Bonelli, R.E.: "Relationship Between Petrographic Characteristics, Engineering Index Properties, and Mechanical Properties of Selected Sandstones," *Bull. Assoc. of Eng. Geol.*, (1991), **28**, No. 1, 55-71.

Sharma, M.M., Garrouch, A., and Dunlap, H.F.: "Effects of Wettability, Pore Geometry, and Stress on Electrical Conduction in Fluid-Saturated Rocks," *The Log Analyst*, (Sept.-Oct., 1991), 511-526.

Sharma, S.K., Nohwar, U.V.S., Raj, H., Koithara, J., and Chilingar, G.V.: "Interrelationships Among Various Petrophysical Parameters of Carbonate Reservoir Rocks in the Bombay High Oil Field, India," *Energy Sources*, (1980), **5**, No. 1, 53-69.

Sigmund, P., Sharma, H., Sheldon, D., and Aziz, K.: "Rate Dependence of Unstable Waterfloods," *SPERE*, (May 1988), 401-409.

Simon, D.E., Kaul, F.W., and Culbertson, J.N.: "Anadarko Basin Morrow-Springer

Sandstone Stimulation Study," paper No. SPE 6757 presented at the 52nd Annual Fall Technical Conference and Exhibition of the SPE, Denver, CO., (Oct. 9-12, 1977), 1-4.

Skopec, R.A.: "Recent Advances in Rock Characterization," *The Log Analyst*, (May-June, 1992), 270-285.

Slack, W.W., and Ehlich, R.: "Immiscible Displacement of Oil By Simultaneous Injection of Water and Nitrogen," paper No. SPE/DOE 9807 presented at the 1981 SPE/DOE Second Joint Symposium on EOR, Tulsa, OK., April 5-8.

Slatt, R.M., and Hopkins, G.L.: "Scaling Geologic Reservoir Description to Engineering Needs," *JPT*, (Feb. 1990), 202-210.

Slobod, R.L., Chambers, A., and Prehn, W.L. Jr.: "Use of Centrifuge for Determining Connate Water, Residual Oil, and Capillary Pressure Curves of Small Core Samples," *Petroleum Trans. AIME*, (1951), **192**, 127-134.

Smith, L.: "Spatial Variability of Flow Parameters in a Stratified Sand," *Math. Geol.*, (1981), **13**, No. 1, 1-21.

Smith, D.H., Covatch, G.L., and Lowry, W.E.: "Three-Fluid Wetting Transitions and their Effects on Three-Phase Flow in Enhanced Oil Recovery," paper No. SPE 21043 presented at the 1991 SPE International Symposium on Oilfield Chemistry, Anaheim, CA., Feb. 20-22.

Soeder, D.J., and Chowdlah, P.: "Pore Geometry in High- and Low-Permeability Sandstones, Travis Peak Formation, East Texas," *SPEFE*, (1990), 421-430.

Sondenaa, E., Bratteli, F., Normann, H.P., and Kollveit, K.: "The Effect of Reservoir Conditions and Wettability on Electrical Resistivity," paper No. SPE 22991 presented at the SPE Asia-Pacific Conference, Perth, Western Australia, Nov. 4-7, 1991, 409-422.

Sprunt, E.S.: "Arun Core Analysis: Special Procedures for Vuggy Carbonates," *The Log Analyst*, (Sept.-Oct., 1989), 353-362.

Stevenson, D.L.: "Salem Limestone Oil, Gas Production in Keenville Field in Illinois," *Oil and Gas J.*, (May 14, 1979), 193-201.

Steward, C.R., Craig, F.F. Jr., and Morse, R.A.: "Determination of Limestone Performance Characteristics by Model Flow Tests," *AIME Trans.*, (1953), **198**, 93-102.

Stout, J.L.: "Pore Geometry as Related to Carbonate Stratigraphic Traps," *AAPG Bull.*, (March 1964), **48**, No. 3, 329-337.

Sudicky, E.A.: "A Natural Gradient Experiment on Solute Transport in a Sand Aquifer: Spatial Variability of Hydraulic Conductivity and Its Role in the Dispersion Process," *Water Resources Research*, (Dec. 1986), **22**, No. 13, 2069-2082.

Svata, M.: "The Application of Mercury Porosimetry to Materials Wetted by Mercury," *Powder Tech.*, (1981), **29**, 145-149.

Sweeney, S.A., and Jennings, H.Y.: "Effect of Wettability on the Electrical Resistivity of Carbonate Rock from a Petroleum Reservoir," *J. of Physical Chem.*, (May 1960), 551-553.

Swanson, B.F.: "A Simple Correlation Between Permeabilities and Mercury Capillary Pressures," *JPT*, (Dec. 1981), 2498-2504.

Taber, J.J., Kamath, I.S.K., and Reed, R.L.: "Mechanism of Alcohol Displacement of Oil from Porous Media," *SPEJ*, (Sept. 1961), 195-212.

Thomas, D.C., and Pugh, V.J.: "A Statistical Analysis of the Accuracy and Reproducibility of Standard Core Analysis," *The Log Analyst*, (Mar.-April, 1989), 71-77.

Thomas, R.D., Stosur, G.T., and Pautz, J.F.: "Analysis of Trends in U.S.A. Enhanced Oil-Recovery Projects," *J. Pet. Sci. and Eng.*, (1989), **2**, 149-157.

Thompson, A.H., Katz, A.J., and Raschke, R.A.: "Estimation of Absolute Permeability From Capillary Pressure Measurements," paper No. SPE 16794 presented at the 1987 Annual Technical Conference and Exhibition of the SPE, Dallas, TX., Sept. 27-30, 475-481.

Thornton, O.F.: "A Note on the Valuation of Relative Permeability," *AIME Trans.*, (Dec. 1949), 328.

Tomutsa, L., Jackson, S.R., and Szpakiewicz, M.: "Geostatistical Characterization and Comparison of Outcrop and Subsurface Facies: Shannon Shelf Sand Ridges," paper No. SPE 15127 presented at the 1986 California Regional Meeting, Oakland, CA., April 2-4.

Tomutsa, L., Mahmood, S.M., Brinkmeyer, A., and Honarpour, M.: "Application of Integrated Pore-to-Core Image Analysis to Study Fluid Distribution in Reservoir Rocks," paper No. SPE 20478 presented at the 65th Annual Technical Conference and Exhibition of the SPE, New Orleans, LA., (Sept. 23-26, 1990), 137-148.

Trantham, J.C., and Clampitt, R.L.: "Determination of Oil Saturation After Waterflooding in an Oil-Wet Reservoir - The North Burbank Unit, Tract 97 Project," *JPT*, (May, 1977), 491-500.

Treiber, L.E., Archer, D.L., and Owens, W.W.: "A Laboratory Evaluation of the

Wettability of Fifty Oil-Producing Reservoirs," *SPEJ*, (Dec. 1972), 531-540.

Trygstad, J.C., Ehrlich, R., and Wardlaw, N.C.: "Physical Modeling of Microscopic Rock-Pore Heterogeneities," paper No. SPE/DOE 14891 presented at the 1986 SPE/DOE Fifth Symposium on EOR, Tulsa, OK., April 20-23.

Unalmiser, S.: "Handling Unconsolidated Sandstone Cores to Preserve Wettability and Pore Structure," paper No. 8803 in the 1988 SCA Conference proceeding.

Unalmiser, S., and Stewart, R.W.: "Boundary Effect on Porosity Measurements and its Resolution by Method and Mathematical Means," *The Log Analyst*, (Mar.-April, 1989), 85-92.

Van Brakel, J., Modry, S., and Svata, M.: "Mercury Porosimetry: State of the Art," *Powder Tech.*, (1981), **29**, 1-12.

Venuto, P.B.: "Tailoring EOR Processes to Geological Environments," *World Oil*, (Nov. 1989), 61-68.

Verma, M.K., Boucherit, M.A.G., and Bouvier, L.: "Evaluation of Residual Oil Saturation After Waterflood in a Carbonate Reservoir," paper No. SPE 21371 presented at the 1991 SPE Middle East Oil Show, Bahrain, Nov. 16-19, 305-320.

Vernik, L., and Nur, A.: Petrophysical Classification of Siliciclastics for Lithology and Porosity Prediction from Seismic Velocities," *AAPG Bull.*, (Sept. 1992), **76**, No. 9, 1295-1309.

Wagner, O.R., and Leach, R.O.: "Improving Oil Displacement Efficiency by Wettability Adjustment," *Trans. AIME*, (1959), **216**, 65-72.

Wall, G.C., and Brown, R.J.C.: "The Determination of Pore-Size Distributions from Sorption Isotherms and Mercury Penetration in Interconnected Pores: The Application of Percolation Theory," *J. of Colloid and Interface Sci.*, (July 1981), **82**, No. 1, 141-149.

Wang, Z., Hirsche, W.K., and Sedgwick, G.E.: "Electrical and Petrophysical Properties of Carbonate Rocks," paper No. SPE 22661 presented at the 66th Annual Tech. Conference and Exhibition of the SPE, Dallas, TX., Oct. 6-9, 1991.

Wardlaw, N.C.: "Pore Geometry of Carbonate Rocks as Revealed by Pore Casts and Capillary Pressure," *AAPG Bull.*, (Feb. 1976), **60**, No. 2, 245-257.

Wardlaw, N.C.: "The Effects of Geometry, Wettability, Viscosity and Interfacial Tension on Trapping in Single Pore-Throat Pairs," *J. of Can. Pet. Tech.*, (May-June 1982), 21-27.

Wardlaw, N.C.: "Rock Texture, Pore Structure and Wettability: Neglected Parameters in

Well Log Interpretation of Fluid Saturation?," *Can. Well Logging Soc.*, (Dec. 1983), **12**, No. 1, 10pp.

Wardlaw, N.C., and Cassan, J.P.: "Estimation of Recovery Efficiency by Visual Observation of Pore Systems in Reservoir Rocks," *Bull. Can. Pet. Geol.*, (Dec. 1978), **26**, No. 4, 572-585.

Wardlaw, N.C., and Cassan, J.P.: "Oil Recovery Efficiency and the Rock-Pore Properties of Some Sandstone Reservoirs," *Bull. Can. Pet. Geol.*, (June 1979), **27**, No. 2, 117-138.

Wardlaw, N.C., and McKellar, M.: "Mercury Porosimetry and the Interpretation of Pore Geometry in Sedimentary Rocks and Artificial Models," *Powder Tech.*, (1981), **29**, 127-143.

Wardlaw, N.C., and McKellar, M.: "Oil Blob Populations and Mobilization of Trapped Oil in Unconsolidated Packs," *The Can. J. of Chem. Eng.*, (Aug. 1985), **63**, No. 4, 525-532.

Wardlaw, N.C., and McKellar, M.: "Pore and Throat Size Distributions Determined by Mercury Porosimetry and by Direct Observation," *Carbonates and Evaporites*, (1988), **3**, No. 1, 1-15.

Wardlaw, N.C., and Taylor, R.P.: "Mercury Capillary Pressure Curves and the Interpretation of Pore Structure and Capillary Behavior in Reservoir Rocks," *Bull. Can. Pet. Geol.*, (June 1976), **24**, No. 2, 225-262.

Warner, H.R. Jr.: "An Evaluation of Miscible CO_2 Flooding in Waterflooded Sandstone Reservoirs," *JPT*, (Oct. 1977), 1339-1347.

Washburn, E.D.: "Note on a Method of Determining the Distribution of Pore Sizes in a Porous Material," *Proc. Nat. Acad. Sci.*, (1921), **7**, 115-116.

Watson, R.W., and Boukadi, F.H.: "Effect of Surface Area and Pore Size Distribution on Oil Recovery at Breakthrough, Oil Recovery at Floodout, Residual Oil Saturation, and Wettability," paper No. 9007 presented at the Soc. of Core Analysts (SCA) Conference, Aug. 1990.

Watson, R.W., and Boukadi, F.H.: "Determination of Fluid Flow Mechanisms in Berea Using Mercury Porosimetry and a Stochastic Model to Relate these Mechanisms to Oil Recovery," paper No. 9123 presented at the SCA Conference, Aug. 1991.

Wei, J-Z., and Lile, O.B.: "Influence of Wettability on Two- and Four-Electrode Resistivity Measurements on Berea Sandstone Plugs," *SPEFE*, (Dec. 1991), 470-476.

Wellington, S.L., and Vinegar, H.J.: "X-Ray Computerized Tomography," *JPT*, (Aug.

1987), 885-898.

Willhite, G.P.: Waterflooding, 326 pp., SPE Textbook Series, Richardson, TX., 3,, 1986.

Winsauer, W.O., Shearin, H.M. Jr., Masson, P.H., and Williams, M.: "Resistivity of Brine-Saturated Sands in Relation to Pore Geometry," *AAPG Bull.*, (Feb. 1952), **36**, No. 2, 253-277.

Withjack, E.M., Graham, S.K., and Yang, C-T.: "CT Determination of Heterogeneities and Miscible Displacement Characteristics," *SPEFE*, (Dec. 1991), 447-452.

Wolcott, J.M., Groves, F.R. Jr., Trujillo, D.E., and Lee, H.G.: Investigation of Crude-Oil/Mineral Interactions: Factors Influencing Wettability Alteration," paper No. SPE 21042 presented at the 1991 SPE International Symposium on Oilfield Chemistry, Anaheim, CA., Feb. 20-22.

Woodbury, A.D., and Sudicky, E.A.: "The Geostatistical Characteristics of the Borden Aquifer," *Water Resources Research*, (April 1991), **27**, No. 4, 533-546.

Wunderlich, R.W.: "Imaging of Wetting and Nonwetting Phase Distributions: Application to Centrifuge Capillary Pressure Measurements," paper No. SPE 14422 presented at the 60th. Annual Tech. Conf. and Exhibition of the SPE, Las Vegas, NV., Sept. 22-25, 1985.

Wyllie, M.R.J., and Gregory, A.R.: "Formation Factors of Unconsolidated Porous Media: Influence of Particle Shape and Effect of Cementation," *AIME Trans.*, (1953), **198**, 103-110.

Wyllie, M.R.J., and Spangler, M.B.: "Application of Electrical Resistivity Measurements to Problem of Fluid Flow in Porous Media," *AAPG Bull.*, (Feb. 1952), **36**, No. 2, 359-403.

Wyman, R.E.: "How Should We Measure Residual Oil Saturation?," *Bull. Canadian Pet. Geol.*, (May 1977), **25**, 233-270.

Yadav, G.D., Dullien, F.A.L., Chatzis, I., and Macdonald, I.F.: "Microscopic Distribution of Wetting and Nonwetting Phases in Sandstones During Immiscible Displacements," *SPERE*, (May 1987), 137-147.

Yan, J., and Sharma, M.M.: "Wettability Alteration and Restoration for Cores Contaminated with Oil-Based Muds," *J. of Pet. Sci. and Eng.*, (1989), **2**, 63-76.

Yeh, S.W., Ehrlich, R., and Emanuel, A.S.: "Miscible-Gasflood-Induced Wettability Alteration: Experimental Observations and Oil Recovery Implications," *SPEFE*, (June 1992), 167-172.

Appendix A.

STATISTICS USED IN EVALUATIONS

Statistics used in evaluation purposes fall into three categories (Isaaks and Srivastava, 1989; and Neter et al., 1990): measures of location, measures of spread and measures of shape. The statistics in the first group give information about where various parts of the distribution lie. The mean, the median and the mode can give us some idea of where the center of the distribution lies, while the location of other parts of the distribution are given by various quartiles. The second group are used to describe the variability of the data values. This group includes the variance, and the standard deviation. The shape of the distribution is described by the coefficient of skewness and the coefficient of variation. The coefficient of skewness provides information on the symmetry while the coefficient of variation provides information on the length of the tail for certain types of distributions.

A.1 Measures of Location

Mean: The mean, $\overline{x}$, is the arithmetic average result of the data values:

$$\overline{x} = \frac{1}{n} \sum_{i=1}^{i=n} x_i \qquad \text{(A.1)}$$

Median: The median, M, is the midpoint of the observed values if they are arranged in increasing order. Half of the data values are below the median and half of the values are above the median. It can be calculated from one of the following equations:

$$M = \begin{cases} x_{\frac{n+1}{2}} & \text{if } n \text{ is odd} \\ (x_{\frac{n}{2}} + x_{\frac{n}{2}+1})/2 & \text{if } n \text{ is even} \end{cases} \qquad \text{(A.2)}$$

Mode: The mode is the value that occurs most frequently. The class with the tallest bar on the histogram gives a quick idea where the mode is.

Minimum and Maximum: The smallest value in the data set is the minimum. Maximum is the largest value in the data set.

Lower and Upper Quartile: Similar to the manner in which the median splits the data into halves, the quartiles split the data into quarters. If the data values are arranged in increasing order, then a quarter of the data falls below the lower or first quartile, Q_1, and a quarter of the data falls above the upper or third quarter, Q_3.

A.2 Measures of Spread

Variance: The variance, σ^2, is the average squared difference of values from their mean. It is sensitive to high erratic values (Isaaks and Srivastava, 1989), and given by:

$$\sigma^2 = \frac{1}{n} \sum_{i=1}^{i=n} (x_i - \overline{x})^2 \qquad \text{(A.3)}$$

Standard Deviation: The standard deviation, σ, is simply the square root of the variance (Isaaks and Srivastava, 1989; and Neter et al., 1990).

A.3 Measures of Shape

Coefficient of Skewness: The coefficient of skewness, C.S., is the most commonly used statistic for summarizing the symmetry (Isaaks and Srivastava, 1989). It is defined as:

$$\text{C.S.} = \frac{\frac{1}{n} \sum_{i=1}^{i=n} (x_i - \overline{x})^3}{\sigma^3} \qquad \text{(A.4)}$$

According to Isaaks and Srivastava (1989), the coefficient of skewness suffers even more

than the mean and variance from a sensitivity to erratic high values.

Coefficient of Variation: A measure of relative dispersion is provided by the coefficient of variation, C.V. It is a statistic that is often used as an alternative to skewness to describe the shape of the distribution. It is defined as the standard deviation of a sample divided by the mean of the sample (Isaaks and Srivastava, 1989; and Thomas and Pugh, 1989):

$$C.V. = \frac{\sigma}{\bar{x}} \tag{A.5}$$

A coefficient of variation greater than 1.0 indicates the presence of some erratic high sample values that may have a strong impact on the final estimates.

A.4 Confidence Intervals and Limits

A confidence interval is an estimate of the interval in which the true value lies. The more commonly used term is confidence limit, C.I. or μ, which has essentially the same meaning as confidence interval. A confidence limit is a range of values within which a sample observation can be expected to fall at a specified probability level. Usually, variation around the mean is discussed as falling within certain confidence limits, for example 95% (Neter et al., 1990).

These values help one to estimate the confidence interval for a given test. The confidence limits around the mean is calculated using the equation (Neter, et al., 1990):

$$\mu = \bar{x} \pm z_c \left[\frac{\sigma}{\sqrt{n}} \right] \tag{A.6}$$

where z_c, depends on the particular level of confidence desired and can be read from statistical tables (Neter et al., 1990). For example 95% and 99% confidence limits for

estimation of the population mean, μ, are given by Eqs. E.7 and E.8 respectively.

$$\mu = \overline{x} \pm 1.96 \left[\frac{\sigma}{\sqrt{n}} \right] \tag{A.7}$$

$$\mu = \overline{x} \pm 2.58 \left[\frac{\sigma}{\sqrt{n}} \right] \tag{A.8}$$

A.5 Level of Significance:

In testing a given hypothesis, the maximum probability with which we would be willing to risk a Type I error is called the level of significance and it is denoted by α (Neter et al., 1990). Frequent use is made of 5% and 1% values of α, although other levels of significance are also used. How much risk one wants to take in a given problem of rejecting a true hypothesis determines the value of α that will be chosen. For example if a .05 or 5% level of significance is chosen in designing a test of hypothesis, then there is approximately a 5% chance that we would then reject the hypothesis when it should be accepted. That is, we are 95% confident that we have made the right decision.

The p-value (also called significance level) indicatess how unusual the discrepancy in an estimation is (Ryan et al., 1985). Assuming one is to test the null hypothesis H_0: $\mu = 0$ against the alternative hypothesis H_1: $\mu \neq 0$. If the p-value is less than α, H_0 is rejected. If it is greater than α, H_0 is not rejected. For example, if we did a test using $\alpha = 0.01$ and p-value = 0.0053, we would reject H_0 since 0.0053 is less than 0.01. If we used $\alpha = 0.001$, we would accept H_0 (Ryan et al., 1985).

☆U.S. GOVERNMENT PRINTING OFFICE: 1995 - 660-029/20035